



# Refining and replacing models of hepatocytes and periportal fibrosis

Philip Michael Evan Probert

Thesis submitted for the degree of Doctor of Philosophy

Newcastle University

Faculty of Medical Sciences

Institute of Cellular Medicine

July 2014

## **Declaration**

I hereby declare that this thesis has been composed by myself and has not been accepted in application of a degree. All work was performed by myself unless otherwise stated. All sources of information have been acknowledged appropriately by means of a reference.

Philip Probert

## Abstract

The liver plays an important role in drug toxicity, in part through its significant expression of drug-metabolising enzymes. For this reason, liver cells are often used in toxicity screening. Chronic liver injury is also a growing health concern, but its study *in-vivo* is limited by the severity of the bile duct ligation (BDL) animal model. In investigating ways to replace animals as a source of liver cells for toxicity screening and reduce and refine the BDL model, rat AR42J-B-13 (B-13) cells have been examined as an alternative to primary hepatocytes and chemical alternatives to BDL have been examined respectively.

B-13 cells were readily converted by glucocorticoid treatment to hepatocyte-like (B-13/H) cells, which expressed functional CYP1A and CYP3A sub-families whose expression could be induced in response to prototypical inducers. CYP2B1 could be induced at mRNA but not protein level. The CYP1A2 gene in B-13 cells was disrupted/non-functional, however stable introduction of human CYP1A2 showed B-13 cells could be humanised and used for assessment of bioactivation-dependent genotoxins. Drug transporter mRNA expression was low in B-13 and B-13/H cells, but HNF4 $\alpha$  overexpression enhanced transporter mRNA expression and function in B-13/H cells.

The chronic administration of methapyrilene and  $\alpha$ -naphthylisothiocyanate in rats and mice respectively, caused liver injury qualitatively equivalent to that seen after BDL but without the associated mortality or severity seen with BDL.

These data suggest that B-13/H cells could be used as an alternative to primary hepatocytes for drug toxicity screening. Chronic administration of methapyrilene and  $\alpha$ -naphthylisothiocyanate could be used as alternative less severe models of periportal fibrosis in rats and mice respectively. Use of B-13/H cells would reduce the number of animals required for hepatocyte derivation and through refinement of the BDL model of periportal fibrosis, fewer rodents would be subject to the associated complications and high mortality rate of BDL.

*For E.M.H*

## Acknowledgements

I would like to firstly thank Matthew Wright for his unrelenting and infectious enthusiasm and advice and guidance over the course of this project. He has helped me in innumerable ways and undoubtedly, it wouldn't have been the same experience without him!

I must also thank my other supervisor Fiona Oakley and the members of the Wright group both past and present: Karen Wallace, Andy Axon, Stephen Hill, Emma Fairhall, Izzy Swindenbank, Stephanie Meyer, Anne Lakey and Aiman Amer, for their technical assistance, suggestions and for enlivening every day, making it all that much more enjoyable.

I must acknowledge Jelena Mann and Fiona Oakley who kindly donated liver tissue from a 14 day rat bile duct ligation study and a 21 day mouse bile duct ligation study respectively. I would also like to thank the numerous other collaborators who generously gifted specific chemicals and materials for this project.

Importantly, thanks to the NC3Rs for funding my PhD, without which this project would not have been possible.

I would like to thank my family for all their support up to and during this point in my life (and hopefully onwards!). Clearly, I would not be where I am now without them.

Finally, I would like to thank my wife, Lucy, for all the support, understanding and love she has shown through every step, including the good and particularly, the bad. This would not have been possible without her.

## Abstracts and Publications

### Publications

**Probert, P.M.**, Ebrahimkhani, M.R, Oakley, F, Mann, J, Burt, A.D, Mann, D.A, Wright, M.C. (2014) 'A reversible model for periportal fibrosis and a refined alternative to bile duct ligation'. *Toxicology Res* **3**: 98-109.

**Probert, P.M.**, Chung, G.W., Cockell, S.J., Agius, L., Mosesso, P., White, S.A., Oakley, F., Brown, C.D. and Wright, M.C. (2014) 'Utility of B-13 Progenitor-Derived Hepatocytes in Hepatotoxicity and Genotoxicity Studies', *Toxicol Sci* **137**:350-70.

---

### Presented abstracts

**Probert, P.M.E.**, Ebrahimkhani, M, Oakley, F, Burt, D.A, Mann, D.A, Wright, M.C. Methapyrilene as an alternative to bile duct ligation for the generation of reproducible hepatic periportal fibrosis. British Toxicology Society Annual Congress 2012.

**Probert, P.M.E.**, Ebrahimkhani, M, Oakley, F, Burt, D.A, Mann, D.A, Wright, M.C. Methapyrilene treatment as an alternative to bile duct ligation for the generation of reproducible hepatic periportal fibrosis. NEPG 2012.

**Probert, P.M.E.**, Oakley, F, Wright, M.C. Metabolic and Toxicity Screening Potential in B13 Progenitor-Derived Hepatocyte-like Cells *In-vitro*. British Toxicology Society Annual Congress 2013

**Probert, P.M.E.**, Ebrahimkhani, M.R, Oakley, F, Burt, A.D, Mann, D.A, Wright, M.C. (2013). Methapyrilene treatment is a refined alternative to bile duct ligation as a model of reproducible and reversible periportal fibrosis in the rat. *Journal of Hepatology*; 58 (S1), Page S244

**Probert, P.M.E.** Mosesso, P. Oakley, F. Wright, M.C. Potential in B-13 Progenitor-Derived Hepatocyte-like Cells for *in-vitro* metabolic and toxicity screening. IVTS annual meeting 2013.

---

**Awards**

- Eurotox registration bursary (2014)
- IVTS mini-travel fellowship (2013)
- EASL registration bursary (2013)
- IVTS Poster Prize (2013)
- BTS annual meeting full bursary (2013)
- BTS annual meeting full bursary (2012)

## Table of Contents

<b>Declaration</b> .....	i
<b>Abstract</b> .....	ii
<b>Acknowledgements</b> .....	iv
<b>Abstracts and Publications</b> .....	v
<b>Table of Contents</b> .....	vii
<b>List of Figures</b> .....	xiv
<b>List of Tables</b> .....	xix
<b>List of Abbreviations</b> .....	xx
<b>Chapter 1. Introduction</b> .....	1
1.1 The Liver .....	2
1.1.1 Anatomy.....	2
1.1.2 Cellular composition, distribution and function .....	2
1.1.3 The biliary system .....	4
1.1.4 Cells of the liver .....	5
1.1.5 Liver zonation .....	6
1.2 Xenobiotic metabolism .....	8
1.2.1 The phases of metabolism.....	8
1.2.2 Cytochrome P450s .....	9
1.2.3 Xenobiotic hepatic bioactivation & toxicity .....	10
1.2.4 CYP450 induction.....	10
1.2.5 Drug transporters.....	18
1.3 Safety testing of drug candidates .....	20
1.3.1 Primary hepatocytes .....	20
1.3.2 Pluripotent stem cell-derived hepatocyte-like cells .....	22
1.3.3 HepG2 .....	24
1.3.4 HepaRG cells .....	24

1.4 AR42J-B-13 cells .....	25
1.4.1 Isolation and properties .....	25
1.4.2 Conservation of transdifferentiation of pancreas to liver.....	26
1.4.3 Molecular basis of transdifferentiation .....	27
1.5 Liver disease & fibrosis .....	30
1.5.1 Pathophysiology .....	30
1.5.2 Liver fibrosis asymmetry .....	32
1.5.3 Ductular reaction and fibrogenesis.....	34
1.5.4 Modelling liver fibrosis.....	35
1.5.5 Treatment of liver fibrosis.....	37
1.6 Study objectives .....	37
<b>Chapter 2. Materials and Methods .....</b>	<b>38</b>
2.1 Materials.....	39
2.2 Animals .....	39
2.2.1 Housing and ethics .....	39
2.2.2 Rats.....	39
2.2.3 C57BL/6 mice .....	40
2.2.4 3x-κB-luc C57BL/6 mice (NF-κB –luc mice) .....	40
2.2.5 PXR knockout mice .....	40
2.3 Cell Culture .....	40
2.3.1 AR42J-B-13 .....	40
2.3.2 B-13 <sup>TR/h1A2</sup> .....	40
2.3.3 HEK293 .....	41
2.3.4 Isolation of Primary Rat Hepatocytes .....	41
2.3.5 Primary rat hepatocyte culture .....	41
2.3.6 Cell passage.....	41
2.3.7 Long term cell storage.....	42

2.3.8 Cell stock revival.....	42
2.3.9 Determining cell number.....	42
2.3.10 Measuring cell viability by trypan blue exclusion .....	43
2.3.11 B-13 transdifferentiation .....	43
2.3.12 CYP450 induction.....	44
2.3.13 Alvetex culture .....	44
2.3.14 PU134 culture .....	44
2.4 Cell transfection, adenoviral titration and infection.....	44
2.4.1 Effectene transfection.....	44
2.4.2 Generation of stably transfected cell lines .....	45
2.4.3 Adenovirus titration – plaque assay .....	45
2.4.4 Determining multiplicity of infection (MOI).....	46
2.4.5 Adenoviral infection of cells.....	46
2.5 Plasmid DNA constructs and sequencing .....	47
2.5.1 Competent cell transformation.....	47
2.5.2 Mini-prep isolation of plasmid DNA .....	47
2.5.3 Maxi-prep isolation of plasmid DNA .....	48
2.5.4 Storage and thawing of transformed bacteria.....	49
2.5.5 DNA extraction from agarose gel .....	49
2.5.6 TOPO cloning .....	50
2.5.7 Restriction digests .....	51
2.5.8 Sequencing and analysis .....	51
2.6 Isolation of RNA and quantification .....	52
2.6.1 RNA isolation .....	52
2.6.2 RNA and DNA quantification.....	53
2.6.3 DNase I treatment of RNA.....	53
2.6.4 RNA cleanup using RNeasy columns .....	53

2.6.5 1 <sup>st</sup> strand synthesis and reverse transcription of RNA .....	54
2.6.6 Polymerase chain reaction (PCR) .....	54
2.6.7 Fusion PCR .....	56
2.6.8 Agarose gel electrophoresis .....	57
2.6.9 Quantitative real-time PCR .....	58
2.6.10 Primer design .....	59
2.6.11 PCR array plates.....	60
2.7 Protein isolation and analysis.....	61
2.7.1 Cell lysate preparation .....	61
2.7.2 Tissue lysate preparation.....	61
2.7.3 Lowry assay .....	61
2.7.4 Sodium-dodecyl sulphate polyacrylamide gel electrophoresis (SDS-PAGE).....	62
2.7.5 Western blotting.....	63
2.8 Histochemistry and immunostaining.....	64
2.8.1 Paraffin embedded section preparation.....	64
2.8.2 Haematoxylin and eosin staining (H&E) .....	65
2.8.3 Sirius red staining of collagen.....	65
2.8.4 Immunohistochemistry.....	65
2.8.5 Sodium-citrate antigen retrieval.....	68
2.8.6 Trypsin antigen retrieval .....	68
2.8.7 Fluorescence immunocytochemistry.....	68
2.8.8 Transmission electron microscopy.....	69
2.8.9 Image analysis.....	69
2.9 Enzyme activity assays .....	69
2.9.1 Rat liver microsome preparation.....	69
2.9.2 Resorufin based probe assays (EROD, MROD and PROD).....	70
2.9.3 Luciferin-IPA CYP3A1 assay.....	72

2.9.4 Dye retention assays.....	72
2.10 Measurement of DNA damage.....	74
2.10.1 The single cell gel electrophoresis assay (comet assay) .....	74
2.10.2 DNA diffusion assay .....	75
2.10.3 Assessment of cell proliferation.....	75
2.11 Spectrophotometric CYP450 assays .....	76
2.11.1 Total CYP450 dual-beam spectroscopy.....	76
2.11.2 Total cytochrome b <sub>5</sub> dual beam spectroscopy .....	76
2.12 Serum activity assays .....	77
2.13 Hydroxyproline assay.....	77
2.14 Luminescent imaging of mice.....	78
2.15 Statistics .....	78
<b>Chapter 3. Expression and induction of drug metabolising enzymes in B-13/H cells.....</b>	<b>79</b>
3.1 Introduction .....	80
3.2 B-13 cells undergo transdifferentiation in response to DEX treatment .....	80
3.3 B-13/H cells express male CYP450 isoforms.....	84
3.4 B-13/H cells are not receptive to GH.....	87
3.5 The AhR activator $\beta$ -naphthoflavone ( $\beta$ -NF) induces CYP1A1 expression in B-13 and B-13/H cells and sensitises cells to the genotoxic effects of benzo[ $\alpha$ ]pyrene. ....	90
3.6 CAR activators induce CYP2B1 mRNA in B-13/H cells.....	97
3.7 PXR activators induce a quantitatively liver equivalent induction of CYP3A1 in B-13/H cells .....	100
3.8 B-13/H cells express the PPAR $\alpha$ and agonists induce peroxisome proliferation .....	109
3.9 Chapter discussion .....	113
<b>Chapter 4. Generation of a humanised B-13 line and its suitability for genotoxicity screening of novel drugs and chemicals.....</b>	<b>116</b>
4.1 Introduction.....	117

4.2 The CYP1A2 gene is mutated in B-13 cells .....	117
4.3 CYP1A1 but not CYP1A2 can be induced by $\beta$ -NF.....	119
4.4 Isolation and amplification of the hCYP1A2 coding sequence .....	122
4.5 B-13 <sup>-TR/h1A2</sup> cells express hCYP1A2 independent of tetracycline .....	127
4.6 Cloned hCYP1A2 in B-13 <sup>-TR/h1A2</sup> /H cells is functional and inhibited by furafylline...129	
4.7 hCYP1A2 expression significantly increases the susceptibility of B-13 <sup>-TR/h1A2</sup> /H cells to PhIP induced genotoxicity.....	130
4.8 PhIP induced DNA damage is inhibited by furafylline in B-13 <sup>-TR/h1A2</sup> /H cells .....	133
4.9 PhIP bioactivation is dependent on SULT activity .....	134
4.10 B-13/H cells express functional SULTs and are susceptible to 1-hydroxyestragole induced DNA damage .....	135
4.11 1-hydroxyestragole induced damage is sulphation dependent.....	140
4.12 Chapter discussion .....	141
<b>Chapter 5. Expression and function of transporters in B-13/H cells.....</b>	<b>144</b>
5.1 Introduction .....	145
5.2 Transdifferentiation of B-13 cells is associated with up-regulation of drug transporter mRNA expression.....	146
5.3 3D culture does not markedly change B-13/H expression of drug transporters .....	147
5.4 Culture on PU134 does not up-regulate B-13/H expression of drug transporters .....	151
5.5 Introduction of liver enriched transcription factor HNF4 $\alpha$ increases expression of drug transporters.....	154
5.6 Co-expression of HNF4 $\alpha$ with SGK1F or FOXA2 does not improve drug transporter expression .....	158
5.7 Ad-HNF4 $\alpha$ infected B-13/H cells show significantly increased MDR and BCRP activity.....	162
5.8 Chapter discussion .....	165
<b>Chapter 6. Chronic administration of MP causes reversible and modulatable periportal fibrosis comparable to BDL.....</b>	<b>168</b>
6.1 Introduction .....	169

6.2 Chronic administration of MP significantly inhibits weight gain.....	171
6.3 Administration of MP causes significant and reversible portal tract inflammation.....	172
6.4 MP treatment causes activation of hepatic regeneration pathways.....	175
6.5 MP administration causes expansion of hepatic pro-fibrogenic cell populations.....	176
6.6 MP administration causes significant and reversible periportal fibrosis .....	180
6.7 MP treatment causes a ductular reaction.....	182
6.8 MP treatment significantly up-regulates expression of fibrosis-associated markers ...	184
6.9 Chapter discussion .....	185
<b>Chapter 7. The PXR is anti-fibrogenic in an <math>\alpha</math>-naphthylisothiocyanate-induced model of periportal fibrosis in the mouse .....</b>	<b>188</b>
7.1 Introduction .....	189
7.2 ANIT treatment causes hepatic injury.....	190
7.3 Acute ANIT administration induces hepatic NF- $\kappa$ B signalling <i>in-vivo</i> .....	192
7.4 ANIT treatment causes portal tract inflammation in WT and PXR KO mice .....	199
7.5 Hepatic pro-fibrogenic cell populations expand in response to ANIT treatment .....	202
7.6 The PXR protects against ANIT-induced periportal fibrosis.....	202
7.7 ANIT administration causes a ductular reaction and induces NTCP expression.....	206
7.8 Chapter discussion .....	208
<b>Chapter 8. General discussion.....</b>	<b>214</b>
<b>References.....</b>	<b>219</b>
<b>Appendix A. List of primers used for PCR .....</b>	<b>247</b>
<b>Appendix B. Published papers .....</b>	<b>252</b>

## List of Figures

Figure 1.1: The two principal models of liver structure.....	3
Figure 1.2: The human biliary tree.....	5
Figure 1.3: Liver and hepatocyte zonation.....	7
Figure 1.4: The cytochrome P450 catalytic cycle.....	9
Figure 1.5: Mechanisms of A. AhR, B. direct CAR, C. indirect CAR, D. PXR and E. PPAR $\alpha$ mediated CYP450 induction .....	17
Figure 1.6: Factors contributing to dedifferentiation of hepatocytes.....	21
Figure 1.7: Hypothesised signalling pathway linking DEX (and other glucocorticoids) to C/EBP $\beta$ activation and transdifferentiation .....	29
Figure 1.8: Changes in liver structure resulting from fibrosis .....	32
Figure 1.9: Zonal nature of liver fibrosis .....	34
Figure 1.10: Pattern of hepatic fibrosis induced by CCl <sub>4</sub> and BDL.....	36
Figure 2.1: B-13 blasticidin kill curve. ....	45
Figure 2.2: TOPO cloning system.....	50
Figure 2.3: The events of a PCR cycle.....	55
Figure 2.4: The steps of fusion PCR.....	57
Figure 2.5: Metabolism of 7-ethoxyresorufin, 7-methoxyresorufin and 7-pentoxyresorufin. ....	71
Figure 2.6: Metabolism of luciferin-IPA by CYP3A1 and luciferase .....	72
Figure 2.7: Principal of fluorescence transporter efflux assays. ....	73
Figure 3.1: B-13 cells change morphology and cease proliferation in response to DEX. ....	81
Figure 3.2: B-13/H cells express hepatic markers. ....	82
Figure 3.3: B-13/H cells contain haem-bound CYP450 and cytochrome b <sub>5</sub> .....	83
Figure 3.4: B-13/H cells partially recapitulate a male pattern of CYP450 expression ...	86
Figure 3.5: B-13/H cells are sensitive to methapyrilene.....	87
Figure 3.6: B-13/H cells express signalling machinery required for JAK/STAT signalling. ....	88
Figure 3.7: B-13/H cells are not responsive to hGH.....	89

Figure 3.8: hGH does not affect the rate of sex-dependent CYP450 up-regulation during transdifferentiation .....	90
Figure 3.9: B-13 and B-13/H cells express inducible CYP1A1.....	92
Figure 3.10: B-13/H cells express inducible CYP1A1 protein which is functional and inducible.....	94
Figure 3.11: Benzo[a]pyrene dose response in vehicle or $\beta$ -NF induced B-13 and B-13/H cells measured by comet assay.....	95
Figure 3.12: DNA damaging compounds did not induce significant cell death or division in treated cells.....	96
Figure 3.13: B-13/H cells express inducible CYP2B1 .....	98
Figure 3.14: B-13/H cells express no detectable CYP2B1 protein.....	99
Figure 3.15: Cyclophosphamide dose response in vehicle or PB induced B-13 and B-13/H cells measured by comet assay.....	100
Figure 3.16: B-13/H cells express inducible CYP3A1 .....	102
Figure 3.17: Western blot for CYP3A1 in induced B-13 and B-13/H cells and primary rat hepatocytes.....	102
Figure 3.18: Induced CYP3A1 in B-13/H cells is functional .....	104
Figure 3.19: Aflatoxin B1 dose response in vehicle, DEX or PCN induced B-13 and B-13/H cells measured by comet assay.....	105
Figure 3.20: DEX induced B-13/H cells are significantly more sensitive to inhibitable AFB1 induced DNA damage .....	107
Figure 3.21: DEX pretreatment of B-13/H cells causes nuclear accumulation of $\gamma$ -H2AX in response to AFB1 .....	108
Figure 3.22: The coding region of <i>rCyp4a2</i> is mutated in B-13 cells. ....	109
Figure 3.23: B-13/H cells express PPAR $\alpha$ but only weakly induce CYP4A1.....	110
Figure 3.24: B-13/H cells are sensitive to peroxisome proliferators .....	112
Figure 4.1: The coding region of <i>rCyp1a2</i> in B-13 cells is mutated.....	118
Figure 4.2: Neither <i>rCyp1a2</i> nor rCYP1A2 mRNA can be detected in B-13 cells .....	120
Figure 4.3: Western blot for CYP1A1 and CYP1A2.....	121
Figure 4.4: EROD but not MROD activity is inducible in B-13 and B-13/H cells .....	122
Figure 4.5: Planned final vector for transformation.....	123
Figure 4.6: Construction of the hCYP1A2 coding sequence .....	124

Figure 4.7: Restriction digest of miniprep isolated plasmid DNA from transformants. .....	125
Figure 4.8: Clone 2.4 was cloned with the complete coding sequence of hCYP1A2*1. .....	126
Figure 4.9: The hCYP1A2 insert was successfully transferred from the gateway vector to the destination vector .....	127
Figure 4.10: B-13 <sup>-TR/h1A2</sup> cells express hCYP1A2 independent of tetracycline.....	128
Figure 4.11: B-13 <sup>-TR/h1A2</sup> cells can transdifferentiate. ....	129
Figure 4.12: Transdifferentiated B-13 <sup>-TR/h1A2</sup> /H cells express functional hCYP1A2. ..	130
Figure 4.13: Metabolism of PhIP .....	131
Figure 4.14: B-13 <sup>-TR/h1A2</sup> /H cells are susceptible to PhIP induced DNA damage. ....	132
Figure 4.15: PhIP does not induce significant cell death or division.....	133
Figure 4.16: PhIP genotoxicity is inhibited by furafylline in B-13 <sup>-TR/h1A2</sup> /H cells.....	134
Figure 4.17: PhIP genotoxicity is SULT dependent. ....	135
Figure 4.18: B-13 and B-13/H cells express a number of SULTs and PAPSS.....	137
Figure 4.19: B-13/H and B-13 <sup>-TR/h1A2</sup> /H cells are sensitive to 1-hydroxyestragole .....	138
Figure 4.20: B-13 <sup>-TR/h1A2</sup> /H cells are more sensitive to 1-hydroxyestragole than B-13/H cells. ....	139
Figure 4.21: 1-hydroxyestragole induced DNA damage is SULT dependent .....	140
Figure 5.1: B-13/H cells express several drug transporters at liver levels.....	147
Figure 5.2: B-13 cells adhere to and transdifferentiate on alvetex .....	149
Figure 5.3: Alvetex does not enhance B-13/H expression of drug transporters .....	150
Figure 5.4: Culture on PU134 does not affect B-13 transdifferentiation.....	152
Figure 5.5: Culture on PU134 does not cause up-regulation of transporter expression. .....	153
Figure 5.6: Calculation of B-13/H MOI.....	155
Figure 5.7: Adenoviral infection with HNF4 $\alpha$ causes a phenotype change and induction of BSEP and MRP2 expression .....	156
Figure 5.8: Adenoviral overexpression of HNF4 $\alpha$ induces expression of transporters including MRP2 and BSEP .....	157
Figure 5.9: Adenoviral overexpression of SGK1F or FOXA2 does not enhance transporter expression in B-13/H cells.....	159
Figure 5.10: RT-PCR for hSGK1F, hFOXA2 and HNF4 $\alpha$ in indicated cell samples ..	160

Figure 5.11: Adenoviral overexpression of SGK1F or FOXA2 does not increase drug transporter expression .....	161
Figure 5.12: Western blot for MRP2 and NTCP in B-13 cells, adenoviral infected B-13/H cells and rat liver .....	162
Figure 5.13: HNF4 $\alpha$ overexpression significantly increases MDR and BCRP, but not MRP or BSEP activity .....	164
Figure 6.1: Main MP metabolites produced <i>in-vitro</i> by male primary rat hepatocytes	170
Figure 6.2: MP treatment inhibits weight gain and increases relative liver size.....	172
Figure 6.3: MP treatment and 14 day BDL cause periportal inflammation.....	174
Figure 6.4: MP causes liver specific injury.....	175
Figure 6.5: 6 weeks chronic MP treatment and 14 day BDL cause hepatocyte and cholangiocyte proliferation .....	177
Figure 6.6. Chronic MP treatment and 14 day BDL cause a significant increase in periportal vimentin staining .....	178
Figure 6.7. Chronic MP treatment and 14 day BDL cause a significant increase in periportal $\alpha$ -SMA staining .....	179
Figure 6.8. Chronic MP treatment and 14 day BDL cause significant periportal fibrosis .....	181
Figure 6.9: Chronic MP treatment and BDL cause significant hepatic fibrosis .....	182
Figure 6.10: Chronic MP treatment and 14 day BDL cause activation of a ductular reaction.....	183
Figure 7.1: ANIT treatment does not give rise to weight loss but does increase serum ALP activity. ....	191
Figure 7.2: ANIT treatment causes portal tract inflammation and fibrosis .....	192
Figure 7.3: Acute dosing of 50mg/kg but not 30mg/kg ANIT causes long term hepatic inflammation .....	194
Figure 7.4: Acute dosing of 50mg/kg ANIT causes long term hepatic inflammation..	196
Figure 7.5: Acute treatment of 50mg/kg ANIT causes long term significant hepatic inflammation. ....	197
Figure 7.6: Abdominal luminescence was proportional to hepatic inflammation following acute 50mg/kg ANIT treatment.....	198

Figure 7.7: Chronic ANIT treatment significantly increases serum ALP and ALT activity.....200

Figure 7.8: Chronic ANIT treatment causes significant portal tract inflammation. ....201

Figure 7.9: Chronic ANIT treatment causes a significant increase in periportal vimentin staining .....203

Figure 7.10: Chronic ANIT treatment causes a significant increase in periportal myofibroblast recruitment/activation. ....204

Figure 7.11: Chronic ANIT treatment causes periportal fibrosis significantly more severe in PXR KO mice .....205

Figure 7.12: Chronic ANIT treatment causes activation of a ductular reaction. ....207

Figure 7.13: Chronic ANIT treatment significantly increases NTCP expression.....208

## List of Tables

Table 1.1: Cell types found in the liver.....	2
Table 1.2: Major phase I and all phase II pathways of xenobiotic metabolism.....	8
Table 1.3: CYP450 inducing receptors.....	11
Table 1.4: Important hepatocyte transporters and their properties. ....	18
Table 1.5: Common causes of chronic liver disease and their incidence.....	30
Table 2.1: Details of antibodies used .....	67
Table 2.2: Substrates and inhibitors used to measure indicated transporter activity .....	73
Table 5.1: Average fold change in expression of all measured transcripts in B-13/H cells and rat liver relative to B-13 cells. ....	147
Table 5.2: Average fold change in expression of all measured transcripts in rat liver and B-13 and B-13/H cells cultured on plastic or PU134 relative to B-13/H cells cultured on plastic. ....	154
Table 5.3: Average fold change in expression of all measured transcripts in rat liver or B-13/H cells following adenoviral infection relative to Ad-null infected B-13/H cells. ....	158
Table 5.4: Average fold change in expression of all measured transcripts in B-13/H cells infected with different adenovirus constructs alone or in combination relative to Ad-null infected cells.....	161
Table 6.1: MP dosing regime .....	171
Table 6.2: Whole liver changes in gene expression after MP treatment or 14 day BDL as measured by qPCR.....	185
Table 7.1: Pilot animal dosing groups .....	190
Table 7.2: Pilot NF- $\kappa$ B-luc mouse study groups.....	193
Table 7.3: Animal dosing groups for ANIT and PCN study.....	199

## List of Abbreviations

- 18S rRNA**- 18S ribosomal RNA
- $\alpha$ -NF**-  $\alpha$ -naphthoflavone
- $\alpha$ -SMA**-  $\alpha$ -smooth muscle actin
- ABC**- ATP binding cassette
- AFB1**- Aflatoxin B1
- AhR**- Aryl hydrocarbon receptor
- AIP**- Hepatitis B virus x-associated protein 2
- ALP**- Alkaline phosphatase
- ALT**- Alanine transaminase
- ANIT**-  $\alpha$ -naphthylisothiocyanate
- ARNT**- Aryl hydrocarbon receptor nuclear translocator
- $\beta$ -NF**-  $\beta$ -naphthoflavone
- B-13**- AR42J-B-13 cell
- B-13/H**- B-13 derived hepatocyte-like cell
- BCRP**- Breast cancer resistance protein
- BrdU**- Bromodeoxyuridine
- BSA**- Bovine serum albumin
- BSEP**- Bile salt export pump
- CAR**- Constitutive androstane receptor
- CCl<sub>4</sub>**- Carbon tetrachloride
- CCRP**- Cytoplasmic constitutive androstane receptor retention protein
- cDNA**- Complementary DNA
- C/EBP**- CCAAT/enhancer-binding protein
- CMFDA**- 5-Chloromethylfluorescein diacetate
- CPS-1**- Carbamoyl-phosphate synthetase 1
- CsA**- Cyclosporin A
- CYP450**- Cytochrome P450
- DAB**- 3,3'-Diaminobenzidine
- DAPI**- 4',6-Diamidino-2-phenylindole
- DEX**- Dexamethasone

**DILI**- Drug induced liver injury  
**DME**- Drug metabolising enzyme  
**DMEM**- Dulbecco's modified eagle medium  
**DMN**- Dimethylnitrosamine  
**DMSO**- Dimethyl sulfoxide  
**DNA**- Deoxyribonucleic acid  
**dsDNA**- Double stranded DNA  
**DTT**- Dithiothreitol  
**ECM**- Extracellular matrix  
**EDTA**- Ethylenediaminetetraacetic acid  
**EROD**- 7-ethoxyresorufin O-deethylation  
**ESCs**- Embryonic Stem Cells  
**FCS**- Foetal calf serum  
**FITC**- Fluorescein isothiocyanate  
**FOXA2** – Forkhead box protein A2  
**FXR**- Farnesoid X receptor  
**GAPDH**- Glyceraldehyde 3-phosphate dehydrogenase  
**GFP**- Green fluorescent protein  
**GH**- Growth hormone  
**Ghr**- Growth hormone receptor  
**GSK3**- Glycogen synthase kinase 3  
**GST**- Glutathione transferases  
**H&E**- Haematoxylin and eosin  
**H<sub>2</sub>FDA**- Dihydrofluorescein diacetate  
**H33342**- Hoechst 33342  
**HEK293**- Human embryonic kidney 293 cell  
**HEPs**- Hepatocytes  
**hGH**- human growth hormone  
**HNF**- Hepatocyte nuclear factor  
**HRP**- Horse-radish peroxidase  
**HSP90**- 90kDa heat shock protein  
**ICC**- Immunocytochemistry  
**IHC**- Immunohistochemistry  
**i.p.**- Intraperitoneal

**iPSC**- Induced pluripotent stem cell  
**IVIS**- *In-vivo* imaging system  
**KO**- Knockout  
**LAP**- C/EBP $\beta$ -liver enriched activator protein  
**LB**- Luria-Bertani medium  
**LETf**- Liver enriched transcription factor  
**LIP**- C/EBP $\beta$ -liver enriched inhibitory protein  
**MDR**- Multiple drug resistance protien  
**M-MLV**- Moloney murine leukemia virus  
**MMP-2**- Matrix metalloproteinase-2  
**MOI**- Multiplicity of infection  
**MP**- Methapyrilene  
**mRNA**- Messenger RNA  
**MROD**- 7-methoxyresorufin O-deethylation  
**MRP**- Multidrug resistance-associated protein  
**NADH**- Nicotinamide adenine dinucleotide  
**NADPH**- Nicotinamide adenine dinucleotide phosphate  
**NAPQI**- N-acetyl-p-benzoquinoneimine  
**NAT**- N-acetyl transferases  
**NF- $\kappa$ B-luc**- 3x- $\kappa$ B-luc C57BL/6 mice  
**NTCP**- Na<sup>+</sup>-taurocholate cotransporting polypeptide  
**OAT**- Organic anion transporter  
**OATP**- Organic anion-transporting polypeptide  
**OCT**- Organic cation transporter  
**OD**- Optical density  
**PAPS**- 3'-phosphoadenosine-5'-phosphosulphate  
**PAPSS**- 3'-phosphoadenosine-5'-phosphosulphate synthase  
**PB**- Phenobarbital  
**PBS**- Phosphate buffered saline  
**PCN**- Pregnenolone-16 $\alpha$ -carbonitrile  
**PCNA**- Proliferating cell nuclear antigen  
**PCP**- Pentachlorophenol  
**PCR**- Polymerase chain reaction  
**PDK1**- 3-phosphoinositide dependent protein kinase-1

**Pfu**- Plaque forming units  
**PhIP**- 2-Amino-1-methyl-6-phenylimidazo(4,5-b)pyridine  
**PI3K**- Phosphatidylinositol-4,5-bisphosphate 3-kinase  
**PKB/AKT**- Protein kinase B  
**PMP70**- 70kDa Peroxisomal membrane protein  
**PNP**- 4-nitrophenol  
**PP2A**- Protein phosphatase 2A  
**PPAR $\alpha$** - Peroxisome proliferator-activated receptor  $\alpha$   
**PROD**- 7-pentoxoresorufin O-dealkylation  
**PU134**- Polyurethane 134  
**PXR**- Pregnane X receptor  
**qPCR**- Quantitative-PCR  
**RACK1**- Receptor for activated C kinase 1  
**rmh**- Rat/mouse/human  
**RNA**- Ribonucleic acid  
**ROS**- Reactive oxygen species  
**RT-PCR**- Reverse transcription polymerase chain reaction  
**RXR**- Retinoid X receptor  
**SD**- Standard deviation  
**SDS**- Sodium dodecyl sulphate  
**SDS-PAGE**- Sodium dodecyl sulphate- polyacrylamide gel electrophoresis  
**SE**- Standard error  
**SGK**- Serum/glucocorticoid regulated kinase  
**SULT**- Sulphotransferase  
**TAA**- Thioacetamide  
**TCF/LEF**- T cell factor/lymphoid enhancer factor  
**TCPOBOP**- 1,4-Bis[2-(3,5-dichloropyridyloxy)]benzene  
**TEMED**- Tetramethylethylenediamine  
**TetR**- Tetracycline repressor  
**TGF $\beta$** - Transforming growth factor beta  
**TIMP1**- Tissue inhibitor of metalloproteinases  
**UGT**- UDP glucuronosyl-transferases  
**WT**- Wildtype

## **Chapter 1. Introduction**

## 1.1 The Liver

### 1.1.1 Anatomy

The liver is the largest internal organ in humans; it is located under the ribcage and below the diaphragm in the upper right region of the abdominal cavity. It is surrounded by the Glisson's capsule, a collagenous tissue capsule similar to that which surrounds the kidneys and other organs. The liver is split into lobes of differing sizes; humans, mice and rats each have 4 liver lobes [1], although the number is variable in other animals. Blood is supplied to the liver from two sources. The portal vein carries in deoxygenated blood, rich in the products of digestion, direct from the gut, pancreas and spleen. The remaining blood is supplied from the hepatic artery which is fully oxygenated.

### 1.1.2 Cellular composition, distribution and function

Within the liver are at least 15 different cell types, as outlined in table 1.1. The bulk of the liver is composed of hepatocytes (80% of the liver by volume) which are responsible for the majority of liver functions [2]. However, although hepatocytes make up the bulk of the liver, the numerous other cell types are required for the liver to function correctly.

<b>Hepatocytes</b>	<b>Progenitor cells</b> Oval cell (rodents) Hepatoblasts (humans)
<b>Biliary epithelia</b>	<b>Fibroblasts</b>
<b>Endothelia</b> Sinusoids Blood vessels (arteries and veins) Lymphatics	<b>Smooth muscle cells (blood vessels)</b>
<b>Sinusoids</b>	<b>Mesothelia</b>
<b>Blood vessels (arteries and veins)</b>	<b>Nerves (unmyelinated)</b>
<b>Lymphatics</b>	<b>Neuroendocrine cells</b>
<b>Kupffer cells</b>	<b>Hematopoietic cells</b>
<b>Hepatic stellate cells (Ito cells)</b>	<b>Blood (erythrocytes, leukocytes, etc.)</b>
<b>Lymphocytes</b>	

Table 1.1: Cell types found in the liver

The liver acts as the regulator of intermediary metabolism as well as the primary organ involved in metabolism of ingested xenobiotics. Its functions specifically include carbohydrate and protein metabolism, control of lipid uptake and metabolism, production of numerous serum proteins (such as albumin and clotting factors) and xenobiotic metabolism.

At a structural level, the liver is composed of lobules (figure 1.1) – polygonal units that contain all hepatic cell types centred around points of blood entry and exit and bile exit. At a functional level, the liver is composed of acini which similar to lobules, are focused around the point of blood entry and exit. However acini take into account the heterogeneous conditions experienced by cells depending on their position along the porto-central axis as outlined in figure 1.3.

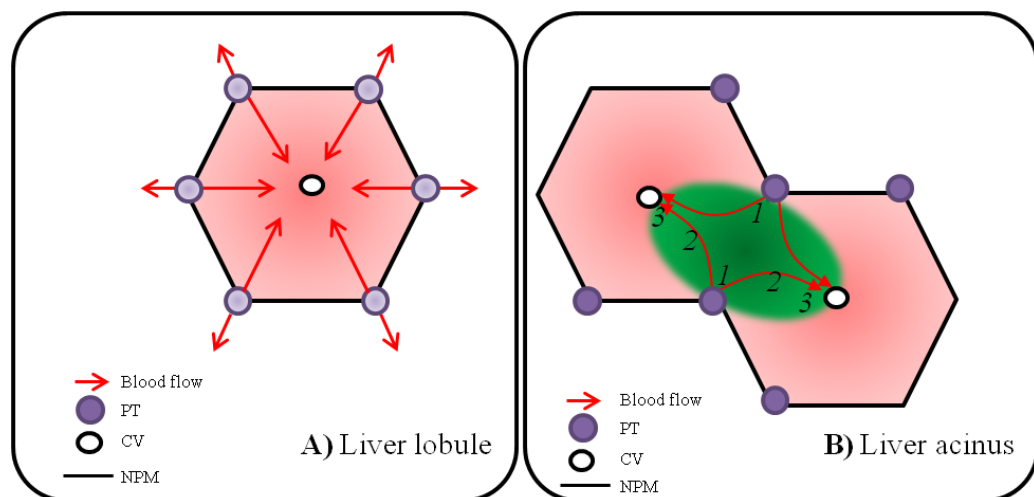


**Figure 1.1: The two principal models of liver structure.** In the Kiernan lobule, **A**, blood flows toward the central vein within a lobule but also between lobules with oxygen and nutrient concentrations falling as blood flows away from the portal tract. In the Rappaport acinus, **B**, blood similarly flows from the portal tract to the central vein through zones 1-3. Blood however is restricted to a single acinus and is considered not to flow into adjacent acini. Abbreviations: PT, portal tract; CV, central vein; NPM, nodal point of Mall.

Within the lobule or acinus, hepatocytes are organised into cell sheets flanked by sinusoids on either side. The hepatocytes are polarised so that on the sinusoidal surface (basolateral) they have numerous microvilli whereas on the lateral surface, they are bound by tight junctions to form canals (canaliculi) into which they secrete bile that drains into bile ducts located in portal tracts [2].

Between the hepatocytes and the sinusoid, fenestrated endothelial cells enclose an extravascular region called the space of Dissé. In this space are found hepatic stellate cells, which, in the absence of inflammation, are quiescent retinoid and vitamin A storing cells. The close proximity of hepatocytes to portal vein blood and the fenestrated nature of sinusoidal endothelial cells allows hepatocytes to carry out their aforementioned roles [2]. Since the liver is highly perfused with blood vessels and is the first organ exposed to absorbed compounds from the gut, it expresses proteins required for xenobiotic metabolism and clearance. The liver therefore acts as the primary site of ingested xenobiotic metabolism and can effectively metabolise xenobiotics absorbed from the gut before they reach distal organs through systemic circulation (referred to as first pass metabolism). The consequence of this is that because many xenobiotics are toxic, hepatocytes are particularly susceptible to necrosis and apoptosis in response to ingestion of toxic xenobiotics.

### ***1.1.3 The biliary system***

The biliary tree consists of specialised vessels which run the length of the liver and transport bile secreted by hepatocytes within the liver out through ever enlarging vessels to the gut as outlined in figure 1.2. In humans and mice, the gall bladder acts to store bile when it is not needed, but not in rats which lack a gall bladder. Cholangiocytes (bile duct epithelial cells) line all parts of the biliary tree. Bile facilitates the intestinal digestion and absorption of lipids and lipophilic vitamins. Bile acids, which are the primary constituents of bile, are synthesised by hepatocytes from cholesterol and pumped into the canaliculi which drain into bile ducts in portal tracts. Aside from its role in digestion, the bile is used as an important route of excretion of a range of xenobiotic metabolic products from hepatocytes that are too hydrophobic to be excreted via the kidneys.

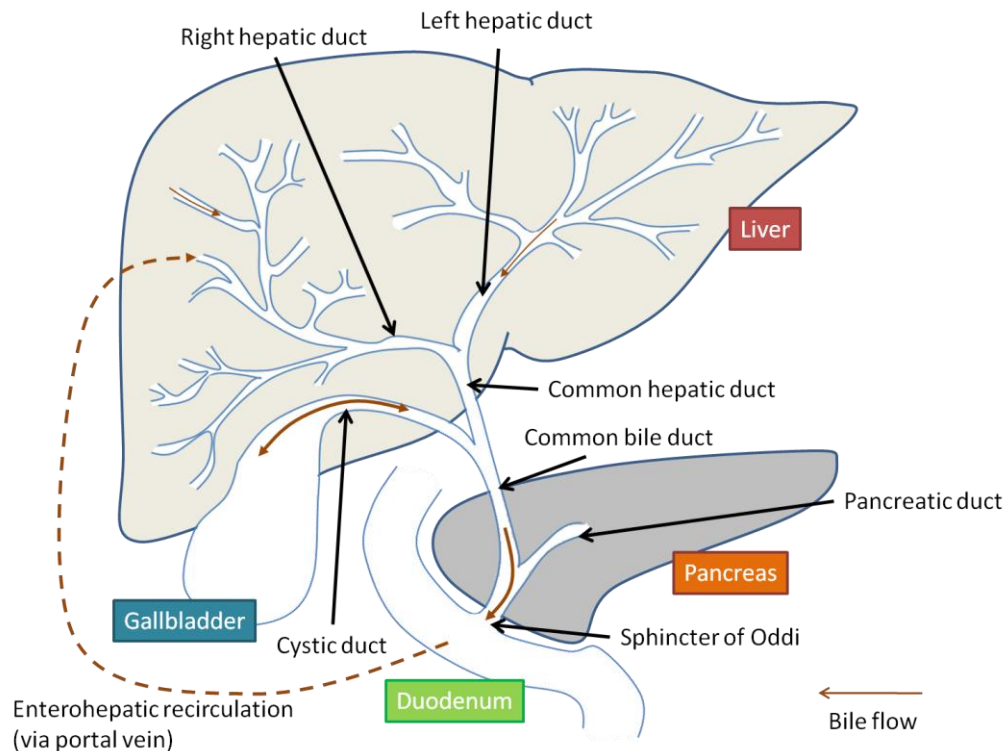


**Figure 1.2: The human biliary tree.** Bile produced by hepatocytes is transported through the biliary tree which emerges from the liver as the common bile duct. From here bile either is stored in the gall bladder or released into the duodenum through the sphincter of Oddi. Most intestinal bile acids are recirculated back to the liver by enterohepatic recirculation via the portal vein. From Probert., (2011) [3].

#### 1.1.4 Cells of the liver

**Hepatocytes** - Hepatocytes make up the bulk of the liver and are responsible for most of its unique functions. They are appropriately specialised and, at the ultrastructure level, are packed with rough and smooth endoplasmic reticulum, mitochondria and glycogen granules. The tight junctions between adjacent hepatocytes on the lateral membrane act to form a barrier to blood and bile between the basal and apical membranes. Hepatocyte transporters also show polarised expression with specific transporters expressed on the basal and apical surfaces. The tight junctions and polarised expression of transporters allows for the partitioning of different substrates between the blood and the bile, aiding in the control of whole body homeostasis by hepatocytes.

**Cholangiocytes** – Cholangiocytes, cuboidal epithelial cells that line the biliary tree, are responsible for regulating bile homeostasis. As a population they are heterogeneous – they show a different phenotype depending on their location within the biliary tree. In terms of morphology their size is directly correlated to the size of the vessels that they

line. Small cholangiocytes (i.e. those surrounding small bile ducts) do not significantly modify the contents of the bile. Large cholangiocytes, lining larger bile ducts, conversely secrete hormones and electrolytes and alkalinize the bile [4].

**Hepatic stellate cells** - Hepatic stellate cells under normal hepatic conditions are quiescent vitamin A storing cells that lie between sinusoidal endothelial cells and hepatocytes. Pro-inflammatory signalling from liver injury leads to the activation of hepatic stellate cells; they lose vitamin A and transdifferentiate to proliferative and pro-fibrogenic contractile myofibroblasts [5]. As part of this phenotypic change they up-regulate  $\alpha$ -smooth muscle actin ( $\alpha$ -SMA) expression.

**Portal tract fibroblasts** - Fibroblasts within the portal tracts normally act to maintain extracellular matrix (ECM) within the portal tract. The portal tract fibroblast population is heterogeneous, however they can generally be considered to be composed of cells that do not express  $\alpha$ -SMA (portal tract fibroblasts) and those that do (portal tract myofibroblasts) [6]. In response to biliary and periportal hepatic injury, differentiation of portal tract fibroblasts to a myofibroblast collagen secreting phenotype ( $\alpha$ -SMA positive) may occur [7, 8]. However, evidence suggests that significant populations of portal tract fibroblasts can remain undifferentiated whilst still contributing to the fibrogenic deposition of fibrotic collagens [9, 10].

**Kupffer cells** - Kupffer cells are the liver-resident macrophage population. They adhere to the sinusoidal side of endothelial cells and are found primarily in the periportal region of the liver [11]. The primary role of Kupffer cells, under normal conditions, is to maintain blood homeostasis through the phagocytosis of large particles (>10nm) such as cell debris, damaged erythrocytes and microorganisms. In response to hepatic insult, they become activated and release a wide range of inflammatory mediators including cytokines through which they act to regulate liver-specific responses to inflammation and recruitment of extra-hepatic inflammatory cells [12].

### ***1.1.5 Liver zonation***

Hepatocytes are morphologically the same but demonstrate different specialisations according to their position along the porto:central axis. Several functions of hepatocytes

appear uniform across all hepatocytes such as production of serum. However, as indicated in figure 1.3, numerous hepatic functions such as glucose, ammonia and drug metabolism show zonal localisation and this is a consequence of the proteins required for these processes being differentially expressed in the specific regions of the lobule. Zonation is a complex phenomenon with important ramifications on how the liver functions.

Current evidence indicates that zonation is a consequence of Wnt signalling; Wnt up-regulated genes are high in centrilobular regions and low in periportal regions (figure 1.3) [13]. Liver-wide activation of Wnt signalling leads to a reprogramming of all liver hepatocytes to a centrilobular phenotype. Conversely, liver-wide inhibition of Wnt signalling leads to a phenotypic change of all hepatocytes to a periportal phenotype [13, 14].

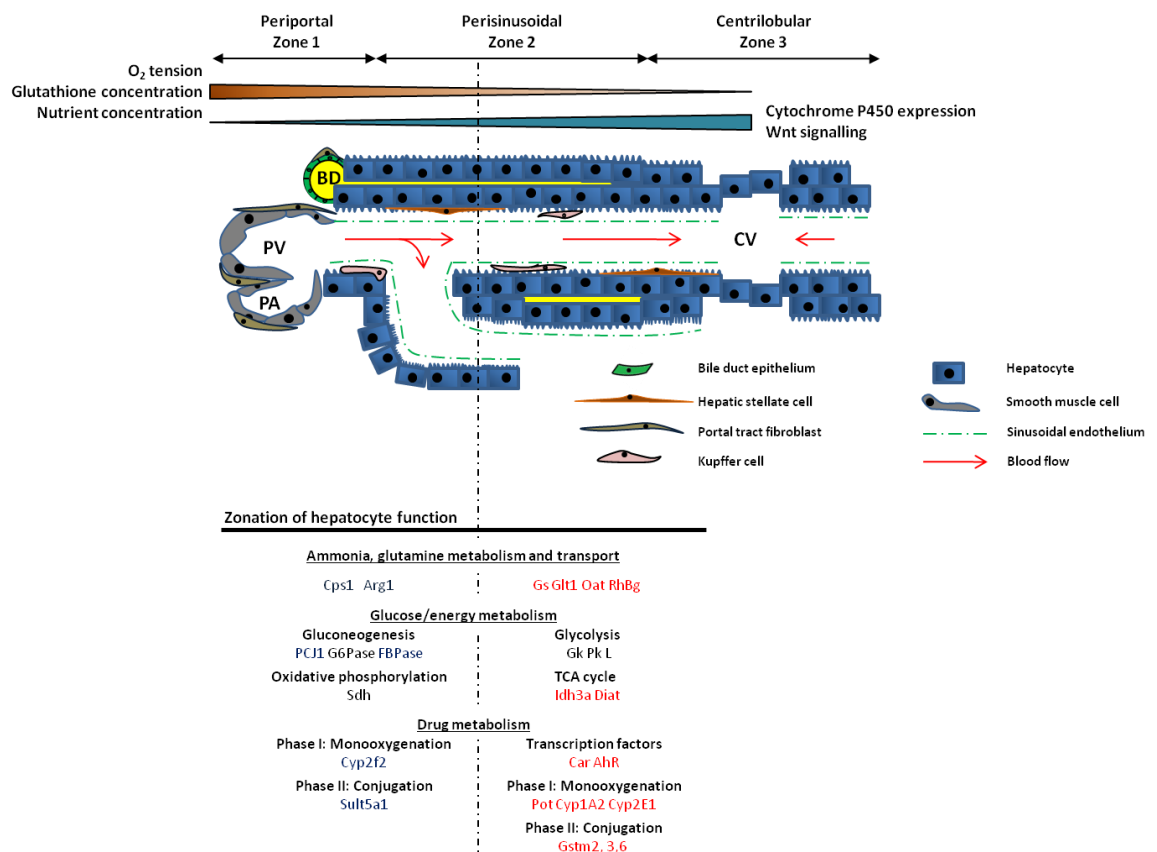


**Figure 1.3: Liver and hepatocyte zonation.** As blood flows from the portal tract in zone 1 to the central vein in zone 3, the oxygen and glutathione concentration decreases and cytochrome P450 expression and Wnt signalling increases. Several hepatocyte functions are zoned in a process that appears to be controlled by a Wnt signalling concentration gradient which is high in centrilobular regions and low in periportal regions. The proteins involved in the indicated processes are shown. Genes down-regulated by Wnt signalling are blue and genes up-regulated by Wnt signalling are red. Adapted from Colnot *et al.*, (2011) [15] and Wallace *et al.*, (2008) [16].

## 1.2 Xenobiotic metabolism

### 1.2.1 The phases of metabolism

The xenobiotic metabolising properties of the liver are due to the expression of drug metabolising enzymes (DMEs) in hepatocytes. These DMEs primarily act to modify lipophilic xenobiotics, absorbed from the gut, to create more water soluble metabolites that can be excreted via the bile or urine. The process of xenobiotic metabolism has historically been split into 3 distinct phases: phase I, phase II and phase III which correspond to xenobiotic modification, conjugation and cellular efflux respectively. Table 1.2 outlines the primary DMEs of phase I and II in humans. Phase I metabolism can involve hydrolysis, reduction and oxidation reactions, which permit the subsequent conjugation of hydrophilic groups by phase II conjugation enzymes. In humans, the majority of phase I reactions consist of mono-oxygenation reactions catalysed by cytochrome P450s (CYP450) and flavin-containing monooxygenases.

Phase (I or II)	Reaction type	Enzyme family involved	Number of human isoforms
<b>Phase I (modification)</b>	Mono-oxygenation	Cytochrome P450s (CYP450s)	57 isoforms classified into 37 families
	Mono-oxygenation	Flavin-containing monooxygenases (FMOs)	5 isoforms
<b>Phase II (conjugation)</b>	Glucuronidation	UDP glucuronosyl transferases (UGT)	22 isoforms classified into 8 families
	Sulphation	Sulphotransferases (SULT)	13 total, 6 expressed in the liver
	Glutathione conjugation	Glutathione transferases (GST)	17 isoforms divided into 8 different classes
	Acetylation	N-acetyl transferases (NAT)	2 distinct isoforms with several genetic polymorphisms
	Methylation	Methyl transferases	10 distinct enzymes classified according to substrate
	Amino acid conjugation	ATP dependent acid:CoA ligases and Acyl:CoA amino acid N-acyltransferases	2 known enzymes but more enzymes have been postulated

**Table 1.2: Major phase I and all phase II pathways of xenobiotic metabolism.** Adapted from Apte *et al.*, (2011) [17].

Although most chemicals undergo modification followed by conjugation, some chemicals undergo conjugation directly followed by modification, or are directly conjugated and excreted. Gemfibrozil for example is conjugated (to glucuronic acid), prior to CYP2C8 mediated hydroxylation [18] and paracetamol, under normal conditions, is directly sulphated or glucuronidated prior to cellular elimination [19].

### 1.2.2 Cytochrome P450s

The CYP450 family is the largest family of DMEs and in humans consists of 57 separate genes which in the liver are grouped into 4 main subfamilies (CYP1A, 2B, 3A and 4A). They are responsible for the majority of drug metabolising activity (~75% [20]) and although there are numerous human CYP450s, 2 isoforms, CYP2D6 and CYP3A4 metabolise over 50% of clinically administered drugs [21, 22]. CYP450s catalyse the mono-oxygenation of their substrates following the catalytic cycle shown in figure 1.4 in which they first bind their substrate followed by two stepwise electron reductions. Their ubiquity in drug metabolism is explained by their broad substrate specificity, afforded by a flexible active site which allows them to bind and modify numerous substrates [23, 24].

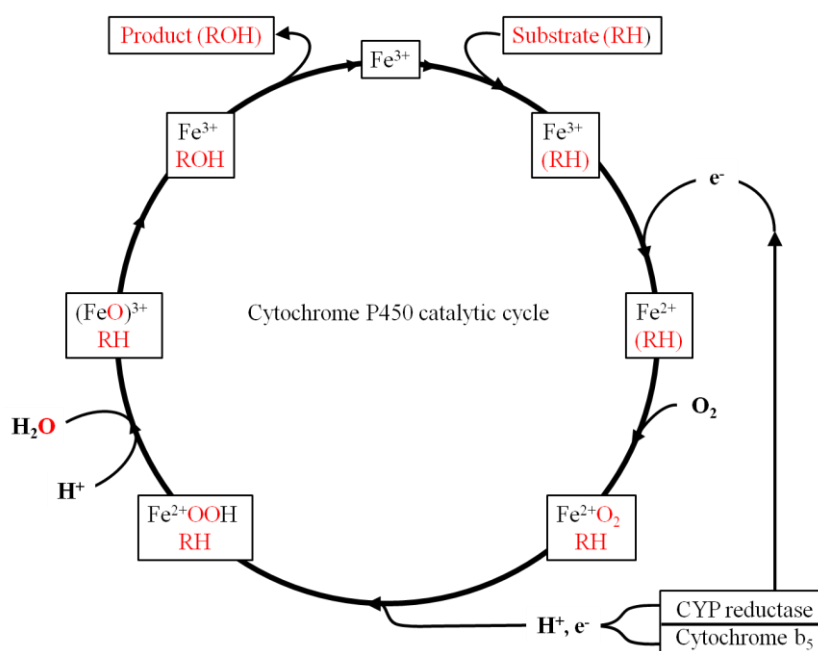


**Figure 1.4: The cytochrome P450 catalytic cycle.** The first electron required for catalysis is donated by CYP reductase and the second electron may be donated by CYP reductase or cytochrome  $b_5$ . Adapted from Apte *et al.*, (2011) [17].

### ***1.2.3 Xenobiotic hepatic bioactivation & toxicity***

Although liver xenobiotic metabolism is considered a sequence of detoxification reactions, both modification and conjugation reactions can result in an increase in compound toxicity (a process referred to as bioactivation). The standard example for this is paracetamol overdose, in which CYP450s catalyse the production of the reactive metabolite N-acetyl-p-benzoquinoneimine (NAPQI) from paracetamol. Bioactivation reactions are generally associated with the production of reactive intermediates. These are normally generated electrophiles and radicals which are postulated to cause toxicity through modification of cellular macromolecules (including DNA) and oxidative stress [25].

Bioactivation reactions cannot occur in the absence of functional DMEs and therefore the liver is susceptible to drug induced liver injury (DILI). Due to this susceptibility, hepatocytes contain particularly high concentrations of the cryoprotectant reduced glutathione, which is their main detoxification mechanism for reactive intermediates, including for NAPQI from paracetamol [19]. However, when detoxification pathways are saturated, then liver damage can occur unimpeded.

DILI is a major cause of acute liver failure [26, 27]. Unexpected hepatotoxicity is also the leading cause of drug attrition during development and following approval [28, 29]. CYP450s, possibly because of their role in the metabolism of most xenobiotics and mechanism of catalysis, are the DME family most commonly implicated in drug bioactivation. Indeed, many structural alerts for toxicity (chemical groups associated with bioactivation), are such because they are bioactivated by CYP450s [20, 25] and reactive intermediates resulting from CYP450 metabolism are considered a major cause of DILI [30].

### ***1.2.4 CYP450 induction***

Due to the importance of CYP450s in xenobiotic metabolism, the liver has evolved robust mechanisms to control CYP450 expression; in response to specific compounds, CYP450 activity can be increased by either up-regulation of CYP450 expression or stimulation of existing CYP450 activity (homotrophic or heterotrophic induction

respectively). The induction of CYP450 expression is primarily regulated by the receptors described in table 1.3. The agonists of the receptors are frequently substrates of the CYP450s that the receptors act to up-regulate and the inductive property of CYP450s can therefore be considered a homeostatic mechanism to promote clearance of xenobiotics.

Receptor	Main rat CYP450 induced	Prototypical agonists	Response elements
<b>Aryl hydrocarbon receptor (AhR)</b>	CYP1A1	$\beta$ -naphthoflavone, 3-methylcholanthrene	XRE
<b>Constitute androstane receptor (CAR)</b>	CYP2B1	Phenobarbital	XREM & PBREM (DR-3, DR-4, ER-6)
<b>Pregnane X receptor (PXR)</b>	CYP3A1/23	Pregnane 16 $\alpha$ -carbonitrile, dexamethasone, rifampicin	XREM & PBREM (DR-3, DR-4, ER-6, ER-8)
<b>Peroxisome proliferator-activated receptor-<math>\alpha</math> (PPAR<math>\alpha</math>)</b>	CYP4A1	Bezafibrate, clofibrate	PPRE (DR-1)

**Table 1.3: CYP450 inducing receptors.** Based on Tompkins, 2008 [31].

**The aryl hydrocarbon receptor** - the AhR is a basic helix-loop-helix receptor, a member of the PAS domain superfamily which, when activated, causes the up-regulation of CYP1A1, CYP1A2 and CYP1B1 expression as well as the expression of several conjugating enzymes [32]. It is expressed in most tissues including liver and its prototypical ligands are polyaromatic hydrocarbons and heterocyclic amines such as  $\beta$ -naphthoflavone ( $\beta$ -NF), 3-methylcholanthrene, benzo[a]pyrene and 2,3,7,8-tetrachlorodibenzodioxin [33, 34]. Several dietary agonists have also been identified including curcumin and quercetin [35, 36].

As illustrated in figure 1.5, under non-induced conditions, AhR is partitioned into the cytoplasm heterocomplexed to 90kDA heat shock protein (HSP90), hepatitis B virus x-associated protein 2 (AIP) and p23. These protein chaperones (and potentially others to a lesser degree) act to fold and stabilise AhR, maintain ligand responsiveness and to retain the AhR in the cytoplasm [32, 37]. On binding of an agonist to AhR, AIP dissociates and the AhR translocates to the nucleus still bound to HSP90. Within the nucleus, AhR nuclear translocator (ARNT) binds to AhR in place of HSP90 and the

heterocomplex binds to XRE sites, recruiting coactivators and transcriptional machinery to up-regulate gene expression [32].

Historically, the evolution of the AhR has been viewed as an adaptation to exogenous chemical insults as its identified ligands were essentially all xenobiotics. However, there is increasing evidence that the true physiological role of the AhR is concerned with regulation of endocrine and immunological functions and that induction with exogenous ligands may disrupt its normal function [32]. For example, AhR knockout mice demonstrate defective leukocyte, liver and vascular development [38, 39]. Female knockout mice are also poor breeders and this has been linked to the AhR regulating oestrogen synthesis via the ovarian CYP450 CYP19 [40]. In this study, it was shown that a AhR ligand could modulate AhR regulation of oestrogen synthesis suggesting that AhR agonists/antagonists could disrupt endocrine signalling. A further endogenous role of the AhR has been demonstrated by Opitz *et al.*, [41]. In this work, kynurenine produced by tryptophan catabolism in tumour cells activated the AhR to promote tumour malignancy by suppression of immune responses and tumour cell death. The authors further showed that in human glioblastoma tissue, AhR activity was inversely correlated with a positive outcome.

From a toxicological perspective, the induction of CYP450s by the AhR in response to exogenous compounds is the most important when considering drug development and potential DILI. However, it is clear that the AhR plays important roles regulating endogenous physiological functions that are yet to be fully elucidated and these may become increasingly important to take into account when designing drugs in terms of off target effects of AhR activators.

**The constitutive androstane receptor and pregnane X receptor** - the CAR and PXR are orphan nuclear receptors that are almost exclusively expressed in the liver, with some overlap of ligands and response elements [42]. CAR is constitutively active in that it is able to bind response elements in the absence of ligand binding [42]; its activity can therefore be regulated by agonists and antagonists. mCAR prototypical activators include phenobarbital (PB), bilirubin and 1,4-Bis[2-(3,5-Dichloropyridyloxy)]benzene (TCPOBOP); androstane and androstenol are antagonists [42]. The mechanism of CAR activation differs between agonists as is illustrated in figure 1.5B-C: it can be activated

either directly or indirectly such as in the case of TCPBOP and PB respectively. In the cytoplasm, similar to AhR, CAR appears to bind HSP90 as a chaperone and additionally to the co-chaperone cytoplasmic CAR retention protein (CCRP) which is required for cytoplasmic retention [43, 44]. The mechanism of CAR inhibition appears to depend upon disruption of co-activator association with CAR. Androstane, for example, inhibits the interaction of hCAR with the co-activator SRC-1 [45].

In the case of direct ligand binding, such as by TCPOBOP, it is thought that the ligand binds within the ligand binding domain leading to the up-regulation of SRC-1 and protein phosphatase 2A (PP2A) association [44, 46]. Nuclear translocation requires dephosphorylation of threonine 38 of hCAR (threonine 48 in mCAR) and is aided by serine 202 dephosphorylation [47, 48]. PP2A may catalyse the dephosphorylation, although additional proteins are required for PP2A-mediated dephosphorylation of threonine residues. The dephosphorylation of threonine 38 and serine 202 leads to nuclear translocation and once within the nucleus, hCAR associates with co-activating proteins and heterodimerises with retinoic X receptors (RXR) to mediate transcription [42]. Within the nucleus it appears that phosphorylation of CAR or an associated protein is required for CAR transactivation, as inhibition of Ca<sup>2+</sup>/calmodulin-dependent kinase activity inhibits CAR mediated up-regulation of CYP2B10 but not nuclear accumulation of CAR [49].

PB is an indirect activator of CAR in that it is able to induce CAR transactivation but does not bind to CAR. Recently, pioneering work by Mutoh *et al.*, [50], has demonstrated that PB activates CAR by preventing the activation of the epidermal growth factor receptor by epidermal growth factor (figure 1.5C). Activated epidermal growth factor receptor normally inhibits the interaction of receptor for activated C kinase 1 (RACK1) with PP2A and CAR by activating SRC kinase, which deactivates RACK1 through phosphorylation (of RACK1) at tyrosine 52. *In-vitro* dephosphorylation assays showed that RACK1 was required for PP2A mediated dephosphorylation of CAR at threonine 38. By inhibiting this activation of epidermal growth factor receptor, PB promotes the interaction of CAR, RACK1 and PP2A, dephosphorylation of threonine 38 by PP2A and subsequent nuclear localisation of CAR. Once in the nucleus, activated CAR may initiate gene expression similar to when it is ligand bound. In the ligand binding model of CAR activation, the involvement of

RACK1 is not known, but conceivably ligand binding of CAR may cause a conformational change allowing PP2A, CAR and RACK1 to associate; this would permit PP2A to dephosphorylate CAR at threonine 38 thereby promoting CAR nuclear translocation.

PXR activation is similar to that of CAR. The PXR is activated by a wide range of prototypical activators in humans such as rifampicin and hyperforin [42]. In humans *in-vitro*, hPXR appears to be constitutively localised in the nucleus where, in the absence of ligand binding, it acts as a gene silencer through association with co-repressors and histone de-acetylases [51]. Binding of ligands leads to dissociation of co-repressors and the recruitment of co-activators, the same as those that associate with CAR, leading to transcriptional up-regulation of genes [42]. In mice *in-vivo*, mPXR appears to be localised in the cytoplasm (figure 1.5D) bound to HSP90 and CCRP [52]. Activation through ligand binding leads to association with co-activators and nuclear translocation, heterodimerisation with RXR and activation of gene transcription.

Activated CAR and PXR both up-regulate the expression of a broad range of DMEs, many of which overlap. This is because CAR and PXR both bind to XREM and PBREM sites. The major genes they regulate include CYP3A4, CYP3A5 and CYP2B6 as well as some hepatic transporters and phase II conjugation enzymes [42]. They also both have specific genes that they alone regulate. Although PXR and CAR bind at the same response elements, they have different affinities for the consensus motifs and therefore their binding affinity at different response elements varies. PXR therefore favours CYP3A regulation whereas CAR favours CYP2B regulation [42, 53, 54]. This system allows for fine control of gene regulation by the two receptors.

The CAR and PXR play a significant role in the regulation of xenobiotic metabolism as they regulate the expression of CYP450s responsible for the metabolism of the majority of drugs [42, 55]. Similar to the AhR, however, they also have a range of endogenous physiological functions. These functions vary but both the PXR and CAR have been shown to regulate gluconeogenesis and endocrine signalling through modulation of steroid and thyroid metabolism [55]. In particular, an important role of the PXR is its regulation of bile acid homeostasis. The PXR is responsive to bile acid precursors and several secondary bile acids and its activation leads to significant up-regulation of

DMEs within hepatocytes, which promotes the detoxification of bile acids and their clearance back into the biliary tree [56-59]. PXR also inhibits CYP7A1, which catalyses the rate limiting step of bile acid synthesis, in order to reduce further bile acid accumulation within the liver [60]. The role of the PXR in this context is evident in PXR knockout mice that have undergone bile duct ligation which show a significantly greater hepatic injury than wild type mice subject to the same procedure [61]. CAR also appears to aid in regulation of bile acid and cholesterol homeostasis, although to a less marked extent [62].

**The peroxisome proliferative activating receptor  $\alpha$**  - the PPAR $\alpha$ , part of the nuclear receptor gene superfamily, is expressed in tissues associated with fatty acid catabolism including the liver, heart, kidneys and muscle [63]. PPAR $\alpha$  has a range of synthetic and biological ligands; its biological ligands include fatty acids and metabolites from fatty acid anabolism and catabolism [63, 64]. Prototypical synthetic ligands are fibrate drugs such as clofibrate and bezafibrate. Unlike the AhR, CAR and PXR, PPAR $\alpha$  activation does not lead to up-regulation of DMEs generally involved in clinical drug metabolism and bioactivation of xenobiotics by PPAR $\alpha$  regulated DMEs is uncommon. In the absence of agonist activation, PPAR $\alpha$  is localised to the nucleus where, heterodimerised with RXR, it inhibits transcription of target genes through recruitment of co-repressors at PPRE sites (figure 1.5E). Binding of ligands causes the release of co-repressors and the subsequent recruitment of co-activators which leads to the initiation of target gene transcription [63].

PPAR $\alpha$  was first investigated when it was found that the chronic administration of anti-hyperlipidaemia drugs (later discovered to be PPAR $\alpha$  agonists) caused peroxisomal proliferation, hepatomegaly and the development of liver tumours in rodents independent of any genotoxicity. Use of knockout mice demonstrated unequivocally that PPAR $\alpha$  was responsible for the phenotype seen [65]. More generally, PPAR $\alpha$  knockout mice show hepatic accumulation of lipids when fed a high fat diet or, when fasted, show hypoglycaemia and elevated concentrations of plasma free fatty acids. These are phenotypes indicative of disrupted fatty acid oxidation and gluconeogenesis [66]. Further work has demonstrated that the PPAR $\alpha$  is a crucial regulator of fatty acid  $\beta$ -oxidation through which, particularly in the liver, it acts as a mediator of whole body energy homeostasis [63]. In response to high concentrations of fatty acids and their

intermediate breakdown products, the PPAR $\alpha$  up-regulates genes associated with all three fatty acid oxidation pathways (mitochondrial, peroxisomal and microsomal)[63]. This negative feedback loop leads to a reduction of cellular fatty acid concentrations and plasma triglyceride and very low density lipoproteins levels. Synthetic PPAR $\alpha$  agonists (mainly fibrates) have been used for years to effect these very changes in patients with hyperlipidemia and can be taken without risk of carcinogenesis. This is because the link between PPAR $\alpha$  activation and carcinogenesis that is seen in rodents is not recapitulated in humans due to species differences in PPAR $\alpha$  activity [67].

In rodents, PPAR $\alpha$  activation causes an increase in hepatocyte oxidative stress and hepatocyte size whilst also promoting proliferation and inhibiting apoptosis, responses not seen in humans [68]. In humans, PPAR $\alpha$  is expressed at levels significantly lower than that seen in rodents (roughly one tenth of the level in rodents) and it does not regulate growth and apoptosis, unlike rodent PPAR $\alpha$  [69]. The reduced sensitivity of the human PPAR $\alpha$  and differences in transcriptional regulation are thought to be the primary reason for the species difference observed.

In terms of the relevance of the PPAR $\alpha$  to xenobiotic metabolism, PPAR $\alpha$  is activated by environmental contaminants including herbicides and phthalate esters which humans may be exposed to via the diet [70]. In rodents, phthalate ester exposure leads to a typical peroxisomal proliferation response [71]. There is consequently a growing concern that chronic exposure of humans to these compounds may have toxicological consequences.

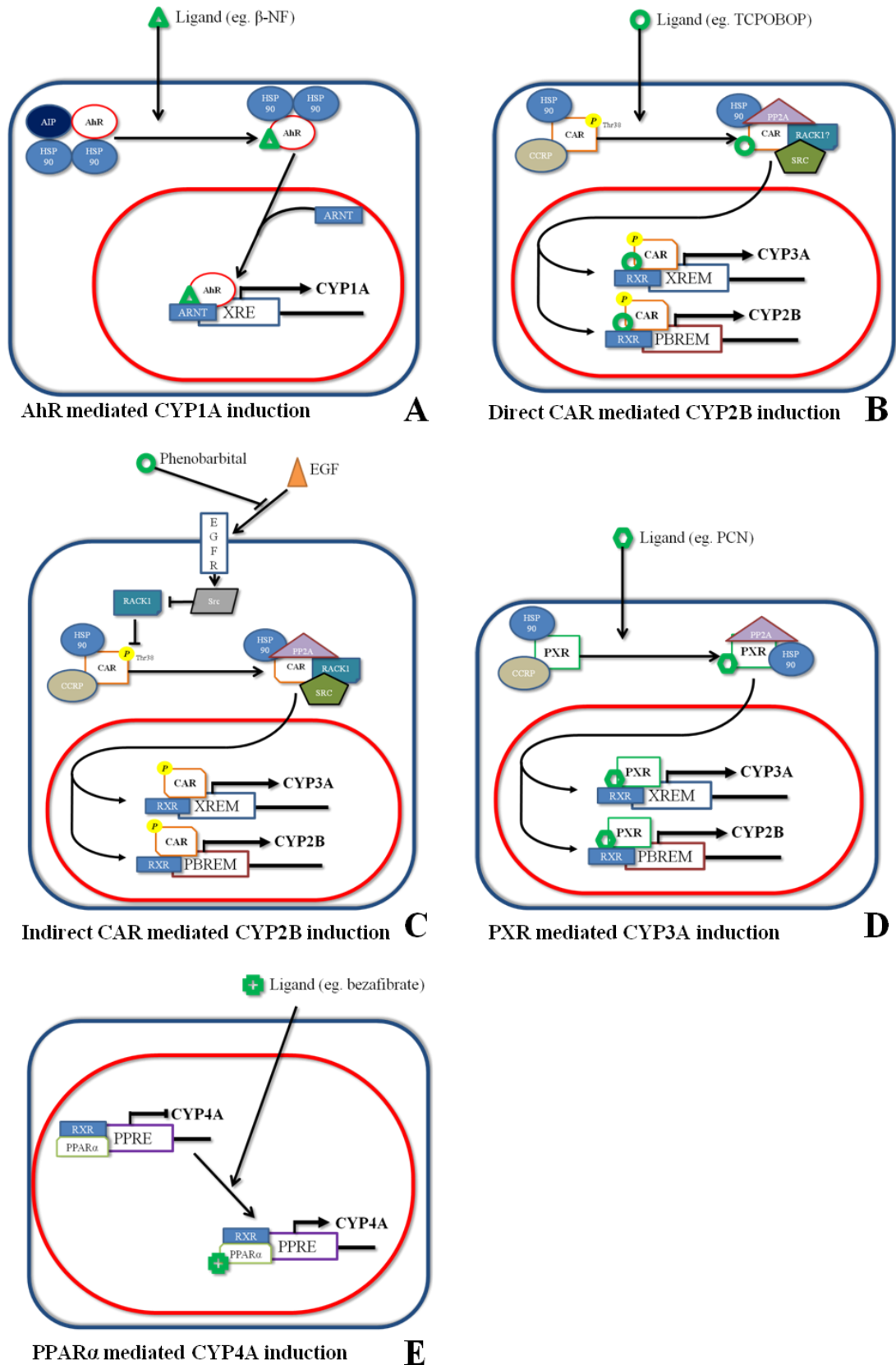


**Figure 1.5: Mechanisms of A. AhR, B. direct CAR, C. indirect CAR, D. PXR and E. PPAR $\alpha$  mediated CYP450 induction. D shows mPXR induction (cytoplasmic in absence of ligand binding). See text for details.**

### 1.2.5 Drug transporters

The transport of drugs and chemicals, both prior to and after metabolism, plays a fundamental role in determining the rate of xenobiotic clearance and route of excretion. Hepatocytes express a broad range of transporters as summarised in table 1.4. These transporters, due to the polarised nature of hepatocytes, are expressed either basolaterally or apically, and allow hepatocytes to selectively partition endogenous moieties or xenobiotics into general circulation or the biliary tree.

Transporter	Location	Role	Example substrate	ATP dependent
<b>Solute carriers</b>				
<b>NTCP</b>	Basal	Major influxer of bile salts	Taurine and glycine conjugated bile acids [72]	No
<b>OCTs</b>	Basal	Influx of organic cations	Choline	No
<b>OATs</b>	Basal	Influx of organic anions	Salicylates [73]	No
<b>OATP1s</b>	Basal	Influx of organic anions, amphiphatic organic solutes and bile salts	Dihydroxy bile salts [74]	No
<b>OATP2A1</b>	Basal	Influx of prostaglandins and eiscanoids	Prostaglandin E2 [75]	No
<b>OATP2B1</b>	Basal	Influx of organic anions	Atorvastatin [75]	No
<b>ABC transporters</b>				
<b>BCRP</b>	Apical	Efflux mainly of sulphate conjugates	Gefitinib [76]	Yes
<b>BSEP</b>	Apical	Major effluxer of conjugated bile salts although may also pump out some xenobiotics	Monovalent bile acids [72]	Yes
<b>MDR1</b>	Apical	Efflux of cationic compounds	Colchicine [77]	Yes
<b>MDR3</b>	Apical	Efflux of phospholipids via flippase activity	Phosphatidylcholine [77]	Yes
<b>MRP1</b>	Apical	Efflux of glutathione conjugates	LTC4 [78]	Yes
<b>MRP2</b>	Apical	Efflux of organic anions and GSH	Glucuronidated bilirubin	Yes
<b>MRP3</b>	Basal	Efflux of glucuronidated conjugates	Bilirubin diglucuronide	Yes
<b>MRP4</b>	Basal	Efflux of glucuronide and sulphate conjugates	Chenodeoxycholyglycine (+GSH) [79]	Yes

**Table 1.4: Important hepatocyte transporters and their properties.** Adapted from Arias, (2009) [80].

**Basolateral uptake transporters** – Drugs or endogenous compounds may enter hepatocytes either by passive diffusion or basolateral transporter mediated active uptake. Uptake transporters are members of the solute carrier superfamily which power uptake through secondary active transport (electrochemical gradient dependent) [81]. The primary uptake solute carriers are the major organic anion transporting polypeptides (OATPs), sodium-dependent taurocholate co-transporting polypeptide (NTCP), major hepatic organic cation transporters (OCTs) and major hepatic organic anion transporters (OATs).

**Efflux transporters** – The hepatic transporters involved in the efflux of xenobiotics, their metabolites and endogenous metabolism products belong to the ATP binding cassette (ABC) superfamily which catalyse the unidirectional export of substrates powered by ATP hydrolysis. The primary efflux ABC transporters are the multidrug resistance P-glycoproteins (MDRs), bile salt export pump (BSEP), multidrug resistance proteins (MRPs) and the breast cancer resistance protein (BCRP). The majority of these transporters are on the apical membrane and efflux substrates into the bile, however MRP3 & MRP4 are located on the basolateral membrane and pump water soluble conjugated-metabolites into the blood.

**Hepatobiliary transport** - The transport of bile acids in hepatocytes is primarily mediated by NTCP, which uptakes bile salts from the blood, and BSEP, which exports bile salts into canaliculi. Other transporters including OATPs (particularly OATP1B1) and MRPs (particularly MRP2 and MRP3), also have a role in bile salt transport. The farnesoid-X receptor (FXR) transcriptionally regulates the expression of bile acid production and transport [82]. It is activated by a range of bile acids in response to which it induces BSEP expression whilst inhibiting the expression of NTCP and OATP1B1, and CYP7A1, the rate determining enzyme in bile acid synthesis [83]. This response acts to maintain bile acid homeostasis by promoting hepatocyte bile acid clearance. Under cholestatic conditions, this response acts to protect hepatocytes from toxicity resulting from intracellular bile acid accumulation. Although the FXR is the main regulator of hepatobiliary transport, the PXR and CAR also play a secondary role through similar regulation of bile acid transport and metabolism [84].

### 1.3 Safety testing of drug candidates

The further a potential drug candidate progresses through drug development, the greater the potential loss if its development is halted due to safety concerns; consequently, companies try to detect potentially toxic candidates early on during drug development using a range of toxicological endpoints [85].

Important aspects of a candidate drug determined during the discovery phase include assessing whether a drug causes CYP450 or transporter induction or inhibition, forms adducts with proteins or DNA, and its route of metabolism [85]. Much of the discovery phase work of drug development is carried out *in-vitro* as it is cheaper, has higher throughput and requires smaller quantities of a drug candidate [86]. The proportion of this work carried out *in-vitro* will increase in the future as a consequence of the increasing public and legislative pressure to reduce animal use in research and promotion of the 3Rs principles of research; these encourage the refinement, reduction and replacement of animals in research [87].

The liver metabolises the majority of clinical drugs and it is hepatocytes that are primarily responsible for liver functionality. Hepatocyte function is therefore the determining factor that governs drug toxicity and pharmacokinetics. To this end, hepatocyte models are utilised in drug research for *in-vitro* assessment of candidate drug metabolic parameters in terms of routes of metabolism and potential DME induction/inhibition. These hepatocyte models are described below.

#### 1.3.1 Primary hepatocytes

The gold standard model for *in-vitro* toxicity screening of novel drugs and chemicals are primary human hepatocytes. However, there are numerous issues associated with their sourcing and culture. Primary human hepatocytes for research are mainly sourced from liver excised as part of surgical procedures and the demand for donor tissue consequently outstrips the supply available. Beyond supply issues, as the donor liver comes from patients undergoing hepatic surgery, the tissue itself maybe diseased or proxy to diseased tissue and the liver has in most cases been exposed to a range of

therapeutic drugs taken by the patient. These issues can cause significant variability between donor samples [88].

In culture, primary hepatocytes are non-proliferative and rapidly dedifferentiate to a more fibroblastic phenotype within a few days, losing the majority of relevant drug metabolising activity, particularly CYP450s [89, 90]. Their senescence prevents their expansion in culture and the rapid dedifferentiation means that all experiments must be carried out within a short period of time. The cause of hepatocyte dedifferentiation *in-vitro* is thought to be related to the loss of ECM and ischemia experienced by hepatocytes during isolation. This leads to initiation of inflammatory (through NF- $\kappa$ B) and proliferative (through mitogen-activated protein kinase) signalling as outlined in figure 1.6 [86, 91]. This response has the effect of priming hepatocytes for division, increasing ribonuclease expression and repressing liver enriched transcription factors such as hepatocyte nuclear factor 1 $\alpha$  (HNF1 $\alpha$ ) and 4 $\alpha$ , and CCAAT/enhancer-binding protein  $\alpha$  (C/EBP $\alpha$ ) and C/EBP $\beta$  [92-94]. These transcription factors promote a hepatocyte phenotype and their repression is thought to lead to dedifferentiation and the gradual loss of DME expression [86, 95, 96].

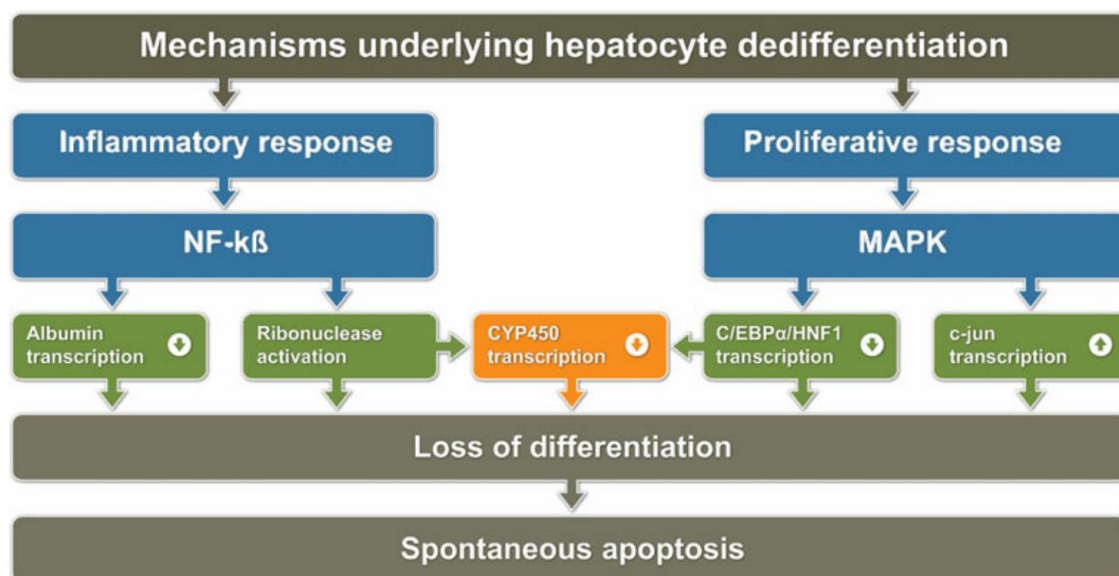


**Figure 1.6: Factors contributing to dedifferentiation of hepatocytes.** From Fraczek et al., (2013) [86].

The limited supply of human hepatocytes means that non-human hepatocytes are frequently used for *in-vitro* toxicity screening as an alternative. To enhance survival and maintenance of drug metabolising activity in hepatocyte cultures, numerous approaches

have been investigated. The most common approach is to sandwich hepatocytes between collagen and matrigel [89, 97]. Other approaches include supplementation of serum free medium with dexamethasone (DEX) or epigenetic modifying agents such as dimethyl sulfoxide (DMSO) and trichostatin A [98-100]. Although the use of these different techniques alone or in combination diminishes the rate of hepatocyte dedifferentiation, they have only limited effect and they introduce complications in examination of endpoints and results.

### ***1.3.2 Pluripotent stem cell-derived hepatocyte-like cells***

In an attempt to solve the problems of human hepatocyte availability, numerous groups have attempted to derive hepatocytes from pluripotent stem cells, usually human embryonic stem cells (hESCs) or induced pluripotent stem cells (hiPSCs). Hepatocyte-like cells can be derived from either of these populations and a wide range of different techniques have been used, generally by attempting to recapitulate liver embryogenesis [101]. Specifically, this involves the application of growth factors at defined times in order to differentiate the stem cells from pluripotency to endoderm induction, hepatic lineage specification and finally maturation [102]. Hepatocyte growth factor, fibroblast growth factor 4, oncostatin M and activin A are used almost universally for these protocols although there is no universal protocol and methods used vary significantly [101]. To determine if hepatic differentiation of stem cells has been successful, a range of endpoints are commonly measured and the most common of these is the assessment of albumin,  $\alpha$ -fetoprotein and  $\alpha$ -1-antitrypsin expression by PCR and/or immunocytochemistry [102].

Hepatocytes derived from pluripotent stem cells could solve many of the issues associated with the use of primary human hepatocytes. Pluripotent stem cells are proliferative so offer an unlimited source of hepatocytes for xenobiotic toxicity testing and if a standardised protocol was developed, variation seen in primary human hepatocyte preparations could be reduced. The use of hiPSCs as the pluripotent stem cells used for generation would be superior to the use of hESCs, as the ethics involved with their derivation are significantly more straightforward since hiPSCs are derived from somatic cells unlike hESCs which must come from fertilised embryos. Additionally, the use of hiPSCs could allow for hepatocytes with different drug

metabolising phenotypes to be generated from genetically distinct individuals, thereby improving the predictive capacity of toxicity screening.

Although there are significant resources focused on this area of research, hepatocyte-like cells generated using these protocols demonstrate substantial variability in terms of the percentage of cells differentiated to a hepatic lineage and the functionality of the “mature” hepatocyte-like cells. A review of the recent literature has showed that the number of derived hepatocyte-like cells expressing albumin varies between ~9-90% using different protocols [101]. Drug metabolism activity has been assessed in several experiments involving the generation of hepatocyte-like cells and this similarly shows a large variation. The hepatocyte-like cells have shown 0-100% of primary human hepatocyte CYP3A4 activity (the most commonly measured CYP450) and 4-100% of CYP1A2 activity [101]. Of recent studies, work by Chen *et al.*, and Duan *et al.*, using hiPSCs and hESCs respectively have shown promise in producing hepatocyte-like cells with physiologically relevant drug metabolising activity [103, 104]. Chen *et al.*, demonstrated the generation of hepatocyte-like cells from hiPSCs that showed equivalent CYP3A4 expression to primary human hepatocytes and these cells, when injected, could rescue mice treated with a fatal dose of carbon tetrachloride (CCl<sub>4</sub>). Using hESCs, Duan *et al.*, describe hepatocyte-like cells which showed similar levels of CYP3A4, CYP1A2 and CYP2D6 activity to primary human hepatocytes. Aside from assessment of a limited subset of genes, characterisation of hepatocyte-like cells derived from stem cells is incomplete, particularly in respect to conjugation and transporter activity. Importantly, it is suggested that hepatocyte-like cells derived from pluripotent stem cells are foetal like cells that require maturation for complete function, similar to hepatocytes following dedifferentiation [105]. To improve their function, methods will need to be devised so that the derived cells can be matured to fully functional hepatocytes.

Although the work deriving hepatocyte-like cells from pluripotent stem cells is encouraging, their use for drug and chemical toxicity screening is currently limited. This is mainly because of the considerable variation in batch to batch differentiation and function and general lack of significant drug metabolising activity. They are however also expensive to generate due to the numerous growth factors required which would become particularly pronounced considering the huge numbers that would be required

for screening purposes. Finally, if physiologically relevant hepatocytes are generated from pluripotent stem cells, then it is likely that they would spontaneously dedifferentiate similar to primary hepatocytes, limiting their utility.

### ***1.3.3 HepG2***

The HepG2 cell line was derived from a male human hepatoblastoma in the 1970s and found to have a parenchymal hepatocyte morphology and express a range of liver synthesised plasma proteins whilst being proliferative and straightforward to culture [106, 107]. Although they are the most widely used alternative to primary human hepatocytes and consistently express a range of conjugating enzymes and a number of transporters, their expression of CYP450s is more varied and limited. In particular they generally express some CYP1A and, in most cases, low to undetectable levels of CYP2B/C and CYP3A. Although they express AhR, PXR and low levels of CAR, HepG2 cells induce CYP1A but usually not CYP2B/C or CYP3A in response to the different receptor agonists [93, 108-113].

A consequence of their limited CYP450 activity means that un-modified HepG2 cells are generally not very predictive of toxicity when exposed to bioactivation dependent hepatotoxins compared to primary hepatocytes [109]. However, as they express machinery required for CYP450 function (particularly CYP reductase [113]), some success has been achieved using HepG2 cells stably expressing CYP450 variants [114, 115] and these could potentially be used for drug and chemical toxicity screening. A disadvantage of this approach is that the potential for induction and therefore study of drug interactions is lost as the introduced genes are either constitutively expressed or tetracycline induced/inhibited.

### ***1.3.4 HepaRG cells***

HepaRG cells are emerging as a useful model of hepatocytes. They were derived from a human female hepatocellular carcinoma and under normal conditions they are phenotypically stable and proliferative with a non-hepatocyte phenotype [116]. When the cells are confluent they are treated with 2% DMSO which gives rise to two distinct populations, one of hepatocyte-like and one of cholangiocyte-like cells, within 7-10

days [116, 117]. Measurement of CYP450 expression shows that non-differentiated HepaRG cells (prior to DMSO treatment) express low to undetectable levels of a range of CYP450s including CYP3A4 and CYP2D6 similar to HepG2 cells. Following DMSO induced differentiation, CYP3A4 in particular was expressed at higher levels than in freshly isolated human hepatocytes. Other CYP450s measured were also up-regulated though to a lesser extent but to levels greater than that seen in HepG2 cells [108]. Aside from CYP450s, they also express a number of conjugation enzymes and transporters required for phase II and III metabolism though their activity has not yet been determined [118].

HepaRG cells express AhR and the nuclear receptors CAR and PXR; these receptors appear functional as induction of the CYP450s CYP1A2, CYP2B6 and CYP3A4 has been documented [108, 118]. Recent literature has assessed the potential of HepaRG cells for drug and chemical toxicity screening based on their similarity to primary human hepatocytes. In comparison to HepG2 cells and primary human hepatocytes, it has been shown that HepaRG cells were more comparable to HepG2 cells than primary hepatocytes in terms of their response to hepatotoxins; primary human hepatocytes were ~42% sensitive, HepaRG cells ~12.5% and HepG2 cells ~6% sensitive to the hepatotoxins tested [109]. This data suggests that although they express a similar drug metabolising complement to primary human hepatocytes, this alone is not sufficient to confer similar sensitivity. Potentially this may be because HepaRG cells, as hepatoma cells, may be more resistant to apoptosis and necrosis than primary hepatocytes.

## **1.4 AR42J-B-13 cells**

### ***1.4.1 Isolation and properties***

The pancreatic acinar cell line AR42J was derived from a pancreatic adenocarcinoma in male Wistar rats treated with azaserine [119, 120]. They have been suggested to be a “cancerous version of primordial pancreatic ductular epithelium” as they express acinar markers (such as amylase) but also some neuroendocrine markers, as well as being highly proliferative [120]. In response to activin A and betacellulin in combination, or hepatocyte growth factor alone, it was shown by the Kojima lab that a proportion of AR42J cells began to produce insulin [121, 122]. These responsive cells were isolated and expanded to produce the AR42J-B-13 (B-13) cell line. In 2000, the Tosh group

demonstrated that treatment of B-13 cells with DEX caused them to flatten, cease proliferation and up-regulate the expression of liver specific markers including albumin, glucose-6-phosphatase and transferrin within 14 days [123]. The activation of C/EBP $\beta$  was shown in the same paper to be the crucial event inducing transdifferentiation as, in the absence of DEX, transfection of C/EBP $\beta$  was sufficient to induce transdifferentiation. Furthermore, use of the dominant negative form of C/EBP $\beta$  inhibited transdifferentiation [123].

Subsequent work has shown that hepatocyte-like cells derived from B-13 cells (B-13/H cells) express several CYP450 isoforms including CYP2C11, CYP2A and CYP2E1, most of which are up-regulated significantly by 5 days following initiation of DEX treatment and are expressed at similar levels to freshly derived hepatocytes [124, 125]. The up-regulation of CYP450s has been demonstrated to lead to similarly high levels of cell death in response to the hepatotoxin paracetamol to freshly isolated hepatocytes [124]. Cell death conversely was not seen in undifferentiated B-13 cells.

#### ***1.4.2 Conservation of transdifferentiation of pancreas to liver***

Based on the observed transdifferentiation of B-13 cells to B-13/H cells, the effect of glucocorticoids on exocrine pancreatic tissue *in-vivo* has been investigated. Treatment of rats for 21 days with DEX led to a significant increase in the number of CYP2E1 positive cells in the pancreas compared to control animals [126]. Similarly, in transgenic mice which have constitutively elevated levels of glucocorticoids, significant expression of CYP2E1 was seen in pancreatic exocrine tissue [127]. Removal of the adrenal glands of these transgenic mice inhibited the expression of CYP2E1 in the pancreas indicating that glucocorticoids were responsible for the CYP2E1 positive exocrine cells in the pancreas. Perhaps most importantly, hepatic markers could be detected in the pancreas of a human patient treated for over 20 years with glucocorticoid (prednisolone) [128]. Furthermore, culture of primary and immortal adult human acinar cells with high concentrations of DEX leads to expression of hepatic markers [128]. The ubiquitous nature of the transdifferentiation of pancreatic exocrine cells to hepatocyte-like cells in response to glucocorticoid interspecies provides strong proof that rather than being an artefact of cell culture, the transdifferentiation response is a conserved pathophysiological response and is likely related to the similar developmental origins of

the liver and pancreas which are both foregut endoderm derived. It also suggests that glucocorticoids may play developmental roles in the specification of the liver and pancreas in the foetus [123].

### ***1.4.3 Molecular basis of transdifferentiation***

The signalling pathway responsible for the transdifferentiation of B-13 cells to B-13/H cells is still being elucidated, particularly at the level of gene regulation. However significant progress has been made in linking the administration of glucocorticoids to the induction of C/EBP $\beta$  as outlined in figure 1.7 and it has become clear that the suppression of Wnt signalling is the crucial early stage event of transdifferentiation. The involvement of the canonical Wnt signalling pathway in the transdifferentiation response was first suggested when it was observed that, following DEX treatment but prior to any phenotypic changes, Wnt3a expression was significantly down-regulated and  $\beta$ -catenin cytoplasmic localisation, phosphorylation and degradation were significantly increased [129]. The role of  $\beta$ -catenin in the transdifferentiation response was confirmed when introduction of a mutant form of  $\beta$ -catenin, that cannot be phosphorylated, prevented DEX induced transdifferentiation [129]. Active  $\beta$ -catenin regulates gene expression through the T cell factor/lymphoid enhancer factor (TCF/LEF) family of transcription factors. Chemical activation of TCF/LEF inhibited transdifferentiation and its inhibition, using quercetin, potentiated transdifferentiation [129]. That TCF/LEF inhibition is not sufficient alone to induce transdifferentiation suggests that  $\beta$ -catenin does not act solely through TCF/LEF to repress C/EBP $\beta$  expression.

Further up the signalling cascade, the glucocorticoid receptor has been shown to be required for glucocorticoid induced transdifferentiation in B-13 cells [130]. It has also been observed that transdifferentiation was associated with a significant up-regulation of serum/glucocorticoid inducible kinase 1 (SGK1) expression [130]. SGK1 knockdown was subsequently shown to inhibit transdifferentiation whereas SGK1 overexpression promoted it [130]. Importantly, evidence suggests that SGK1C is able to phosphorylate  $\beta$ -catenin, providing a causal link between SGK1 activation and transdifferentiation [130]. The SGK1 promoter contains a glucocorticoid response

element, which the glucocorticoid receptor has been shown to bind in rat fibroblast and mammary cell lines [131, 132], allowing transcriptional regulation of SGK1 expression.

The phosphatidylinositol-4,5-bisphosphate 3-kinase (PI3K)/protein kinase B (PKB/AKT) pathway has been implicated in transdifferentiation because inhibition of PI3K using the small molecule inhibitor LY294002 inhibits transdifferentiation as does expression of a dominant negative form of PKB/AKT [130, 133]. PI3K can be activated by the glucocorticoid receptor leading to the downstream activation of 3-phosphoinositide dependent protein kinase-1 (PDK1) [134] and this potentially may occur in B-13 cells following DEX treatment. Generally activation of PDK1 would be expected to enhance Wnt signalling as active PKB/AKT, activated by PDK1, can deactivate glycogen synthase kinase 3 (GSK3) through phosphorylation [135]. However, it has been more recently shown that PDK1 can activate SGK1C [136], which could lead to a net repression of Wnt signalling as SGK1C acts downstream of PKB/AKT. Potentially therefore, activation of the glucocorticoid receptor by DEX in B-13 cells may lead to increased glucocorticoid receptor mediated SGK1 transcription and also the activation of a signalling cascade in which PI3K activates PDK1, which in turn activates SGK1C. Activated SGK1C may then inhibit Wnt signalling through the phosphorylation of  $\beta$ -catenin, causing the de-repression and subsequent up-regulation of C/EBP $\beta$  expression leading to transdifferentiation.

Once C/EBP $\beta$  is activated, the mechanism of cellular reprogramming that causes transdifferentiation is unknown. Unpublished work from this lab suggests that DEX treatment is associated with major epigenetic reprogramming within hours of treatment which commit the cells to transdifferentiation, even when DEX is removed after only 6 hours of treatment. C/EBP $\alpha$  and C/EBP $\beta$  are thought to be the first transcription factors induced, followed by the liver transcription factors HNF4 $\alpha$  and RXR $\alpha$  [137]. Significant work is required however to elucidate the mechanism, though once established, it could be used to generate a human equivalent B-13/H cell which could be used for drug and chemical toxicity screening as an alternative to primary human hepatocytes.

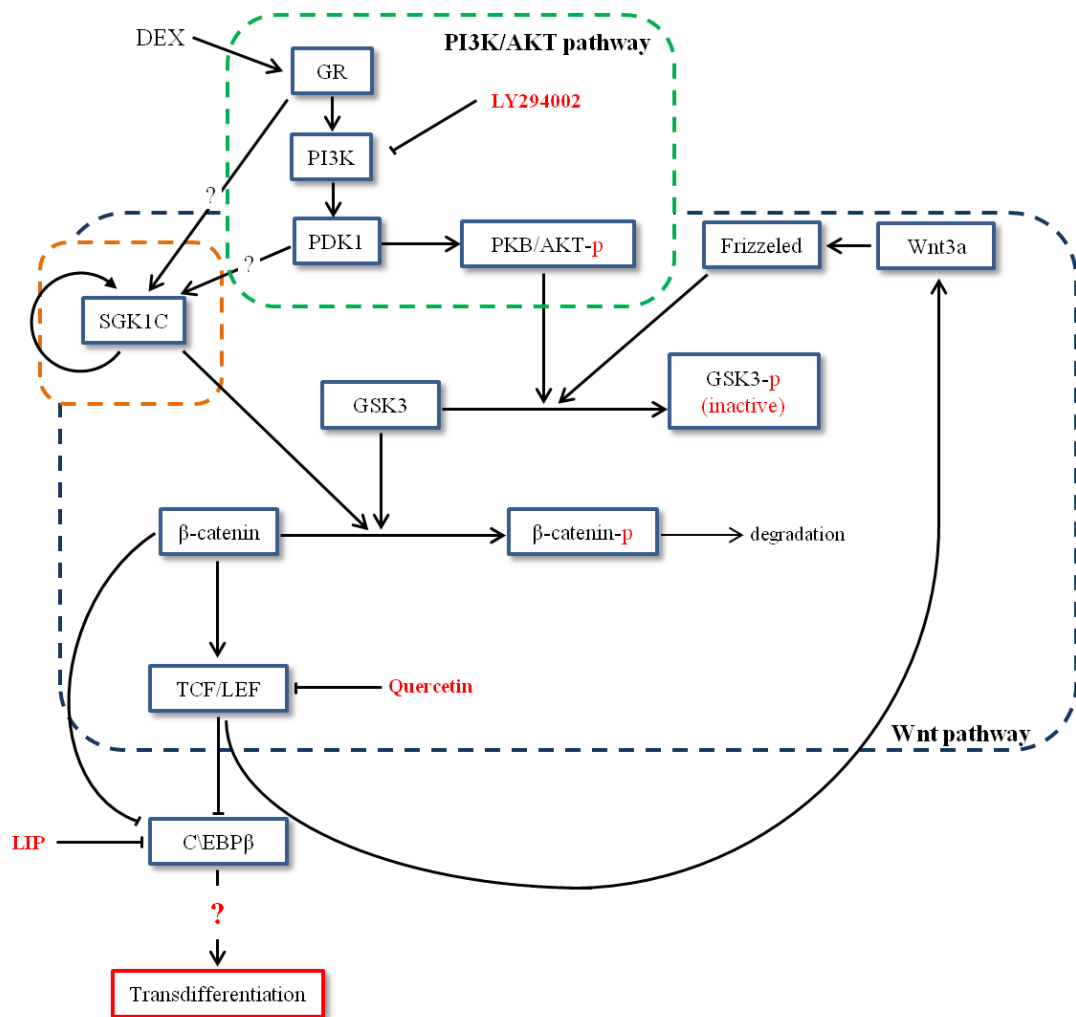


**Figure 1.7: Hypothesised signalling pathway linking DEX (and other glucocorticoids) to C/EBP $\beta$  activation and transdifferentiation.** See text for details. Abbreviations: p, phosphorylated; GR, glucocorticoid receptor; LIP, C/EBP $\beta$ -liver enriched inhibitory protein.

## 1.5 Liver disease & fibrosis

Liver disease is a significant worldwide cause of mortality; it is the 5<sup>th</sup> most common cause of mortality in the UK, the 12<sup>th</sup> in the USA and 14<sup>th</sup> in the world overall [138]. The liver has the unique ability to regenerate when up to 70% of its mass is removed, restoring former mass and function within a relatively short period of time [16]. The liver can therefore regenerate in response to acute injury to restore full function. However, when the liver is challenged by chronic injury/insult, as from the diseases listed in table 1.5, the regenerative capacity of the liver results in the excess deposition of collagen I rich ECM. The unrestricted accumulation of this fibrotic matrix restricts liver regeneration and function [2, 16].

Disease	Incidence
<b>Hepatitis B</b>	370 million individuals worldwide [139]
<b>Hepatitis C</b>	130 million individuals worldwide [139]
<b>Alcoholic liver disease (ALD)</b>	Difficult to gauge, caused nearly 5,000 deaths in England and Wales in 2008 and death rates due to ALD have increased 69% in 30 years [140]
<b>Non-alcoholic fatty liver disease (NAFLD) and non-alcoholic steatohepatitis (NASH)</b>	Possibly up to 60 million individuals worldwide and increasing due to a continual global rise in obesity [141]
<b>Primary biliary cirrhosis</b>	About 1 in 4000 individuals in England, lower in non-Western countries. Disproportionally effects women (only ~10% of sufferers are men) [142]

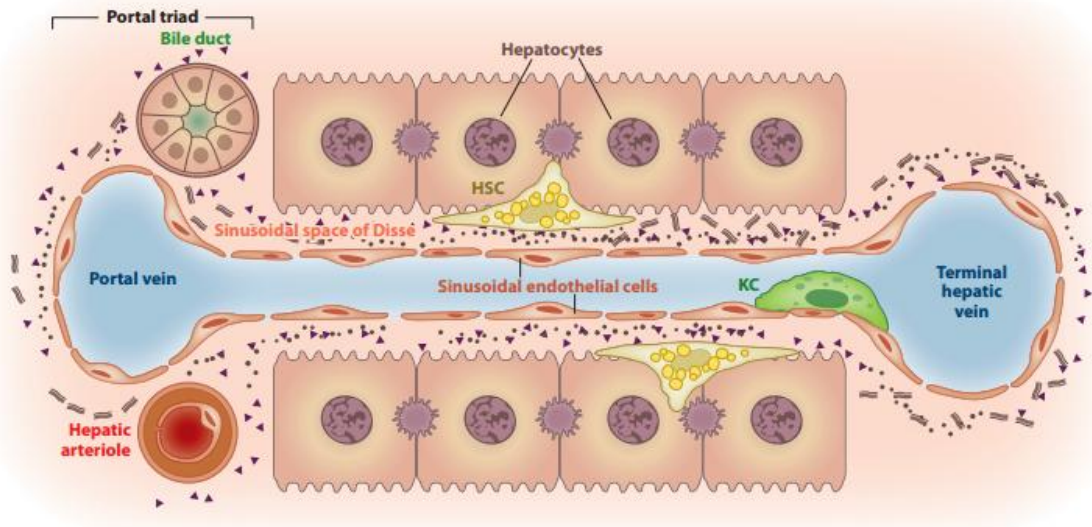
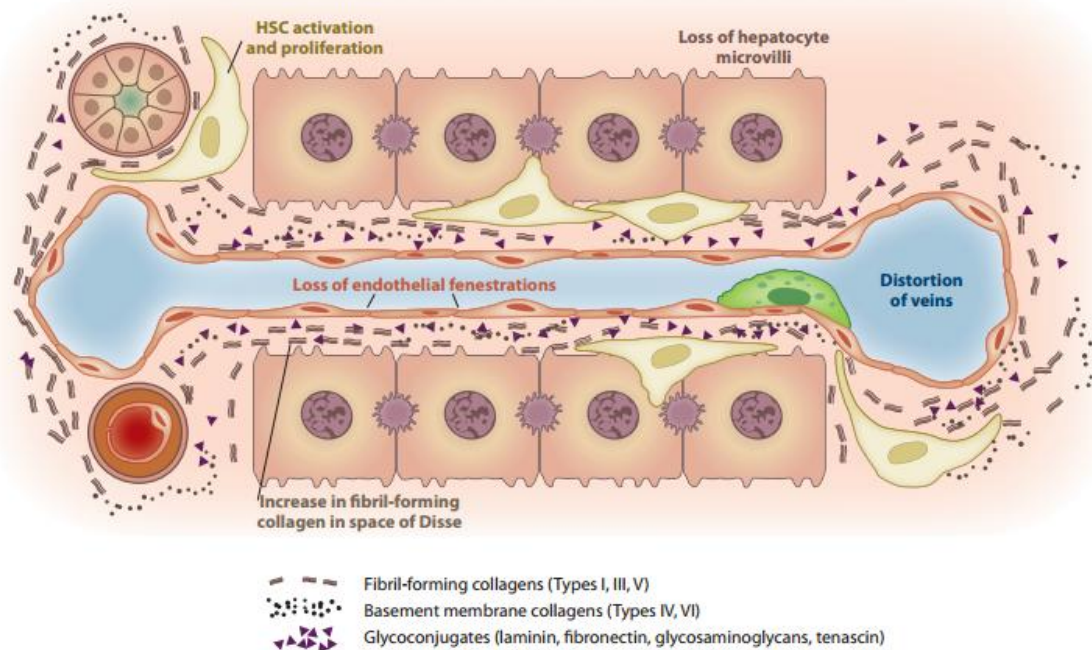
**Table 1.5: Common causes of chronic liver disease and their incidence.** Adapted from Probert (2011) [3].

### 1.5.1 Pathophysiology

Chronic liver injury resulting from a variety of causative agents results in cell injury and death within the liver. The release of intracellular components resulting from cellular necrosis leads to activation of Kupffer cells and initiation of an inflammatory response through the release of pro-inflammatory mediators [5, 16]. Exposure of collagen, a consequence of endothelium damage, also activates platelets which release pro-inflammatory mediators [143]. These factors cause the recruitment of extra-hepatic leukocytes, which contribute to the inflammation, and the activation of fibroblasts (i.e. hepatic stellate cells and portal tract fibroblasts) causing them to replace the damaged liver parenchyma with fibrous matrix. In the context of wound healing, fibroblasts

deposit ECM which acts as a scaffold for regeneration. However, the constant pro-inflammatory environment of chronically injured liver results in the prolonged activation and proliferation of pro-fibrotic myofibroblast cell populations leading to a net increase in ECM formation. This manifests as a reduction in “normal” matrix protein, mainly collagens IV and VI, and an increase in crosslinked fibrillar collagens I and III and fibronectin [5].

Initially, the deposition of fibrous tissue within the space of Disse leads to a loss of endothelial fenestrations and hepatocyte microvilli in the sinusoids which retards metabolic exchange between hepatocytes and the blood resulting in attenuated hepatic function (figure 1.8)[5]. Over time, ongoing cycles of hepatic injury and scar tissue deposition may result in the development of cirrhosis. Cirrhosis is considered the final stage of fibrosis and is characterised by the development of regenerative and irregular hepatic nodules [144]. Initially the liver is able to functionally compensate for cirrhosis, however as the severity of fibrosis increases and portal hypertension develops, due to increased resistance faced by blood passing through the liver, cirrhosis may become decompensated, ultimately culminating in liver failure [5].

**a Normal liver****b Fibrotic liver**

**Figure 1.8: Changes in liver structure resulting from fibrosis. A.** In normal liver hepatocytes are separated from the sinusoid by a thin-like basement membrane within the space of Disse and blood flows unimpeded through from afferent blood vessels in the portal tract to the central vein. **B.** In fibrotic liver metabolic exchange between hepatocytes and the blood is inhibited by the deposition of ECM within the space of Disse and loss of hepatocyte microvilli and endothelial fenestrations. ECM causes constriction of blood vessels causing portal hypertension. From Hernandez-Gea and Friedman, (2011) [5].

### 1.5.2 Liver fibrosis asymmetry

Liver fibrosis develops in different regions of the liver lobule depending on the causative injury as outlined in figure 1.9. Hepatotoxins primarily target centrilobular regions due to the elevated expression of CYP450s and low concentrations of the

cytoprotectant glutathione in the region (because of liver lobule zonation). Conversely, viral hepatitis primarily infects periportal hepatocytes, at least during the early stages of the disease, due to their immediate proximity to the afferent blood supply.

The asymmetric nature of liver lobule injury gives rise to asymmetric fibrosis: centrilobular liver damage causes centrilobular fibrosis and periportal injury leads to periportal fibrosis. The regulation of fibrogenesis varies depending on the location of lobule injury and this is in part due to the heterogeneity of hepatic (myo)fibroblast populations. The main sources of myofibroblasts in the liver are hepatic stellate cells and portal tract fibroblasts, which express both distinct and shared markers and demonstrate different behaviour *in-vivo* and *in-vitro* [145].

Until recently, it was thought that fibrogenesis in centrilobular and perisinusoidal regions of the liver was mediated by hepatic stellate cells whereas, in periportal regions, it was mediated by portal tract fibroblasts [6, 16]. This was based on a number of studies including one by Beaussier *et al.*, who showed that most myofibroblasts following bile duct ligation (BDL) were negative for the hepatic stellate cell marker desmin [146]. Furthermore, portal tract fibroblasts are activated, proliferate and deposit ECM during the early stages of liver injury following bile duct ligation prior to activation of hepatic stellate cells [145]. However, a recent study using lineage tracing suggests that the majority of myofibroblasts (>80%) in several murine models of liver disease including BDL are derived from hepatic stellate cells, which are also responsible for the majority of collagen production [147]. The role of portal tract fibroblasts and derived myofibroblasts in periportal fibrogenesis is therefore controversial; it is likely that, regardless of their apparently minor contribution to collagen deposition, they play a role in regulation of fibrogenesis, particularly during the initial phases and are an important determining characteristic of periportal fibrogenesis [145]. Their ablation would allow their absolute contribution to fibrogenesis to be determined. However this is prevented by the heterogeneous nature of portal tract fibroblast populations and lack of consistent markers to allow for their selective targeting compared to hepatic stellate cells [145].

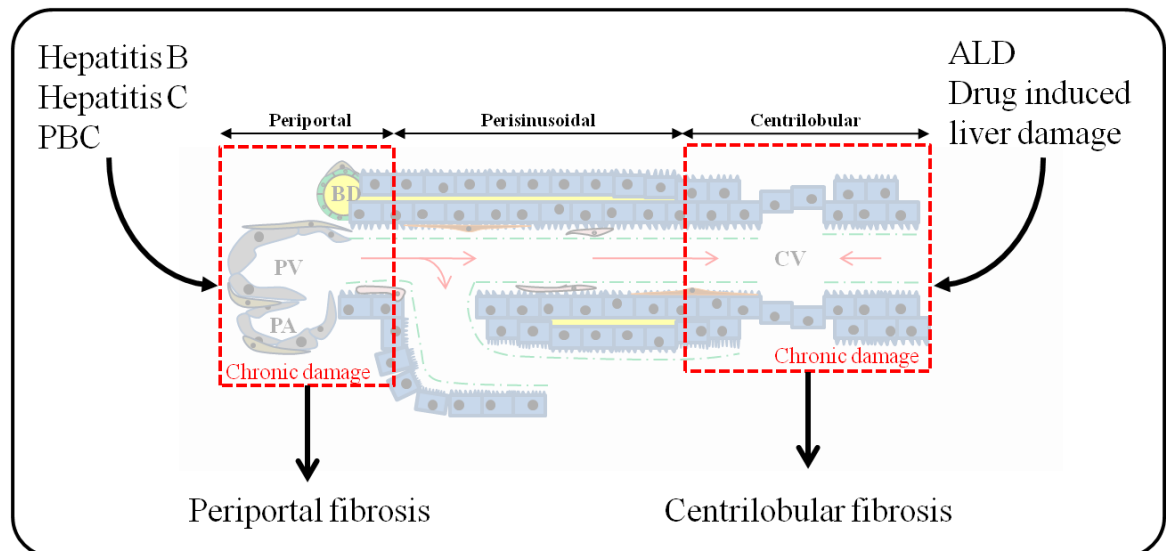


**Figure 1.9: Zonal nature of liver fibrosis.** Different causative agents preferentially damage the liver in different regions. Based on Wallace *et al.*, (2008) [16].

### 1.5.3 Ductular reaction and fibrogenesis

Apart from differences in fibrogenic cell populations involved in fibrogenesis in different regions of the liver, other factors affect the development of fibrosis. Arguably the most important of these is the regulation of fibrogenesis by bile duct epithelia which is particularly pronounced during portal/periportal fibrogenesis due to the local activation of a ductular reaction. Ductular reaction describes the expansion of a potential stem niche within the small branches of the intra-hepatic biliary tree, such as occurs during chronic liver injury [4]. These stem cells are described as oval cells in rodents and hepatic progenitor cells in humans and have a cholangiocyte phenotype (cytokeratin-7 & -19 positive). They divide to form cords of bipotent cells, able to differentiate into hepatocytes or cholangiocytes, which stream out of the portal tract to aid in hepatic regeneration. A consequence of this reaction is an increase in the number of reactive biliary ductules within and around the portal tract. Although ductular reaction may be seen during chronic liver injury generally regardless of insult or localisation, it is particularly associated with portal and periportal injury [4].

In terms of their ability to modulate fibrogenesis, in rats with biliary fibrosis following bile duct ligation, biliary epithelial cells have been shown to be able to release a range of pro-fibrogenic and inflammatory factors. These include including connective tissue growth factor, transforming growth factor  $\beta$  (TGF $\beta$ ) -2 and platelet-derived growth factor [148-150]. There is also evidence for hedgehog mediated paracrine signalling

with myofibroblasts, in which cholangiocytes act to promote myofibroblast growth, which in turn promotes cholangiocyte proliferation [151].

#### ***1.5.4 Modelling liver fibrosis***

Liver fibrosis is a complex disease involving the contribution of a range of cell types. The most straightforward modelling of liver fibrosis involves the *in-vitro* culture of hepatic stellate cells, isolated by collagenase and pronase digestion of the liver [152]. Hepatic stellate cells are isolated on the basis of their low density, a by-product of their high lipid content. This mechanism therefore primarily isolates quiescent cells which, on prolonged culture with plastic, rapidly acquire a myofibroblast phenotype similar to that seen *in-vivo* during chronic liver disease. Although useful for basic research, culture of single cell types fails to reflect the complexity of liver fibrosis, thereby necessitating the use of *in-vivo* models. The most common *in-vivo* models of liver fibrosis are detailed below:

**Carbon tetrachloride (CCl<sub>4</sub>) treatment** - chronic administration of the hepatotoxin CCl<sub>4</sub>, particularly in rodents, is the most commonly used model of fibrosis. Most commonly it is dosed at 1ml/kg body weight twice a week by intra-peritoneal (i.p) injection for 4 to 8 weeks [153]. CCl<sub>4</sub> is metabolised by hepatic CYP2E1 to form a reactive radical (trichloromethyl radical) which causes hepatocyte death through lipid peroxidation and alkylation of cellular components [154]. CYP2E1 is highly expressed in centrilobular hepatocytes and therefore CCl<sub>4</sub> administration results in fibrosis that develops out of the central vein eventually forming central-central bridging fibrosis as shown in figure 1.10. Due to their low expression of CYP2E1, periportal hepatocytes are relatively unaffected [16].

**Dimethylnitrosamine (DMN) administration** - DMN is injected i.p in rats and mice to generate centrilobular fibrosis. Similar to CCl<sub>4</sub>, DMN is bioactivated by CYP2E1 to produce methanol and formaldehyde which through methylation of cellular components (particularly DNA) causes hepatocyte and endothelial cell apoptosis [155, 156]. It is commonly administered by i.p injection at 40-100mg/kg body weight 1 to 4 times a week for up to 15 weeks in rats. Mice are often treated by adding DMN to the drinking water at 0.1mg/L [153]. The progressive injury leads to centrilobular haemorrhagic

necrosis, coagulation and ultimately centrilobular and central-central bridging fibrosis [157].

**Thioacetamide (TAA) treatment** - thioacetamide is administered either by i.p injection or in the drinking water of rats and mice to generate primarily centrilobular fibrosis and eventually central-central bridge fibrosis [16]. Fibrosis is normally generated either by dissolving TAA in drinking water at 200mg/L or by i.p injection of 50-100mg/kg body weight 3 times a week for up to 12 to 16 weeks [153]. It is bioactivated by CYP2E1 resulting in generation of the highly reactive sulfdioxide metabolite which, through covalent modification of cellular proteins, causes oxidative stress and necrosis in hepatocytes [158, 159].

**Bile duct ligation (BDL)** - BDL is a surgical procedure involving the double ligation of the common bile duct for 3-4 weeks. This ligation causes cholestasis and the subsequent accumulation of bile acids within bile ducts. In bordering hepatocytes and cholangiocytes, these bile acids either cause apoptosis through disruption of mitochondrial function or, at higher concentrations, necrosis through solubilisation of the cell membrane [160]. Figure 1.10 shows that the location of the bile duct in the portal tract means that BDL causes periportal injury and fibrosis, leading to portal-portal bridging fibrosis [161]. The severity of the injury induced by BDL however means that within 4 weeks, fibrosis is generally seen throughout the lobule [162].

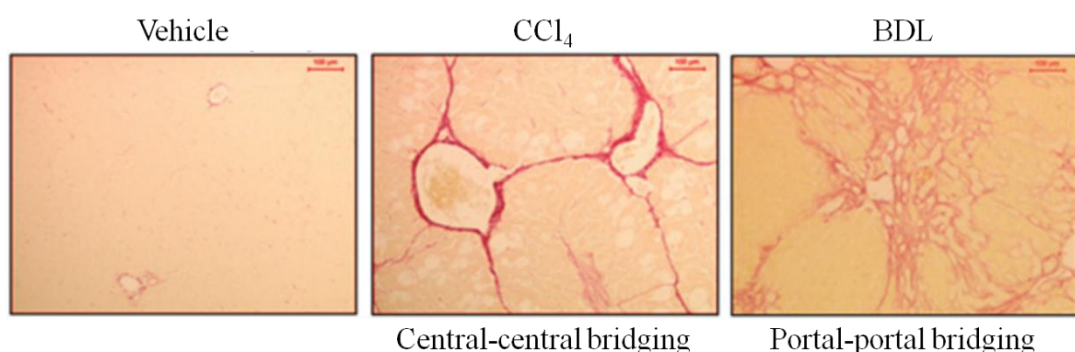


**Figure 1.10: Pattern of hepatic fibrosis induced by CCl<sub>4</sub> and BDL.** Adapted from Wallace *et al.*, (2008) [16].

### ***1.5.5 Treatment of liver fibrosis***

Liver fibrosis, where the underlying causative agent is removed, has been shown to be reversible in many animal models of hepatic fibrosis and cirrhosis. In human patients, regression or complete reversal of fibrosis resulting from a range of diseases has been documented where the underlying insult has been treated [5, 163]. However, not all patients are responsive to treatment and therefore development of anti-fibrogenic drugs could be an important tool to treat fibrosis. Currently though, there are no approved anti-fibrogenic drugs in clinical use for the treatment of hepatic fibrosis as novel drugs tested clinically have generally failed due to lack of efficacy in human patients [143]. There is therefore an ongoing demand for models of fibrosis with which to develop anti-fibrogenic drugs.

### **1.6 Study objectives**

Development of novel drug treatments requires robust models with which to identify drug targets and consequently determine drug safety and efficacy. The rate of drug discovery and validation can be significantly limited by a shortage of robust, relevant and practical models. Application of the 3Rs principles of research to existing models can result in development of superior models for research whilst reducing animal usage. The aims of this thesis were therefore to apply the 3Rs to two models within the field of liver toxicology and disease, primary hepatocytes and periportal fibrosis respectively, in order to develop more refined models and reduce animal usage. The aims specifically were to:

- Investigate the expression and function of drug metabolising enzymes and transporters in B-13/H cells
- Determine if B-13 cells can be humanised with human drug metabolising enzymes
- Investigate if chronic administration of methapyrilene in rats and  $\alpha$ -naphthylisothiocyanate in mice could be used as alternative models of periportal fibrosis to BDL

## **Chapter 2. Materials and Methods**

## 2.1 Materials

Unless otherwise stated, all materials were bought from Sigma-Aldrich at the highest purity available (Poole, UK). 2-Amino-1-methyl-6-phenylimidazo(4,5-b)pyridine (PhIP) and 1-hydroxyestradiol were kindly donated by Professor Nigel Gooderham (Imperial College London, UK) and Professor Ivonne Rietjens (Wageningen University and Research centre, Netherlands) respectively. Polyurethane 134 (PU134) coated slides were donated by Dr David Hay (The University of Edinburgh, UK). Professor Matthew Wright (Newcastle University, UK) provided the B-13 genomic sequence and DNA produced from rat liver and B-13 and B-13/H cells. Adenovirus constructs Ad-null, Ad-C/EBP $\alpha$  encoding mouse C/EBP $\alpha$ , Ad-HNF1 $\alpha$  encoding human HNF1 $\alpha$ , Ad-HNF4 $\alpha$  encoding human HNF4 $\alpha$ , Ad-LAP encoding liver activatory protein of unknown species and Ad-LIP encoding liver inhibitory protein of unknown species were donated by Professor David Tosh (University of Bath, UK). Adenoviral construct Ad-EGFP, encoding green fluorescent protein, was donated by Dr Audrey Brown (Newcastle University, UK).

## 2.2 Animals

### 2.2.1 Housing and ethics

Rats and mice were housed in the Comparative Biology Centre at Newcastle University and kept in accordance with Home Office guidelines. They were kept in separate rooms in an air-conditioned environment on a 12 hour light/dark cycle with regulated humidity (50%  $\pm$  10%) and temperature (23°C  $\pm$  1°C). Rats and mice were provided with food and water *ad-libitum* and kept no more than 5 (rats) or 6 (mice) to a cage. Experiments were performed under a UK Home Office licence (PPL 60/3907) and Newcastle University Ethics Committee permitted the use of animals for this project. Prior to a study starting, a protocol was prepared and approved by the Head Animal Technician.

### 2.2.2 Rats

Male Sprague-Dawley rats were purchased from Charles River (Margate, UK) and kept as per 2.2.1. Rats were between 200-300g body weight at the beginning of all

experiments.

### **2.2.3 C57BL/6 mice**

C57BL/6 mice (wild type) were either bred on site or purchased from Charles River and kept as per 2.2.1. Mice were at least 8 weeks old and between 15-22g body weight at the beginning of all experiments.

### **2.2.4 3x- $\kappa$ B-luc C57BL/6 mice (NF- $\kappa$ B –luc mice)**

NF- $\kappa$ B –luc mice [164] were re-derived from zygotes from Charles River. Mice were kept as per 2.2.1 and were at least 8 weeks old and between 15-22g body weight at the beginning of all experiments.

### **2.2.5 PXR knockout mice**

PXR knockout mice [60] were bred on site and kept as per 2.2.1. They were at least 8 weeks old and between 25-35g body weight at the beginning of all experiments.

## **2.3 Cell Culture**

### **2.3.1 AR42J-B-13**

AR42J-B-13 cells (B-13s, rat pancreatic progenitor cells) were generously provided by Dr Karen Wallace (Aberdeen University, UK) and routinely cultured in low glucose Dulbecco's Modified Eagle Medium (1g glucose/L, DMEM) supplemented with 10% foetal calf serum (v/v, FCS), 100U/ml penicillin, 100 $\mu$ g/ml streptomycin and 2mM L-glutamine. Cells were incubated at 37°C in 95% air and 5% CO<sub>2</sub>. Medium was changed every 2-3 days.

### **2.3.2 B-13<sup>TR/h1A2</sup>**

B-13<sup>TR/h1A2</sup> cells (B-13 cells stably transfected with wild type human CYP1A2 and a tetracycline control vector) were cultured as per 2.3.1 but in medium additionally

supplemented with 250µg/ml geneticin (G418, Invitrogen, Paisley, UK) and 4µg/ml blasticidin (Invitrogen).

### **2.3.3 HEK293**

HEK293 (Human embryonic kidney 293) cells were kindly provided by Dr Audrey Brown (Newcastle University, UK) and were routinely cultured as per 2.3.1.

### **2.3.4 Isolation of Primary Rat Hepatocytes**

Primary rat hepatocytes were generously provided by Professor Lorraine Agius (Newcastle University, UK) and were isolated following a conventional collagenase perfusion [165]. Viability was determined from an aliquot as described in 2.3.10. Assuming adequate viability (>75%), hepatocytes were seeded at  $0.8 \times 10^6$  per well of a 6 well plate or snap frozen as day 0 (T0) samples.

### **2.3.5 Primary rat hepatocyte culture**

Primary rat hepatocytes were initially cultured in low glucose DMEM (1g glucose/L) supplemented with 10% (v/v) FCS, 100U/ml penicillin, 100µg/ml streptomycin and 2mM L-glutamine. After 4 hours, once hepatocytes had adhered to the culture vessel, the medium was replaced with low glucose DMEM (1g glucose/L) supplemented with 100U/ml penicillin, 100µg/ml streptomycin and 2mM L-glutamine. Cells were incubated at 37°C in 95% air and 5% CO<sub>2</sub>. Medium was changed every 2-3 days.

### **2.3.6 Cell passage**

When adherent cells reached 75-95% confluence they were subcultured. All medium was removed from cells and washed once in phosphate buffered saline (PBS, 137mM NaCl, 2.6mM KCl, 10mM K<sub>n</sub>H<sub>n</sub>PO<sub>4</sub>, pH 7.4) to remove all medium. After removal of the PBS, 1x trypsin-EDTA diluted in PBS was added to cells (5ml per T75<sup>2</sup> flask and 0.5ml per well of a 6 well plate) and the cells incubated at 37°C and 5% CO<sub>2</sub> for 5-15 minutes. The culture vessel was then tapped gently to promote cell detachment which was confirmed by light microscopy. Detached cells were then transferred to a 50ml

centrifuge tube (Fisher, Loughborough, UK) and an equal volume of complete culture medium was added to inhibit trypsin activity. Cells were then centrifuged at 800g for 5 minutes. The supernatant was aspirated and the cells re-suspended in fresh medium. The cells were then seeded as required for cell maintenance or an experimental protocol.

### ***2.3.7 Long term cell storage***

Cell lines were regularly frozen down and stored at -80°C or in liquid nitrogen. Cells were detached from the cell culture vessel when 70-80% confluent and pelleted as outlined in 2.3.6. Following supernatant removal the pellet was re-suspended in freezing medium (10% (v/v) DMSO in FCS – normally 2ml per T75<sup>2</sup> flask). This was aliquoted into sterile cryovials (1ml/tube). Cryovials were placed in a Mr Frosty cooling device (Thermo scientific, Loughborough, UK) which was prefilled with isopropanol and pre-chilled at -80°C. The Mr Frosty chills cells at ~1°C/minute for optimal cell survival. Cryovials were left overnight following which they were either left at -80°C or submerged in liquid nitrogen for long term storage.

### ***2.3.8 Cell stock revival***

Cryovials were removed from storage and placed in a water bath preheated to 37°C. Once thawed, 1ml of complete culture medium was added to the cryovial and the cryovial contents were carefully pipetted into 20ml of complete culture medium in a T75<sup>2</sup> flask. The cells were incubated under normal conditions as outlined in 2.3.1 until cells had adhered to the culture flask (4-8 hours). The culture medium was then aspirated, fresh medium added and the cells returned to the incubator. Medium was renewed the following day.

### ***2.3.9 Determining cell number***

Following trypsinisation and pelleting as described in 2.3.6, cells were re-suspended in a defined volume of medium (1-10ml). An aliquot of 100µl of the cell suspension was then diluted 1:1 (v/v) in 0.4% (w/v) trypan blue in PBS. 50µl of the cell:trypan blue solution was then pipetted onto a haemocytometer counting grid. The number of cells in 4-16 small squares was counted (depending on cell density). 3 counts were taken per

sample and averaged. The number of viable cells excluding trypan blue (i.e. colourless cells) per ml was then calculated as follows:

$$\text{Cell number ml}^{-1} = \text{average cell count} \times 2 \times \frac{16}{\text{no. of squares counted}} \times 10^4$$

The cell suspension was then diluted as necessary based on the count.

### ***2.3.10 Measuring cell viability by trypan blue exclusion***

Trypan blue is excluded by cells with an intact plasma membrane (live cells), whereas compromised or dead cells fail to exclude the dye, turning them blue. Therefore, by counting the number of colourless and then blue cells, the viability of a cell suspension can be calculated. To measure cell viability, when trypsinising cells as in 2.3.6, instead of discarding the original culture medium, it was pipetted into a 50ml centrifuge tube. Following cell detachment using trypsin-EDTA, the detached cells were added to the original culture medium and centrifuged at 800g for 5 minutes. The supernatant was discarded and the pellet re-suspended in culture medium. Either an aliquot of this suspension or all was mixed 1:1 (v/v) with 0.4% (w/v) trypan blue in PBS and 50 $\mu$ l pipetted onto the grid of a haemocytometer. 4-16 small squares were counted in three different regions of the grid and the number of colourless (viable) and blue cells (non-viable) counted. The viability was then calculated as follows:

$$\% \text{ viability} = 100 \times \left( \frac{\text{mean no. of viable cells}}{\text{Total cell number}} \right)$$

### ***2.3.11 B-13 transdifferentiation***

B-13 cells were cultured in 10nM DEX to transdifferentiate them to hepatocyte-like cells. DEX was added to their culture medium from a 1000x concentrated stock solution (10 $\mu$ M in ethanol). B-13 cells treated with DEX were cultured like normal B-13 cells as per 2.3.1 with medium and DEX changed every 2-3 days. Within 4-7 days hepatocyte-like cells began to appear. B-13 cells were considered transdifferentiated to hepatocyte-like cells (B-13/H) and ready for experiments following 14 days of culture in 10nM DEX unless otherwise specified.

### ***2.3.12 CYP450 induction***

For induction studies, cells were routinely dosed daily with inducing agents for 3 days, with a medium change every day. Cells were harvested on day 4 (24 hours after the last treatment with inducer). Inducers were used at the following final concentrations:  $\beta$ -NF, 20 $\mu$ M; androstrenol, 5 $\mu$ M; PB, 1mM; TCPOBOP, 1.5 $\mu$ M; DEX, 10 $\mu$ M; pregnenolone-16 $\alpha$ -carbonitrile (PCN), 2 $\mu$ M; bezafibrate, 250 $\mu$ M.

### ***2.3.13 Alvetex culture***

Alvetex scaffolds (AMS Biotechnology, Abingdon, UK) were briefly washed in 70% ethanol then PBS to prepare for cell seeding.  $1 \times 10^6$  cells were seeded onto the alvetex in a volume of 150 $\mu$ l and initially left for 1.5 hours for the cells to adhere. Following this incubation, 10ml of complete growth medium was added and the cells cultured as outlined in 2.3.1. Transdifferentiation was carried out by addition of 10nM DEX to the culture medium as outlined in 2.3.11.

### ***2.3.14 PU134 culture***

B-13 cells were seeded on to PU134 coated slides in 24 well plates at  $3 \times 10^4$  cells/well following which they were cultured as described in 2.3.1.

## **2.4 Cell transfection, adenoviral titration and infection**

### ***2.4.1 Effectene transfection***

For stable transfection, cells were transfected using effectene (Qiagen, Manchester, UK) in T75<sup>2</sup> flasks essentially following the manufacturer's guidelines under normal culture conditions. Effectene forms a cationic complex with DNA, promoting transfer through the cell plasma membrane facilitating transfection of DNA. Enhancer, EC buffer and plasmid DNA were mixed at a ratio of 10 $\mu$ l enhancer: 150 $\mu$ l buffer: 1 $\mu$ g DNA and briefly mixed using a vortex. Following a 5 minute incubation at room temperature, 15 $\mu$ l of effectene was added per 1 $\mu$ g of DNA and vortexed again. After 15 minutes at

room temperature, the master mix was added dropwise to cells 60-70% confluent in fresh medium. Transfected cells were cultured for 48 hours under standard conditions after which they were washed in PBS and fresh medium added.

#### 2.4.2 Generation of stably transfected cell lines

Transfected cells were cultured in medium containing the appropriate selection agent for 7-14 days until the majority of cells had died leaving small numbers of resistant colonies. For the cells transfected with the pcDNA6/TR vector (Invitrogen), selection was carried out by treating transfected cells with 8 $\mu$ g/ml blasticidin which was determined to be the optimal concentration (figure 2.1). B-13 cells transfected with human CYP1A2 (in the pT-REX-DEST30 vector, Invitrogen) were selected using 400 $\mu$ g/ml geneticin which has been used previously in B-13 cells to select stable transformants (personal communication).

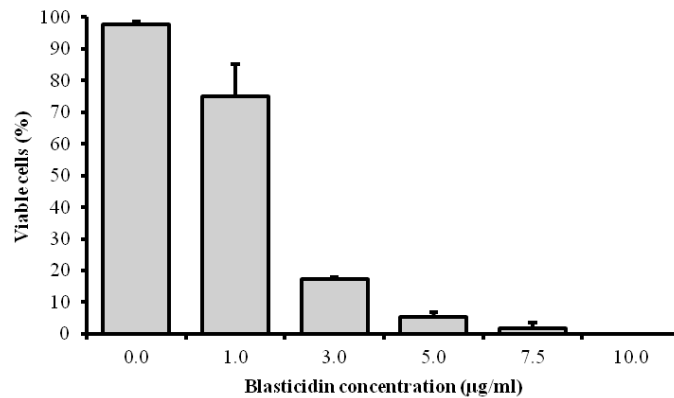


**Figure 2.1: B-13 blasticidin kill curve.** B-13 cells were treated with the indicated concentrations of blasticidin for 3 consecutive days. Absolute viability was then determined for each treatment by trypan blue exclusion. Results are the mean and SD of 3 independent determinations from the same experiment.

#### 2.4.3 Adenovirus titration – plaque assay

HEK293 cells were seeded into 6 well plates at  $1 \times 10^5$  cells/ well and cultured as per 2.3.3 until approximately 80% confluent. Viral stocks to be titred were serially diluted between  $10 \times 10^{-4}$  –  $10^{-9}$ . Medium was removed from the HEK293 cells and 300 $\mu$ l of each adenoviral dilution added to each well and the plate gently rocked to ensure coverage of all cells by the viral solution. Cells were then returned to the incubator and cultured per normal for 1 hour. During this incubation, a 5% agarose solution in PBS

was melted and cooled to approximately 45°C. Complete growth medium was pre-heated to 45°C also. After the 1 hour incubation, the viral dilutions were aspirated from the cells. The 5% agarose solution was diluted to 0.5% in the complete growth medium and 2ml of this solution was added per well and left to set. Once set, 2ml of complete growth medium was added per well and the cells cultured as per 2.3.3 for 7-10 days. After this time the medium was removed and replaced with a 0.03% (w/v) solution of neutral red in PBS and incubated for 2 hours to stain living cells. The neutral red solution was aspirated and the number of plaques counted. The titre of the virus was then calculated using the following equation, from the dilution which gave between 15-150 plaques per well:

$$\frac{\text{\# of plaques}}{\text{dilution factor} \times 0.3} = \text{pfu/ml}$$

#### ***2.4.4 Determining multiplicity of infection (MOI)***

Cultured cells were infected with Ad-GFP (adenovirus encoding green fluorescent protein) serially diluted over 3 logs (i.e.  $10^0$  to  $10^{-3}$ ). The following day, cells were imaged using a fluorescence microscope and the percentage of cells positive for green fluorescent protein (GFP) per field calculated. The number of plaque forming units (pfu) required for >85% infection efficiency was then calculated from this using the known viral titre, determined by a plaque assay (see 2.4.3), to give the MOI.

#### ***2.4.5 Adenoviral infection of cells***

Per experiment, the number of cells in each well was calculated from a single well as per 2.3.9. Using this and the known MOI of the cell line, the volume of virus to be added per well was calculated. This was then added per well and the cells cultured as per normal for 24 hours. At this point the medium was changed to remove all virus and the cells cultured as normal (5% CO<sub>2</sub> and 37°C) until required. Ad-SGK1F encoding human SGK1F and Ad-FOXA2, encoding human forkhead box protein A2, were from Vector Biosystems (Philadelphia, USA). For all adenoviral constructs used, overexpression of the virus encoded protein coding sequence in infected cells was driven by a linked constitutively active promoter.

## 2.5 Plasmid DNA constructs and sequencing

### 2.5.1 *Competent cell transformation*

Plasmid DNA was replicated in TOP10 cells (Invitrogen). When required, TOP10 cells were thawed on ice and 2µl of TOPO cloning reaction was added to the vial after which the cells were incubated on ice for 30 minutes. The cells were then heat shocked in a water bath, equilibrated at 42°C, for 30 seconds without shaking. Heat shocked cells were transferred to ice and 250µl of super optimal broth (20mM glucose, 10mM NaCl, 2.5mM KCL, 10mM MgCl<sub>2</sub>, 10mM MgSO<sub>4</sub>, 2% tryptone and 0.5% yeast extract) added to the vial. The vials were then placed in a 37°C incubator shaking at 200rpm for 1 hour. The transformed cells were spread onto 2 agar plates containing the appropriate selection agent (kanamycin 25µg/ml or ampicillin 100µg/ml); one plate was spread with 20µl and the other with 200µl. The plates were incubated overnight at 37°C.

The next morning a colony was picked and placed into 5ml of Luria-Bertani medium (LB, 10g/L NaCl 10g/L tryptone and 5g/L yeast extract) with antibiotics as required and incubated overnight at 37°C shaking at 220rpm. The following day the cells were either mini- or maxi-prepped or frozen down as outlined in 2.5.2, 2.5.3 and 2.5.4 respectively.

### 2.5.2 *Mini-prep isolation of plasmid DNA*

Isolation of plasmid DNA was carried out using Qiagen Qiaprep Miniprep spin columns to rapidly isolate pure plasmid DNA from ~5ml of bacteria in LB. The purification works by the alkaline lysis of bacterial cell walls followed by the adsorption of plasmid DNA onto a permeable silica membrane under high salt conditions [166]. Contaminating RNA is removed by RNase in buffer P1.

DNA was isolated essentially as per the manufacturer's protocol. 5ml of culture was centrifuged in eppendorf tubes at 16,000g for 1 minute. The supernatant was discarded and the pellet re-suspended in 250µl of buffer P1 following which 250µl of buffer P2 was added (salt solution with sodium dodecyl sulphate). The tube was inverted to produce a clear solution to which 350µl of buffer N3 was added (containing acetic acid to neutralise alkaline lysis buffer) and rapidly inverted. The cloudy solution was

centrifuged for 10 minutes at 16,000g to pellet cell debris and genomic DNA. The supernatant was pipetted into a Qiaprep spin column and centrifuged for 1 minute at 16,000g. The flow through was discarded and 500µl of buffer PB added to the column which was then centrifuged again as before. The flow through was discarded and 750µl of buffer PE added to the column which was centrifuged at 16,000g for 1 minute. The flow through was discarded and the column centrifuged once more for 1 minute to remove residual residue. The column was transferred to a nuclease free eppendorf and 50µl of nuclease free water added directly to the column membrane. The column was left to stand for 1 minute then centrifuged for 1 minute at 16,000g to elute the plasmid DNA. Plasmid DNA was then quantified spectrophotometrically as described in 2.6.2.

### ***2.5.3 Maxi-prep isolation of plasmid DNA***

To purify large quantities of plasmid DNA (up to 500µg), a maxi-prep was carried out using the Qiagen Maxiprep kit. It is based on the same theory as the miniprep but designed to produce larger yields.

250ml of overnight culture in a 1L Erlenmeyer flask was decanted to 50ml centrifuge tubes and centrifuged at 6,000g for 10 minutes at 4°C. The pellets were re-suspended and combined in 10ml of buffer P1 (RNase containing) and 10ml of buffer P2 was then added and mixed by inversion. This solution was left to stand for 5 minutes following which 10ml of buffer P3 was added (pre-chilled on ice) and mixed by inversion. This was left on ice for 20 minutes and subsequently centrifuged at 6,000g for 30 minutes at 4°C. The supernatant was then applied to a Qiagen-tip 500 column that had been equilibrated by the addition of 10ml of buffer QBT left to drain through. The supernatant was left to enter the column after which the column was washed 2 times with 30ml of buffer QC. The flow through was discarded. The plasmid DNA was eluted by the addition of 15ml of buffer QF into a 50ml centrifuge tube and precipitated by the addition of 10.5ml of absolute isopropanol. The sample was inverted to mix then centrifuged at 6,000g for 30 minutes at 4°C. The supernatant was discarded and the pellet washed with 70% ethanol. After another centrifugation step (6,000g for 30 minutes at 4°C), the supernatant was all removed and the DNA pellet left to air dry for 10 minutes. The pellet was then re-suspended in nuclease free water and quantified as per 2.6.2.

#### ***2.5.4 Storage and thawing of transformed bacteria***

TOP10 cells transformed with plasmid DNA were stored long term as glycerol stocks at -80°C. 500µl of an overnight culture, picked from a single colony, was diluted 1:1 (v/v) with sterile LB containing 30% (v/v) glycerol then transferred to a cryovial, labelled and frozen long term at -80°C.

When required, previously stored bacteria were thawed and a small volume (20-30µl) streaked out on an agar plate supplemented with the appropriate antibiotic to select for transformed bacteria. The glycerol stock was then returned to the -80°C freezer for storage. After incubation overnight at 37°C, a single colony was picked from the plate and grown up overnight in LB, with antibiotics as required, and plasmid DNA purified using a miniprep (2.5.2) or maxiprep (2.5.3).

#### ***2.5.5 DNA extraction from agarose gel***

DNA subject to agarose gel electrophoresis (see 2.6.8) was imaged using a UV light box and the band of interest excised using a sterile scapel blade, weighed and placed into a nuclease free eppendorf tube. The DNA was then extracted using a QIAquick gel extraction kit (Qiagen) which, similar to the miniprep system, utilises the adsorption of DNA onto a silica membrane under high salt concentrations. 3 volumes of buffer QG was added to the plasmid DNA in an eppendorf. This was placed in a heat block set at 50°C for ~10 minutes until melted. One volume of absolute isopropanol was then added and mixed and the entire solution applied to a gel extraction column. The column was centrifuged at 16,000g for 1 minute and the flow through discarded. 750µl of buffer PE was then added to the column and centrifuged again as before to wash the DNA. The flow through was discarded and the column centrifuged dry at 16,000g for 1 minute to remove residual buffers. The DNA was eluted by the application of 30µl of nuclease free water to the centre of the silica membrane. After standing for 1 minute the column was centrifuged at 16,000g for 1 minute. The flow through was then reapplied to the membrane and centrifuged once more to increase yield. The eluted DNA was quantified as detailed in 2.6.2.

### 2.5.6 TOPO cloning

DNA was cloned into a gateway vector (pENTR/D-TOPO) using the TOPO cloning system (Invitrogen) as outlined in figure 2.2. This system utilises *Vaccinia* topoisomerase I which cleaves the phosphodiester backbone of duplex DNA at 5'-(C/T)CCTT-3' sequences and binds the 3' thymidine [167]. The DNA sequence to be cloned was amplified using primers that add a 5' complementary sequence (CACC). The vector contains an overhang which binds the DNA in only one orientation facilitating directional cloning into the vector. The topoisomerase can then ligate the DNA and plasmid together using the energy stored from the original cleavage.

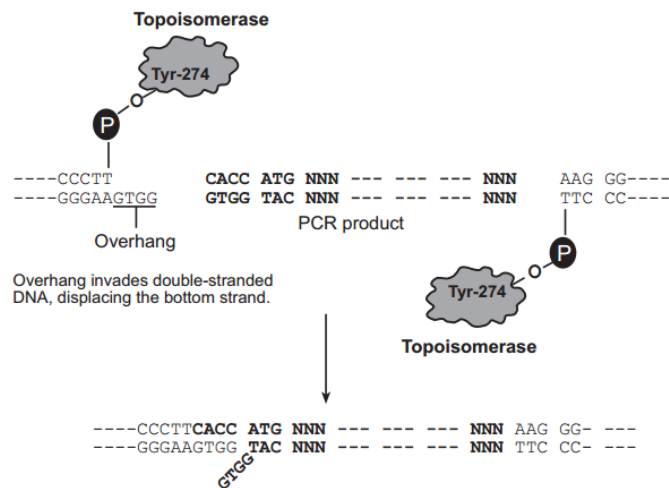


**Figure 2.2: TOPO cloning system.** From [http://tools.invitrogen.com/content/sfs/manuals/pentr\\_dtopo\\_man.pdf](http://tools.invitrogen.com/content/sfs/manuals/pentr_dtopo_man.pdf)

Following insertion into the gateway vector, the insert was transferred to a destination vector using a LR recombination reaction (Invitrogen). This reaction utilises LR clonase to directionally transfer DNA between the gateway restriction sites attL1 and attL 2 to the destination vector with corresponding attR1 and attR2 sites in a single quick reaction.

Target DNA sequences (containing the nucleotide sequence 5'-CACC-3' in the required orientation) were prepared by reverse-transcription polymerase chain reaction (RT-PCR) and cloned into the gateway pENTR/D-TOPO vector following the manufacturer's instructions. Briefly, DNA was mixed at a 1:1 molar ratio with the gateway vector (1µl of vector/reaction). 1µl of salt solution (1.2M NaCl and 60mM

MgCl<sub>2</sub>) was then added to the DNA followed by nuclease free water up to a final volume of 6µl. The reaction was mixed and incubated for 30 minutes at room temperature following which the vector was transformed as described in 2.5.1.

To transfer the DNA insert from the gateway vector to the destination vector (pT-REX-Dest30), 150ng of the pENTR/D-TOPO containing insert was mixed with 150ng of pT-REX-Dest30 and Tris-EDTA buffer pH 8.0 (10mM Tris, 1mM EDTA pH 8) up to 8µl. LR Clonase II enzyme mix (Invitrogen) was thawed on ice briefly then vortexed twice. 2µl was then added to the reaction and vortexed twice to mix. The reactions were incubated for 1 hour at 25°C then terminated by the addition of 1µl of proteinase K. The reaction was then transformed into TOP10 cells as per 2.5.1.

### ***2.5.7 Restriction digests***

Restriction of plasmid DNA was carried out essentially following the restriction enzyme manufacturer's guidelines (New England Biolabs, Hitchin, UK). Briefly, the reaction mixture was composed of 2µl 10x reaction buffer (optimal buffer determined based on restriction enzymes being used), 0.2µl of acetylated bovine serum albumin (BSA, 10µg/µl), up to 1µg of plasmid DNA, 0.5µl of restriction enzyme(s) and nuclease free water up to 20µl. This was incubated for 1 hour at 37°C. The samples were then mixed with DNA loading buffer and subjected to agarose gel electrophoresis as outlined in 2.6.8 to determine the size of fragments produced.

### ***2.5.8 Sequencing and analysis***

Miniprep plasmids were sequenced by DNAseq (Dundee, UK) using either M13 or sequence specific primers. Sequencing chromatograms were analysed using Sequence Scanner Software v1.0 (Applied Biosystems, Paisley, UK).

The B-13 genomic sequence was analysed using the Integrative Genomic Viewer software [168]. The sequence was aligned to the Wistar rat genome reference assembly RN4.

## 2.6 Isolation of RNA and quantification

### 2.6.1 RNA isolation

Total RNA, from cell and tissue samples, was isolated using TRIzol (Invitrogen) essentially following the recommended protocol. TRIzol is a monophasic solution of guanidine isothiocyanate and phenol which allows for the 3 step isolation of RNA by isolation, precipitation and washing. The underlying principal is based on acid guanidinium thiocyanate-phenol-chloroform extraction [169].

To extract RNA from cells, after a PBS wash, cells were scraped and centrifuged at 16,000g for 1 minute to pellet after which 1ml of TRIzol was added and pipetted up and down. If the cells were cultured in 6 well plates, after the PBS wash, 1ml of TRIzol was added directly to the cells in the well and left on an orbital shaker for 5 minutes. The TRIzol was then transferred to RNase free eppendorf tubes. After a 5 minute incubation, 200µl of chloroform was added and mixed by inversion. This was then centrifuged at 16,000g for 15 minutes to promote the formation of an aqueous phase, interphase and organic phase. RNA partitions in the aqueous phase whereas DNA and proteins are localised to the interphase and organic phases. The aqueous phase was transferred to a fresh tube and 500µl of isopropanol was added to precipitate the RNA. The tube was then mixed by inversion and left to stand on ice for 15 minutes. To pellet the RNA the tube was centrifuged at 16,000g for 10 minutes. The isopropanol was aspirated off and 1ml of 70% ethanol used to wash the pellet. The samples were centrifuged again as before and all the ethanol removed. After 5-10 minutes of air drying at room temperature the pellets were re-suspended in RNase free water. The RNA was then quantified as per 2.6.2 and frozen at -80°C until needed.

Tissue preparations were carried out following the same protocol but were prepared differently; tissues were snap frozen in TRIzol (in liquid nitrogen) immediately after culling and when needed were thawed on ice. The samples were then homogenised using a hand homogeniser and then briefly sonicated if required prior to RNA extraction.

### ***2.6.2 RNA and DNA quantification***

The peak absorbance of RNA and DNA is at 260nm. The optical density (OD) at 260nm using a 1cm pathlength is 1.0 for double stranded DNA at 50 $\mu\text{g ml}^{-1}$  and 40 $\mu\text{g ml}^{-1}$  for single stranded RNA. The concentration of nucleic acids in a pure solution can therefore be easily calculated by UV spectrophotometry.

To determine the quantity of RNA and DNA in samples, their absorbance at 260nm was measured using a Nanodrop 2000 spectrophotometer (Thermo Scientific) using RNase free water as the blank. The purity of samples was measured by calculating the OD<sub>260</sub>/OD<sub>280</sub> ratio. For pure nucleic acid samples this should be between 1.8-2.1. Lower ratios suggest contamination, likely by phenol or protein. A peak absorbance at 270nm rather than 260nm indicates significant phenol contamination [170].

### ***2.6.3 DNase I treatment of RNA***

To remove contaminating genomic DNA from TRIzol purified RNA, samples were routinely treated with RQ1 RNase-free DNase (Promega, Southampton, UK). DNase selectively hydrolyses the phosphodiester backbone of single and double stranded DNA to degrade DNA whilst leaving RNA intact.

8 $\mu\text{l}$  of RNA was added to 1 $\mu\text{l}$  of 10x RQ1 buffer (400mM Tris-HCl pH 8.0, 100mM MgSO<sub>4</sub> and 10mM CaCl<sub>2</sub>) and 1 $\mu\text{l}$  of RQ1 RNase free DNase. The reactions were mixed by pipetting and incubated at 37°C for 30 minutes. 1 $\mu\text{l}$  of stop solution (20mM EGTA pH 8.0) was then added and incubated at 65°C for 10 minutes to deactivate the DNase.

### ***2.6.4 RNA cleanup using RNeasy columns***

To remove contaminating DNase from samples following DNase treatment for PCR array plates (see 2.6.11), samples were cleaned using RNeasy columns (Qiagen). RNeasy columns utilise the selective binding of mRNA (>200 base pairs in length) to a silica membrane under high salt conditions.

Following DNase treatment of RNA (as detailed in 2.6.3), the RNA solution was made up to 100µl with RNase free water, following which 350µl of buffer RLT was added and mixed. 250µl of absolute ethanol was added and mixed by inversion. The RNA solution was then transferred to an RNeasy spin column, incubated for 2-5 minutes then centrifuged at 16,000g for 15s and the flow through discarded. 500µl of buffer RPE was added to the column which was centrifuged for 15s at 16,000g and the flow through was discarded. This step was then repeated to remove any residual buffer. The RNeasy spin column was transferred to a fresh RNase free eppendorf and 30µl of RNase free water applied directly to the membrane to elute the RNA. This was left to stand for 1 minute then centrifuged for 1 minute at 16,000g. The RNA was then quantified as per 2.6.2 and frozen at -80°C until needed.

### ***2.6.5 1<sup>st</sup> strand synthesis and reverse transcription of RNA***

Reverse transcription was carried out using Moloney Murine Leukemia Virus reverse transcriptase (M-MLV), a RNA-dependent DNA polymerase, essentially following the manufacturers guidelines (Promega). Briefly, DNase treated RNA was diluted to 200ng/µl and 5µl (i.e. 1µg total) transferred to a 200µl reaction tube. 1µl of 50ng/µl random primers (Promega) were added to each tube, mixed by pipetting and incubated at 90°C for 3 minutes. Incubation at 90°C melts the RNA secondary structure and following this, the temperature was brought down quickly to 4°C to allow annealing of the random primers to the RNA.

To the 1<sup>st</sup> strand synthesis reactions on ice was added 14µl of reverse transcription mastermix. This was composed of 2µl 10mM dNTPs (Promega), 4µl of 5x M-MLV buffer (50mM Tris-HCl pH 8.3, 3mM MgCl<sub>2</sub>, 75mM KCl, and 10mM DTT), 7µl of nuclease free water and 1µl of M-MLV. The reverse transcription reactions were incubated for 1 hour at 42°C after which they were diluted accordingly (usually to 10-20ng/µl) with nuclease free water and frozen at -20°C

### ***2.6.6 Polymerase chain reaction (PCR)***

PCR is a technique which uses thermostable DNA polymerases and thermal cycling to rapidly and accurately amplify target DNA sequences. As summarised in figure 2.3,

during a cycle of PCR, double stranded DNA is separated at high temperatures (95°C) then short '5-3' oligonucleotides (upstream and downstream primers) anneal complementary cDNA at a target sequence to be amplified. Thermostable DNA polymerase then binds and elongates the DNA strand 5'-3'. In principle, the abundance of the target sequence (the amplicon) should double every cycle (i.e. exponentially) meaning that, very rapidly, a huge amount of amplicon is generated which can be visualised by agarose gel electrophoresis (detailed in 2.6.8)

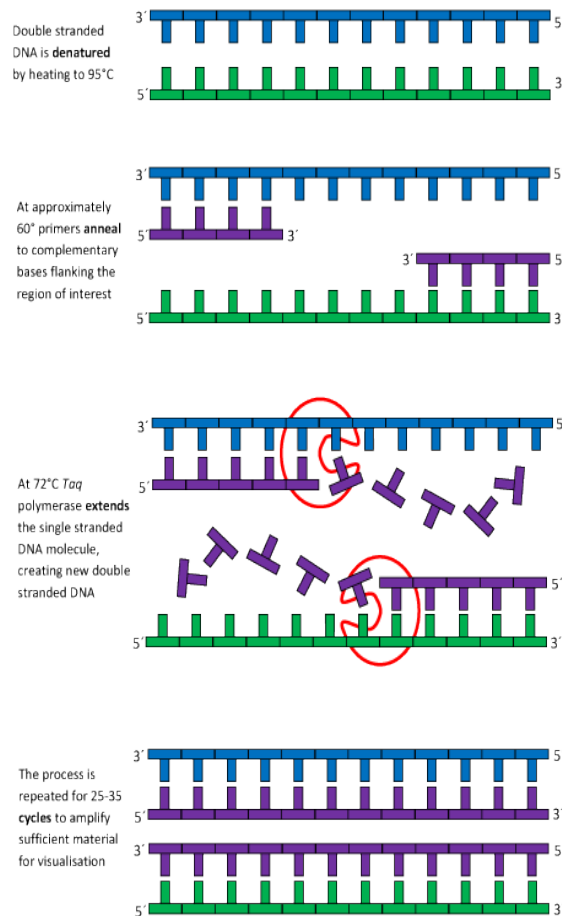


**Figure 2.3: The events of a PCR cycle.** From <http://www2.le.ac.uk/departments/emfpu/genetics/explained/images/PCR-process.gif>

Semi-quantitative PCR was routinely carried out using GoTaq green 2x mastermix (Promega), which contains Taq polymerase. For cloning work, *Pfu* DNA polymerase (Promega) was used as this has 3'-5' exonuclease proofreading capability. The mutation rate of Taq is approximately one error per  $2.0 \times 10^5$  base pairs whereas for *Pfu* the error rate is only one error per  $1.6 \times 10^6$  base pairs, due to its proofreading activity [171].

Using GoTaq green, the reaction mix for PCR, made up on ice, was as follows: 10-40ng of cDNA was added to 10µl of GoTaq green 2x mastermix, 2µl each of upstream and downstream primers (from 10µM primer stocks, 1µM final concentration) and nuclease free water up to 20µl.

For *Pfu*, the reaction was composed on ice as follows: 40-100ng of cDNA was added to 5µl of 10x *Pfu* buffer (200mM Tris-HCl (pH 8.8 at 25°C), 100mM KCl, 100mM (NH<sub>4</sub>)<sub>2</sub>SO<sub>4</sub>, 20mM MgSO<sub>4</sub>, 1% (v/v) Triton X-100 and 1µg/µl BSA), 1µl 10mM dNTPs, 5µl of forward and reverse primers (from 10µM primer stocks, 1µM final concentration) and nuclease free water up to 49.3µl. 0.7µl *Pfu* was then added and mixed by pipetting.

Once samples were prepared, thermal cycling was carried out using a Px2 (Thermo Scientific) thermocycler. The programme used varied according to the primers used (listed in appendix A) but was essentially as follows:

<b>Initial denaturation</b>	-	95°C	1 minute
Then 30-35 cycles of:			
<b>Denature</b>	-	95°C	1 minute
<b>Anneal</b>	-	X°C	30s
<b>Elongate</b>	-	72°C	1 minute per Kbp (GoTaq) 2 minutes per Kbp ( <i>Pfu</i> )
<b>Final elongation</b>	-	72°C	5 minutes
<b>Hold</b>	-	4°C	∞

Annealing temperature was optimised according to individual primer pairs but was 55°C in most cases. After the run was complete samples were stored at 4°C.

### 2.6.7 Fusion PCR

To amplify sequences greater than 1Kbp using *Pfu*, which would not amplify in a single reaction, both halves of the sequence were amplified in separate reactions then fused in

a third reaction as illustrated in figure 2.4. The primers were designed so that the 5'-3' sequence of the 1<sup>st</sup> fragment was complementary to the 3'-5' sequence of the 2<sup>nd</sup> fragment. Following amplification of a fragment by *Pfu*, the PCR products were separated using agarose gel electrophoresis (see 2.6.8) and the correct size product gel purified (see 2.5.5). When both fragments were amplified and purified, fusion PCR was run using *Pfu* DNA polymerase as before but using a modified method. Specifically, *Pfu* reactions were set up using equimolar amounts of the DNA sequences to be fused (50ng total) and run for 10 cycles without either the forward or reverse primers to allow the fragments to anneal at their complementary ends and prime one another for elongation by the polymerase. After 10 cycles the primers were added and the PCR run for another 25 cycles. Agarose gel electrophoresis and gel extraction was used to separate and purify the completed sequence from any fragment left over.

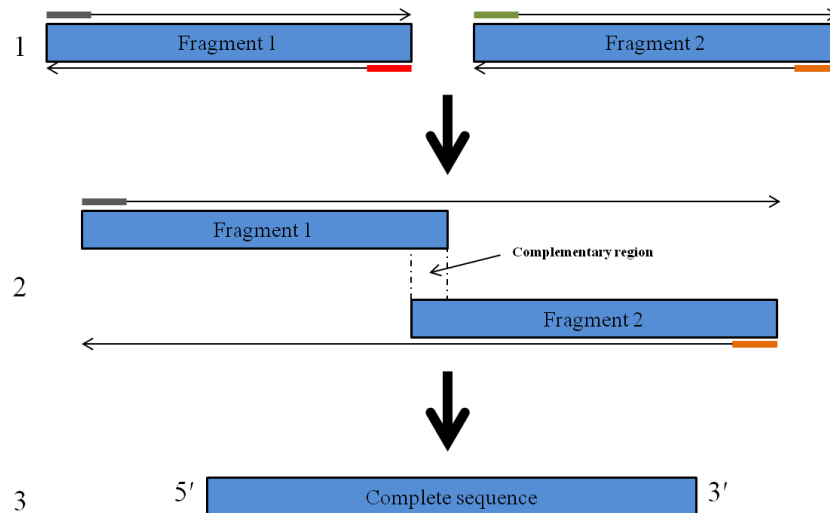


**Figure 2.4: The steps of fusion PCR.** First the two halves of the complete sequence are amplified in 2 separate reactions using primers that give complementary ends. The 2 fragments are separated using electrophoresis and purified. In the fusion PCR reaction, the two fragments anneal and are amplified to produce a complete sequence.

### 2.6.8 Agarose gel electrophoresis

When DNA is placed within an electric field, it migrates towards the positive electrode because the sugar phosphate backbone of DNA is negatively charged. All DNA migrates towards the anode, but larger fragments experience more resistance in a polymerised agarose matrix and therefore migrate at a slower rate. This is exploited in agarose gel electrophoresis to separate DNA fragments by size. PCR reactions were routinely separated in 1-2% agarose (1-2% (w/v) agarose and 5µg/ml ethidium bromide

in TAE (40mM Tris, 20mM acetic acid, 1mM EDTA)). The gels were prepared by boiling the TAE and agarose together in a microwave until dissolved then left to cool. Once cool enough to hold, the ethidium bromide was added. Gels were then cast in a casting stand and a comb added to form wells. This was then left to set prior to electrophoresis. To resolve amplicons greater than 400bp, a 1% agarose gel was used; for amplicons smaller than 400bp, a 2% agarose gel was used.

Prior to electrophoresis, 9µl of 6x DNA loading dye (Promega) was added per *Pfu* PCR reaction and mixed. This was required so that samples sank to the bottom of the wells. GoTaq PCR reactions did not need DNA loading dye added because the mastermix already contained it. 10µl of reaction was generally loaded into an agarose gel alongside 100bp or 1Kbp DNA ladder (New England Biolabs) and separated for 30-45 minutes at 90V. TAE, sufficient to cover the gel, was used as the running buffer. Once amplicons were resolved, they were imaged using a G:BOX transilluminator and bundled software.

### **2.6.9 Quantitative real-time PCR**

In principle, per PCR cycle, each template of DNA produces 2 copies. This principle is utilised in real-time PCR to quantitatively measure the amount of target DNA in different samples. SYBR green is a dye that is fluorescent when bound to double stranded DNA and therefore, by measuring its fluorescence, the amount of target DNA can be measured in real time during PCR.

A quantitative real-time PCR (qPCR) mastermix was prepared by mixing 6.5µl of SYBR Green JumpStart Taq ReadyMix, forward and reverse primers to final optimised concentration (between 125-250nM) and nuclease free water up to a volume of 12µl per well. 12µl of mastermix was added per well of an optical 96 well reaction plate (Applied Biosystems) and 1µl of cDNA added (usually from a 10ng/µl stock). The plates were sealed using optical film (Applied Biosystems) and centrifuged at 300g for 1 minute to collect samples at the bottom of the wells. Plates were then either run immediately or stored at -80°C for up to a week. Plates were run in a 7500 Fast real-time PCR thermocycler (Applied Biosystems) using the included software (SDS 2.0.6). The run method was as follows:

**Initial denaturation** - 95°C 5s

Then 40 cycles of:

**Denature** - 95°C 5s

**Anneal** - X°C 30s

**Elongate** - 72°C 30s

The annealing temperature was optimised for each primer pair. Following the cycling, melt curve analysis was run using the default software programme. SYBR green fluorescence was measured during the extension phase of cycling. Once the run was complete, the cycle threshold ( $C_T$ ) was set manually by setting the threshold in the lower half of the exponential phase of amplification.

Relative amounts of target DNA were calculated using the comparative  $\Delta\Delta C_T$  method using 18S ribosomal RNA (18S rRNA) as the housekeeping control. Relative expression was calculated as follows:

$$\Delta C_T = C_T \text{ target} - C_T \text{ 18S rRNA}$$

$$\Delta\Delta C_T = \Delta C_T \text{ sample} - \Delta C_T \text{ control}$$

$$\text{Fold change} = 2^{-\Delta\Delta C_T}$$

Standard deviation was calculated as described by Yuan *et al.*, (2006) [172] from the  $\Delta\Delta C_T$  values as follows:

$$\text{Positive SD value} = 2^{-(\Delta\Delta C_T \text{ Avg} - \text{SD}(\Delta\Delta C_T \text{ Avg}))} - \text{fold change}$$

$$\text{Negative SD value} = \text{fold change} - 2^{-(\Delta\Delta C_T \text{ Avg} + \text{SD}(\Delta\Delta C_T \text{ Avg}))}$$

### 2.6.10 Primer design

Nucleotide sequences were downloaded from the NCBI database ([www.ncbi.nlm.nih.gov](http://www.ncbi.nlm.nih.gov)) and primer-blast was then used to design primer sequences for RT-PCR. In general, primers were designed so that they had minimal complementarity with themselves and their pair. They were 18-25 bases in length, with 40-60% guanine

and cytosine content and with an annealing temperature within 1-2°C of one another. Where possible, they were also designed to span an exon-exon junction. For normal PCR, primers were designed to amplify a sequence of 200-600bp whereas for qPCR the target amplicon size was 50-200bp.

### ***2.6.11 PCR array plates***

PCR arrays (SAbiosciences, Crawley, UK) were used to perform rapid quantitative RT-PCR screens for related transcripts. The arrays were used as outlined in the manufacturer's protocol, firstly by preparing cDNA using the RT<sup>2</sup> first strand kit (SAbiosciences). Briefly, 1µg total RNA was added to 2µl of genomic DNA elimination buffer and water up to 10µl. This was then incubated at 42°C for 5 minutes then placed on ice. A reverse transcription mastermix was prepared by combining 4µl of 5x buffer BC3, 1µl of control P2, 2µl of RE3 reverse transcriptase mix and 3µl of water per reaction. 10µl of this mix was added to the DNA eliminated RNA solution and mixed by pipetting. The reaction was subsequently incubated at 42°C for 15 minutes, then the reverse transcriptase deactivated by incubation at 95°C for 5 minutes. Finally 91µl of nuclease free water was added and mixed. The qPCR mastermix was then immediately prepared by mixing 102µl of cDNA, 1350µl of 2x RT<sup>2</sup> SYBR green mastermix (SAbiosciences) and 1248µl of RNase free water. This was mixed by pipetting and 25µl added to each well of the PCR array plate which was sealed with optical film and centrifuged at 300g for 1 minute. The plate was run in a 7500 Fast thermocycler using the included software with the following settings:

1 cycle of:

<b>Initial denaturation</b>	-	95°C	10 minutes
-----------------------------	---	------	------------

Then 40 cycles of:

<b>Denature</b>	-	95°C	15s
-----------------	---	------	-----

<b>Anneal and elongate</b>	-	60°C	60s
----------------------------	---	------	-----

Followed by melt curve analysis

Following the end of the run the  $C_T$  values were calculated as described in 2.6.9 and the excel-based PCR array data analysis template used to analyse the data (available at <http://www.sabiosciences.com/pcrarraydataanalysis.php>).

## **2.7 Protein isolation and analysis**

### ***2.7.1 Cell lysate preparation***

Cultured cells were washed once in PBS then scraped into 1ml of ice cold PBS. The samples were centrifuged at 16,000g for 1 minute and the pellet re-suspended in an appropriate volume of 20mM Tris (pH 7.5). Samples were then quantified by Lowry assay (2.7.3) and frozen as aliquots at -80°C until required.

### ***2.7.2 Tissue lysate preparation***

Tissue from culled animals was flash frozen in liquid nitrogen then stored at -80°C until needed. When required, it was thawed on ice and rinsed in PBS to remove any blood. The tissue was then homogenised by hand and sonicated in 20mM Tris (pH 7.5). Samples were quantified by Lowry assay (2.7.3) and frozen at -80°C until required.

### ***2.7.3 Lowry assay***

The Lowry assay was used to determine protein concentration [173]. The mechanism is that, under alkaline conditions, copper reacts with peptide bonds. Folin-ciocalteu reagent is then added which is reduced, through a poorly understood mechanism, to produce a blue colouration. The intensity of colour is proportional to the amount of protein present at 750nm. With the use of protein standards, the concentration of protein in samples can therefore be easily calculated.

Assay buffers were prepared fresh each time. Buffer ABC was made up as follows: Lowry A (2% (w/v)  $\text{Na}_2\text{CO}_3$  and 4% (w/v) NaOH), Lowry B (2% (w/v) sodium tartrate) and Lowry C (1% (w/v)  $\text{CuSO}_4$ ) were combined at a ratio of 100:1:1 (v:v:v). Folin-ciocalteu was diluted 1:1 in distilled water prior to use. BSA was used as the protein standard and was made up in 20mM Tris (pH 7.5) in concentrations ranging from 0-

20mg/ml. To 5µl of standard or protein sample was added 50µl of distilled water and 1ml of buffer ABC. This was briefly vortexed and incubated at room temperature for 10 minutes. 100µl of diluted folin-ciocalteu reagent was added and mixed then incubated for 15-20 minutes until blue colouration was visible. The samples were then transferred to 1cm plastic cuvettes and OD<sub>750</sub> measured using the 0mg/ml standard to blank. The OD<sub>750</sub> of the standards was plotted against concentration and used to calculate the protein concentrations of samples using the equation  $y = m\chi + c$ .

#### ***2.7.4 Sodium-dodecyl sulphate polyacrylamide gel electrophoresis (SDS-PAGE)***

In 1970 Laemmli first described the use of SDS-PAGE to separate proteins based on their molecular weight [174]. This system of electrophoresis utilises sodium dodecyl sulphate (SDS), an anionic detergent. When a potential difference is applied to SDS bound polypeptides, they migrate towards the anode (due to the binding of negatively charged SDS) through the polyacrylamide gel at a rate proportional to their molecular weight, which allows for separation of proteins in a solution. The proteins are initially denatured to polypeptide chains by heating in the presence of SDS and the reducing agent DL-dithiothreitol (DTT) which reduces thiol groups, so that they lose their secondary, tertiary and quaternary structure which would otherwise interfere with migration.

SDS-PAGE was carried out using the Bio-Rad protean minigel system (Hereford, UK). Briefly, front and back glass plates (0.75mm) were clamped and petroleum jelly applied to the underside to prevent leakage. The polyacrylamide gel used is composed of a resolving gel and a stacking gel in which samples are loaded. Use of a stacking gel improves resolution as proteins accumulate at the stacking/resolving interface. Resolving gel acrylamide percentage varied according to the molecular weights of the proteins of interest but 9% was most commonly employed (optimally resolves ~20-100kDa). The stacking gel was always 4%. A 9% resolving gel was composed of 9% acrylamide/bis (w/v) (using acrylamide/bis-acrylamide, 37.5:1 ratio), 375mM Tris-HCL (pH 8.8), 0.1% (w/v) SDS, 0.05% (w/v) ammonium persulphate and 0.05% (v/v) tetramethylethylenediamine (TEMED) The ammonium persulphate and TEMED were added last as they catalyse the polymerisation of the acrylamide. 200µl of isopropanol was layered over the resolving gel whilst it set to create a level interface for the stacking

gel. Once the resolving gel had set (within 1 hour), the isopropanol was washed off with distilled water. The stacking gel consisted of 4% acrylamide/bis (w/v), 125mM Tris (pH 6.8), 0.1% (w/v) SDS, 0.1% (w/v) ammonium persulphate and 0.1% (w/v) TEMED. This was immediately poured over the resolving gel and a comb inserted into the polymerising gel to form wells. Once set, the glass plates were unclamped and either stored in electrode running buffer (25mM Tris, 0.1% (w/v) SDS and 192mM glycine, pH 8.3) at 4°C for 2-3 days or placed in a gel tank filled with electrode running buffer for immediate use.

Samples for SDS-PAGE were diluted at least 1:1 (v/v) in reducing loading buffer (120mM Tris (pH 6.8), 20% glycerol (v/v), 3.9% (w/v) SDS, 0.74% (w/v) bromophenol blue and 20mM DTT) and heated at 95°C for 5 minutes. Typically 20µg of protein was loaded per well alongside a ladder containing coloured proteins of known molecular weights (ColorBurst Electrophoresis Marker, molecular weight 8-220kDa). Electrophoresis was run at 100V until the migrating front reached the stacking/resolving interface at which point the voltage was increased to 160V. When the migrating front reached the bottom of the gel, the proteins were transferred to nitrocellulose for Western blotting (detailed in 2.7.5).

### ***2.7.5 Western blotting***

Western blotting describes the detection of specific proteins separated using SDS-PAGE using immunodetection. Whilst samples were being separated by electrophoresis, filter paper and nitrocellulose membrane (Fisher) were cut to size and incubated in pre-chilled transfer buffer (25mM Tris, 192mM glycine and 20% (v/v) methanol, pH 8.3). Following the end of SDS-PAGE, the plates were removed and the gel transferred to the nitrocellulose membrane. The gel and nitrocellulose membrane were sandwiched between filter paper and a scouring pad on both sides in a transfer cassette with the nitrocellulose membrane closest to the anode. A roller was used to remove air bubbles between the gel and nitrocellulose membrane. The cassette was placed in a tank filled with pre-chilled transfer buffer and an ice pack. Transfer was run for 2 hours at 100V.

After transfer, the nitrocellulose membrane was removed from the cassette and transfer buffer washed off by a rinsing in TBS-T (200mM NaCl, 20mM Tris (pH 7.4) and

0.05% (v/v) Tween 20, pH 7.4). The membranes were then blocked in 3% (w/v) skimmed milk powder in TBST-T for 1 hour at room temperature or 16 hours at 4°C to block non-specific antibody binding. After blocking, membranes were given 3 washes with TBS-T followed by 2 incubations in 10ml of TBS-T for 10 minutes. The membranes were then incubated in primary antibody (diluted in 0.3% (w/v) skimmed milk powder in TBS-T, see table 2.1 for dilutions) for 1 hour at room temperature or 16 hours at 4°C. The primary antibody solution was removed and then membranes washed as before. The appropriate secondary antibody (horseradish peroxidase (HRP) bound, diluted in 0.3% (w/v) skimmed milk powder in TBS-T) was added and left for 1 hour at room temperature. The secondary antibody was removed and the membrane was finally washed again as before.

To detect bound secondary antibody by HRP catalysed chemiluminescence, Pierce ECL Western blotting substrate (Thermo scientific) was used. 0.75ml of reagents 1 and 2 were added to the membrane and mixed briefly by rocking. The membrane was then blotted with tissue paper and sandwiched between saran wrap in a film cassette. CL-Xposure film (Thermo scientific) was exposed to the membrane in a dark room for varying degrees of time (dependent on antibodies used) then developed using an automated developer (RP X-OMAT, Kodak, Hertfordshire, UK). Following development, the position of the ladder proteins was marked on the film.

Nitrocellulose membranes in some cases were re-probed for an additional protein. After the initial probing, membranes were stripped by washing for 1 hour at room temperature in TBS-T, changing the TBS-T every 10 minutes. The membranes were then blocked and probed again as before.

## **2.8 Histochemistry and immunostaining**

### ***2.8.1 Paraffin embedded section preparation***

Tissue from freshly culled animals was fixed in 10% buffered formalin (3.7% (v/v) formaldehyde in PBS) for 24 hours then transferred to 70% ethanol for at least 24 hours. Fixed tissue was then processed and embedded and sequentially cut by microtome into 5µm sections onto Superfrost Plus slides (Fisher) and stored.

### ***2.8.2 Haematoxylin and eosin staining (H&E)***

Prior to staining of sections, they were first dewaxed by incubation in xylene for 10 minutes then rehydrated by incubation in 100% then 95% ethanol. Sections were incubated in haematoxylin for 1 minute which stains nuclei blue. The blue colour of haematoxylin was developed by incubation in Scott's tap water (2% (w/v) NaHCO<sub>3</sub> and 0.35% (w/v) MgSO<sub>4</sub> in distilled water) for 10s. After a wash in tap water, sections were stained in eosin for 15 seconds then again washed in tap water. Sections were dehydrated by incubation in an increasing ethanol gradient (50%, 75%, 90% and 100% (v/v)) each for 5 minutes followed by a 10 minute incubation in xylene. Sections were mounted using DPX and allowed to dry overnight prior to imaging.

### ***2.8.3 Sirius red staining of collagen***

At acidic pH, sirius red F3B specifically binds to basic amino acids in collagen due to its 6 sulphonic acid groups [175]. Fibrotic ECM is primarily composed of collagen; sirius red staining is therefore used to easily visualise fibrosis in tissue sections. Following dewaxing and dehydration as outlined in 2.8.1, sections were incubated for 1 hour in sirius red (0.001% (w/v) direct red 80 (Fisher) in saturated picric acid). The stain was then fixed by 2 washes in 0.5% (v/v) acetic acid in distilled water. Dehydration and mounting was then carried out as described in 2.8.2.

### ***2.8.4 Immunohistochemistry***

Following dewaxing and dehydration as described in 2.8.2, endogenous peroxidase activity was quenched in sections by an incubation in hydrogen peroxide (3% H<sub>2</sub>O<sub>2</sub> (v/v) in absolute methanol) for 15 minutes. After a wash in PBS for 5 minutes, sections were then subject to antigen retrieval which was either sodium citrate heat based (see 2.8.5) or trypsin protease based (see 2.8.6). Antigen retrieval was required because fixation can lead to cross-linking of amino acids, thereby masking the epitope. Antigen retrieval reverses some of this cross-linking improving the efficacy and specificity of immunostaining.

After antigen retrieval, a hydrophobic pen was used to outline the sections to keep solutions localised over the section. Sections were then blocked in 20% (v/v) FCS in PBS for 20 minutes at room temperature to block non-specific binding of antibodies followed by 3 PBS washes, each for 5 minutes. The primary antibody was incubated overnight at 4°C and was diluted in 0.05% (v/v) FCS in PBS (see table 2.1 for antibody details). To control for non-specific secondary antibody binding, a no primary antibody control (no primary) section was routinely stained alongside other sections and treated the same except that, during this primary antibody incubation period, it was incubated in diluent (0.05% (v/v) FCS) alone. The primary antibody was then washed off and the sections washed 3 times in PBS each for 5 minutes. The secondary antibody, diluted as for the primary antibody, was incubated for 1 hour at room temperature. This was then removed and washed as before with PBS. Antibody binding was detected using 3,3'-diaminobenzidine (DAB, Dako, Ely, UK) which is oxidised, in a peroxidase conjugated reaction, to a brown insoluble product, which can be imaged microscopically. The DAB substrate solution was made up by combining 1ml of substrate buffer with a drop of DAB+ chromagen solution. 200µl of this solution was added per section. The time for development varied depending on the antibody combination used and was optimised for each combination. Generally it was between 1 to 3 minutes. After the required development time, the sections were washed in a large volume of distilled water then counterstained in haematoxylin for 1 minute. Sections were then incubated in Scott's tap water for 10s, washed in tap water and dehydrated and mounted as previously described in 2.8.2.

Antigen	Approximate molecular weight (kDa)	Antibody raised in	Dilution	Source
<b>Primary antibodies</b>				
<b><math>\alpha</math>-SMA</b>	42	Mouse	1/250 IHC	Abcam (ab134813)
<b>Albumin</b>	60	Rabbit	1/3000 WB	Unknown
<b>Amylase</b>	55	Rabbit	1/3000 WB	Abcam (ab21156)
<b><math>\beta</math>-actin</b>	44	Mouse	1/3000 WB	Sigma (A1978)
<b>BrdU</b>	n/a	Mouse	1/50 ICC	BD bioscience (347580)
<b>CK-19</b>	40	Rabbit	1/250 IHC	Abcam (ab84632)
<b>CPS-I</b>	160	Rabbit	1/1000 WB	Abcam (ab3682)
<b>CYP reductase</b>	70	Rabbit	1/3000 WB	Santa Cruz (sc13984)
<b>CYP1A1/1A2</b>	56	Goat	1/3000 WB	Daiichi
<b>CYP2B1/2B2</b>	56	Mouse	1/1500 WB	Abcam (ab22721)
<b>CYP2C11</b>	57	Goat	1/3000 WB	Daiichi
<b>CYP2E1</b>	50	Rabbit	1/3000 WB 1/150 ICC	Abcam (ab28146)
<b>CYP3A1</b>	51	Mouse	1/3000 WB	Abcam (ab22724)
<b>CYP4A1</b>	50	Rabbit	1/1500 WB	Abcam (ab3573)
<b>HNF4<math>\alpha</math></b>	50	Goat	1/1500 WB	Santa Cruz (sc6556)
<b><math>\gamma</math>H2AX (S139)</b>	17	Rabbit	1/1000 WB	Abcam (ab2939)
<b>MRP2</b>	185	Mouse	1/100 WB	Santa Cruz (sc59608)
<b>NTCP</b>	38	Rabbit	1/200 WB	Abcam (ab85611)
<b>PCNA</b>	29	Mouse	1/300 IHC	Abcam (ab2426)
<b>PMP70</b>	70	Rabbit	1/3000 WB	Abcam (ab3421)
<b>SGK1</b>	50	Rabbit	1/1500 WB	Sigma (S5188)
<b>Vimentin</b>	58	Rabbit	1/250 IHC	Abcam (ab92547)
<b>Secondary antibodies</b>				
<b>Anti-mouse FITC</b>	n/a	Rabbit	1/50 Comet staining	Sigma (F9137)
<b>Anti-mouse HRP</b>	n/a	Goat	1/3000 WB 1/200 IHC	Dako (P0447)
<b>Anti-goat HRP</b>	n/a	Rabbit	1/200 WB	Sigma (A5420)
<b>Anti-rabbit FITC</b>	n/a	Sheep	1/200 ICC	Dako (F7512)
<b>Anti-rabbit HRP</b>	n/a	Goat	1/3000 WB 1/200 IHC	Dako (P0448)

**Table 2.1: Details of antibodies used** (abbreviations: ICC - immunocytochemistry, IHC – immunohistochemistry, WB – Western blot)

### ***2.8.5 Sodium-citrate antigen retrieval***

Sections were placed in 10mM sodium citrate pH 6.0 in a plastic rack then microwaved at high power for 20 minutes. The sodium citrate was topped up every 5 minutes to replace that lost by evaporation. After microwaving the sections were cooled down by slowly adding distilled water to the sodium citrate buffer. Once at room temperature immunostaining was continued.

### ***2.8.6 Trypsin antigen retrieval***

For protease antigen retrieval, a trypsin solution (0.1% (v/v) trypsin-EDTA in PBS) was pre-warmed at 37°C. Sections were then incubated in this solution for 30 minutes at 37°C prior to continuation of immunostaining.

### ***2.8.7 Fluorescence immunocytochemistry***

Cells in 6 well plates were washed twice in PBS then permeabilised with 2ml of ice cold absolute methanol at 4°C for 10 minutes. This was then aspirated off and the cells washed twice with PBS. 2ml of fixative solution (0.2% (v/v) glutaraldehyde and 2% (v/v) formaldehyde in PBS, pH 7.4) was then added and left for 15 minutes at room temperature. Following removal of fixative, non specific binding sites were blocked by incubation in 5% (v/v) FCS in PBS for 10 minutes. The cells were washed twice in PBS and the primary antibody added (diluted in PBS, see table 2.1 for antibody details). To control for non-specific secondary antibody binding, no primary antibody control (no primary) cells were routinely stained alongside other cells and treated the same except that, during this primary antibody incubation period, they were incubated in diluent (PBS) alone. After 1 hour incubation at room temperature, the cells were washed twice in PBS then incubated in the appropriate secondary antibody for 1 hour at room temperature. Cells were then incubated in 4',6-diamidino-2-phenylindole (DAPI, 6µg/ml in PBS) for 20 minutes to label DNA. DAPI is a fluorescent cell permeable dye that binds in the minor groove of DNA at AT rich clusters allowing for specific fluorescent detection of DNA [176]. The DAPI solution was aspirated off and the cells washed 3 times with PBS before being stored in 5ml of PBS at 4°C in the dark prior to visualisation.

### ***2.8.8 Transmission electron microscopy***

Cells were suspended in 10mM EDTA in PBS, pelleted then fixed in 2% glutaraldehyde in Sorenson's phosphate buffer (0.1M sodium phosphate, pH 7.2). The fixed cells were then processed and embedded in resin by the Newcastle University Electron Microscopy Research Service. Samples were viewed using a Philips CM100 transmission electron microscope.

### ***2.8.9 Image analysis***

Stained slides were imaged using a Lecia bright field microscope (Milton Keynes, UK) using the accompanying software, setting the white balance as required. Fluorescently stained cells were imaged using either a Zeiss fluorescence (Cambridge, UK) or a Nikon SP2 laser scanning confocal (Kingston-upon-Thames, UK) microscope. Qwin software (Leica) was used to assess the percentage staining of immunostained sections. The threshold for positive staining was specified manually and kept constant for each batch of stained slides. 70kDa peroxisomal membrane protein (PMP70) fluorescence from cells was determined using ImageJ [177], by applying a threshold, kept constant, to images to remove the background. The analyse particle mode, with particle size set to exclude background staining, was used to count the number of positive staining foci. This was divided by the cell number to give mean relative normalised PMP70 staining.

## **2.9 Enzyme activity assays**

### ***2.9.1 Rat liver microsomal preparation***

The majority of hepatic CYP450s are located in the endoplasmic reticulum in hepatocytes. Microsomes are therefore often used to assess drug bioactivation and metabolism. Liver from a freshly culled rat was chopped roughly in ice-cooled TKMS buffer (50mM Tris; 25mM KCl, 5mM MgCl<sub>2</sub> and 250mM sucrose, pH 7.5). The tissue was then homogenised using a dounce homogeniser in 5 times the volume of tissue on ice, filtered through bolting cloth and centrifuged at 12,000g for 20 minutes at 4°C (pellets nuclei, mitochondria and lysosomes). The top layer of fat was removed and the

supernatant transferred to a fresh centrifuge tube and the samples centrifuged again at 12,000g for 20 minutes at 4°C. The supernatant was aliquoted into ultracentrifuge tubes and centrifuged at 100,000g at 4°C for 1 hour. The supernatant was removed and the pellet (microsomes) washed in fresh TKMS buffer. The pellet was re-suspended in TKMS buffer once more then transferred to a fresh ultracentrifuge tube. This was centrifuged in an ultracentrifuge as before. Following the spin, the supernatant was removed and the pellet re-suspended in 1ml of microsome buffer (10mM  $K_nH_nPO_4$ , 1mM EDTA and 20% (v/v) glycerol, pH 7.2). The microsomes were then aliquoted and stored at -80°C. The protein concentration of samples was calculated by Lowry assay (2.7.3).

### ***2.9.2 Resorufin based probe assays (EROD, MROD and PROD)***

CYP1A1, CYP1A2 and CYP2B1 activities were determined in cellular lysates, using 7-ethoxyresorufin, 7-methoxyresorufin and 7-pentoxyresorufin respectively. These modified forms of resorufin that are not fluorescent are metabolised to resorufin which is highly fluorescent. Different CYP450 enzymes specifically metabolise these different substrates as summarised in figure 2.5 and therefore they can be used to measure the activity of these enzymes [178-180].

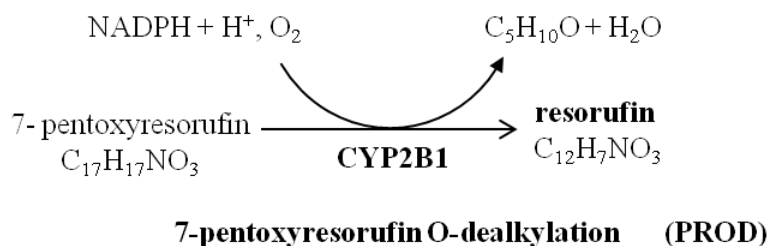
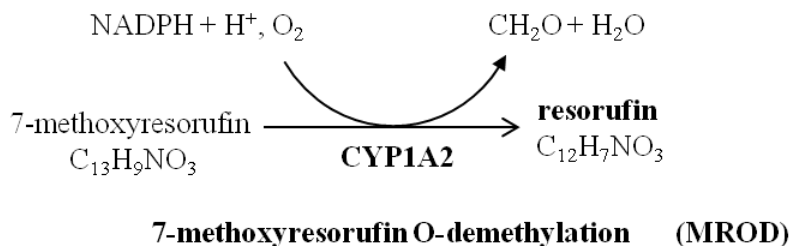
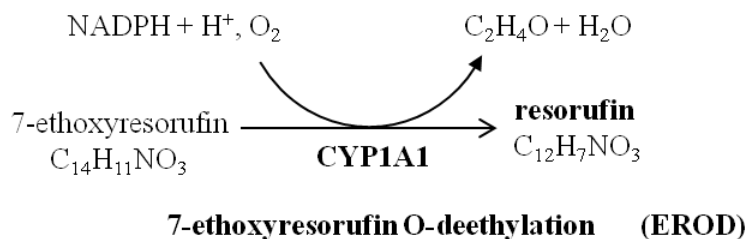


**Figure 2.5: Metabolism of 7-ethoxyresorufin, 7-methoxyresorufin and 7-pentoxyresorufin.**

Following treatment, cells were washed once in PBS then scraped using a rubber policeman into fresh PBS and transferred into an eppendorf tube. The cells were centrifuged at 16,000g for 30s and the supernatant discarded. The pellets were then re-suspended in TM buffer (50mM Tris-HCl, 25mM MgCl<sub>2</sub> pH7.5). 50µl of the cell lysate was added to 100µl of either 4µM 7-ethoxyresorufin, 2µM 7-methoxyresorufin or 20µM 7-pentoxyresorufin in TM buffer depending on the CYP450 being measured. This was then prewarmed at 37°C for 15 minutes after which 50µl of 500µM nicotinamide adenine dinucleotide phosphate (NADPH) was added per well to initiate the reaction. Immediately after NADPH addition, fluorescence was measured ( $\lambda_{\text{excitation}}$ : 522nm,  $\lambda_{\text{emission}}$ : 586nm) routinely every 1 minute for up to 20 minutes at 37°C. A resorufin standard curve was prepared fresh for every assay on the same plate with concentrations ranging from 0-32pmol/well resorufin in TM buffer. Following the end of the assay, fluorescence readings were plotted against time and a line of best fit fitted to the linear region of activity to give a rate of change in fluorescence. The amount of resorufin

produced was then calculated from the standard curve and normalised to protein concentrations measured by Lowry assay (detailed in 2.7.3) to give an absolute rate of activity.

### 2.9.3 Luciferin-IPA CYP3A1 assay

To measure CYP3A1 activity in cell lysates, luciferin-IPA (Promega) metabolism was measured which, in rats, is primarily catalysed by CYP3A1 (personal communication with Promega). The metabolism of the proprietary substrate yields D-luciferin which is then catalysed by luciferase to produce light which can be measured as outlined in figure 2.6.

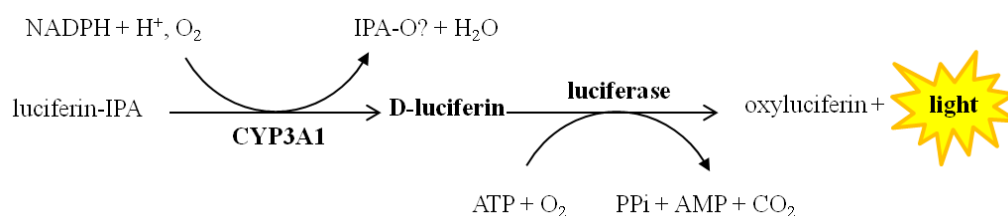


**Figure 2.6: Metabolism of luciferin-IPA by CYP3A1 and luciferase**

To measure luciferin-IPA metabolism, cell pellets or microsomes were re-suspended in TM buffer as described in 2.9.1. A fourfold concentrated reaction mastermix was prepared by mixing 0.05 $\mu$ l of 3mM luciferin-IPA, 22.5 $\mu$ l of distilled water and 5 $\mu$ l of 1M potassium phosphate buffer. 27.5 $\mu$ l of mastermix was added to each well with 5 $\mu$ l of each cell sample in 96 well white walled plates. Plates were pre-incubated for 10 minutes at 37°C then the reaction started by addition of 17.5 $\mu$ l of 4.3mM NADPH (final concentration of 1.5mM). Reactions were incubated for 30 minutes at 37°C then 50 $\mu$ l luciferin detection reagent added per well. Plates were tapped to mix then luminescence determined using a Tecan infinite 200 plate reader (Männedorf, Switzerland) using a 1 second integration time.

### 2.9.4 Dye retention assays

Efflux transporter activity was determined using dye retention assays. As outlined in figure 2.7, if cells are cultured in a medium containing a lipophilic compound, the compound will enter cells and over time equilibrium is reached between its entry and

exit. Transporter efflux determines the accumulation of the compound and their inhibition causes enhanced retention of the dye. Through the use of specific compounds and transporter inhibitors, the relative activity of transporters can be determined.

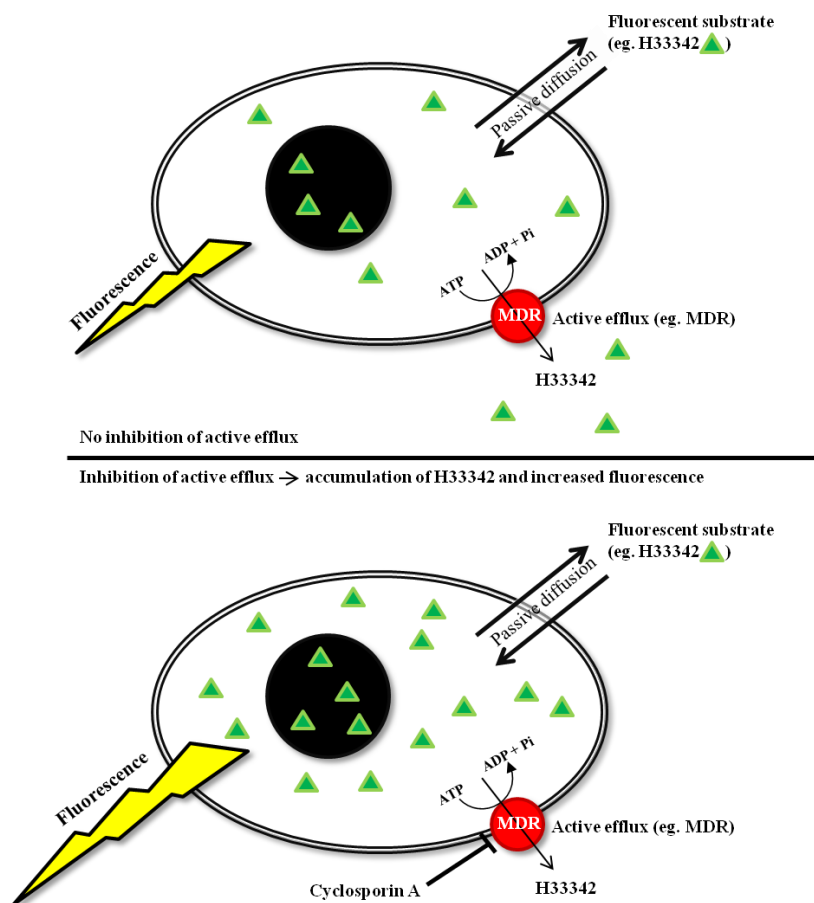


**Figure 2.7: Principal of fluorescence transporter efflux assays.**

The specific fluorophores and inhibitors used to determine the activity of different transporters is detailed in table 2.2.

Transporter activity measured	Substrate	Inhibitor	Fluorescent read settings	
			Excitation	Emission
<b>MDR</b>	1 $\mu$ M Hoechst 33342 (H33342)	5 $\mu$ M Cyclosporin A	355nm	455nm
<b>BCRP</b>	1 $\mu$ M H33342	1 $\mu$ M Ko143	355nm	455nm
<b>MRP</b>	1 $\mu$ M 5-chloromethylfluorescein diacetate (CMFDA)	10 $\mu$ M MK571	490nm	520nm
<b>BSEP</b>	1 $\mu$ M dihydrofluorescein diacetate (H <sub>2</sub> FDA)	100 $\mu$ M Troglitazone 50 $\mu$ M Glibenclamide	490nm	530nm

**Table 2.2: Substrates and inhibitors used to measure indicated transporter activity.** CMFDA was from Life technologies (Paisley, UK).

To determine activity, cells were first incubated with the respective inhibitor or vehicle in serum free medium for 30 minutes at 37°C. After this incubation, the medium was replaced with serum free medium containing both the inhibitor and the appropriate fluorescent substrate for a further 30 minutes at 37°C. The cells were then washed twice with ice cold PBS. After the final wash, ice cold PBS was added to each well and fluorescence read using the settings shown in table 2.2. Gain was optimised individually for each substrate and inhibitor combination per day then kept constant between different plates to ensure results could be directly compared. Background readings were subtracted from all values which were then normalised to protein concentration as calculated by Lowry assay (see 2.7.3). Values were expressed as percentage change in fluorescence relative to vehicle treated controls.

## **2.10 Measurement of DNA damage**

### ***2.10.1 The single cell gel electrophoresis assay (comet assay)***

DNA damage was routinely measured by the alkaline comet assay [181]. Essentially, cells are embedded in agarose and proteins and membranes removed with a lysis solution. A strong basic solution is then used to denature and unwind the DNA, following which a potential difference is applied. Damaged DNA with breaks is more mobile than unbroken DNA and therefore migrates further towards the anode. The amount of DNA migration (“the tail”) from the nucleus (the “head”) can be determined using a DNA intercalating dye and used as a measure of DNA damage.

Treated cells were detached using trypsin as described in 2.3.6 then centrifuged at 600g for 5 minutes to pellet the cells. The cells were re-suspended in a small volume of ice cold medium and counted by haemocytometer, following which cell density was adjusted to  $1 \times 10^6 \text{ ml}^{-1}$ . Cell viability was also measured by trypan blue exclusion (as outlined in 2.3.9) and cells with viability less than 80% were discarded. 6µl of the cell solution was added to 54µl of low melt point agarose (0.9% (w/v) in PBS), which had been melted in boiling water then equilibrated to 37°C. 50µl of this mix was then immediately pipetted onto slides pre-coated with agarose (0.75% (w/v) in PBS). The embedded cells were incubated in a fridge for 10 minutes to harden the agarose then in

comet lysis buffer (10 mM Tris, 2.5M NaCl and 100 mM EDTA pH 10.0 supplemented on the day with 2% (v/v) DMSO and 1% (v/v) triton X-100) for 1 hour at 4°C, which lyses the cell membranes. Slides were briefly washed in PBS then were incubated for 30 minutes in electrophoresis buffer (0.3 M NaOH, 1 mM EDTA pH>13).

Electrophoresis was run at 30V (~0.9V/cm) 300mA for 30 minutes at 4°C. The embedded cells were incubated in neutralisation buffer (0.5M Tris pH 7.5) for 15 minutes then washed in PBS. Slides were incubated for 5 minutes in 1x SYBR gold nucleic acid stain (Invitrogen) in PBS. Finally, they were washed twice in distilled water and left to air dry in the dark at room temperature overnight. Slides were stored long term at 4°C in the dark. SYBR staining was imaged by fluorescence microscopy using the fluorescein isothiocyanate (FITC) filter and comets measured using CometScore software (<http://www.autocomet.com>). DNA damage was expressed as the olive tail moment, a parameter which takes into account the comet tail length and the percentage of DNA in the comet tail.

### ***2.10.2 DNA diffusion assay***

Following preparation, embedding and lysis of cells as described in 2.10.1, slides were incubated in comet lysis buffer for 1 hour then 0.5M Tris pH 7.4 for 5 minutes. They were then washed and stained with SYBR gold as previously outlined in 2.10.1. Slides were visualised using a fluorescent microscope.

### ***2.10.3 Assessment of cell proliferation***

To check that DNA damage caused by treatments was not due to DNA replication, cells were labelled with the thymidine analogue BrdU (bromodeoxyuridine) which is incorporated by cells into their DNA during S-phase of the cell cycle. Cells, the morning after treatment, were treated with 15µM BrdU for 2 hours. Cells were then subjected to the comet assay as described to 2.10.1 but following incubation in the neutralisation buffer, cells were incubated with anti-BrdU (see table 2.1 for details) diluted in 0.5% (v/v) FCS in PBS for 1 hour at room temperature. Slides were washed three times in PBS then incubated with a FITC conjugated secondary antibody in 0.5% (v/v) FCS in PBS for 1 hour at room temperature. This was then washed off and slides

were soaked in 6µg/ml DAPI for 15 minutes to stain DNA followed by a 15 minute wash in distilled water. Slides were air dried overnight at room temperature in the dark and imaged the following day.

## 2.11 Spectrophotometric CYP450 assays

### 2.11.1 Total CYP450 dual-beam spectroscopy

The haem bound in cytochromes demonstrates different absorbance properties depending on its oxidation and ligation state and can be used to identify specific cytochrome concentrations in a solution. Reduced CYP450 has a characteristic absorbance peak at 450nm and therefore, by measuring the absorbance difference between reduced and oxidised samples, the concentration of total CYP450 in a sample can be measured [182].

To measure total haem-bound CYP450 concentrations in samples, cell pellets were re-suspended in 2ml of TST buffer (20mM Tris, 250mM sucrose and 0.01% (v/v) triton X-100 pH 7.4). 5µl was removed to measure total protein concentration by Lowry assay as described in 2.7.3. 1-5mg of sodium dithionite was added to the sample and inverted to mix. The reduced solution was then split into 2 cuvettes. Carbon monoxide was bubbled through one cuvette for 30s at about 1 bubble per second. The absorbance difference between the two cuvettes was then measured between 400-500nm. The total haem bound CYP450 concentration was then calculated using the following equation, where 91,000 M<sup>-1</sup> cm<sup>-1</sup> is the extinction coefficient of CYP450 [182]:

$$\text{Total CYP450 concentration (M)} = \frac{\text{OD}_{450} - \text{OD}_{490}}{91000 \text{ M}^{-1}\text{cm}^{-1}}$$

### 2.11.2 Total cytochrome b<sub>5</sub> dual beam spectroscopy

The concentration of total cytochrome b<sub>5</sub> in a sample can be calculated similar to CYP450, however the reduced absorbance peak is at 424nm [182]. Cell pellets were re-suspended in 2ml of TST buffer and 5µl taken to measure total protein concentration by Lowry assay (see 2.7.3). The solution was split equally between 2 cuvettes and one solution reduced by addition of 50µg of nicotinamide adenine dinucleotide (NADH).

The absorbance difference of the oxidised and reduced solutions was measured between 400-460nm. The total cytochrome b<sub>5</sub> concentration was then found using the following equation, where 18,500 M<sup>-1</sup> cm<sup>-1</sup> is the extinction coefficient of cytochrome b<sub>5</sub> [182]:

$$\text{Cytochrome b}_5 \text{ concentration (M)} = \frac{\text{OD}_{424} - \text{OD}_{409}}{185000}$$

### 2.12 Serum activity assays

Blood was collected from animals by tail vein bleeding or after culling and was left to clot at room temperature (~1 hour). Blood was centrifuged at 16,000g for 5 minutes and the serum transferred to a fresh tube. Analysis of alanine transaminase (ALT) and alkaline phosphatase (ALP) serum activities, biomarkers of hepatocyte and cholangiocyte injury respectively, was carried out by the Royal Victoria Infirmary Clinical Biochemistry Department in Newcastle Upon Tyne.

### 2.13 Hydroxyproline assay

The hydroxyproline content of the liver is proportional to the severity of fibrosis due to the abundance of hydroxyproline specifically in collagen [183]. The Quickzyme hydroxyproline assay (2B Scientific, Upper Heyford, UK) was used to calculate total hydroxyproline content of rat liver samples, essentially following the recommended protocol. Briefly, 100µl of 6M hydrochloric acid was added per 10mg of liver tissue (wet weight) and incubated overnight at 110°C. The samples were then centrifuged at 16,000g for 15 minutes and 35µl of the supernatant added to 75µl of included assay buffer then incubated for 20 minutes at room temperature. Whilst incubating, the detection reagent was prepared by mixing detection reagent A and B at a ratio of 2:3. 75µl of detection reagent was added to each sample and these were then incubated at 60°C for 60 minutes and then the OD<sub>570</sub> measured. A series of hydroxyproline standards were run alongside samples ranging from 0 to 300µM diluted in 4M hydrochloric acid to generate a standard curve which was used to calculate hydroxyproline content of samples using a line of best fit and  $y = m\chi + c$ . Sample readings were normalised to protein concentration as calculated by Lowry assay (outlined in 2.7.3).

### 2.14 Luminescent imaging of mice

NF- $\kappa$ B –luc mouse luminescence was detected and quantified using the Xenogen IVIS (*in-vivo* imaging system) 200 Spectrum imaging system using the bundled Living Image 4.0 software (Caliper Life Sciences, Hopkinton, USA). Prior to imaging, mice were anaesthetised with isoflurane and their abdominal fur shaved off. The mice were then given an intra-peritoneal (i.p.) injection of 200 $\mu$ l  $D$ -luciferin (Caliper Life Sciences) at 15mg/ml in PBS. Mice were typically imaged 0, 5 and 10 minutes following  $D$ -luciferin injection using a 1 minute integration time. Following imaging, mice were either returned to their cages or culled by cervical dislocation. The major organs of culled mice were quickly excised and imaged in the IVIS again using a 1 minute integration time to determine the source of luminescence. From captured images, regions of interest were manually specified using the Living Image 4.0 software to calculate total flux values (photons/s).

### 2.15 Statistics

Statistically significant differences between groups were determined by the Student's 2-tailed t-test unless otherwise specified. Regardless of hypothesis test used, significance was achieved where  $p < 0.05$ .

**Chapter 3. Expression and induction of drug metabolising enzymes in  
B-13/H cells**

### 3.1 Introduction

Hepatic bioactivation is implicated in the toxicity of numerous drugs [30]. Hepatocytes are the primary defining cell type of the liver and are responsible for most of its functions, including drug and chemical metabolism. Hepatocytes, particularly human hepatocytes, are consequently the gold standard for novel drug and chemical toxicity screening to assess for potential toxicity. However, as outlined in the introduction, there are numerous problems associated with the sourcing and culture of primary hepatocytes for screening purposes, meaning that alternatives are sought.

Functional hepatocytes produced from the B-13 cell line could be an alternative to primary hepatocytes; the cells are easily expanded in standard culture medium and consistently, when treated with nanomolar concentrations of DEX, transdifferentiate to hepatocyte-like cells. B-13 cells also have a stable phenotype in that, although they have an abnormal karyotype, they have maintained the ability to transdifferentiate and, unlike tumorigenic cells, do not grow in soft agar [184].

To date, although the expression of some drug metabolising enzymes has been demonstrated in transdifferentiated B-13 cells [124, 125], their drug metabolising properties remain poorly characterised as does their ability to induce CYP450s, a physiologically important response. To this end, the aim was to fully characterise the expression of drug metabolising enzymes, particularly CYP450s in B-13/H cells, and to investigate their potential for induction in response to the relevant AhR, CAR, PXR and PPAR $\alpha$  ligands. The hypothesis was that B-13/H, but not B-13 cells, would express a similar range of functional CYP450s to rat hepatocytes with a similar capacity for induction.

### 3.2 B-13 cells undergo transdifferentiation in response to DEX treatment

B-13 cells were routinely transdifferentiated to B-13/H cells by 14 days treatment with 10nM DEX. As shown in figure 3.1A, DEX treated B-13 cells flattened and spread. When proliferation was measured (figure 3.1B), it was observed that DEX treatment arrested proliferation of B-13 cells compared to vehicle treated cells as has been documented previously [124]. B-13/H cells also expressed a range of hepatic markers

including carbamoyl phosphate synthetase 1 (CPS-1), CYP2E1 and CYP reductase, similar to rat liver, that were not expressed in untreated B-13 cells (figure 3.2). B-13/H cells retained expression of amylase following transdifferentiation as has been previously shown [124]. CYP450s contain a haem cofactor required for function. Split beam spectrophotometry demonstrated that B-13/H but not B-13 cells contained haem bound CYP450 as has been documented previously (figure 3.3A & B) [184]. CYP reductase is the main electron donor for CYP450s. However cytochrome  $b_5$ , which also contains haem, can also act as an electron donor to CYP450s and its addition to microsomes has been shown to enhance their metabolic capacity [185]. Measurement of haem bound cytochrome  $b_5$  showed that B-13/H but not B-13 cells contained an equivalent amount of haem bound cytochrome  $b_5$  to freshly isolated hepatocytes (figure 3.3C & D).

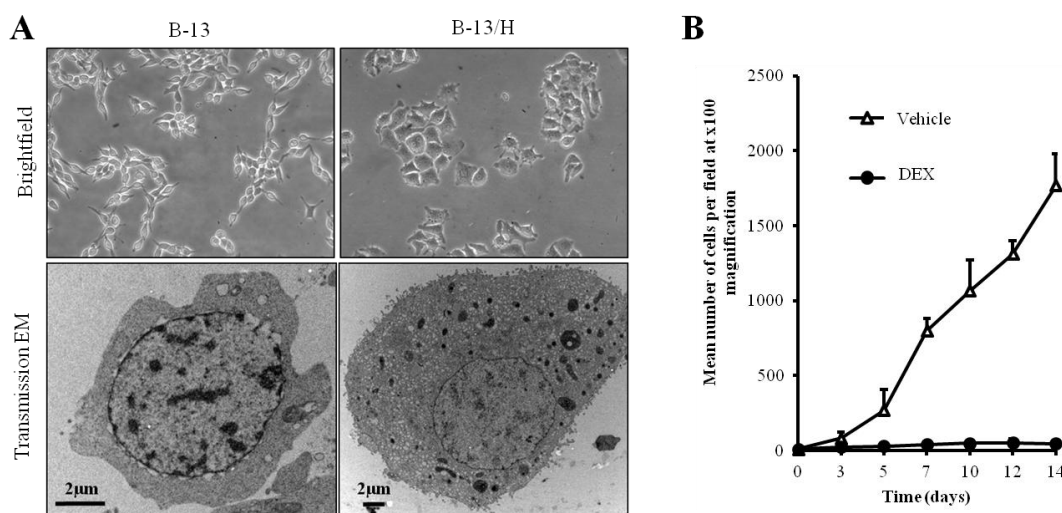


**Figure 3.1: B-13 cells change morphology and cease proliferation in response to DEX. A. Change in morphology in response to DEX.** Representative brightfield and transmission electron photomicrographs at 100x and 34000x magnification respectively. **B. Proliferation of vehicle and DEX treated cells.** The total number of cells treated with vehicle (0.1% (v/v) ethanol) or 10nM DEX were counted per field of view per time point. Results are the mean and SD of 3 independent determinations from a single experiment, typical of at least 3 separate experiments. Statistical analysis was not performed.

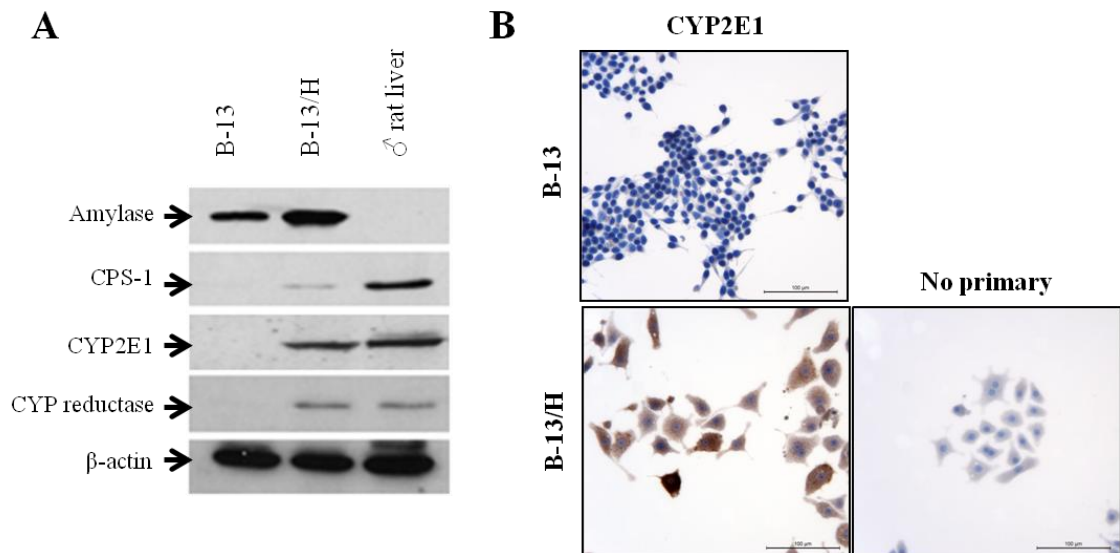


**Figure 3.2: B-13/H cells express hepatic markers. A. Western blot for the indicated proteins in B-13 and B-13/H cells and control rat liver.** Lysates were prepared and quantified by Lowry assay. 20 $\mu$ g of protein/well was separated by SDS-PAGE and transferred to a nitrocellulose membrane which was blocked and probed. Antibody binding was detected using ECL Western blot substrate. **B. CYP2E1 immunostaining in B-13 and B-13/H cells.** Fixed cells were blocked then immunostained for CYP2E1, using DAB to detect bound antibody before counterstaining with haematoxylin. Cells were analysed using a Leica upright microscope. Scale bar indicates 100 $\mu$ m. Results are typical of at least 3 separate experiments.

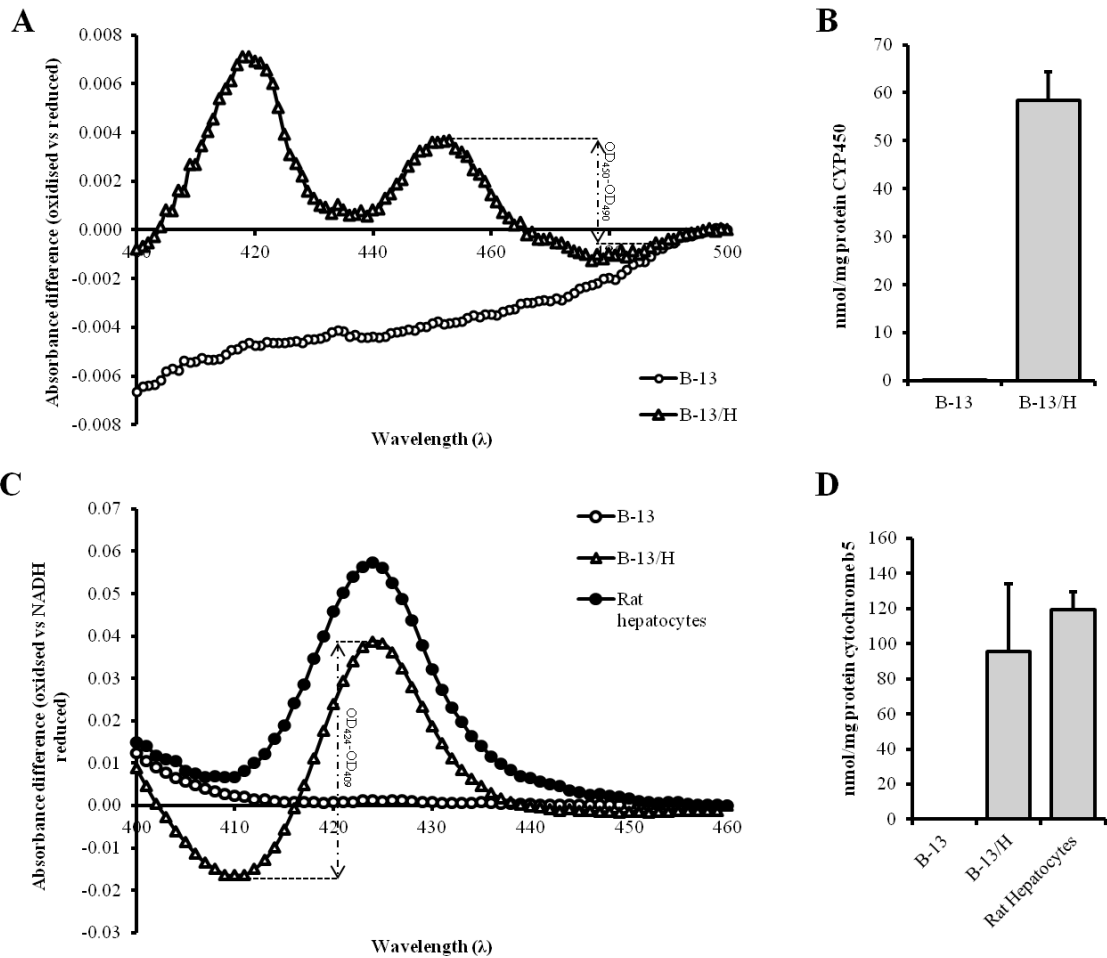


**Figure 3.3: B-13/H cells contain haem-bound CYP450 and cytochrome b<sub>5</sub>.** **A. Total CYP450 absorbance spectrum.** Lysates prepared from B-13 and B-13/H cells were re-suspended in TS buffer containing sodium dithionite and then split into 2 different cuvettes. Carbon monoxide was bubbled through one of the paired cuvettes and then the absorbance difference measured between the reduced and oxidised samples between 400nm and 500nm. **B. Quantified total CYP450 content in B-13 and B-13/H cells.** The  $OD_{450}-OD_{490}$  was calculated from the absorbance difference spectrum as in **A** and the total CYP450 content calculated using the extinction coefficient as outlined in the methods. CYP450 content was normalised to protein concentration. **C. Total cytochrome b<sub>5</sub> absorbance spectrum.** Lysates from B-13 cells, B-13/H cells and freshly isolated primary rat hepatocytes were re-suspended in TS buffer and split into 2 cuvettes. 50µg of NADH was added to one of the paired cuvettes and absorbance difference measured between the reduced and oxidised samples between 400nm and 460nm. **D. Quantified total cytochrome b<sub>5</sub>.** The  $OD_{424}-OD_{409}$  was calculated from the absorbance difference spectrum as in **C** and the total cytochrome b<sub>5</sub> content calculated using the extinction coefficient as outlined in the methods. Cytochrome b<sub>5</sub> content was normalised to protein concentration. For **A** and **B**, results are the mean and SD of 3 independent determinations from a single experiment, typical of 2. Statistical analysis was not performed. For **C** and **D**, results are the mean and SD of 3 separate experiments. There was no significant difference between B-13/H cells and rat hepatocytes.

### 3.3 B-13/H cells express male CYP450 isoforms

Several DMEs, including some CYP450 isoforms, are sex specific; their expression is dependent on specific patterns of growth hormone (GH) release from the pituitary gland, which may be influenced by the actions of gonadal hormones such as testosterone or oestrogen [186]. In adult male rats GH is released in an ultradian manner every 3.3 hours. Between these pulses the basal blood plasma level of GH is less than 5ng/ml [187]. Conversely, in adult female rats, GH peaks are on average lower than in males, but they occur more frequently and the basal level of plasma GH is generally greater than 5ng/ml [188]. To determine the expression of sex-dependent CYP450s in B-13 cells, which are male cells [128], RT-PCR was carried out. As shown in figure 3.4A, B-13/H cells expressed all CYP450 transcripts measured with the exception of CYP3A2.

To quantitatively determine the expression of the expressed CYP450s, qPCR was carried out on B-13 and B-13/H cells, and male and female rat liver (figure 3.4B). CYP2C11 is the main CYP450 in male rats, making up around 50% of total CYP450 content [189]. Conversely, in female rats, CYP2C12 is the dominant CYP450 isoform, making up around 40% of total CYP450 content [190, 191]. B-13/H cells expressed about 10 times less CYP2C11 mRNA than male rat liver but around 10 times more than that expressed in female rat liver (figure 3.4B). In contrast, CYP2C12 mRNA was, as expected, highly expressed in female rat liver with significantly reduced expression in male liver and even lower expression in B-13/H cells.

Analysis of the expression of other sexual-dimorphic CYP450s showed that B-13/H cells expressed greater mRNA levels of the male specific isoform CYP2C13 compared to female liver but 100 fold less than that seen in male liver (figure 3.4B) [186]. The mRNA expression of male isoforms CYP3A2 and CYP3A18 was significantly higher in male liver than in B-13/H cells or female liver. B-13/H cells expressed equivalent levels to that seen in female rat liver. Expression of CYP2A mRNA, a female predominant CYP450 [192], was significantly higher in female liver than male liver. B-13/H cells showed expression significantly lower than male liver. CYP2C7, which has been previously reported as a female predominant isoform [193], showed equivalent mRNA expression in male and female rat liver samples. Considering that the expected

difference between male and female rat liver expression of CYP2C7 is only 2-3 fold, the small sample sizes in this work may explain the lack of significant difference. B-13/H cells expressed significantly lower levels of CYP2C7 mRNA than male liver. CYP2C6, which is not generally considered sex-dependent [194], was expressed at the level of mRNA at similar levels by male and female rat liver. B-13/H cells expressed significantly greater levels than male liver and B-13 cells expressed only around 1/300<sup>th</sup> of that expressed in B-13/H cells.

The pattern of mRNA expression of the main sexual-dimorphic CYP450s, CYP2C11 and CYP2C12, suggests that B-13/H cells recapitulate a male pattern of CYP450 expression. This is essentially supported by the pattern of mRNA expression of the other sexually dimorphic CYP450s. In culture, primary hepatocytes rapidly lose expression of CYP3A2 and this may explain why B-13/H cells expressed only similar levels to female liver [195]. Previous work also suggests that CYP3A2 takes longer than 14 days following transdifferentiation to be expressed [124]. These reasons may also account for the low expression of CYP3A18 mRNA observed. Western blotting for CYP2C proteins essentially supports the transcript data. Figure 3.4C indicates that there was no detectable CYP2C protein in B-13 cells whereas B-13/H cells expressed immunodetectable protein.

To establish whether the CYP2C11 expressed in B-13/H cells was functional, B-13 and B-13/H cells were treated with methapyrilene, which some evidence suggests is activated to a toxic product by CYP2C11 [196]. Figure 3.5 shows that the viability of B-13 cells was unaffected by methapyrilene exposure at concentrations of up to at least 500 $\mu$ M whereas methapyrilene treatment caused a dose-dependent loss of viability in B-13/H cells, with an EC<sub>50</sub> concentration of approximately 20 $\mu$ M.

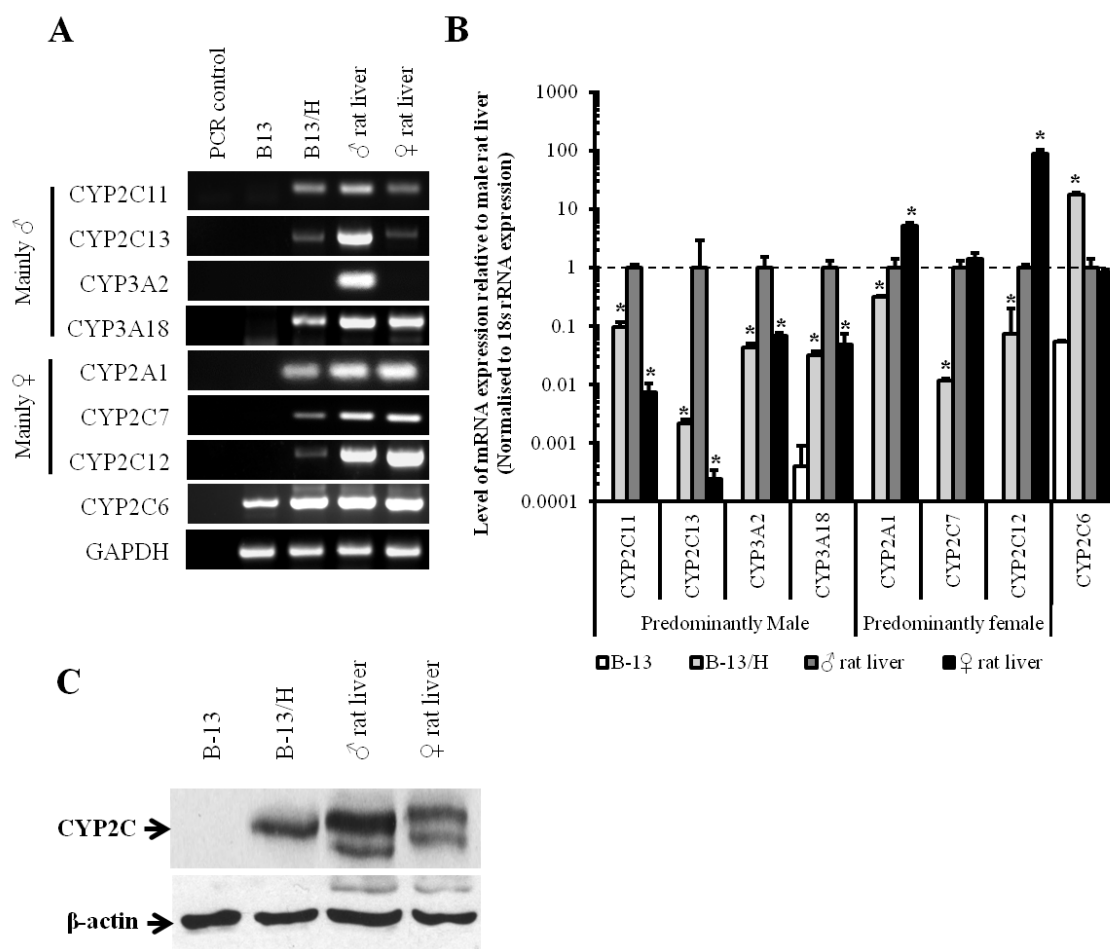


**Figure 3.4: B-13/H cells partially recapitulate a male pattern of CYP450 expression. A. RT-PCR for the indicated transcripts in B-13 cells, B-13/H cells, male rat liver and female rat liver.** Total RNA was extracted from samples using TRIzol and cDNA produced which was used as the template for PCR. Following PCR, samples were separated by agarose gel electrophoresis and visualised by UV transillumination. **B. qPCR for sex-dependent CYP450s.** Total RNA was extracted from B-13 cells, B-13/H cells, and male and female rat liver samples using TRIzol and reverse transcribed. The cDNA was used as template for qPCR to measure the expression of the indicated transcripts. Readings were normalised to 18S rRNA expression and fold change expressed relative to male rat liver. Bars are the mean and SD of 3 independent determinations from a single experiment, typical of at least 3 separate experiments. \*significantly different to male liver at  $p < 0.05$ . **C. Western blot for CYP2C11.** Lysates were prepared and quantified by Lowry assay. 20 $\mu$ g of protein/well was separated by SDS-PAGE and transferred to a nitrocellulose membrane which was blocked and probed. Antibody binding was detected using ECL Western blot substrate. Blot is representative of at least 3 separate experiments.

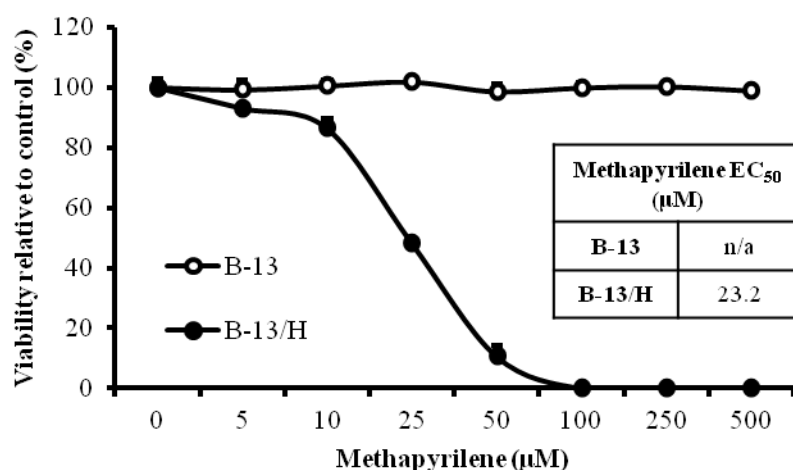


**Figure 3.5: B-13/H cells are sensitive to methapyrilene.** B-13 or B-13/H cells were treated with different concentrations of methapyrilene and their viability assessed by trypan blue 24 hours later. EC<sub>50</sub> was calculated using GraphPad Prism. Additional statistical analysis was not performed. Results are the mean and SD of 3 independent determinations from the same experiment, typical of at least 3 separate experiments.

### 3.4 B-13/H cells are not receptive to GH

GH control of sex-dependent CYP450 expression in hepatocytes is regulated by the growth hormone receptor (Ghr) acting through the JAK/STAT signalling pathway (particularly requiring JAK2 and STAT5b) [186]. To determine if B-13/H cells would be sensitive to GH, mRNA expression of JAK/STAT signalling components was investigated by qPCR array. Figure 3.6 shows that both B-13 and B-13/H cells expressed the majority of pathway components including JAK2, STAT5b and Ghr, which were expressed at similar mRNA levels in both cell types.

To determine if expression of CYP2C11 could be induced in B-13/H cells, B-13/H cells were cultured either serum-free or in serum-containing media and were treated with different concentrations of GH (human growth hormone (hGH)). CYP2C11 mRNA expression in these cells did not significantly change following treatment suggesting that, at least under the conditions tested, B-13/H cells do not respond to GH (figure 3.7A). To confirm the qPCR, CYP2C11 was probed by Western blotting which similarly indicated that GH had no effect on CYP2C11 protein expression (figure 3.7B).

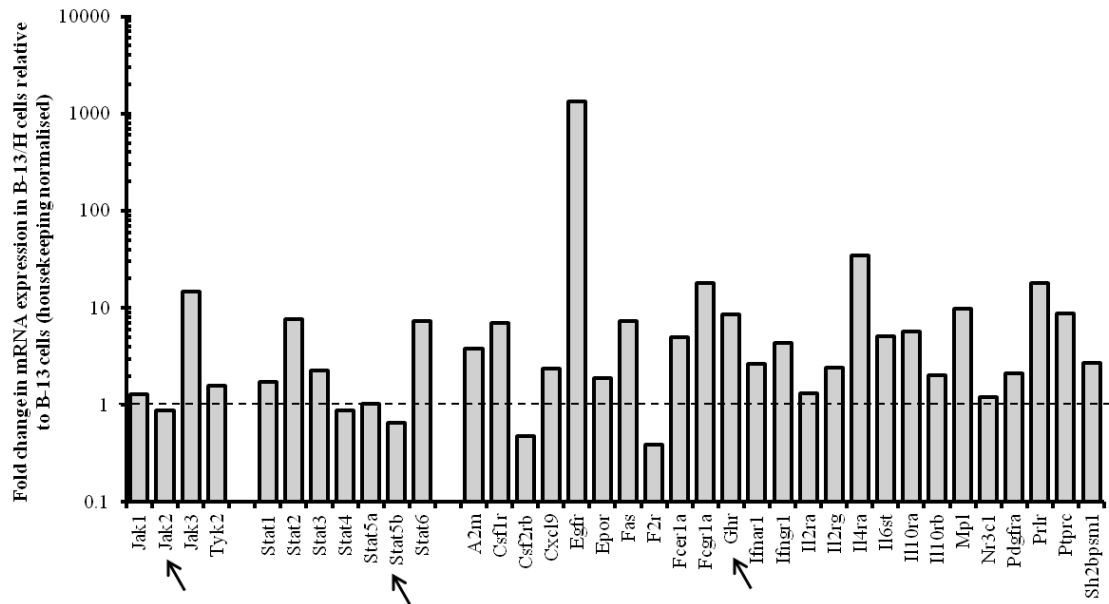


**Figure 3.6: B-13/H cells express signalling machinery required for JAK/STAT signalling.** JAK/STAT signalling qPCR array. Total RNA was produced from B-13 and B-13/H cells using TRIzol, which was then cleaned up, reverse transcribed and the resulting cDNA used as a template for the JAK/STAT signalling arrays. Results are normalised to 5 housekeeping genes. Arrows indicate Jak2, Stat5b and Ghr. Values are the mean fold change in expression in B-13/H cells relative to B-13 cells from 1 sample.

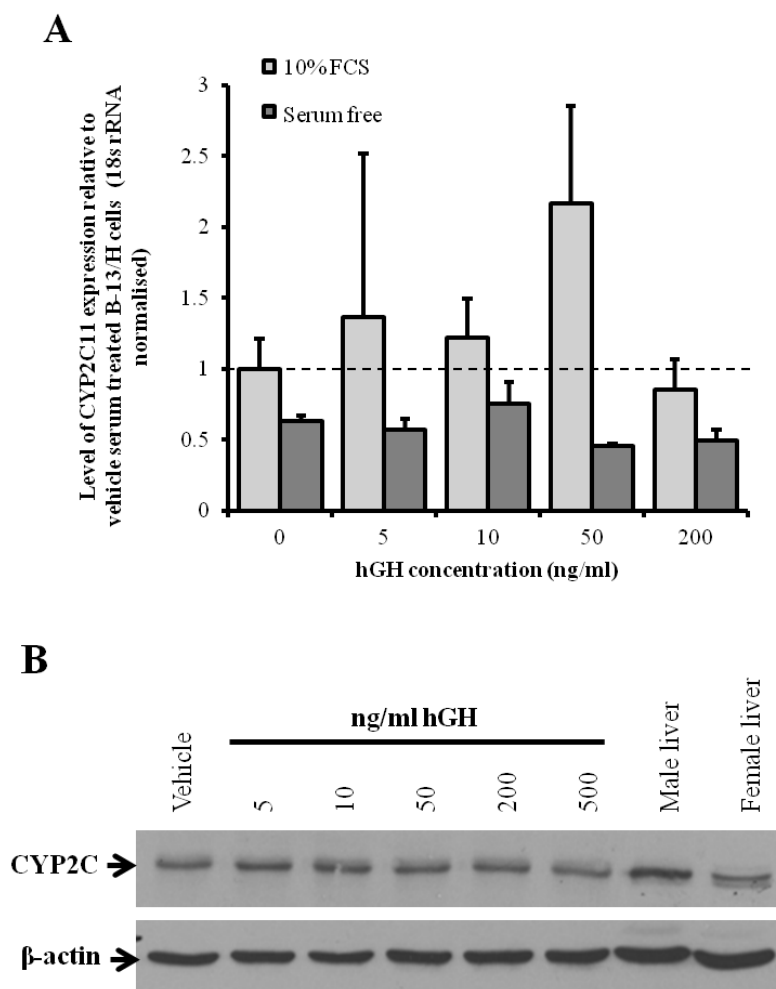


**Figure 3.7: B-13/H cells are not responsive to hGH. A. Expression of CYP2C11 in B-13/H cells treated with different concentrations of hGH measured by qPCR.** B-13/H cells (cultured normally or serum free for 1 day) were treated with the indicated concentrations of hGH for 24 hours following which RNA was extracted using TRIzol. The RNA was reverse transcribed and cDNA used as template for qPCR. Readings were normalised to 18S rRNA expression and fold change expressed relative to vehicle treated B-13/H cells (+FCS). Values are the mean and SD of 3 independent determinations from the same experiment, typical of 2 (SF) or 3 (+FCS) separate experiments. No statistical analysis was performed. **B. Western blot for CYP2C11.** Lysates were prepared from B-13/H cells treated as in A, and quantified by Lowry assay. 20µg of protein/well was separated by SDS-PAGE and transferred to a nitrocellulose membrane which was blocked and probed. Antibody binding was detected using ECL Western blot substrate.

Based on the lack of CYP2C11 induction by GH in B-13/H cells (figure 3.7), it was postulated that the B-13/H cells were fully mature by 14 days and un-receptive to GH. To investigate if less mature B-13/H cells would be sensitive to the CYP450 modulating capacity of GH, B-13 cells were transdifferentiated in the presence or absence of GH. Measurement of sex-dependent CYP450 mRNA transcripts in these cells (figure 3.8) indicated that GH did not have a marked effect on CYP450 expression suggesting the cells are unresponsive to this pattern of GH at all stages of transdifferentiation under the conditions tested.

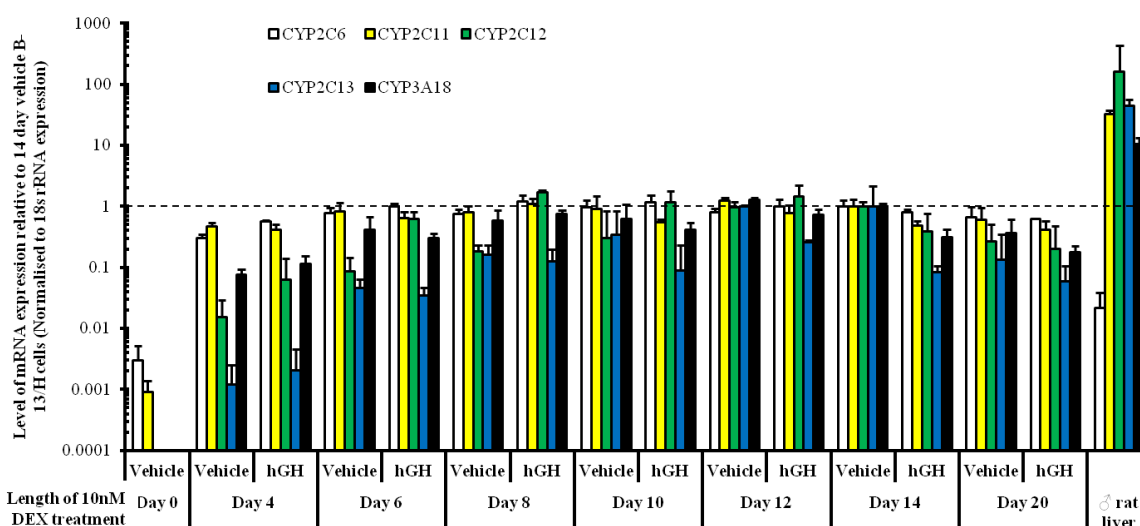


**Figure 3.8: hGH does not affect the rate of sex-dependent CYP450 up-regulation during transdifferentiation.** B-13 cells were treated with 10nM DEX with or without 50ng/ml hGH over 20 days with medium changed daily. From each time point RNA was isolated using TRIzol and used as template for reverse transcription. The cDNA was used as template for qPCR to measure the expression of the indicated transcripts and results were normalised to 18S rRNA expression. Fold change is expressed relative to 14 day vehicle treated B-13/H cells. Results are the mean and SD of 3 independent determinations from a single experiment. No statistical analysis was performed.

### 3.5 The AhR activator $\beta$ -naphthoflavone ( $\beta$ -NF) induces CYP1A1 expression in B-13 and B-13/H cells and sensitises cells to the genotoxic effects of benzo[a]pyrene.

The CYP1A sub-family is of toxicological significance due to its metabolism of a range of carcinogens such as polyaromatic hydrocarbons and heterocyclic amines [33, 34]. These genes are inducible through their regulation by the AhR [32] as outlined in the introduction.

To initially determine the potential of B-13 and B-13/H cells to induce CYP1A1, the expression of the AhR and ARNT, as well as the CYP1A family members CYP1A1, CYP1A2 and CYP1B1 was analysed by RT-PCR (figure 3.9A). This showed that both B-13 and B-13/H cells expressed AhR and ARNT mRNA similar to intact rat liver. They also both expressed CYP1A1 mRNA but not CYP1A2. Interestingly, the related CYP1B1 mRNA transcript, often expressed at high levels in tumour cells [197], was expressed in B-13 cells but down-regulated to near hepatocyte levels in B-13/H cells (figure 3.9A).

To quantitatively assess expression of CYP1A1 following induction, B-13 and B-13/H cells were treated with a range of prototypical CYP450 inducers including  $\beta$ -NF, a AhR ligand [198], and resulting CYP1A1 mRNA expression measured by qPCR. As shown in figure 3.9B, B-13/H cells expressed about 5 times more CYP1A1 mRNA than B-13 cells. When treated with  $\beta$ -NF, both B-13 and B-13/H cells showed a significant induction of CYP1A1 mRNA to levels more than 100 fold greater than in vehicle treated cells. B-13/H cells, but not B-13s, also significantly induced CYP1A1 mRNA in response to 10 $\mu$ M DEX. Primary rat hepatocytes similarly treated also showed a significant induction of CYP1A1 mRNA expression in response to DEX and importantly  $\beta$ -NF (figure 3.9C), suggesting that B-13/H cells respond in an equivalent manner to AhR ligands to primary rat hepatocytes.

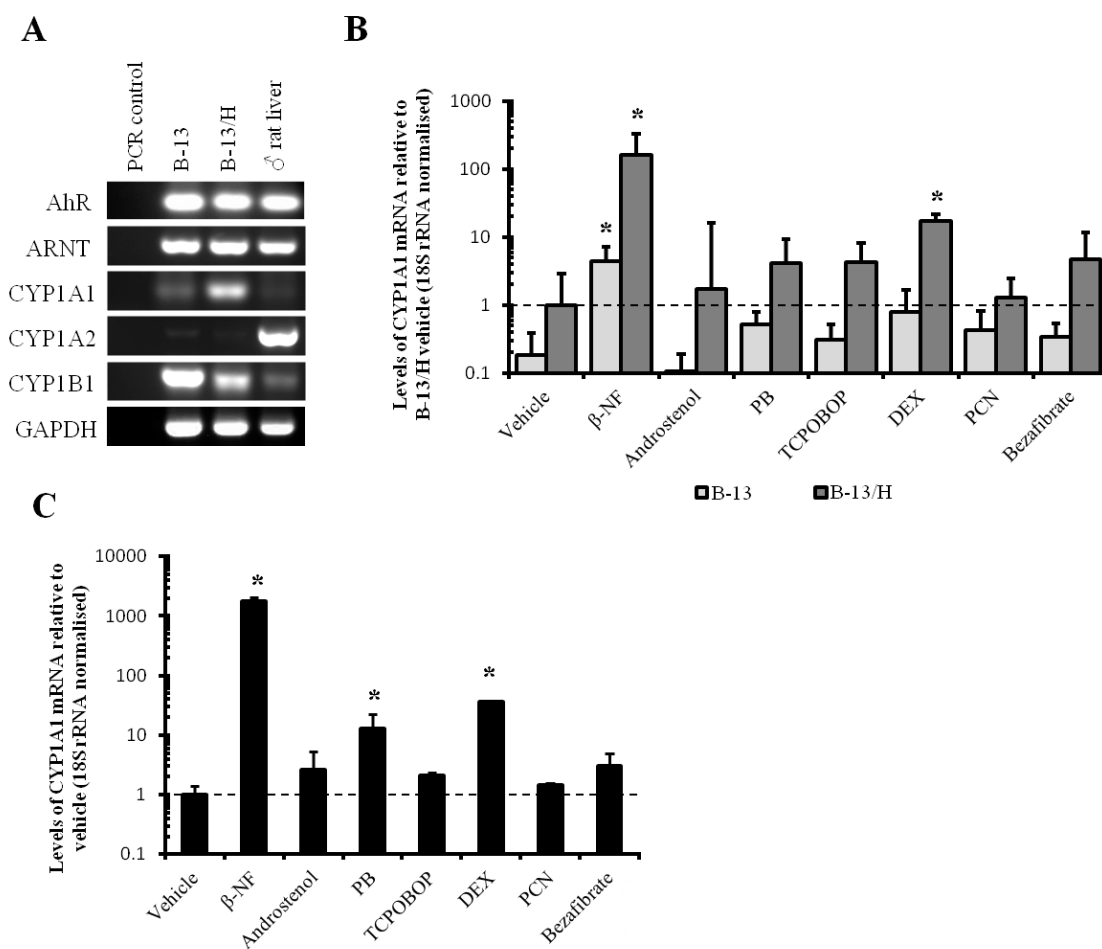


**Figure 3.9: B-13 and B-13/H cells express inducible CYP1A1. A. RT-PCR for CYP1A associated transcripts.** Total RNA was extracted from samples using TRIzol and cDNA produced which was used as the template for PCR. Following PCR, samples were separated by agarose gel electrophoresis and visualised by UV transillumination. **B. qPCR for CYP1A1 in B-13 and B-13/H cells treated with prototypical CYP450 inducers.** B-13 and B-13/H cells were treated for 3 days daily with vehicle (0.1% (v/v) DMSO) or inducer and harvested on the 4<sup>th</sup> day. Total RNA was extracted from the cells using TRIzol and reverse transcribed. cDNA was used as template for qPCR measuring the expression of CYP1A1. Readings were normalised to 18S rRNA expression and fold change expressed relative to vehicle treated B-13/H cells. Bars are the mean and SD of 3 independent determinations from a single experiment, typical of at least 3 separate experiments. \*significantly different to respective vehicle control at  $p < 0.05$ . **C. qPCR for CYP1A1 in primary rat hepatocytes treated with prototypical CYP450 inducers.** From primary rat hepatocytes treated as in B, RNA was extracted and reverse transcribed. The cDNA was used as a template for qPCR measuring the expression of CYP1A1 and results were normalised to 18S rRNA expression. Results are expressed as fold change relative to vehicle treated cells. Bars are the mean and SD of 3 independent determinations from a single experiment, typical of at least 3 separate experiments. \*significantly different to vehicle control at  $p < 0.05$ .

To determine if the induction of CYP1A1 mRNA translated to an induction at the level of protein, Western blotting to detect CYP1A1 was performed on B-13 and B-13/H cells and primary rat hepatocytes treated with  $\beta$ -NF. This demonstrated (figure 3.10) that CYP1A1 protein was induced in all tested cell types.

Based on the induction of CYP1A1 protein by  $\beta$ -NF, it was then investigated if CYP1A1 induction had functional consequences. Using 7-ethoxyresorufin (which as outlined in the methods is a substrate metabolised by CYP1A1 to fluorescent resorufin), CYP1A1 activity was assayed in B-13 and B-13/H cells and primary rat hepatocytes treated with a range of prototypical inducers. Lysates of  $\beta$ -NF and DEX treated B-13/H cells and primary rat hepatocytes showed significantly greater EROD activity than vehicle treated cells (figure 3.10B), suggesting that expressed CYP1A1 was functional. Although B-13 cells expressed a similar amount of CYP1A1 protein to B-13/H cells when induced with  $\beta$ -NF, their induced activity was markedly lower than B-13/H cells. This is likely because B-13 cells do not express CYP reductase which is required for CYP450 function [124]. Although DEX did lead to a significant increase in CYP1A1 mRNA expression in B-13/H cells and primary rat hepatocytes (figure 3.9), the increase was smaller than that seen in response to  $\beta$ -NF. However, when measuring EROD activity, DEX induction led to similar EROD activity to  $\beta$ -NF induction. DEX can induce CYP2B and CYP3A expression through the PXR and it was hypothesised that DEX induced CYP2B and CYP3A may have non-specifically catalysed ethoxyresorufin deethylation. This would account for the significantly increased EROD activity in B-13/H cells and primary rat hepatocytes induced with DEX.

To test this hypothesis, EROD activity was measured in the presence or absence of  $\alpha$ -naphthoflavone ( $\alpha$ -NF), a CYP1A1 inhibitor [199], in B-13/H cells. Compared to lysates from vehicle induced B-13/H cells, only lysates from  $\beta$ -NF treated cells were significantly inhibited by  $\alpha$ -NF (figure 3.10C). This result confirms the hypothesis as the lack of significant difference in lysates from DEX treated cells suggests that DEX was not increasing EROD activity through induction of CYP1A1.

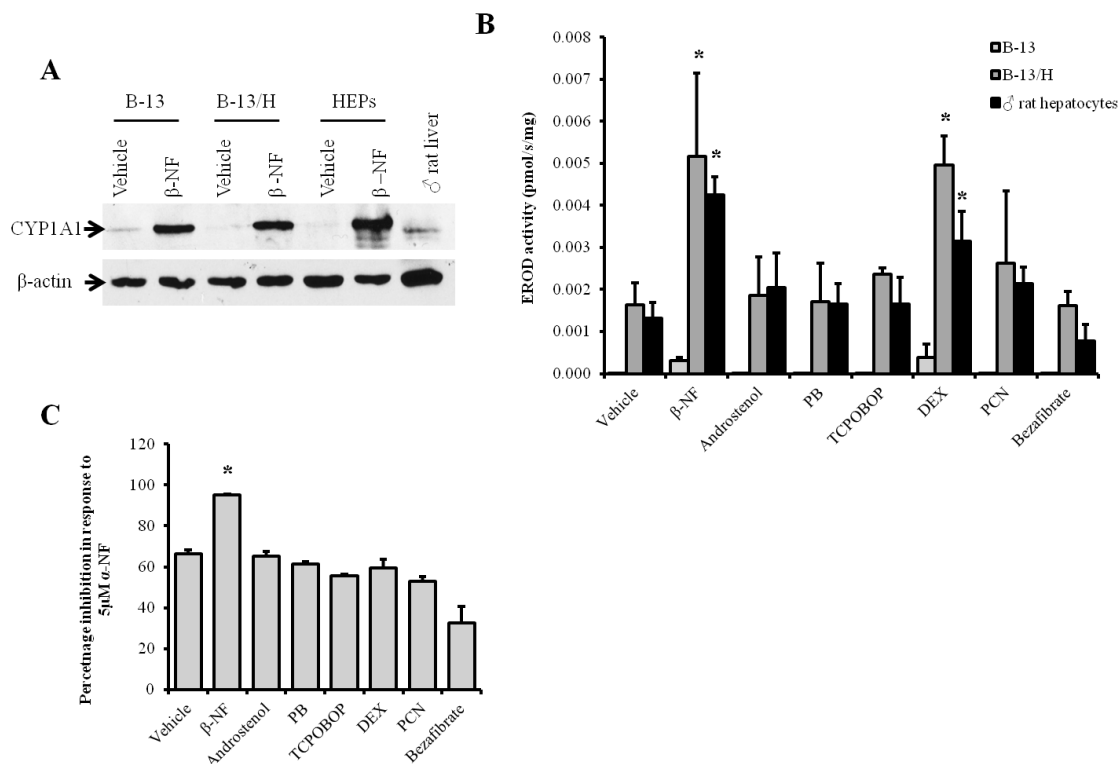


**Figure 3.10: B-13/H cells express inducible CYP1A1 protein which is functional and inducible. A. Western blot for CYP1A1 in normal and induced B-13 cells, B-13/H cells and primary rat hepatocytes.** Cells were treated daily for 3 days with vehicle (0.1% (v/v) DMSO) or 20µM β-NF. On the 4<sup>th</sup> day, lysates were prepared from the treated cells and rat liver and quantified by Lowry assay. 20µg of protein/well was separated by SDS-PAGE and transferred to a nitrocellulose membrane which was blocked and probed. Antibody binding was detected using ECL Western blot substrate. Blot is representative of at least 3 separate experiments. **B. EROD activity in induced B-13 and B-13/H cells, and primary rat hepatocytes.** EROD activity was measured in lysates prepared from B-13 cells, B-13/H cells and primary rat hepatocytes treated as in A. Readings were normalised to lysate protein concentration. Results are the mean and SD of 3 determinations from a single experiment, typical of at least 3 separate experiments. \*statistically significantly different to relevant vehicle treated control at  $p < 0.05$ . **C. Inhibition of EROD activity in induced B-13/H cells following α-NF treatment.** EROD activity was determined in B-13/H lysates prepared as in B. with or without 5µM α-NF. Results are the mean and SD of 3 independent determinations from a single experiment, typical of at least 3 separate experiments. \*statistically greater than vehicle treated cells at  $p < 0.05$ .

Finally, to determine the ability of CYP1A1 expressed in B-13 and B-13/H cells to bio-activate pro-genotoxins to DNA damaging metabolites, vehicle and β-NF induced cells were treated with different concentrations of benzo[a]pyrene. Benzo[a]pyrene is primarily metabolised by CYP1A1 to produce DNA damaging metabolites [200]. As shown in figure 3.11, vehicle induced B-13 and B-13/H cells only showed significant DNA damage when treated with 100µM benzo[a]pyrene. However, B-13/H cells induced with β-NF were significantly more sensitive to benzo[a]pyrene induced DNA damage, as in these cells, DNA damage was detectable from 25µM. Furthermore, at 100µM benzo[a]pyrene, the olive tail moment was approximately 13 whereas in vehicle

induced B-13/H cells it was only around 6. Benzo[a]pyrene induced DNA damage in B-13 cells was unaffected by  $\beta$ -NF induction.

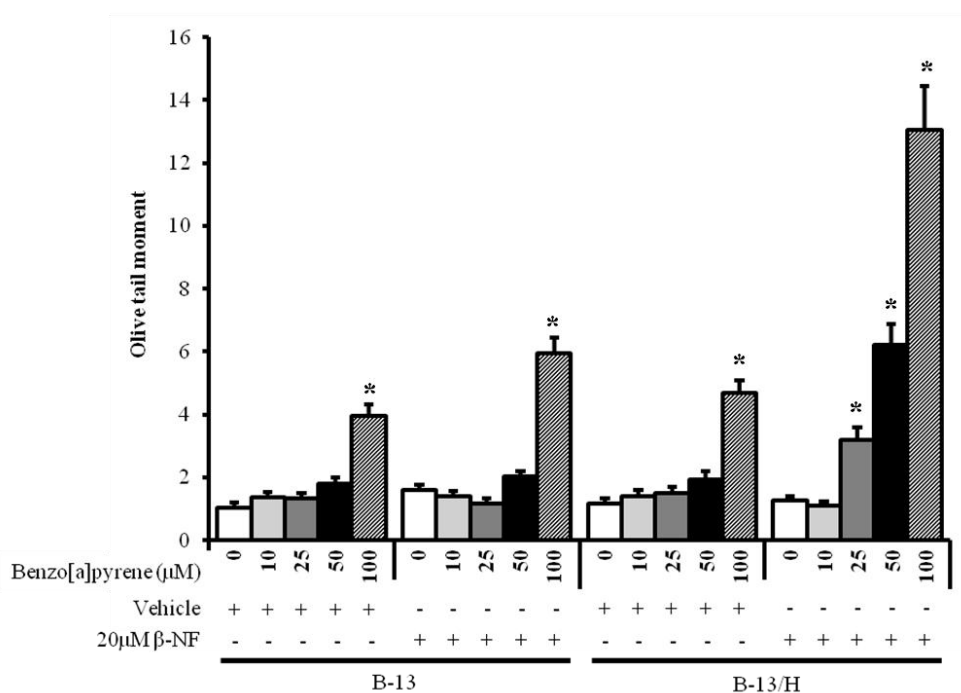


**Figure 3.11: Benzo[a]pyrene dose response in vehicle or  $\beta$ -NF induced B-13 and B-13/H cells measured by comet assay.** B-13 and B-13/H cells were treated daily with vehicle (0.1% (v/v) DMSO) or 20  $\mu$ M  $\beta$ -NF and on the 4<sup>th</sup> day treated additionally with vehicle (1% (v/v) DMSO) or different concentrations of benzo[a]pyrene for 16 hours. Following treatment, cells were subject to the alkaline comet assay and DNA stained with SYBR gold. Slides were viewed using a fluorescence microscope and DNA damage calculated using cometscore software. Data are the mean and SE of 50 cells from a single experiment, typical of at least 3 separate experiments. \*significantly different, as calculated by ANOVA followed by the Bonferroni-Holm post-hoc test, to non-benzo[a]pyrene treated control at  $p < 0.05$ .

Initiation of apoptosis involves the activation of endonucleases which restrict cellular DNA. This could lead to a false positive in a comet assay where apoptotic cells typically have significant comets [201]. DNA replication involves single DNA strand breakage at replication forks, which although required for cell division, may also lead to increased tail length/DNA content and false positive findings [202]. To confirm that DNA damage resulting from treatments was not due to initiation of apoptosis or DNA replication, DNA diffusion and BrdU incorporation in treated cells was determined. Figure 3.12 shows that at the concentration range employed, comets were not associated with cytotoxicity or with a significant increase in DNA synthesis.

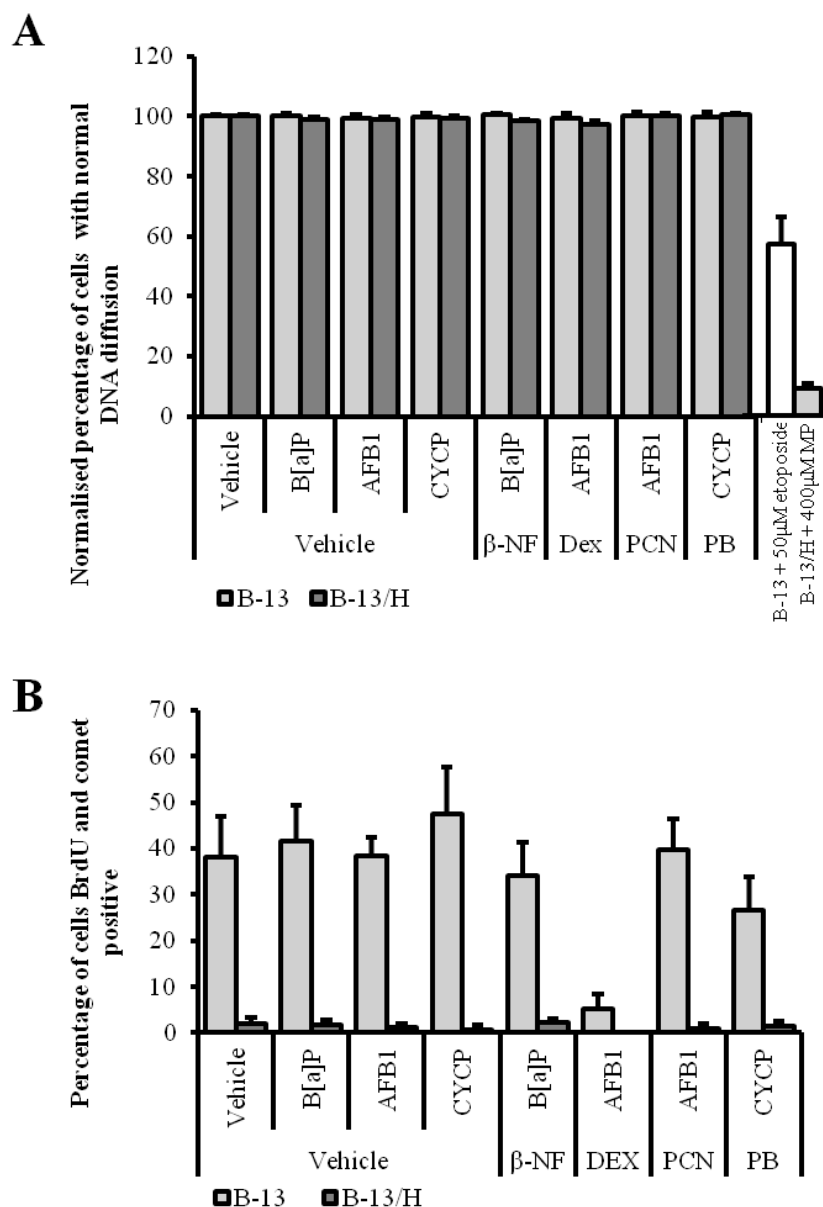


**Figure 3.12: DNA damaging compounds did not induce significant cell death or division in treated cells. A. DNA diffusion assay of cells treated with inducers and pro-genotoxic compounds.** B-13 and B-13/H cells were treated daily for 3 days with vehicle (0.1% (v/v) DMSO) or CYP450 inducer. On The 4<sup>th</sup> day, cells were treated additionally with positive controls (50µM etoposide or 400µM methapyrilene (MP)) or different pro-genotoxic compounds: (B[a]P (benzo[a]pyrene), 100µM; AFB1 (aflatoxin B1), 400nM; CYCP (cyclophosphamide), 200µM). Following treatment cells were embedded in low melting point agarose, lysed and stained with SYBR gold. Slides were viewed using a fluorescence microscope and the percentage of cells with normal DNA diffusion (using the positive controls as a guide) calculated. Results are the mean and SD from 4 fields of view, with at least 100 individual cells counted in total, from a single experiment, typical of at least 3 separate experiments. **B. Percentage of comet cells staining positive for BrdU following inducer and pro-genotoxin treatment.** Cells treated as in **A** were incubated with 15µM BrdU for 2 hours then were subject to the alkaline comet assay and immunostained for BrdU. Following counterstaining with DAPI, slides were viewed using a fluorescence microscope and the percentage of comets staining positive for BrdU calculated. Data are the mean and SD calculated from 4 fields of view, with at least 100 individual cells counted in total. Results are from a single experiment, typical of at least 3 separate experiments. For **A** and **B**, no statistical analysis was performed.

### 3.6 CAR activators induce CYP2B1 mRNA in B-13/H cells

The CYP2B sub-family of CYP450s were some of the first CYP450s to be purified to homogeneity and shown to be markedly induced by PB pre-treatment. Although it has been established that CAR mediates this induction, PB does not bind directly to the CAR. The mechanism has recently been determined, as outlined in the introduction, to be associated with an interference in epidermal growth factor receptor signalling [50].

To determine the expression of CYP2B1 and associated transcripts in B-13/H cells, RT-PCR was carried out. This showed (figure 3.13A) that B-13/H cells expressed CYP2B1 mRNA but not CYP2B2 or CYP2B3. Importantly they also expressed the CAR similar to intact rat liver, suggesting that they would be able to induce CYP2B1.

B-13 and B-13/H cells were therefore treated with a range of prototypical inducers and their CYP2B1 mRNA expression measured using qPCR. In B-13 cells, in agreement with the RT-PCR screening, CYP2B1 mRNA expression could not be detected. Conversely, in B-13/H cells, basal CYP2B1 expression could be detected and treatment with CAR agonists PB and TCPOBOP led to a significant increase in CYP2B1 mRNA expression to levels greater than in intact rat liver (figure 3.13B). Furthermore, treatment of B-13/H cells with the PXR agonist DEX also led to a significant increase in CYP2B1 mRNA expression; this would be expected as the PXR and CAR demonstrate some functional redundancy in that they have an overlapping affinity for consensus sequences in the promoter regions of numerous genes including CYP2B1 and CYP3A1 [42]. In primary rat hepatocytes treated with the same range of inducers (figure 3.13C), all treatments significantly increased expression of CYP2B1 mRNA; bezafibrate induced the largest increase in expression but this was followed by DEX and PB.

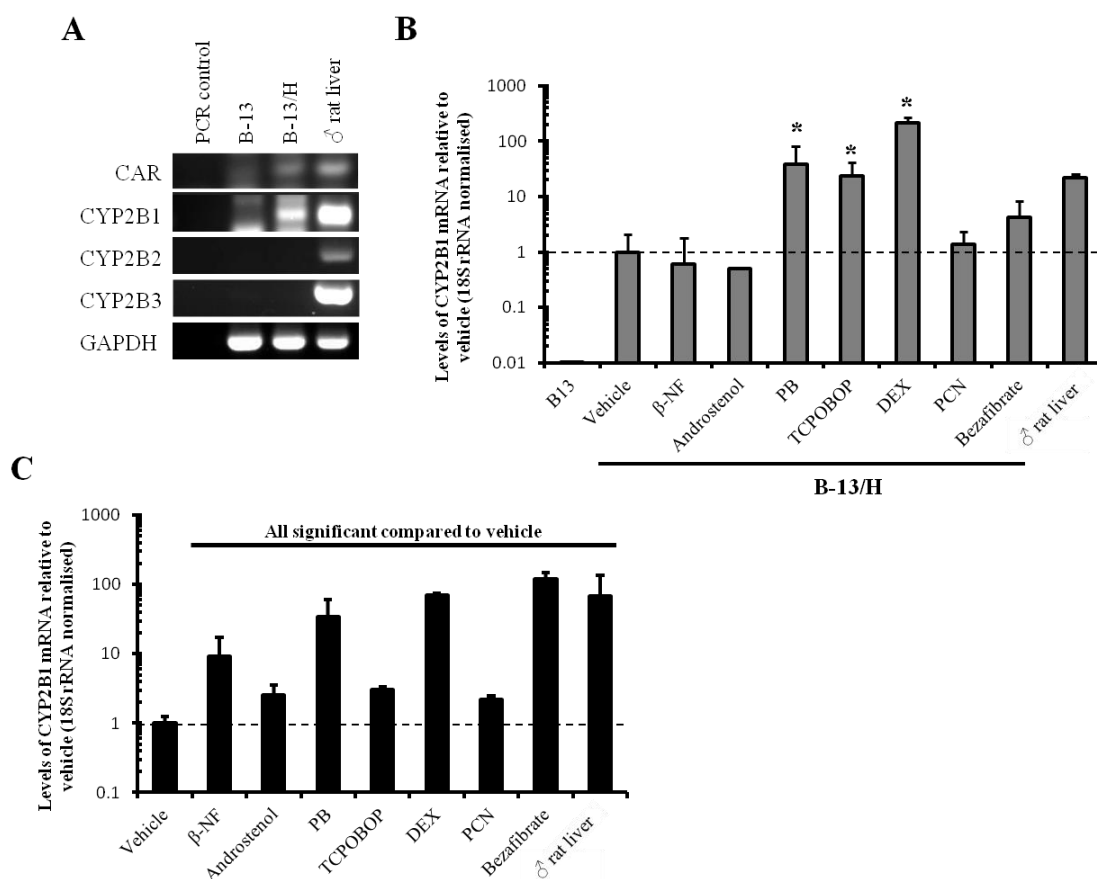


**Figure 3.13: B-13/H cells express inducible CYP2B1. A. RT-PCR for CYP2B associated transcripts.** Total RNA was extracted from samples using TRIzol and cDNA produced which was used as the template for PCR. Following PCR, samples were separated by agarose gel electrophoresis and visualised by UV transillumination. **B. qPCR for CYP2B1 in B-13/H cells treated with prototypical CYP450 inducers.** B-13/H cells were treated for 3 days daily with vehicle (0.1% (v/v) DMSO) or inducer and harvested on the 4<sup>th</sup> day. Total RNA was extracted from the cells using TRIzol and reverse transcribed. cDNA was used as template for qPCR measuring the expression of CYP2B1. Readings were normalised to 18S rRNA expression and fold change expressed relative to vehicle treated cells. Bars are the mean and SD of 3 independent determinations from a single experiment, typical of at least 3 separate experiments. \*significantly different to vehicle control at  $p < 0.05$ . **C. qPCR for CYP2B1 in primary rat hepatocytes treated with prototypical CYP450 inducers.** From primary rat hepatocytes treated as in **B**, RNA was extracted and reverse transcribed. The cDNA was used as a template for qPCR measuring the expression of CYP2B1 and results were normalised to 18S rRNA expression. Results are expressed as fold change relative to vehicle treated cells. Bars are the mean and SD of 3 independent determinations from a single experiment, typical of at least 3 separate experiments. \*significantly different to vehicle control at  $p < 0.05$ .

To assess if induction of CYP2B1 at the level of mRNA translated to an increase in CYP2B1 protein, Western blotting for CYP2B1 was performed on lysates from vehicle, TCPOBOP and PB treated B-13 and B-13/H cells, primary rat hepatocytes and rat liver. As illustrated in figure 3.14A, CYP2B1 protein could only be detected in vehicle and PB induced rat liver but not in any other samples. To test for CYP2B1 activity, a PROD assay was carried out on lysates from B-13 cells, B-13/H cells and primary rat hepatocytes treated with different prototypical inducers. Of all the cells tested, PROD

activity could only be detected in the lysates of B-13/H cells. Lysates from B-13/H cells treated with PB and DEX showed a small but significant increase in PROD activity compared to those from vehicle treated cells (figure 3.14B). These findings suggest that, although B-13/H cells express CYP2B1 mRNA, it is not efficiently translated to protein. This would account for the low basal and induced PROD activity. The induction in PROD activity may also have been a result of PB or DEX mediated induction of CYP3A1 through the CAR/PXR, which may have non-specifically metabolised the 7-pentoxylresorufin, thereby leading to an apparent induction of PROD activity.

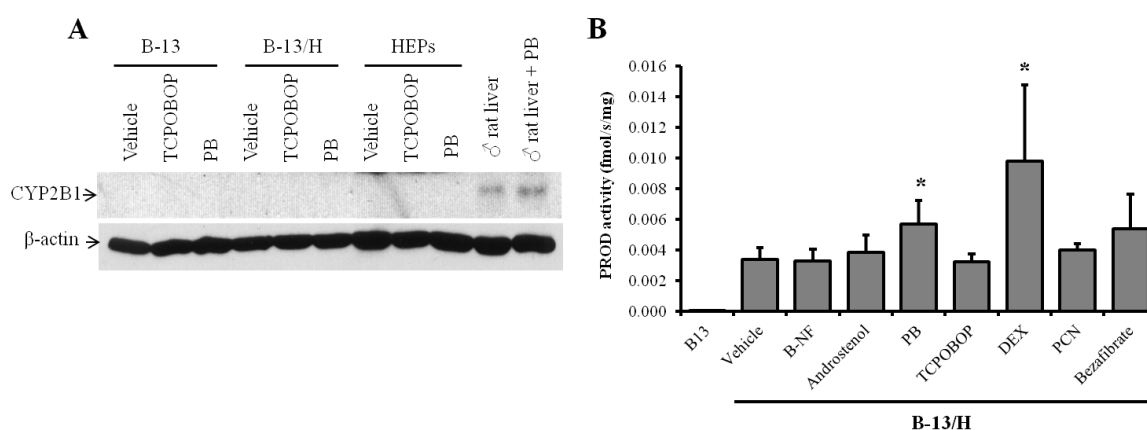


**Figure 3.14: B-13/H cells express no detectable CYP2B1 protein. A. Western blot for CYP2B1 in induced B-13 and B-13/H cells and primary rat hepatocytes.** Cells were treated daily for 3 days with vehicle (0.1% (v/v) DMSO), 1.5 $\mu$ M TCPOBOP or 1mM PB. On the 4<sup>th</sup> day, lysates were prepared from treated cells and rat liver and quantified by Lowry assay. 20 $\mu$ g of protein/well was separated by SDS-PAGE and transferred to a nitrocellulose membrane which was blocked and probed. Antibody binding was detected using ECL Western blot substrate. Blot is representative of at least 3 separate experiments. **B. PROD activity in induced B-13/H cells.** PROD activity was measured in lysates prepared from B-13/H cells treated as in A. Readings were normalised to lysate protein concentration. Readings are the mean and SD of 6 independent determinations from 2 separate experiments. \*significantly different to vehicle treated control at  $p < 0.05$ .

Finally, B-13 and B-13/H cells were treated with cyclophosphamide, a CYP2B bioactivated pro-genotoxin, to determine if they were able to bioactivate it to produce DNA damaging metabolites. The results of this showed that B-13/H but not B-13 cells were susceptible to cyclophosphamide induced DNA damage at the highest tested dose (figure 3.15, 200 $\mu$ M). However, pre-treatment of either B-13 or B-13/H cells with PB, did not significantly change DNA damage resulting from cyclophosphamide treatment. The lack of change in response to PB is in agreement with the Western blot and PROD assay where PB treatment led to little to no change in CYP2B1 expression/function. Based on the low expression of CYP2B1 protein in B-13/H cells, it is likely that the

bioactivation of cyclophosphamide may be a result of non-specific metabolism by other CYP450s expressed more highly in B-13/H cells, rather than CYP2B1. At the concentration range employed, comets were not associated with cytotoxicity or with a significant increase in DNA synthesis (figure 3.12).

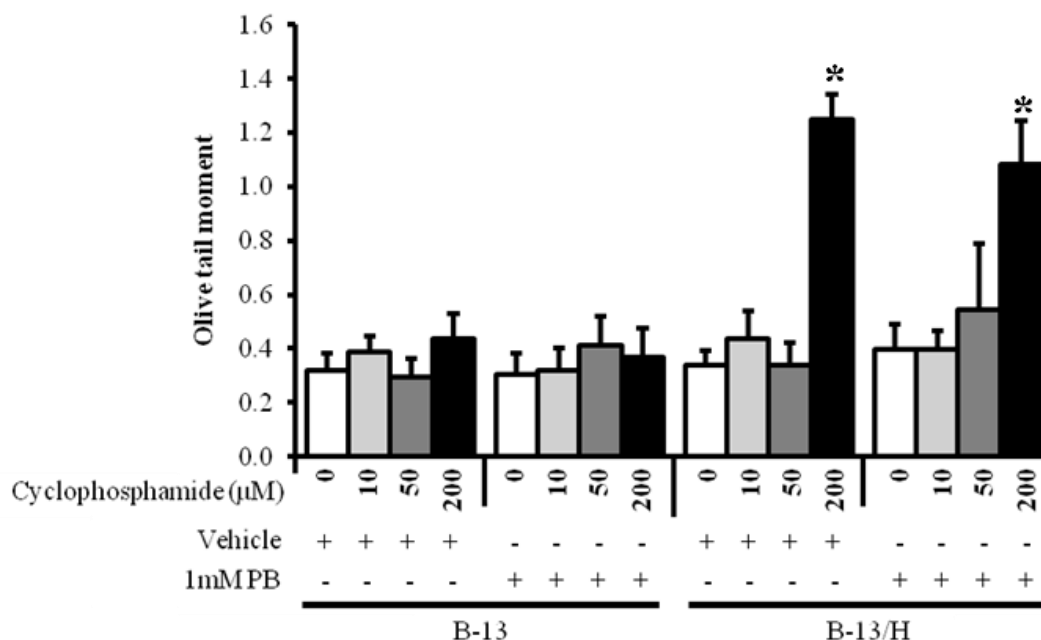


**Figure 3.15: Cyclophosphamide dose response in vehicle or PB induced B-13 and B-13/H cells measured by comet assay.** B-13 and B-13/H cells were treated daily with vehicle (0.1% (v/v) DMSO) or 1mM PB and on the 4<sup>th</sup> day treated additionally with vehicle (0.1% (v/v) DMSO) or different concentrations of cyclophosphamide for 16 hours. Following treatment, cells were subject to the alkaline comet assay and DNA stained with SYBR gold. Slides were viewed using a fluorescence microscope and DNA damage calculated using cometscore software. Data are the mean and SE of 50 cells from a single experiment, typical of at least 3 separate experiments. \*significantly different to non-cyclophosphamide treated control at  $p < 0.05$ , calculated by ANOVA followed by the Bonferroni-Holm post-hoc test.

### 3.7 PXR activators induce a quantitatively liver equivalent induction of CYP3A1 in B-13/H cells

The CYP3A sub-family is constitutively expressed and forms a major expressed sub-family in adult rat liver. The orthologous sub-family in man includes the major expressed gene CYP3A4, which is responsible for the metabolism of approximately 50% of drugs. Both CYP3A4 in man, and CYP3A1 (also referred to as CYP3A23) in the rat, are induced by activators of the PXR [203].

To initially determine the expression of PXR and CYP3A associated transcripts, RT-PCR was carried out on cDNA from B-13 and B-13/H cells, and intact male rat liver.

As shown in figure 3.16A, B-13/H cells, like rat liver, expressed the PXR as well as the transcription factors RXR $\alpha$  and RXR $\beta$ . These form heterodimers with activated PXR and are required for PXR regulated transactivation [42]. B-13/H cells also expressed CYP3A1, CYP3A2 and CYP3A19 mRNA which were not expressed by B-13 cells.

As B-13/H cells expressed PXR, it was hypothesised that CYP3A1 could be induced in the cells using PXR agonists. To test this hypothesis, B-13 and B-13/H cells were treated with a range of prototypical inducers and CYP3A1 mRNA expression measured by qPCR. This demonstrated that B-13/H cells significantly induced CYP3A1 mRNA in response to the PXR ligands, DEX and PCN and this was to levels greater than that seen in male rat liver (figure 3.16B). The previously mentioned crosstalk between PXR and CAR means that CAR can initiate transcription of a range of PXR regulated genes including CYP3A1. Accordingly, B-13/H cells treated with the CAR activators PB and TCPOBOP also significantly increased expression of CYP3A1 mRNA. In B-13 cells, no CYP3A1 mRNA could be detected in either normal or inducer treated cells confirming the RT-PCR results. Primary rat hepatocytes treated in an equivalent manner showed a similar induction profile with DEX and PCN inducing CYP3A1 mRNA the most strongly, followed by PB (figure 3.16C).

Western blotting for CYP3A1 in B-13 and B-13/H cells and primary rat hepatocytes treated with DEX and PCN (figure 3.17) showed that DEX and PCN both increased the amount of CYP3A1 protein in B-13/H cells and primary rat hepatocytes in a quantitatively similar manner. This demonstrates that the induction of CYP3A1 mRNA effectively translated to more CYP3A1 protein.

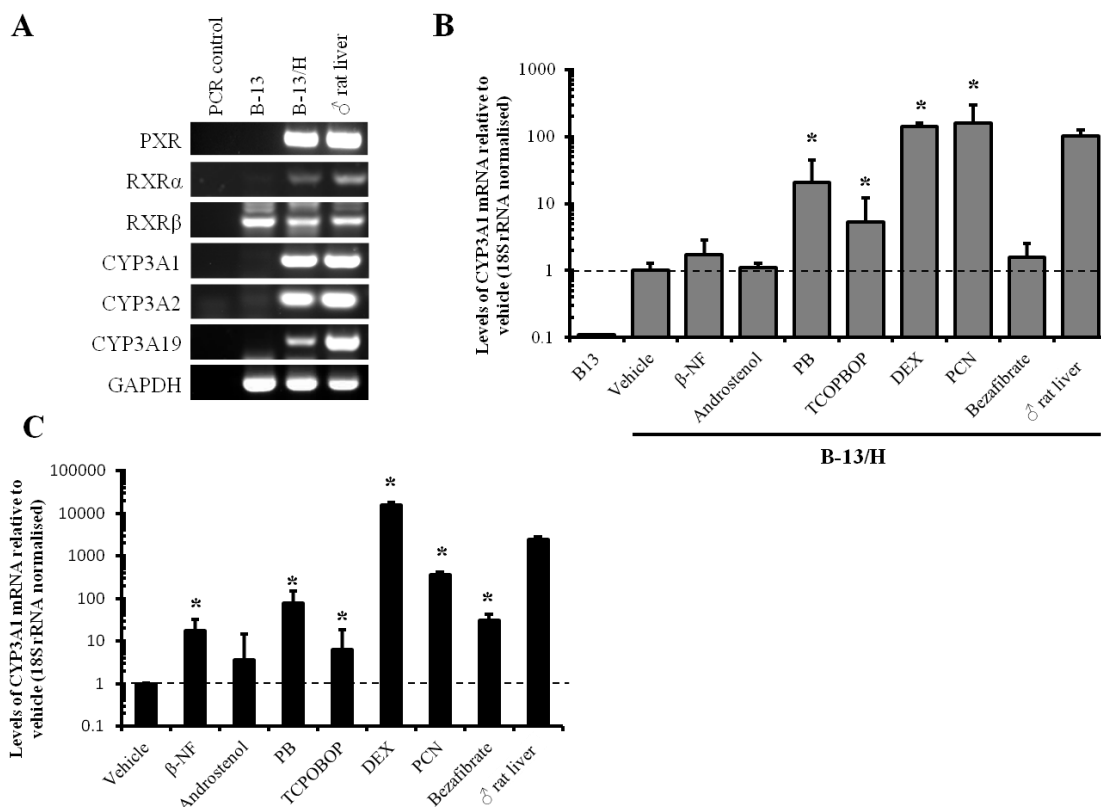


**Figure 3.16: B-13/H cells express inducible CYP3A1. A. RT-PCR for CYP3A associated transcripts.** Total RNA was extracted from samples using TRIzol and cDNA produced which was used as the template for PCR. Following PCR, samples were separated by agarose gel electrophoresis and visualised by UV transillumination. **B. qPCR for CYP3A1 in B-13/H cells treated with prototypical CYP450 inducers.** B-13/H cells were treated for 3 days daily with vehicle (0.1% (v/v) DMSO) or inducer and harvested on the 4<sup>th</sup> day. Total RNA was extracted from the cells using TRIzol and reverse transcribed. cDNA was used as template for qPCR measuring the expression of CYP3A1. Readings were normalised to 18S rRNA expression and fold change expressed relative to vehicle treated cells. Bars are the mean and SD of 3 independent determinations from a single experiment, typical of at least 3 separate experiments. \*significantly different to vehicle control at  $p < 0.05$ . **C. qPCR for CYP3A1 in primary rat hepatocytes treated with prototypical CYP450 inducers.** From primary rat hepatocytes treated as in B, RNA was extracted and reverse transcribed. The cDNA was used as a template for qPCR measuring the expression of CYP3A1 and results were normalised to 18S rRNA expression. Results are expressed as fold change relative to vehicle treated cells. Bars are the mean and SD of 3 independent determinations from a single experiment, typical of at least 3 separate experiments. \*significantly different to vehicle control at  $p < 0.05$ .

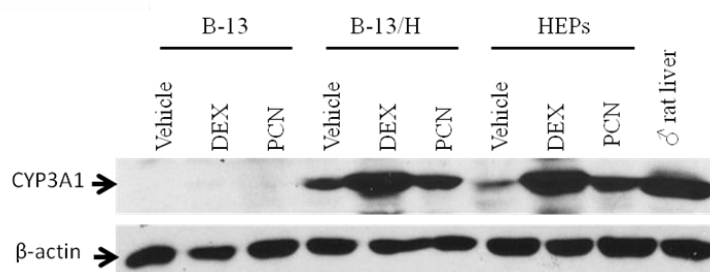


**Figure 3.17: Western blot for CYP3A1 in induced B-13 and B-13/H cells and primary rat hepatocytes.** Cells were treated daily for 3 days with vehicle (0.1% (v/v) DMSO), 10 $\mu$ M DEX or 2 $\mu$ M PCN. On the 4<sup>th</sup> day, lysates were prepared from treated cells and rat liver and quantified by Lowry assay. 20 $\mu$ g of protein/well was separated by SDS-PAGE and transferred to a nitrocellulose membrane which was blocked and probed. Antibody binding was detected using ECL Western blot substrate. Blot is representative of at least 3 separate experiments.

Based on the induction of CYP3A1 protein, it was required to determine if induced CYP3A1 protein was functional. CYP3A1 and CYP3A4 catalyse the 6 $\beta$ -hydroxylation of testosterone and this forms the basis of the most common CYP3A1 activity assay. However, this assay requires high-performance liquid chromatography and is time consuming. As a high throughput alternative, the novel probe substrate luciferin-IPA was identified. This is advertised to be primarily metabolised by CYP3A1 in rats to luciferin, which can be detected photometrically through the addition of luciferase as outlined in the methods. To validate the assay, activity was determined in serially diluted rat liver microsomes. Fitting a line of best fit showed a correlation of 0.999 indicating that there was a linear relationship between microsome concentration and relative light unit production (figure 3.18A). Treating rat liver microsomes with a range of inhibitors (figure 3.18B) showed that the specific CYP3A inhibitors troleandomycin and ketoconazole significantly reduced luciferin-IPA activity as did the general CYP450 inhibitors metyrapone and SKF525A [204-207]. Testosterone did not reduce microsome luciferin-IPA metabolism and the flavin-containing monooxygenase inhibitor methimazole surprisingly significantly increased it [208]. These findings suggest that the metabolism of luciferin-IPA is primarily catalysed by CYP3A1 in a linear manner although flavin-containing monooxygenases may also play a role.

With the assay validated, B-13 and B-13/H cells, and primary rat hepatocytes were treated with a range of prototypical inducers, lysates prepared and CYP3A1 activity determined. The results (figure 3.18C) showed that, in accordance with the mRNA and protein data, DEX and PCN induced a major and significant increase in CYP3A1 activity followed by PB in both B-13/H cells and primary rat hepatocytes. This demonstrates that induced CYP3A1 in B-13/H cells is functional.

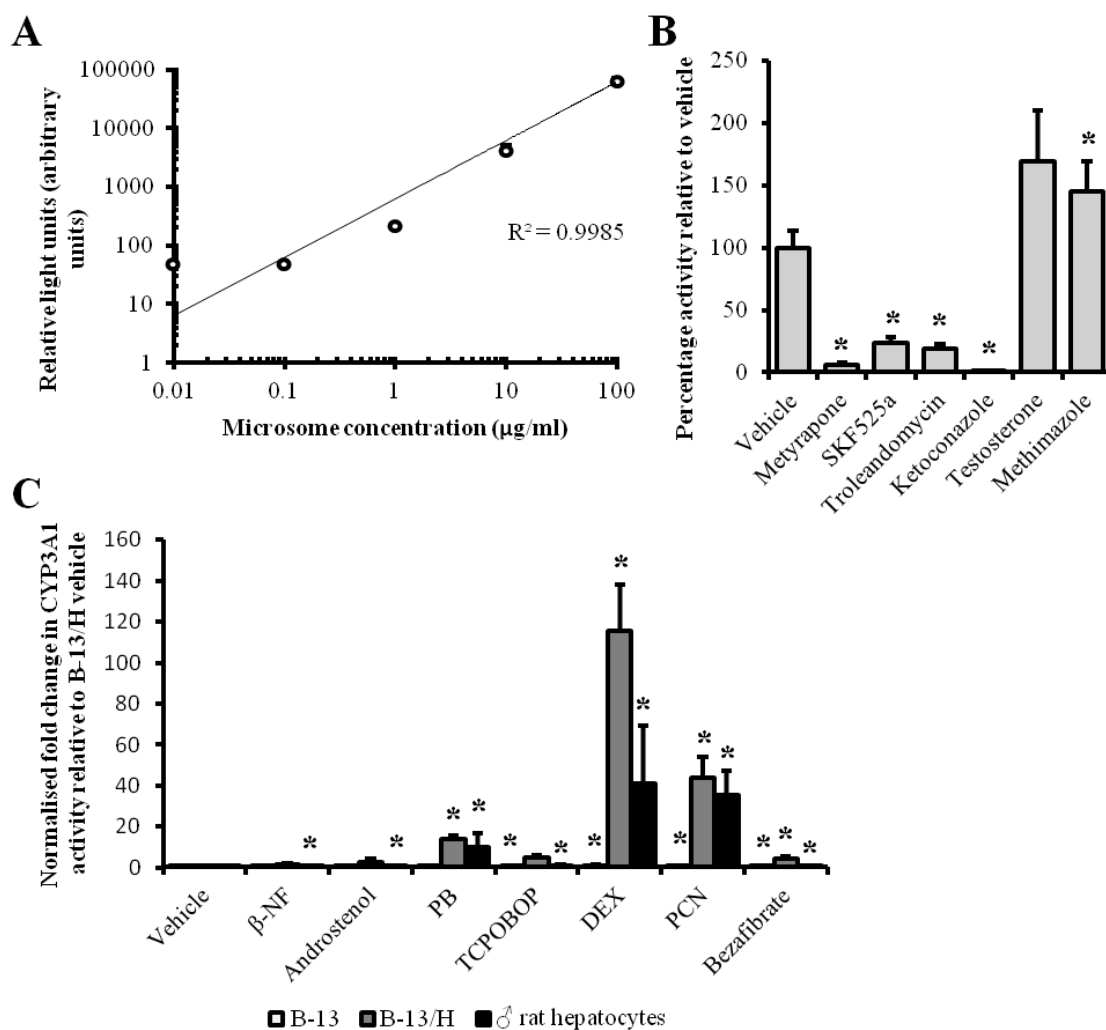


**Figure 3.18: Induced CYP3A1 in B-13/H cells is functional.** **A.** Measurement of luciferin-IPA metabolism in serially diluted microsomes. Rat liver microsomes were diluted 4 logs from 100µg/ml to 0.01µg/ml and luciferin-IPA metabolism measured. Points are the mean of 3 different rat liver microsome preparations. **B.** Percentage change in luciferin-IPA metabolism in response to different CYP450 modulators. Luciferin-IPA metabolism was measured in rat liver microsomes treated with vehicle (0.1% (v/v) DMSO) or the indicated compounds. Bars are the mean and SD of 3 different rat liver microsome preparations. \*significantly different to vehicle treated microsomes at  $p < 0.05$ . **C.** Luciferin-IPA metabolism in induced B-13 and B-13/H cells, and primary rat hepatocytes. Luciferin-IPA metabolism was measured in lysates prepared from B-13 cells, B-13/H cells and primary rat hepatocytes treated with vehicle (0.1% (v/v) DMSO) or the indicated CYP450 inducers daily for 3 days and harvested on the 4<sup>th</sup> day. Readings were normalised to lysate protein concentration. Results are shown as the fold change relative to vehicle treated B-13/H cells. Results are the mean and SD of 3 independent determinations from a single experiment, typical of at least 3 separate experiments. \*significantly different to relevant vehicle treated control at  $p < 0.05$ .

To establish if B-13/H cells could be used to test for CYP3A1 dependent pro-genotoxin bioactivation, normal and induced B-13 and B-13/H cells were treated with the pro-carcinogen aflatoxin B1 (AFB1), which is metabolised to a genotoxic product by CYP3A enzymes [209, 210]. As illustrated in figure 3.19, it was seen that uninduced B-13 cells were insensitive to AFB1 induced DNA damage whereas B-13/H cells showed

significant DNA damage at the highest tested dose (400nM). In both cell types, DEX induction significantly increased their sensitivity to AFB1 induced DNA damage in a dose dependent manner with B-13 cells showing significant damage at 200nM. This is likely due to a glucocorticoid receptor-dependent promotion of B-13/H phenotype and subsequent induction of CYP3A1 expression within the short period of induction. DEX induced B-13/H cells showed significant DNA damage from 100nM AFB1 treatment. Unexpectedly, induction with PCN in either cell type prior to AFB1 treatment had no effect on resulting DNA damage, in contrast to DEX induction. The lack of response with PCN in this experiment was likely because PCN induces a lesser fold increase in protein expression and activity compared to the potent effect of DEX (figure 3.17 and figure 3.18). At the concentration range employed, comets were not associated with cytotoxicity or with a significant increase in DNA synthesis (figure 3.12).

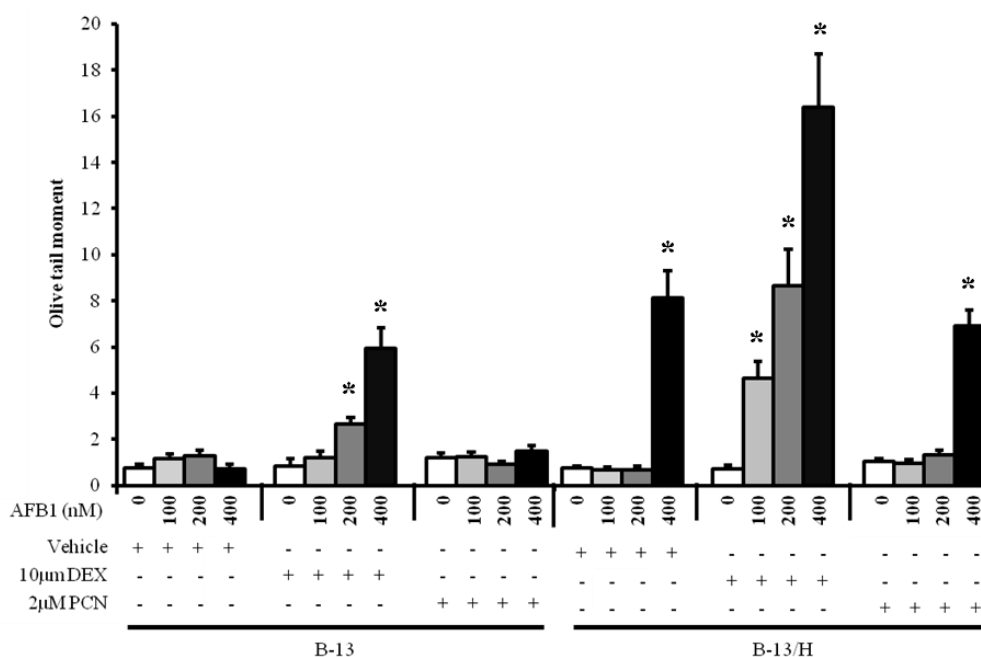


**Figure 3.19: Aflatoxin B1 dose response in vehicle, DEX or PCN induced B-13 and B-13/H cells measured by comet assay.** B-13 and B-13/H cells were treated daily with vehicle (0.1% (v/v) DMSO), 10µM DEX or 2µM PCN and on the 4<sup>th</sup> day treated additionally with vehicle (0.1% (v/v) DMSO) or different concentrations of AFB1 for 16 hours. Following treatment, cells were subject to the alkaline comet assay and DNA stained with SYBR gold. Slides were viewed using a fluorescence microscope and DNA damage calculated using cometscore software. Data are the mean and SE of 50 cells from a single experiment, typical of at least 3 separate experiments. \*significant difference to non-AFB1 treated control at  $p < 0.05$  tested by ANOVA followed by Bonferroni-Holm post-hoc test.

Cellular DNA damage, from endogenous or exogenous sources, causes the initiation of signalling cascades that result in DNA repair. A well documented signalling pathway is the phosphorylation of histone H2AX on serine 139 to  $\gamma$ -H2AX, at the site of double

stranded DNA (dsDNA) breaks, which in turn recruits DNA repair machinery [211, 212]. The quantity of  $\gamma$ -H2AX within a cell can therefore be used as a measure of dsDNA breakage. The alkaline comet assay conversely measures both single and dsDNA breakage.

To investigate the effect of AFB1 on dsDNA breakage, normal and DEX induced B-13 and B-13/H cells were treated with 400nM AFB1 for different lengths of time following which  $\gamma$ -H2AX expression was measured by Western blot. This demonstrated that by 16 hours,  $\gamma$ -H2AX was detectable in untreated B-13/H cells (figure 3.20A). DEX induction prior to AFB1 treatment clearly increased the rate of accumulation of  $\gamma$ -H2AX with saturation of  $\gamma$ -H2AX accumulation by 8 hours. This suggests that DEX induction increased the sensitivity of B-13/H cells to AFB1 induced dsDNA breakage. In B-13 cells,  $\gamma$ -H2AX protein was detected, however its accumulation had no consistent relation to treatments. This variation may be because  $\gamma$ -H2AX accumulation has been shown to be dynamic and variable in proliferating cells such as B-13s [213]. Conversely, B-13/H cells do not proliferate (figure 3.1) and this may explain why they do not show the same variation.

To confirm that increased DNA damage in DEX induced cells from AFB1 was due to enhanced CYP3A expression, vehicle and DEX induced B-13/H cells were treated with AFB1 in the presence or absence of ketoconazole, a CYP3A specific inhibitor. As shown in figure 3.20B, both normal and DEX induced B-13/H cells treated with AFB1 showed  $\gamma$ -H2AX accumulation which was attenuated by ketoconazole treatment. DEX induced AFB1 treated cells showed greater  $\gamma$ -H2AX accumulation than un-induced B-13/H cells and the increased expression of CYP3A1 in DEX treated cells confirms that CYP3A1 was induced by DEX. Immunostaining of  $\gamma$ -H2AX in similarly treated B-13/H cells showed equivalent results with nuclear accumulation of  $\gamma$ -H2AX following AFB1 treatment, which was enhanced by DEX induction (figure 3.21). Treatment with ketoconazole similarly attenuated AFB1 induced  $\gamma$ -H2AX nuclear accumulation. This result suggests that increased sensitivity of B-13/H cells treated with DEX to AFB1 induced DNA damage is primarily due to increased expression of CYP3A1 rather than other CYP450s.

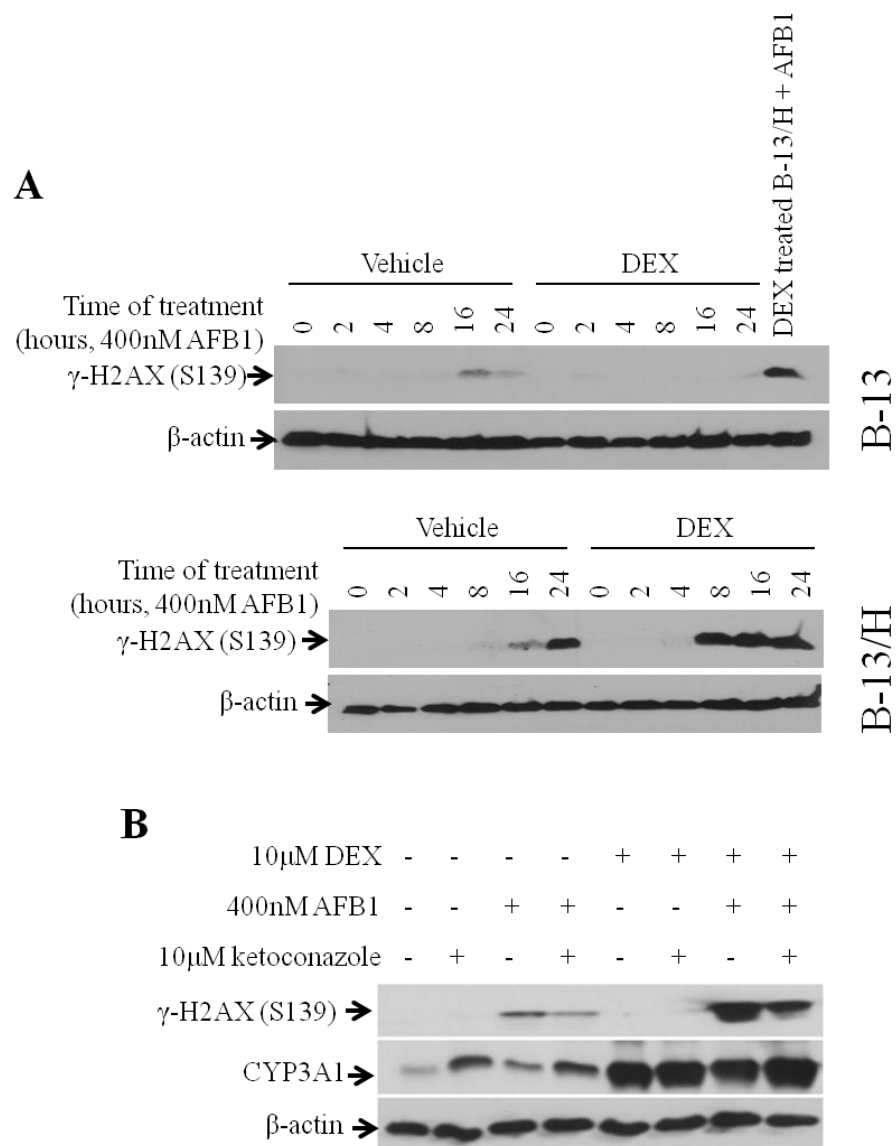


**Figure 3.20: DEX induced B-13/H cells are significantly more sensitive to inhibitable AFB1 induced DNA damage. A. Western blot for  $\gamma$ -H2AX in B-13 and B-13/H cells treated with AFB1 for differing periods of time.** B-13 and B-13/H cells were dosed daily for 3 days with vehicle (0.1% (v/v) DMSO) or 10 $\mu$ M DEX then on the 4<sup>th</sup> day with 400nM AFB1 for different periods of time. **B. Western blot for  $\gamma$ -H2AX in treated B-13/H cells.** B-13/H cells were treated with vehicle (0.1% (v/v) DMSO) or DEX daily for 3 days. On the 4<sup>th</sup> day, cells were additionally incubated with vehicle or 10 $\mu$ M ketoconazole for 6 hours following which they were incubated additionally with vehicle or 400nM AFB1 for 16 hours. For **A** and **B**, following treatment, lysates were prepared and quantified by Lowry assay. 20 $\mu$ g of protein/well was separated by SDS-PAGE and transferred to a nitrocellulose membrane which was blocked and probed. Antibody binding was detected using ECL Western blot substrate. For **B**, blot is representative of at least 3 separate experiments.

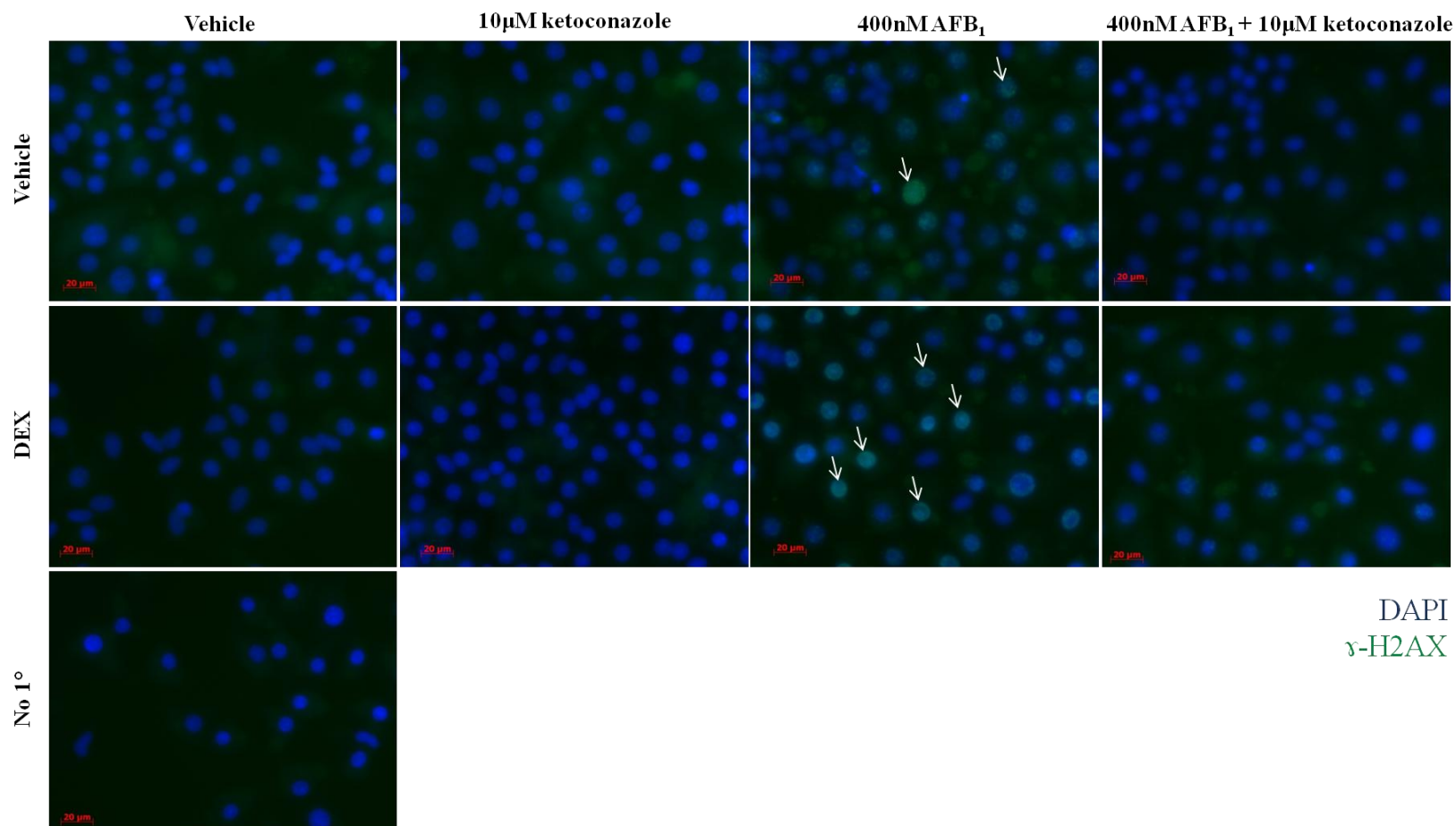


**Figure 3.21: DEX pretreatment of B-13/H cells causes nuclear accumulation of  $\gamma$ -H2AX in response to AFB1.** B-13/H cells were treated with vehicle (0.1% (v/v) DMSO) or DEX daily for 3 days. On the 4<sup>th</sup> day, cells were additionally incubated with vehicle or 10 $\mu$ M ketoconazole for 6 hours following which they were incubated additionally with vehicle or 400nM AFB1 for 16 hours. The cells were then fixed, blocked, immunostained for  $\gamma$ -H2AX and counterstained with DAPI. Cells were analysed using a Zeiss fluorescence microscope. Scale bar indicates 20 $\mu$ m. Images are representative of at least 3 separate experiments.

### 3.8 B-13/H cells express the PPAR $\alpha$ and agonists induce peroxisome proliferation

The CYP4A sub-family primarily catalyses the metabolism of endogenous substrates: mainly fatty acid and prostaglandin  $\omega$ -hydroxylation. The expression of CYP4A is tightly regulated by the PPAR $\alpha$  which is activated by a range of fatty acids and fibrates [63, 64]. Analysis of the B-13 genome indicated that *Cyp4a2* contained a deletion within an exon and *Cyp4a1*, a deletion within an intron (figure 3.22)

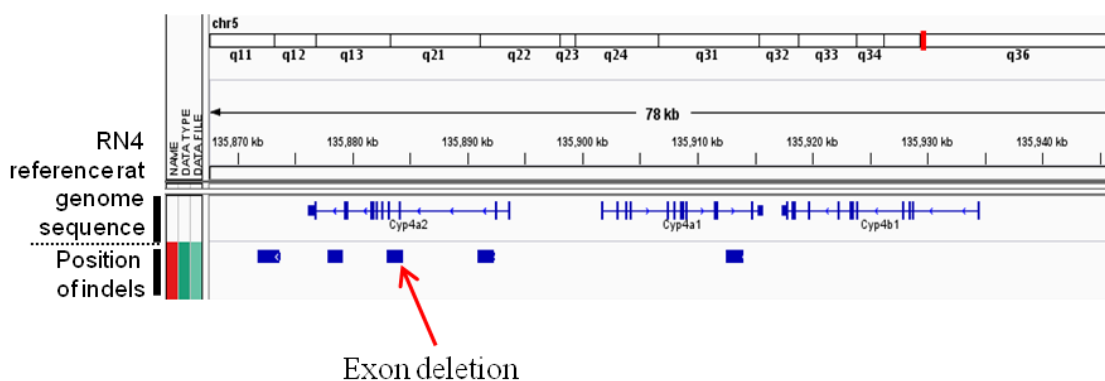


**Figure 3.22: The coding region of *rCyp4a2* is mutated in B-13 cells.** Schematic diagram of B-13 *Cyp4a1*, *Cyp4a2* and *Cyp4b1* genomic region indicating exon deletion of *Cyp4a2*. The sequence of the B-13 cell line (including insertions and deletions) was aligned to *Rattus norvegicus* reference sequence 4 using Integrative Genomics Viewer software.

Analysis of PPAR $\alpha$  and CYP4A expression in B-13 and B-13/H cells by RT-PCR showed that, although they both expressed PPAR $\alpha$  mRNA similar to male rat liver, no CYP4A mRNA could be detected in B-13 or B-13/H cells (figure 3.23A). To determine if B-13 and B-13/H cells could induce CYP4A1 in response to PPAR $\alpha$  activation, they were treated with bezafibrate, a PPAR $\alpha$  agonist. Compared to male rat liver, B-13/H cells expressed very low levels of CYP4A1 mRNA which was increased by treatment with bezafibrate, but only by around 4 fold (figure 3.23B). In B-13 cells, no CYP4A1 mRNA could be routinely detected.

The level of CYP4A1 mRNA expression in primary rat hepatocytes was around 1/10<sup>th</sup> of that seen in male rat liver and was significantly induced more than 200 fold in response to bezafibrate treatment (figure 3.23C). Probing for CYP4A1 protein in vehicle or bezafibrate induced B-13 and B-13/H cells, and primary rat hepatocytes showed that CYP4A1 protein was only detectable in primary rat hepatocytes and rat liver, not in B-13 or B-13/H cells (figure 3.23D). Treatment of primary rat hepatocytes

with bezafibrate caused a clear increase in CYP4A1 protein expression which suggests that the up-regulation of CYP4A1 mRNA in response to bezafibrate directly translated to an increase in CYP4A1 protein.

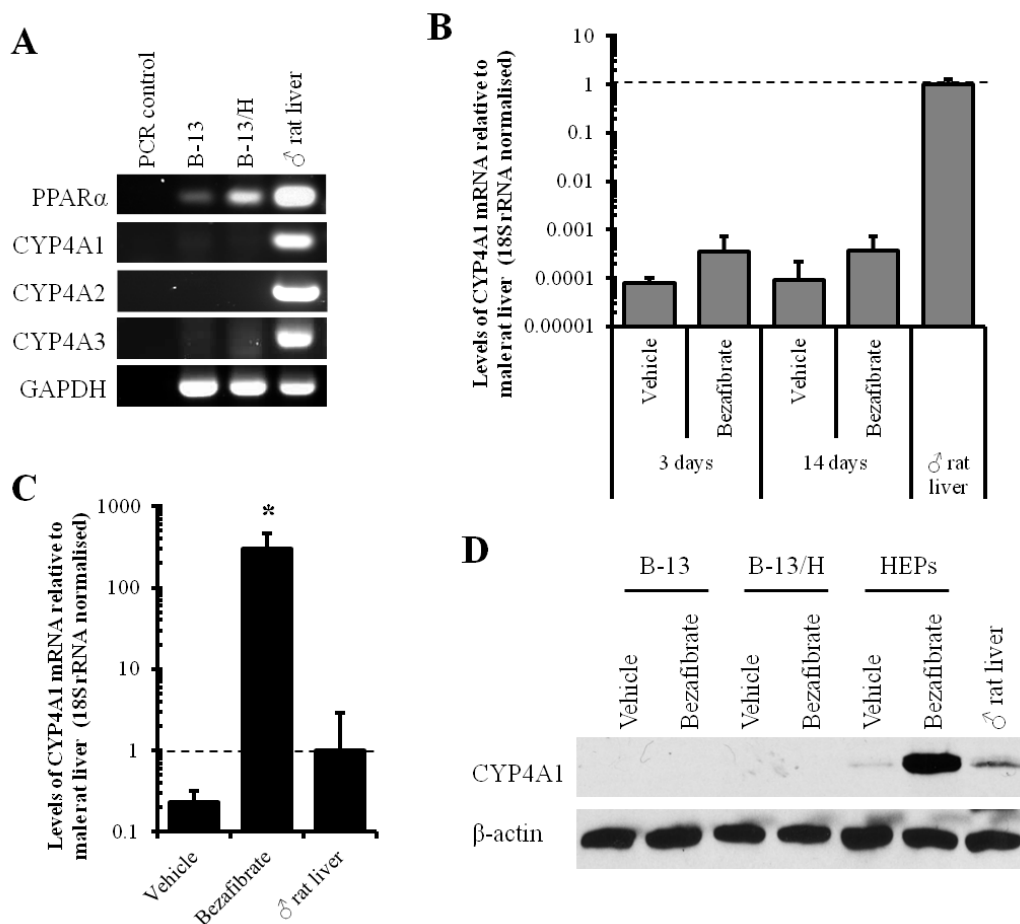


**Figure 3.23: B-13/H cells express PPAR $\alpha$  but only weakly induce CYP4A1. A. RT-PCR for CYP4A associated transcripts.** Total RNA was extracted from samples using TRIzol and cDNA produced which was used as the template for PCR. Following PCR, samples were separated by agarose gel electrophoresis and visualised by UV transillumination. **B. qPCR for CYP4A1 in B-13/H cells treated with bezafibrate.** B-13/H cells were treated for 3 days daily or over 14 days with vehicle (0.1% (v/v) DMSO) or 250 $\mu$ M bezafibrate. Total RNA was then extracted from the cells using TRIzol and reverse transcribed. The cDNA was used as template for qPCR measuring the expression of CYP4A1. Readings were normalised to 18S rRNA expression and fold change expressed relative to male rat liver. Bars are the mean and SD of 3 independent determinations from a single experiment, typical of at least 3 separate experiments. No statistical analysis was performed. **C. qPCR for CYP4A1 in primary rat hepatocytes treated with bezafibrate.** From primary rat hepatocytes treated as in **B**, RNA was extracted and reverse transcribed. The cDNA was used as a template for qPCR measuring the expression of CYP4A1 and results were normalised to 18S rRNA expression. Results are expressed as fold change relative to male rat liver. Bars are the mean and SD of 3 independent determinations from a single experiment, typical of at least 3 separate experiments. \*significant difference to vehicle control at  $p < 0.05$ . **D. Western blot for CYP4A1.** Cells were treated daily for 3 days with vehicle (0.1% (v/v) DMSO) or 250 $\mu$ M bezafibrate. On the 4<sup>th</sup> day, lysates were prepared and quantified by Lowry assay. 20 $\mu$ g of protein/well was separated by SDS-PAGE and transferred to a nitrocellulose membrane which was blocked and probed. Antibody binding was detected using ECL Western blot substrate. Blot is representative of at least 3 separate experiments.

As outlined in the introduction, PPAR $\alpha$  activation in the rat results in proliferation of peroxisomes in the liver [65]. This is a physiologically important response required for control of whole body energy homeostasis through the direct regulation of fatty acid  $\beta$ -oxidation. To first identify if B-13/H cells contained peroxisomes (as has been previously shown [125]), they were imaged by transmission electron microscopy. As shown in figure 3.24A, cellular organelles with the appearance of peroxisome (arrowed) were identified in B-13/H cells. None could be found in B-13 cells. This suggests that the transdifferentiation of B-13 to B-13/H cells involves the initiation of peroxisome production.

Based on the presence of peroxisomes in B-13/H cells, it was hypothesised that PPAR $\alpha$  activation would induce peroxisomal proliferation. Previously, ciprofibrate has been shown to increase catalase activity in select B-13/H cells, but the change has not been quantified [125]. To test the hypothesis, B-13/H cells were treated for 3 or 14 days with vehicle or bezafibrate and the expression of PMP70, which is a major component of peroxisomes [214], measured. Results showed that treatment of B-13/H cells for 3 or 14 days increased PMP70 expression, although the increase was marginal compared to primary rat hepatocytes similarly treated (figure 3.24B). To visualise the distribution of peroxisomes following induction, B-13/H cells were treated with bezafibrate for 14 days and PMP70 then detected by immunostaining. Cells were treated for 14 days because PMP70 induction was more consistent than after only 3 days of treatment. Imaging showed that staining was punctate and cytoplasmic which suggests that PMP70 was labelling peroxisomes in the cells (figure 3.24C). Treatment of B-13/H cells with bezafibrate for 14 days caused an apparent increase in PMP70 staining compared to vehicle treated cells. The mean number of peroxisomes per cell was quantified and this showed that bezafibrate significantly increased the number seen per cell compared to vehicle treated cells.

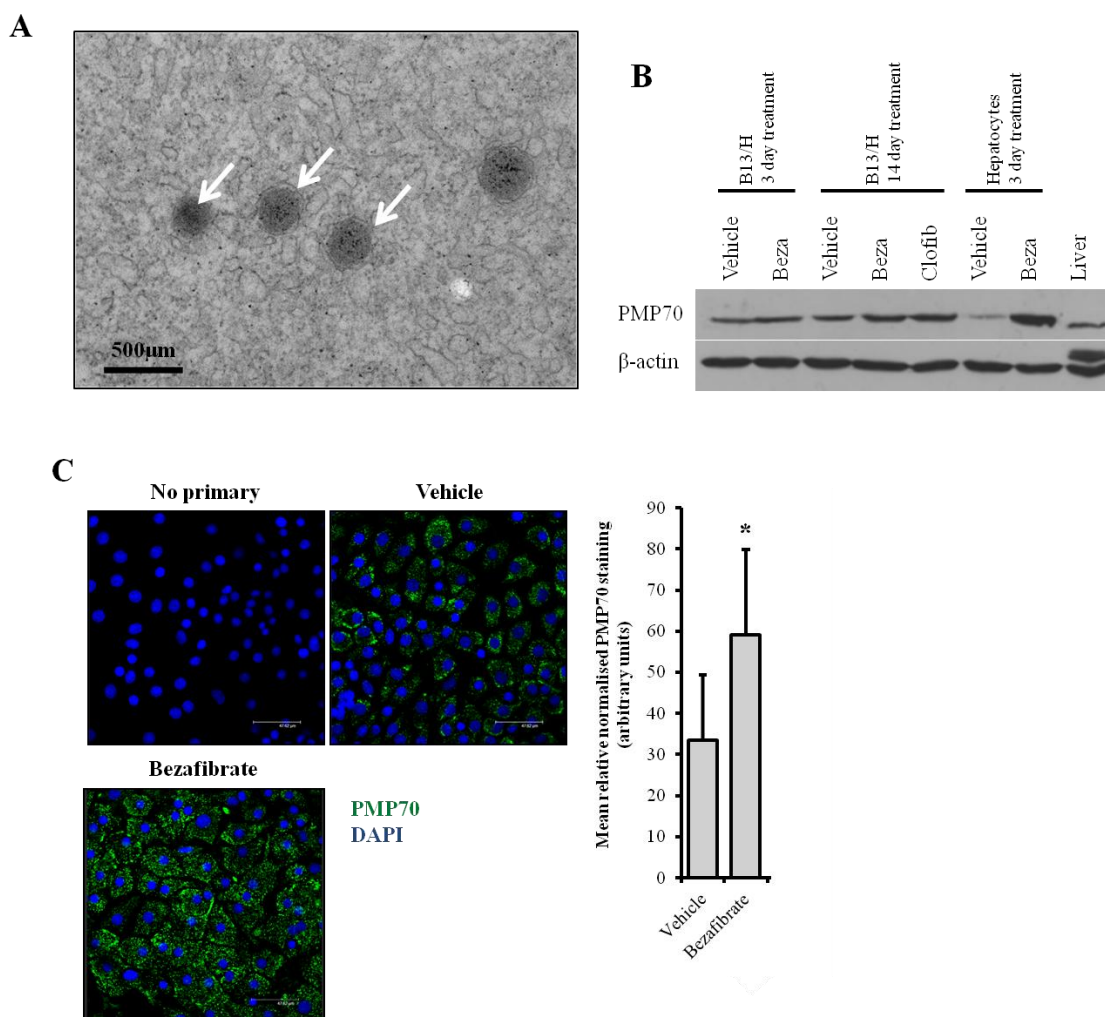


**Figure 3.24: B-13/H cells are sensitive to peroxisome proliferators. A. Peroxisomes in B-13/H cells.** Transmission electron photomicrograph at 34000x magnification of a B-13/H cell. Arrows indicate peroxisomes. **B. Western blot for PMP70 in fibrate treated cells.** Cells were treated daily for 3 days or over 2 weeks (as indicated) with vehicle (0.1% (v/v) DMSO), 250µM bezafibrate (bezafib) or 500µM clofibrate (clofib). Following treatment, lysates were prepared from treated cells and rat liver and quantified by Lowry assay. 20µg of protein/well was separated by SDS-PAGE and transferred to a nitrocellulose membrane which was blocked and probed. Antibody binding was detected using ECL Western blot substrate. Results are representative of at least 3 separate experiments. **C. PMP70 immunostaining in B-13/H cells.** B-13/H cells were treated with vehicle (0.1% (v/v) DMSO) or 250µM bezafibrate for 14 days. Following treatment cells were fixed, blocked and immunostained for PMP70. The cells were then counterstained with DAPI. Cells were photographed using a Zeiss fluorescence microscope and staining quantified using ImageJ particle counter. Results were normalised to cell number. Results are the mean and SD of 5 fields of view from the same experiment, typical of at least 3 separate experiments. Scale bar indicates 48µm. \*significantly different to vehicle control at  $p < 0.05$ .

### 3.9 Chapter discussion

CYP450s are involved in the metabolism of the majority of drugs and it is therefore important that they are expressed in cell models being used for toxicity screening. Other hepatocyte-like cells commonly used for toxicity screening generally show limited expression of CYP450s, particularly HepG2 cells, restricting the extrapolation of results to an *in-vivo* setting. Based on their previously documented expression of several DMEs, it was hypothesised that B-13/H cells expressed a similar range of functional CYP450s to rat hepatocytes and had equivalent inductive capacity.

As expected, treatment of B-13 cells with 10nM DEX caused the induction of hepatic markers, arrested proliferation and formation of haem-bound CYP450 and cytochrome b<sub>5</sub>.

In numerous mammalian species including humans, sex effects numerous aspects of drug kinetics due to the differing levels of expression of different drug metabolising enzymes. Women for example show greater expression of CYP3A4 to men resulting in increased rates of metabolism of numerous drugs including erythromycin [215, 216]. It is therefore a clinically relevant phenomenon. Regulation of sexual dimorphic CYP450 expression is complex and thought to involve epigenetic changes distinct in males and females [186] including the epigenetic patterning of the hypothalamus by gonadal hormones during development [217]. Circulating GH activates the Ghr causing activation of Stat5b in hepatocytes. This promotes male specific gene expression whilst repressing the expression of female specific genes [218]. The Shapiro group have shown restoration of CYP2C11 expression in male rat hepatocytes, derived from hypophysectomized rats, treated with continuous or twice daily pulses of GH [195]. CYP2C13 and CYP3A2 were refractive to induction however and GH had no effect on male CYP450 expression in hepatocytes from female rats.

Measurement of sex-dependent CYP450 mRNA expression in B-13/H cells showed that their pattern of expression was qualitatively similar to male liver, particularly in terms of the main sex-dependent CYP450s, CYP2C11 and CYP2C12. However, even though they expressed JAK/STAT signalling components, B-13/H cells appeared insensitive to GH induction of CYP2C11 at all stages of transdifferentiation. The male pattern of sex-

dependent CYP450 expression in B-13/H cells but insensitivity to GH is surprising. It suggests that the cells retain sex-specific epigenetic patterning but due to defects in signalling pathways are unable to respond to GH. Potentially, recapitulation of an *in-vivo* pattern of GH exposure (i.e. cyclical) could lead to the induction of CYP2C11 and up-regulation of male CYP450s. However, given the complete absence of response of the cells to a range of GH doses, it seems likely that the signalling pathway responsible for GH mediated regulation of sex-dependent CYP450 expression is non- or dysfunctional.

Assessment of the function of the environmental toxin xenosensor AhR showed that it was expressed and, when activated by  $\beta$ -NF, was able to induce CYP1A1 in B-13 and B-13/H cells. Induced CYP1A1 was functional as shown using the probe-substrate 7-ethoxyresorufin, with activity quantitatively similar to hepatocytes. Furthermore, B-13/H cells showed dose responsive DNA damage in response to benzo[a]pyrene and  $\beta$ -NF induced cells showed significantly more DNA damage compared to uninduced controls.

In terms of CAR and CYP2B1, B-13/H but not B-13 cells expressed both CAR and CYP2B1 mRNA, similar to intact rat liver. CAR was also functional as CYP2B1 was inducible in response to CAR agonists. However, CYP2B1 protein was undetectable, basal PROD activity was low and not markedly increased by treatment with CAR agonists and DNA damage was only observed in B-13/H cells treated with a relatively high concentration of cyclophosphamide. This data suggests that although CYP2B1 mRNA is effectively induced by CAR activation, it is not efficiently translated into protein. This may be due to limited haem availability, as the translation of CYP2B in rats is inhibited by low cell haem concentrations [219]. However, haem-bound CYP450 was detectable in B-13/H cells suggesting that they are able to synthesise and incorporate haem. Currently therefore, based on the limited CYP2B1 metabolic activity in B-13/H cells, their utility for determination of toxicity of CYP2B bioactivated drugs is limited. However, the B-13 line could be used for study of transcriptional regulation of CYP2B1 and its translation to protein.

B-13/H cells expressed the xenosensor PXR and a range of CYP3A transcripts. Treatment of B-13/H cells with PXR agonists led to significant induction of CYP3A1

mRNA which was efficiently translated into protein, as induction significantly increased probe substrate activity to levels greater than seen in equivalently treated primary rat hepatocytes. CYP3A1 induction also led to significantly increased sensitivity to AFB1 induced DNA damage. Nuclear accumulation of  $\gamma$ -H2AX was seen in B-13/H cells treated with AFB1 and this was shown to be due to significant induction of CYP3A1 (ketoconazole inhibitable). Similar staining was attempted with lysates from  $\beta$ -NF induced B-13/H cells treated with benzo[a]pyrene, however no  $\gamma$ -H2AX accumulation was seen. Previous work has shown contrasting results regarding benzo[a]pyrene induction of  $\gamma$ -H2AX in different cell types and it is postulated that the response is cell specific due to differential sensitivity and regulation of DNA damage and repair signalling pathways [220, 221].

The lipid sensor and metabolic regulator PPAR $\alpha$  was expressed by B-13 and B-13/H cells but no CYP4A transcripts were detectable. This is possibly attributable to the exon deletion of *Cyp4a2* or intron deletion of *Cyp4a1* which might inhibit effective binding of transcriptional activators including PPAR $\alpha$ . Similarly, although CYP4A1 mRNA could be detected by qPCR and induced, the basal expression and induction were so low as to be irrelevant, particularly when compared to the >200 fold induction seen in bezafibrate induced primary rat hepatocytes. In contrast to the poor expression of CYP4A1, peroxisomes could be detected in B-13/H but not B-13 cells in agreement with a previous study by Tosh *et al.*, (2002) [125]. Quantitative measurement of peroxisomes, using PMP70, showed that although induction by bezafibrate caused only a minor increase in PMP70 protein, immunostaining indicated that there was a significant increase in peroxisome number of around 2 fold. This suggests that B-13/H cells could be used to study peroxisomal proliferation.

The data presented in this chapter demonstrates that B-13/H cells express a range of CYP450s similar to hepatocytes, which are inducible, confirming the initial hypothesis. In particular, expression and function of CYP1A1 and CYP3A1 was quantitatively equivalent to primary rat hepatocytes. This data indicates that B-13/H cells could be used for screening of CYP1A- and CYP3A-dependent hepatotoxins as well as the study of drug induced CYP450 induction.

**Chapter 4. Generation of a humanised B-13 line and its suitability for genotoxicity screening of novel drugs and chemicals**

## 4.1 Introduction

The limited availability of primary human hepatocytes means that rodent hepatocytes are commonly used for drug and chemical toxicity screening. However, it is clear that there are significant differences in the metabolism of numerous drugs in humans compared to other species. These differences are due to variation in expression, substrate specificity and catalytic efficiency of DMEs including CYP450s between species [222]. A consequence of this is that some drugs are toxic to humans but not rodents and vice-versa. An example of this is OT-7100 (5-n-Butyl-7-(3,4,5-trimethoxybenzoylamino)-pyrazolo[1,5-a]pyrimidine), which is metabolised by CYP1A2 in humans to produce a hydroxylated intermediate which is hepatotoxic [223]. Conversely, in rats it is metabolised via a different route which does not generate the toxic intermediate.

In chapter 3, it was seen that B-13/H cells were capable of CYP450 induction and bioactivation of hepatotoxins. However, B-13 cells are rat cells and therefore they may not be a good model of human hepatocytes. The humanisation of cell lines, which have little to no drug metabolising capacity, with human DMEs, is actively used in order to study the metabolism of drugs and chemicals [224-226]. Based on this work, it was hypothesised that genes encoding human DMEs could be cloned into B-13 cells and the resulting proteins would be functional. This would increase the clinical relevance of the cells for toxicity screening of novel drugs and chemicals. To test the hypothesis, B-13 cells were first stably transfected with hCYP1A2. Following this, the susceptibility of the humanised line to CYP1A2 bioactivated pro-carcinogens was assessed.

## 4.2 The CYP1A2 gene is mutated in B-13 cells

CYP1A2, similar to CYP1A1, is associated with the bioactivation of drugs, particularly pro-carcinogenic environmental toxins [33]. However, unlike CYP1A1, which shows significant extra-hepatic expression and which is not constitutively expressed in the liver, CYP1A2 is primarily expressed in the liver and is constitutively expressed [33]. It is therefore responsible for the majority of liver CYP1A activity in the absence of AhR activation.

Analysis of the B-13 cell genome showed that the *rCyp1a2* gene was mutated in the form of a deletion between exon 1 (non coding) and exon 2 (coding), a region which includes the start codon (figure 4.1). The deletion of the start codon likely prevents transcription of the mRNA and therefore it was hypothesised that CYP1A2 would not be expressed by the cells, assuming all alleles were affected.

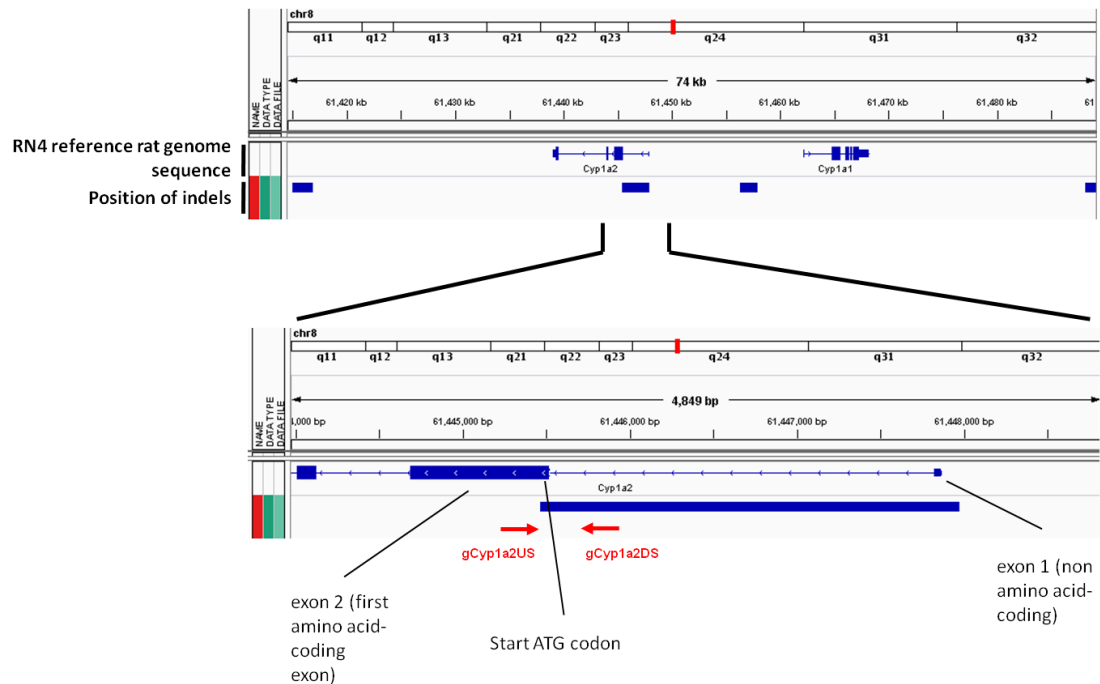


**Figure 4.1: The coding region of *rCyp1a2* in B-13 cells is mutated.** Schematic diagram of the *Cyp1a2* genomic region in the B-13 cell genome, indicating the deletion and the position of genomic primer hybridisation used in PCR amplification. The sequence of the B-13 cell line (including insertions and deletions) was aligned to *Rattus norvegicus* reference sequence 4 using Integrative Genomics Viewer software.

To determine if all alleles were affected, PCR was performed on DNA derived from B-13 and B-13/H cells. Primers were designed with the forward sequence within the undeleted region of *rCyp1a2* and the reverse sequence in the supposedly deleted intron region as shown in figure 4.1. If the deletion was present in all alleles, then only the forward primer would be able to bind as the reverse primer complementary sequence was deleted. If the appropriate size product was produced from B-13 DNA template by PCR therefore, it would suggest that B-13 cells did not contain the deletion in all alleles. Using wild type rat DNA as template, amplification should occur because they have no deletion and both the forward and reverse primers should be able to anneal to target DNA. Using these primers, amplification was only seen when rat liver DNA was used

as template but not B-13 or B-13/H cell DNA, apparently confirming the predicted deletion and suggesting all alleles are affected (figure 4.2A).

Similar to CYP1A1, CYP1A2 can be induced at the transcriptional level by a range of environmental agents and dietary constituents under regulation of the AhR;  $\beta$ -NF, aside from inducing CYP1A1, can also significantly induce CYP1A2 [33]. As shown in figure 4.2B, treating B-13/H cells with  $\beta$ -NF did not cause an induction of CYP1A2 mRNA, which was only detectable in rat liver. Quantitative measurement of CYP1A1 and CYP1A2 mRNA expression (figure 4.2C), using primers which annealed around the deletion site (figure 4.2D), interestingly showed that alongside CYP1A1, CYP1A2 expression could be detected in B-13 and B-13/H cells. However, compared to CYP1A1, which was expressed at greater levels in B-13/H cells than in rat liver, CYP1A2 was expressed at a significantly lower level.

Evidence of CYP1A2 mRNA expression in B-13 and B-13/H cells may mean that, although the CYP1A2 gene is mutated on one chromosome, it is present on another. This is particularly likely considering that B-13 cells have an abnormal karyotype. They have double the normal rat chromosome complement (i.e. tetraploid (42 pairs) rather than diploid (21 pairs)) [184] and are likely therefore to have at least 4 copies of *Cyp1a2*.

### **4.3 CYP1A1 but not CYP1A2 can be induced by $\beta$ -NF**

To determine if CYP1A2 transcript detected in figure 4.2C was translated to protein and if it could be induced by the prototypical CYP1A inducer  $\beta$ -NF, B-13 and B-13/H cells and rat hepatocytes were treated with  $\beta$ -NF and CYP1A1 and CYP1A2 protein expression assessed by Western blot. As shown in figure 4.3, CYP1A1 could be induced by  $\beta$ -NF in all treated cells, but CYP1A2 could only be induced in primary rat hepatocytes induced with  $\beta$ -NF. This suggests that although CYP1A2 mRNA expression was detected, it may be a truncated version and/or not translated to protein.

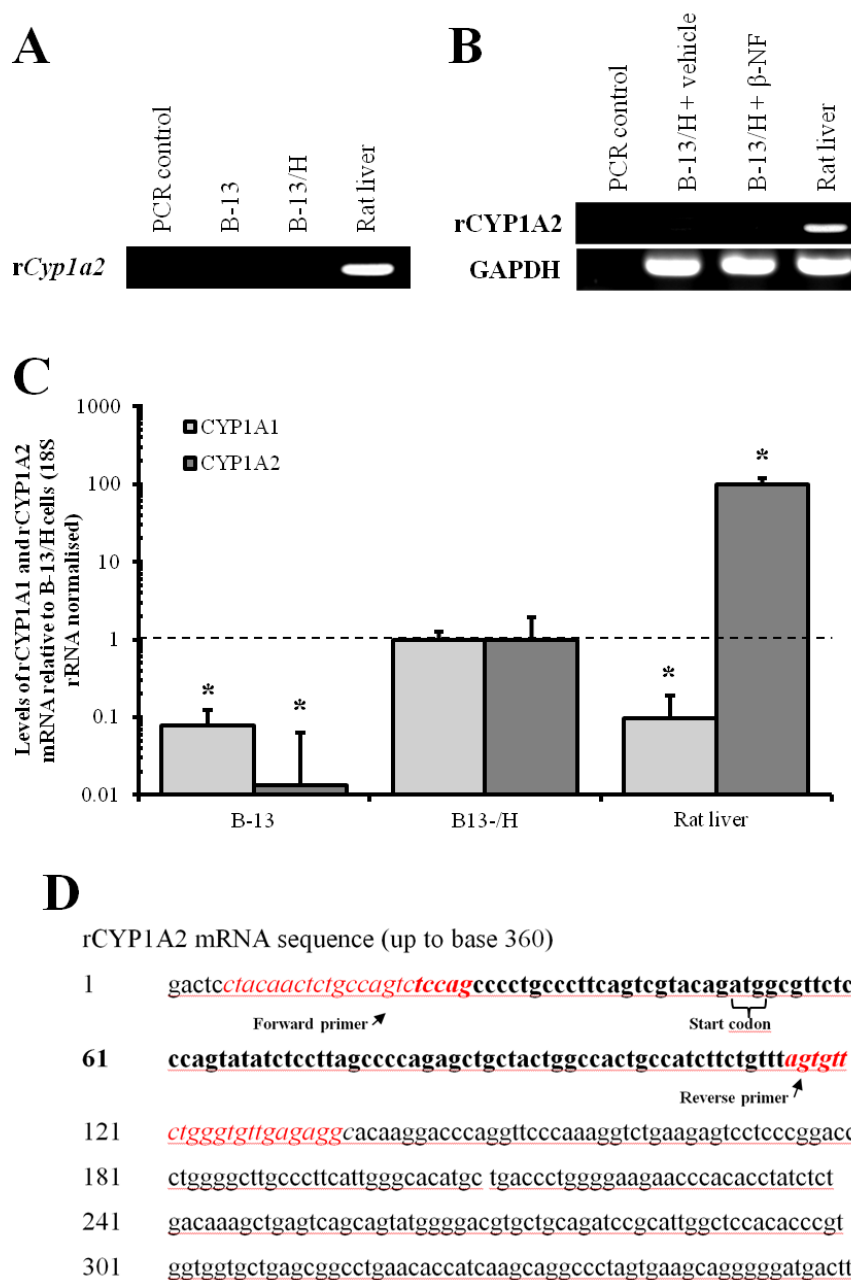


**Figure 4.2: Neither *rCyp1a2* nor rCYP1A2 mRNA can be detected in B-13 cells. A. PCR for genomic CYP1A2.** DNA samples were used as template for *rCyp1a2* using gCyp1a2US and gCYP1A2DS as the forward and reverse primers respectively. Following PCR, samples were separated by agarose gel electrophoresis and visualised by UV transillumination. **B. RT-PCR for rCYP1A2.** B-13/H cells were treated daily for 3 consecutive days with vehicle (0.1% (v/v) DMSO) or 20 $\mu$ M  $\beta$ -NF. On the 4<sup>th</sup> day, total RNA was extracted using TRIzol and cDNA produced which was used as the template for PCR alongside cDNA produced from untreated rat liver. Following PCR, samples were separated by agarose gel electrophoresis and visualised by UV transillumination. **C. qPCR for CYP1A1 and CYP1A2.** Total RNA was extracted from B-13 cells, B-13/H cells and male rat liver using TRIzol and reverse transcribed. cDNA was used as template for qPCR measuring CYP1A1 and CYP1A2. Readings were normalised to 18S rRNA expression and fold change expressed relative to B-13/H cells. Bars are the mean and SD of 3 independent determinations from a single experiment, typical of at least 3 separate experiments. \*statistically significant difference compared to B-13/H cells at  $p < 0.05$ . **D. Binding site of rCYP1A2 qPCR primers.** Forward and reverse primers are in red italics and reported deleted region is in bold.

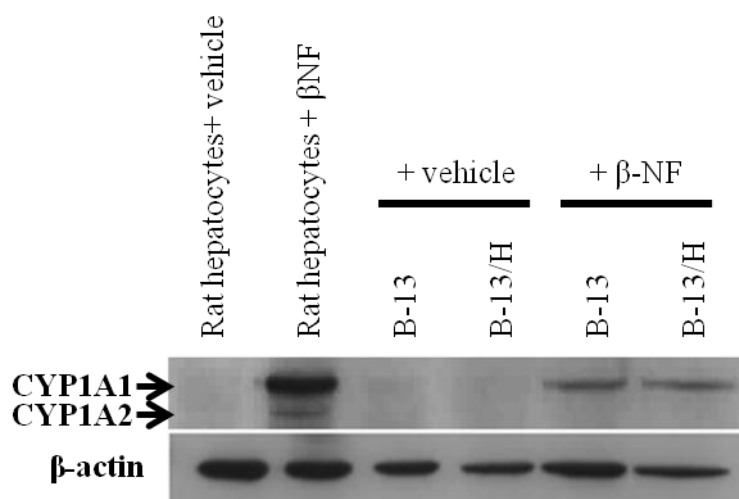


**Figure 4.3: Western blot for CYP1A1 and CYP1A2.** Rat hepatocytes, B-13 and B-13/H cells were treated daily for 3 consecutive days with vehicle (0.1% (v/v) DMSO) or 20 $\mu$ M  $\beta$ -NF. Lysates were prepared and quantified by Lowry assay. 20 $\mu$ g of protein/well was separated by SDS-PAGE and transferred to a nitrocellulose membrane which was blocked and probed. Antibody binding was detected using ECL Western blot substrate. Blot is representative of at least 3 separate experiments.

EROD and MROD activities in B-13 and B-13/H cells (figure 4.4) induced with  $\beta$ -NF showed that only EROD, a marker of CYP1A1 activity, was significantly increased. MROD, which is a marker of CYP1A2 activity, was unaffected by induction. This supports the theory that CYP1A2 mRNA is not translated to protein. The MROD activity documented in the cells is likely from non-specific catalysis by CYP1A2 related proteins such as CYP1A1.

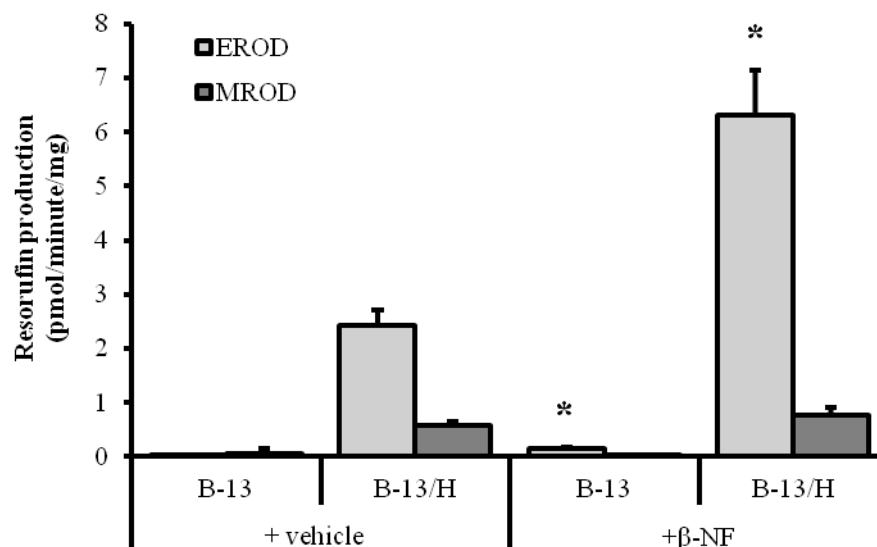


**Figure 4.4: EROD but not MROD activity is inducible in B-13 and B-13/H cells.** EROD and MROD activity in vehicle or  $\beta$ -NF induced B-13 and B-13/H cells. B-13 and B-13/H cells were treated daily for 3 consecutive days with vehicle (0.1% (v/v) DMSO) or 20 $\mu$ M  $\beta$ -NF. Lysates were then prepared and EROD and MROD activity measured. Resorufin production was calculated using a standard curve and values were normalised to protein concentration calculated by Lowry assay. Bars are the mean and SD of 3 independent determinations from the same experiment, typical of at least 3 separate experiments. \*statistically significant difference compared to respective vehicle treated controls at  $p < 0.05$ .

#### 4.4 Isolation and amplification of the hCYP1A2 coding sequence

Due to the absence of functional CYP1A2 expression and the importance of CYP1A2 in the bioactivation of a range of clinically relevant compounds and dietary constituents, it was planned to knock hCYP1A2 into B-13 cells. The hypothesis was that the knocked in hCYP1A2 would produce functional protein with metabolic capacity in B-13/H, but not B-13 cells. Activity was not expected in B-13 cells because, as seen in chapter 3, unlike B-13/H cells they do not express CYP reductase or cytochrome  $b_5$  which are required for CYP450 activity. If the introduced hCYP1A2 was expressed and functional it could be used for analysis of drug and chemical toxicity. Additionally, it would stand as a proof of concept for the cloning of human genes into the B-13 cell line which has not been attempted before.

hCYP1A2 would ultimately be cloned into the pT-REX-DEST30 vector, as illustrated in figure 4.5. When co-expressed with pcDNA6/TR, it in principle only allows expression of the cloned transgene in the presence of tetracycline. In the absence of

tetracycline, tetracycline repressor protein (TetR) binds to tetracycline operator sites in the transgene promoter; this inhibits binding of transcriptional machinery and therefore represses expression.

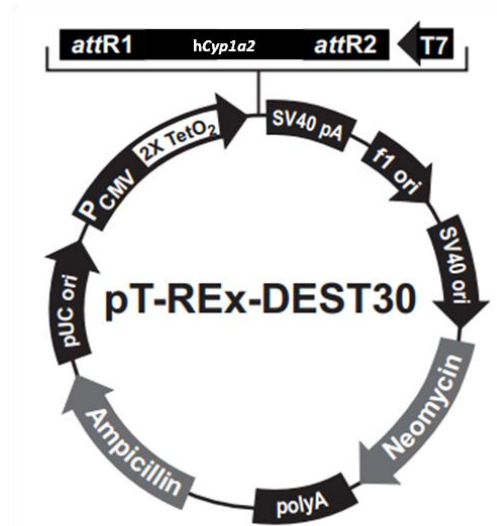


**Figure 4.5: Planned final vector for transformation.** The human complete *CYP1A2* coding sequence would be inserted by LR clonase from a gateway vector to this destination vector. Expression would be driven by the cyclomeglovirus promoter (CMV) in response to tetracycline. The neomycin resistance gene in the vector confers resistance to G418 in order to allow for selection in mammalian cells.

*CYP1A2* is highly polymorphic in humans with more than 15 identified polymorphisms. In order to isolate the prototypical allele of h*CYP1A2* for cloning, h*CYP1A2*\*1, RT-PCR was carried out on RNA isolated from numerous human liver samples. Initially amplification of the entire coding region of h*CYP1A2* (1548bp) was attempted in a single reaction, however most samples did not amplify. In order to isolate the coding sequence of h*CYP1A2* from more donors to maximise the chance of identifying one donor expressing the prototypical allele, the two halves of the coding sequence were amplified separately (figure 4.6A). Interestingly, a huge range in the level of expression of h*CYP1A2* mRNA was seen. The two fragments from different donors were gel extracted and fused by fusion PCR, as outlined in the methods section, to produce the single continuous h*CYP1A2* coding sequence (figure 4.6B).

This was then TOPO cloned into the gateway vector (pENTR/D-TOPO), transformed into bacteria and restriction analysis carried out to determine which bacterial colonies had been transformed with plasmid containing an insert (figure 4.7). Donor sample 4, 6 and 11 had colonies with bands of approximately the correct size (2435bp, 1467bp and

280bp – uncut plasmid 4182bp). Sequencing of the plasmid insert in these colonies showed that one clone was transformed with the full coding sequence of *hCYP1A2\*1* (figure 4.8). This was then transferred to the destination vector (pT-REX-DEST30) by a clonase reaction and transformed into bacteria once more. Colony PCR showed that all colonies transformed with the destination vector contained the cloned *hCYP1A2\*1* coding sequence (figure 4.9). One colony was then expanded and plasmid DNA prepared. Finally, B-13 cells were co-transfected with pcDNA6/TR and pT-REX-DEST30 (containing *hCYP1A2\*1*) and stable transformants selected to create the B-13<sup>TR/h1A2</sup> line.

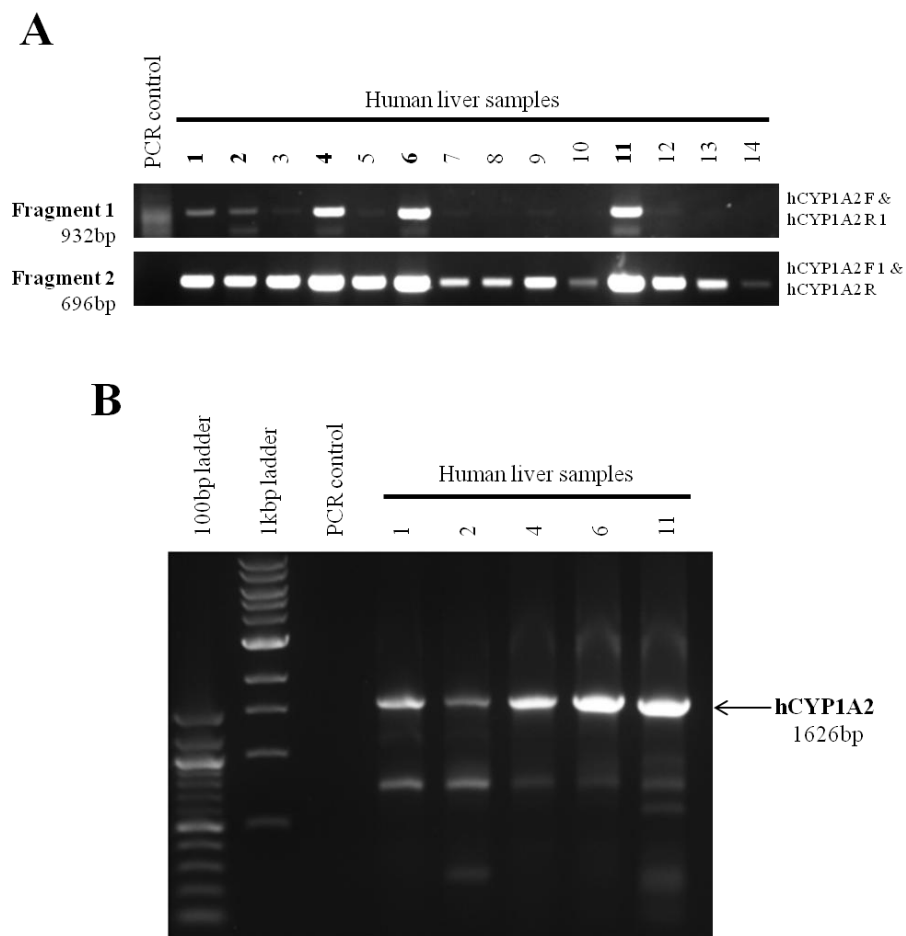


**Figure 4.6: Construction of the *hCYP1A2* coding sequence. A. PCR of the two fragments of *hCYP1A2* from donor liver samples.** Total RNA was extracted from donor liver samples using TRIzol then reverse transcribed. The cDNA was then used as a template for PCR using the primers indicated on the right. The PCR products were separated by agarose gel electrophoresis and visualised by UV transillumination. **B. Fusion PCR of the two *hCYP1A2* fragments.** The two fragments of *hCYP1A2* amplified in A were gel extracted and fused by PCR. The human liver sample numbers correspond to those from A. The resulting PCR products were separated by agarose gel electrophoresis and visualised by UV transillumination.

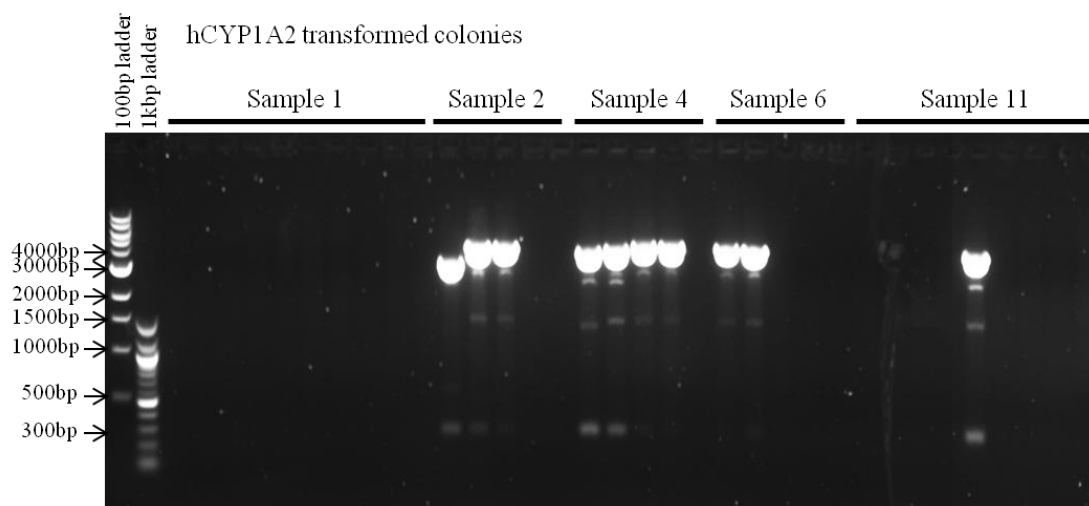


**Figure 4.7: Restriction digest of miniprep isolated plasmid DNA from transformants.** TOP10 cells were transformed with the hCYP1A2 cloned into pENTR/D-TOPO from different donor samples (see Figure 4.6) then cultured overnight at 37°C on agar plates containing kanamycin. In the morning, colonies were picked into LB containing kanamycin and cultured overnight at 37°C shaking at 225rpm. In the morning, minipreps were used to isolate plasmid DNA which was restricted using NotI, EcoRV and BglII. Following digestion, DNA loading dye was added to the reactions and they were separated by agarose gel electrophoresis and visualised by UV transillumination.

Clone-2.4 hCYP1A2*1	CAGATGGCATTGTCCCAGTCTGTCCCTTCTCGGCCACAGAGCTTCTCCTGGCCTCTGCC 360 ---ATGGCATTGTCCCAGTCTGTCCCTTCTCGGCCACAGAGCTTCTCCTGGCCTCTGCC 57 *****	Clone-2.4 hCYP1A2*1	TTCTGTGGTTCTCGAGAAAACAGTCCAGGAGCACTATCAGGACTTTGACAAGAACAGT 1140 TTCTGTGGTTCTCGAGAAAACAGTCCAGGAGCACTATCAGGACTTTGACAAGAACAGT 837 *****
Clone-2.4 hCYP1A2*1	ATCTTCTGCCTGGTATTCTGGGTGCTCAAGGTTTGGAGCCTCGGGTCCCCAAGGCCTG 420 ATCTTCTGCCTGGTATTCTGGGTGCTCAAGGTTTGGAGCCTCGGGTCCCCAAGGCCTG 117 *****	Clone-2.4 hCYP1A2*1	GTCCGGGACATCACGGGTGCCTGTCAAGCAGCAAGAGGGGCTTAGAGCCAGCGGC 1200 GTCCGGGACATCACGGGTGCCTGTCAAGCAGCAAGAGGGGCTTAGAGCCAGCGGC 897 *****
Clone-2.4 hCYP1A2*1	AAAAGTCCACCAGAGCCATGGGGCTGGCCCTTGCTCGGGCATGTGCTGACCCCTGGGGAAG 480 AAAAGTCCACCAGAGCCATGGGGCTGGCCCTTGCTCGGGCATGTGCTGACCCCTGGGGAAG 177 *****	Clone-2.4 hCYP1A2*1	AACCTCATCCCACAGGAGAAGATTGTCAACCTTGTCAATGACATCTTTGGAGCAGGATTT 1260 AACCTCATCCCACAGGAGAAGATTGTCAACCTTGTCAATGACATCTTTGGAGCAGGATTT 957 *****
Clone-2.4 hCYP1A2*1	AACCCGCACCTGGCACTGTCAAGGATGAGCCAGCGCTACGGGGACGTCTGCAGATCCGC 540 AACCCGCACCTGGCACTGTCAAGGATGAGCCAGCGCTACGGGGACGTCTGCAGATCCGC 237 *****	Clone-2.4 hCYP1A2*1	GACACAGTCAACCAGCCATCTCCTGGAGCCTCATGTACCTTGTGACCAAGCCTGAGATA 1320 GACACAGTCAACCAGCCATCTCCTGGAGCCTCATGTACCTTGTGACCAAGCCTGAGATA 1017 *****
Clone-2.4 hCYP1A2*1	ATTGGCTCCACGCCGTGCTGGTGTGAGCCGCCTGGACACCATCCGGCAGGCCCTGGTG 600 ATTGGCTCCACGCCGTGCTGGTGTGAGCCGCCTGGACACCATCCGGCAGGCCCTGGTG 297 *****	Clone-2.4 hCYP1A2*1	CAGAGGAAGATCCAGAAGGAGCTGGACACTGTGATTGGCAGGGAGCGGGGCCCGGCTC 1380 CAGAGGAAGATCCAGAAGGAGCTGGACACTGTGATTGGCAGGGAGCGGGGCCCGGCTC 1077 *****
Clone-2.4 hCYP1A2*1	CGGCAGGGCGACGATTTCAAGGGCCGGCCTGACCTCTACACCTCCACCCTCATCACTGAT 660 CGGCAGGGCGACGATTTCAAGGGCCGGCCTGACCTCTACACCTCCACCCTCATCACTGAT 357 *****	Clone-2.4 hCYP1A2*1	TCGACAGACCCAGCTGCCCTACTTGGAGGCCTTCATCCTGGAGACCTTCCGACACTCC 1440 TCGACAGACCCAGCTGCCCTACTTGGAGGCCTTCATCCTGGAGACCTTCCGACACTCC 1137 *****
Clone-2.4 hCYP1A2*1	GGCCAGAGCTTGACCTTCAAGGACAGACTCTGGACCGGTGTGGGCTGCCCGCCGGCCCTG 720 GGCCAGAGCTTGACCTTCAAGGACAGACTCTGGACCGGTGTGGGCTGCCCGCCGGCCCTG 417 *****	Clone-2.4 hCYP1A2*1	TCCTTCTTGCCCTTACCATCCCCACAGCAACAAGGGACACAACGCTGAATGGCTTC 1500 TCCTTCTTGCCCTTACCATCCCCACAGCAACAAGGGACACAACGCTGAATGGCTTC 1197 *****
Clone-2.4 hCYP1A2*1	GCCCAGAATGCCCTCAACACCTTCTCCATCGCCTCTGACCCAGCTTCTCATCCTCCTGC 780 GCCCAGAATGCCCTCAACACCTTCTCCATCGCCTCTGACCCAGCTTCTCATCCTCCTGC 477 *****	Clone-2.4 hCYP1A2*1	TACATCCCCAAGAAATGCTGTGCTTTCGTAACCAGTGGCAGGTCAACCATGACCCAGAG 1560 TACATCCCCAAGAAATGCTGTGCTTTCGTAACCAGTGGCAGGTCAACCATGACCCAGAG 1257 *****
Clone-2.4 hCYP1A2*1	TACCTGGAGGAGCATGTGAGCAAGGAGGCTAAGGCCCTGATCAGCAGGTTGCAGGAGCTG 840 TACCTGGAGGAGCATGTGAGCAAGGAGGCTAAGGCCCTGATCAGCAGGTTGCAGGAGCTG 537 *****	Clone-2.4 hCYP1A2*1	CTGTGGGAGGACCCCTCTGAGTTCGGCCTGAGCGGTTCCTCACCCGCGATGGCACTGCC 1620 CTGTGGGAGGACCCCTCTGAGTTCGGCCTGAGCGGTTCCTCACCCGCGATGGCACTGCC 1317 *****
Clone-2.4 hCYP1A2*1	ATGGCAGGGCCTGGGCACCTTCGACCCCTTACAATCAGGTGGTGGTGTGAGTGGCCAACGTC 900 ATGGCAGGGCCTGGGCACCTTCGACCCCTTACAATCAGGTGGTGGTGTGAGTGGCCAACGTC 597 *****	Clone-2.4 hCYP1A2*1	ATTAACAAGCCCTTGAGTGAAGATGATGCTGTTTGGCATGGGCAAGCGCCGGTGTATC 1680 ATTAACAAGCCCTTGAGTGAAGATGATGCTGTTTGGCATGGGCAAGCGCCGGTGTATC 1377 *****
Clone-2.4 hCYP1A2*1	ATTGGTGCCATGTGCTTCGGACAGCACTTCCCTGAGAGTAGCGATGAGATGCTCAGCCTC 960 ATTGGTGCCATGTGCTTCGGACAGCACTTCCCTGAGAGTAGCGATGAGATGCTCAGCCTC 657 *****	Clone-2.4 hCYP1A2*1	GGGGAAGTCCTGGCCAAGTGGGAGATCTTCTCTTCTGGCCATCCTGCTACAGCAACTG 1740 GGGGAAGTCCTGGCCAAGTGGGAGATCTTCTCTTCTGGCCATCCTGCTACAGCAACTG 1437 *****
Clone-2.4 hCYP1A2*1	GTGAAGAACACTCATGAGTTCGTGGAGACTGCCCTCCCGGAACCCCTGGACTTCTTC 1020 GTGAAGAACACTCATGAGTTCGTGGAGACTGCCCTCCCGGAACCCCTGGACTTCTTC 717 *****	Clone-2.4 hCYP1A2*1	GAGTTCAGCGTGCCGCCGGGCGTAAAGTCGACCTGACCCCATCTACGGGCTGACCATG 1800 GAGTTCAGCGTGCCGCCGGGCGTAAAGTCGACCTGACCCCATCTACGGGCTGACCATG 1497 *****
Clone-2.4 hCYP1A2*1	CCCATCCTTCGCTACCTGCCTAACCCCTGCCTGCAGAGGTTCAAGGCCTTCAACCAGAGG 1080 CCCATCCTTCGCTACCTGCCTAACCCCTGCCTGCAGAGGTTCAAGGCCTTCAACCAGAGG 777 *****	Clone-2.4 hCYP1A2*1	AAGCACGCCCGCTGTGAACATGTCCAGGCGCGGCTGCGCTTCTCCATCAACTGAAAGGGT 1860 AAGCACGCCCGCTGTGAACATGTCCAGGCGCGGCTGCGCTTCTCCATCAACTG----- 1551 *****

**Figure 4.8: Clone 2.4 was cloned with the complete coding sequence of hCYP1A2\*1.** Sequence alignment of the insert in clone 2.4 with the complete coding sequence of hCYP1A2\*1. Miniprepmed plasmid DNA from clone 2.4 was sequenced twice forward and reverse and the resulting sequences averaged to one sequence. ClustalW2 was used to align the sequences (<http://www.ebi.ac.uk/Tools/msa/clustalw2/>).



**Figure 4.9: The hCYP1A2 insert was successfully transferred from the gateway vector to the destination vector. PCR of colonies transformed with the product of the LR clonase reaction.** Insert in pENTR/D-TOPO was transferred to pT-Rex-DEST30 using LR clonase then the reaction products transformed into TOP10 cells. The colonies were cultured overnight on agar containing ampicillin at 37°C. In the morning, colony picks were used as template for PCR using primers for hCYP1A2. Following PCR, the products were separated by gel electrophoresis and visualised by UV transillumination.

#### 4.5 B-13<sup>-TR/h1A2</sup> cells express hCYP1A2 independent of tetracycline

To determine if B-13<sup>-TR/h1A2</sup> cells expressed the introduced hCYP1A2 and if its expression was regulated by doxycycline (derivative of tetracycline), untransfected B-13 cells and B-13<sup>-TR/h1A2</sup> cells were treated with doxycycline for 24 hours and hCYP1A2 expression assessed by RT-PCR and Western blotting. As can be seen in figure 4.10A, only B-13<sup>-TR/h1A2</sup> cells expressed hCYP1A2 mRNA. However, repression of the transgene in the absence of doxycycline did not occur and therefore hCYP1A2 mRNA was constitutively expressed. To check for successful transfection of the pcDNA6/TR vector in B-13<sup>-TR/h1A2</sup> cells, the expression of TetR, which is required for tetracycline inducible expression, was also assessed. Similar to hCYP1A2, TetR mRNA was only expressed by B-13<sup>-TR/h1A2</sup> cells.

Western blotting complemented the RT-PCR; it showed that B-13<sup>-TR/h1A2</sup> cells, but not untransfected B-13 cells, expressed hCYP1A2 protein similar to human liver (figure 4.10B). At the protein level, doxycycline treatment appeared to cause a small increase in expression of the cloned hCYP1A2. To confirm that B-13<sup>-TR/h1A2</sup> cells could still transdifferentiate, hepatic markers were assessed by Western blotting before and after transdifferentiation. Figure 4.11 shows that B-13<sup>-TR/h1A2</sup> cells could transdifferentiate to hepatocyte-like cells (B-13<sup>-TR/h1A2</sup>/H) as, following DEX induced transdifferentiation, they expressed the hepatic markers albumin, CYP2E1 and CPS-1. They also maintained expression of the hCYP1A2 transgene which showed a small induction of expression in response to doxycycline.

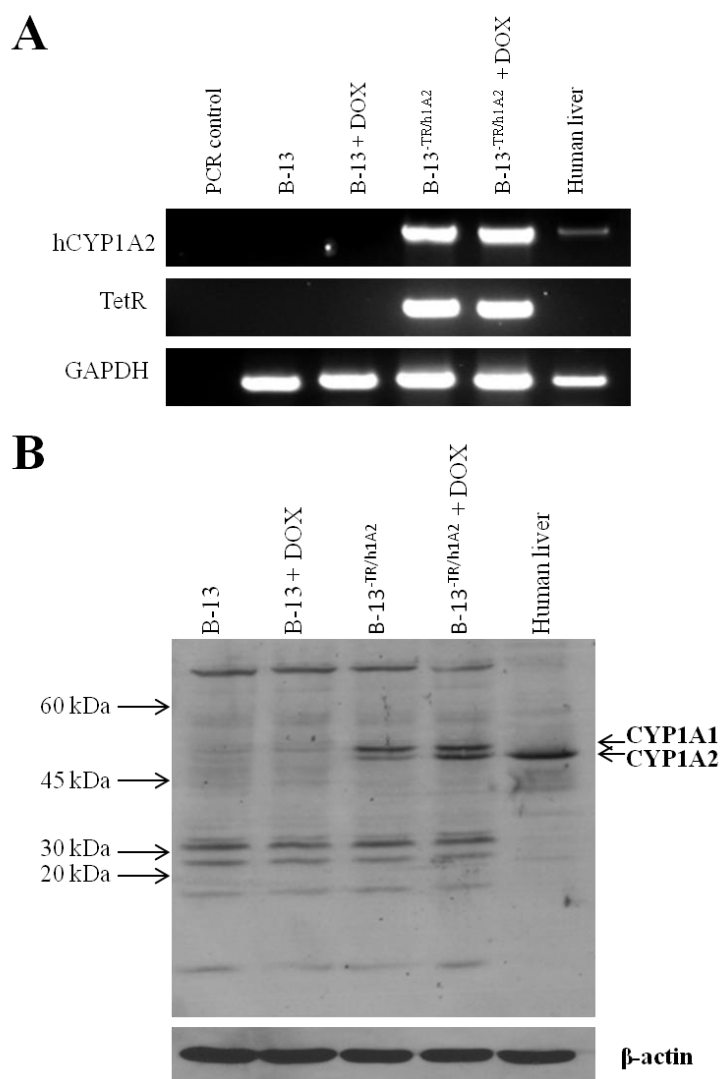


**Figure 4.10: B-13<sup>-TR/h1A2</sup> cells express hCYP1A2 independent of tetracycline.** **A. RT-PCR for hCYP1A2, TetR and GAPDH in the indicated samples.** B-13 and B-13<sup>-TR/h1A2</sup> cells were treated with vehicle (0.1% (v/v) PBS) or 2 $\mu$ g/ml doxycycline (DOX) for 24 hours then total RNA extracted using TRIzol. The RNA was reverse transcribed and used as template for PCR. PCR products were separated using agarose gel electrophoresis and visualised by UV transillumination. **B. Western blot for CYP1A1/1A2 and  $\beta$ -actin in normal and doxycycline induced B-13 and B-13<sup>-TR/h1A2</sup> cells.** Lysates were prepared from samples treated as in **A** and quantified by Lowry assay. 20 $\mu$ g of protein/well was separated by SDS-PAGE and transferred to a nitrocellulose membrane which was blocked and probed. Antibody binding was detected using ECL Western blot substrate. Results are representative of at least 3 separate experiments.

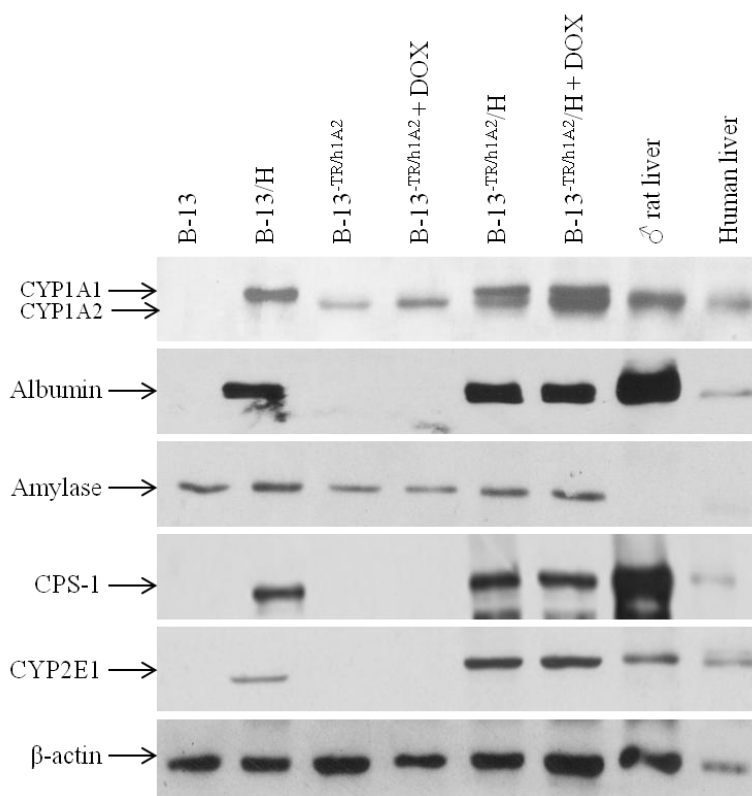


**Figure 4.11: B-13<sup>TR/h1A2</sup> cells can transdifferentiate.** Western blot for CYP1A1/1A2 and liver markers in indicated samples. B-13<sup>TR/h1A2</sup> and B-13<sup>TR/h1A2</sup>/H cells were treated with vehicle (0.1% (v/v) PBS) or 2 $\mu$ g/ml doxycycline (DOX) for 24 hours. Lysates were then prepared from treated cells, B-13 and B-13/H cells and rat and human liver samples and quantified by Lowry assay. 20 $\mu$ g of protein/well was separated by SDS-PAGE and transferred to a nitrocellulose membrane which was blocked and probed. Antibody binding was detected using ECL Western blot substrate.

#### 4.6 Cloned hCYP1A2 in B-13<sup>TR/h1A2</sup>/H cells is functional and inhibited by furafylline

To determine if expressed hCYP1A2 in B-13<sup>TR/h1A2</sup> cells was functional, MROD activity was measured in vehicle and doxycycline induced B-13, B-13/H, B-13<sup>TR/h1A2</sup> and B-13<sup>TR/h1A2</sup>/H cells. This showed that B-13<sup>TR/h1A2</sup>/H cells had significantly higher MROD activity than B-13/H cells, suggesting the introduced hCYP1A2 was functional (figure 4.12A). Furthermore, treating lysates with furafylline, a specific inhibitor of hCYP1A2 [227], caused a significant reduction in MROD activity in B-13<sup>TR/h1A2</sup>/H cells. Doxycycline induced cells showed essentially identical MROD activity to uninduced cells (not shown).

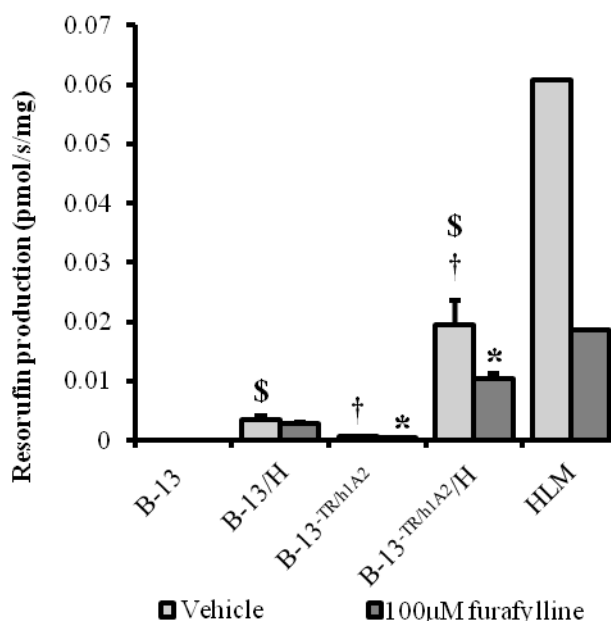


**Figure 4.12: Transdifferentiated B-13<sup>-TR/h1A2</sup>/H cells express functional hCYP1A2.** MROD activity in the indicated samples treated with or without the hCYP1A2 inhibitor furafylline. Lysates were prepared from the indicated samples which were then measured for MROD activity with or without 100µM furafylline. Human liver microsomes (HLM) were run alongside as a positive control. Resorufin production was calculated using a standard curve and readings were normalised to protein concentration measured using the Lowry assay. Results are the mean and SD of 3 independent determinations from the same experiment, typical of at least 3 separate experiments. \*significantly different activity compared to extract without addition of furafylline, \$significantly different activity compared to respective B-13 equivalent, †significantly different activity compared to parent B-13 cells all at  $p < 0.05$ . Abbreviations: HLM, human liver microsomes.

#### 4.7 hCYP1A2 expression significantly increases the susceptibility of B-13<sup>-TR/h1A2</sup>/H cells to PhIP induced genotoxicity

2-Amino-1-methyl-6-phenylimidazo(4,5-b)pyridine (PhIP) is a carcinogenic heterocyclic amine carcinogen derived from the prolonged cooking of meat at high temperatures, particularly by barbequing. It is ingested as a pro-genotoxin and metabolised to a genotoxic metabolite. Specifically, in the liver, PhIP is N-hydroxylated primarily by CYP1A2, and to a lesser extent CYP1A1 and CYP1B1 [228, 229]. N-hydroxy-PhIP then undergoes O-esterification, catalysed by N-acetyltransferases or sulphotransferases (SULTs) as outlined in figure 4.13, to form reactive esters that bind and damage DNA [228, 229].

Due to the relative specificity of hCYP1A2 in bioactivation of PhIP, a dose response, using DNA damage as the endpoint, was performed on B-13 and B-13<sup>-TR/h1A2</sup> cells and

their transdifferentiated forms. Measurement of DNA damage showed that B-13<sup>TR/h1A2</sup>/H cells were significantly more sensitive to DNA damage resulting from PhIP treatment than B-13/H cells (figure 4.14). Undifferentiated B-13 and B-13<sup>TR/h1A2</sup> cells did not show any marked genotoxicity in response to PhIP. Treatment of B-13<sup>TR/h1A2</sup>/H cells with doxycycline, prior to PhIP treatment, had no effect on resulting DNA damage.

To confirm that DNA damage resulting from PhIP treatment was not due to initiation of apoptosis or DNA replication, DNA diffusion and BrdU incorporation in PhIP treated cells was determined. Figure 4.15 shows that at the concentration range employed, comets were not associated with cytotoxicity or with a significant increase in DNA synthesis.

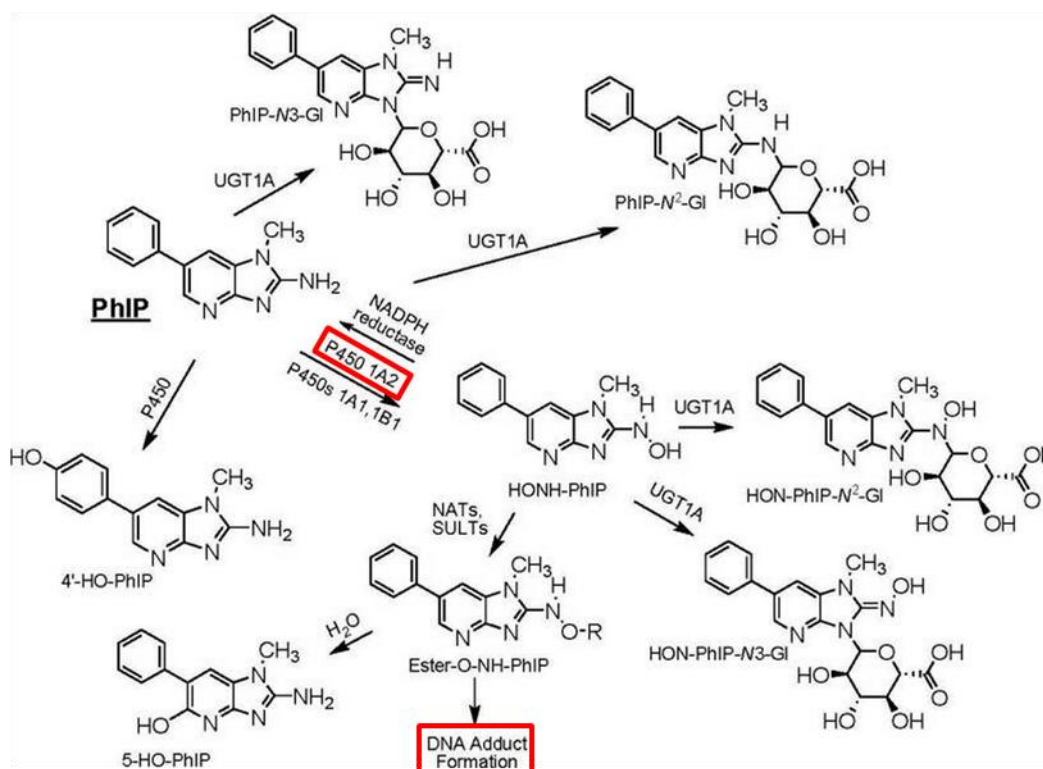


**Figure 4.13: Metabolism of PhIP.** From Gu *et al.*, (2010) [230].

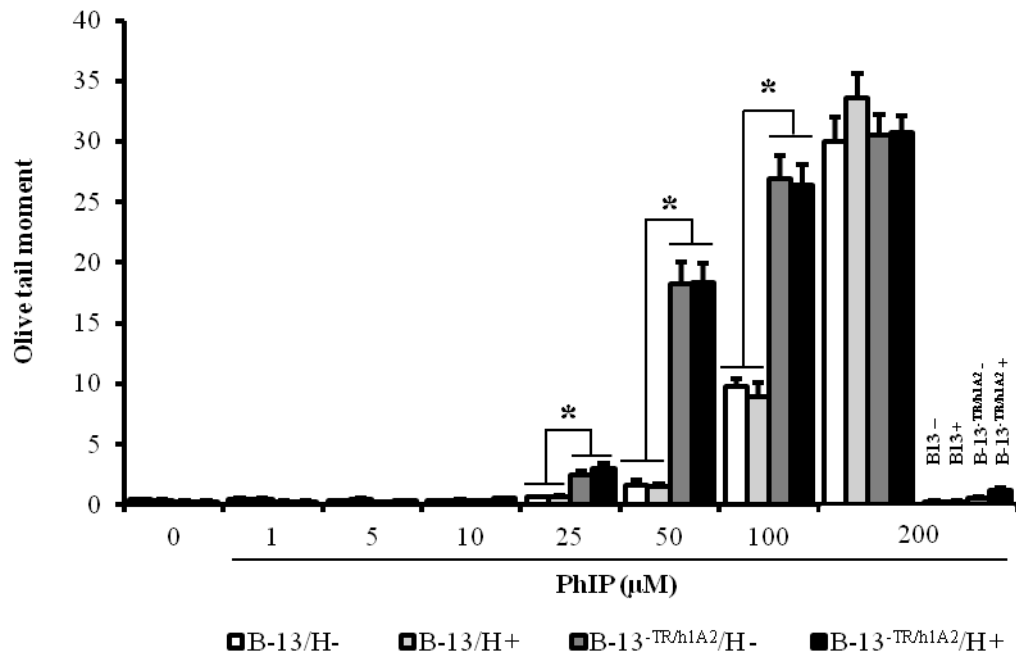


**Figure 4.14: B-13<sup>-TR/h1A2</sup>/H cells are susceptible to PhIP induced DNA damage.** Dose response olive tail moment of indicated cells treated with different concentrations of PhIP. B-13, B-13/H, B-13<sup>-TR/h1A2</sup> and B-13<sup>-TR/h1A2</sup>/H cells were treated with (+) or without (-) 2 μg/ml doxycycline for 24 hours then additionally with different concentrations of PhIP for 16 hours. Following treatment cells were subject to the alkaline comet assay and DNA stained with SYBR gold. Slides were viewed using a fluorescence microscope and DNA damage calculated using cometscore software. Data are the mean and SE of 100 cells from 2 separate experiments, typical of at least 3 separate experiments. \*indicates significant difference between indicated groups at  $p < 0.05$ , calculated by ANOVA followed by the Bonferroni-Holm post-hoc test.

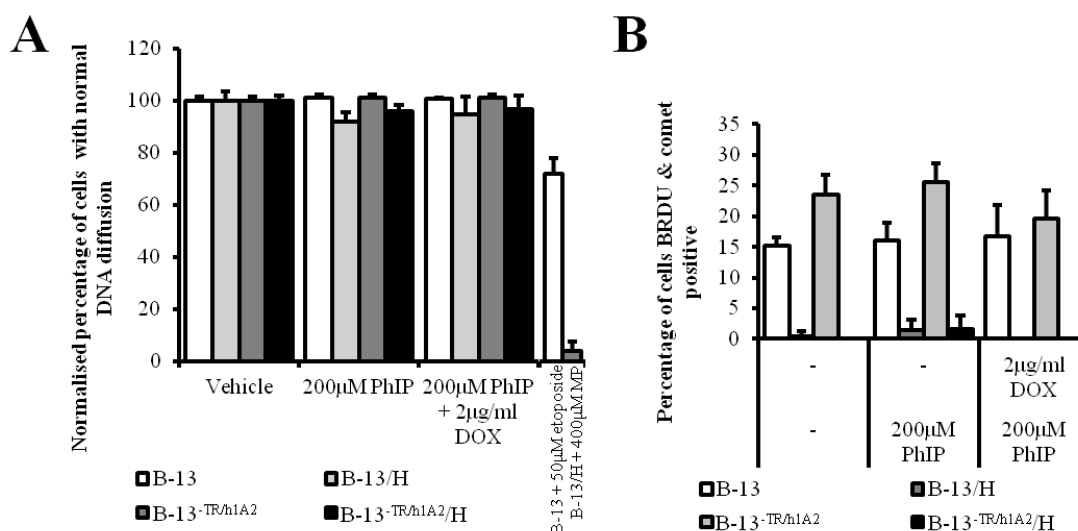


**Figure 4.15: PhIP does not induce significant cell death or division. A. DNA diffusion assay of PhIP treated cells.** B-13, B-13/H, B-13<sup>-TR/h1A2</sup> and B-13<sup>-TR/h1A2</sup>/H cells were treated with (+) or without (-) 2μg/ml doxycycline (DOX) for 24 hours then additionally with 200μM PhIP or positive controls (50μM etoposide or 400μM methapyrilene (MP)) for 16 hours. Following treatment, cells were embedded in low melting point agarose, lysed and stained with SYBR gold. Slides were viewed using a fluorescence microscope and the percentage of cells with normal DNA diffusion (using the positive controls as a guide) calculated. Results are the mean and SD from 4 fields of view, with at least 100 individual cells counted in total, from a single experiment, typical of at least 3 separate experiments. **B. Percentage of comet cells staining positive for BrdU following PhIP treatment.** Cells treated as in **A** were incubated with 15μM BrdU for 2 hours then were subject to the alkaline comet assay and immunostained for BrdU. After counterstaining with DAPI, slides were viewed using a fluorescence microscope and the percentage of comets staining positive for BrdU calculated. Data are the mean and SD calculated from 4 fields of view, with at least 100 individual cells counted in total. Results are from a single experiment, typical of at least 3 separate experiments. For **A** and **B**, no statistical analysis was performed.

#### 4.8 PhIP induced DNA damage is inhibited by furafylline in B-13<sup>-TR/h1A2</sup>/H cells

To determine if the introduced hCYP1A2 in B-13<sup>-TR/h1A2</sup>/H cell was responsible for enhanced sensitivity of B-13<sup>-TR/h1A2</sup>/H cells to PhIP compared to B-13/H cells, B-13/H and B-13<sup>-TR/h1A2</sup>/H cells were co-treated with PhIP as well as either the hCYP1A2 inhibitor furafylline, the general CYP450 inhibitor metyrapone or CYP1A1 inhibitor  $\alpha$ -NF (figure 4.16). B-13/H cells showed significantly reduced DNA damage in response to  $\alpha$ -NF and metyrapone but not furafylline. In B-13<sup>-TR/h1A2</sup>/H cells, furafylline but not metyrapone or  $\alpha$ -NF, caused a significant reduction in DNA damage in response to PhIP. The almost complete inhibition of PhIP induced DNA damage in response to  $\alpha$ -NF in B-13/H cells suggests that CYP1A1 was primarily responsible for the bioactivation in these cells. The inhibition of DNA damage by furafylline in B-13<sup>-TR/h1A2</sup>/H cells suggests that hCYP1A2 is responsible for the majority of PhIP

bioactivation in these cells and explains why they are more sensitive to PhIP induced DNA damage than B-13/H cells.

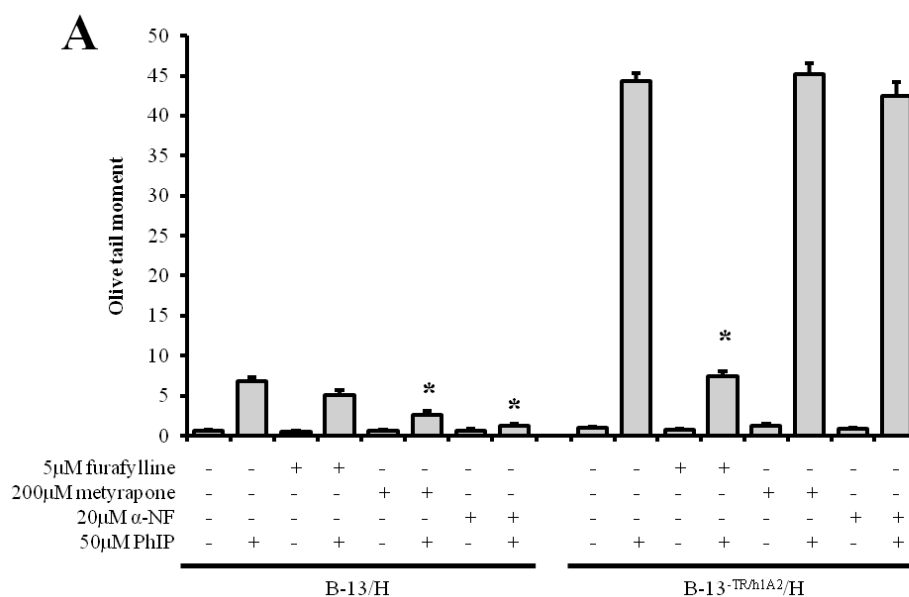


**Figure 4.16: PhIP genotoxicity is inhibited by furafylline in B-13<sup>-TR/h1A2</sup>/H cells.** DNA damage in B-13/H and B-13<sup>-TR/h1A2</sup>/H cells treated with PhIP and CYP450 inhibitors measured by comet assay. B-13/H and B-13<sup>-TR/h1A2</sup>/H cells were treated with vehicle (0.1% (v/v) DMSO), furafylline, metyrapone or α-NF for 6 hours then additionally with vehicle (1% (v/v) DMSO) or 50µM PhIP for 16 hours. Following treatment cells were subject to the alkaline comet assay and DNA stained with SYBR gold. Slides were viewed using a fluorescence microscope and DNA damage calculated using cometscore software. Data are the mean and SE of 50 cells from a single experiment, typical of 2 separate experiments. \*indicates significant difference to cells treated with 50µM PhIP alone at p<0.05.

#### 4.9 PhIP bioactivation is dependent on SULT activity

Sulphation reactions, in the context of drug metabolism, involve the transfer of the sulfonyl moiety from 3'-phosphoadenosine-5'-phosphosulphate (PAPS) to xenobiotics, catalysed by SULTs. Sulphation reactions are important in the liver for drug detoxification, but also for drug bioactivation. CYP1A proteins (including CYP1A2) are involved in the bioactivation of a range of pro-carcinogens which are subsequently sulphated to genotoxic forms, such as benzylic alcohols from polycyclic aromatic hydrocarbons and aromatic hydroxylamines (including hydroxylated PhIP and benzo[a]pyrene) [231]. If wild type or humanised B-13 cells, including B-13<sup>-TR/h1A2</sup> cells, were to be used for genotoxicity screening therefore, they would need to express functional SULTs.

Based on the sensitivity of B-13/H and B-13<sup>-TR/h1A2</sup>/H cells to PhIP, which requires sulphation for genotoxicity, cells were pretreated with 4-nitrophenol (PNP) or quercetin, prior to addition of PhIP. PNP is a substrate and quercetin an inhibitor of a range of SULTs, particularly SULT1A1. In humans, SULT1A1 and SULT1A2, and in rats SULT1A1, SULT1B1 and SULT1C1 have been shown to be able to sulphate hydroxylated PhIP [232-234].

The competitive inhibition of SULT activity by PNP significantly inhibited PhIP induced genotoxicity only in B-13/H cells whereas quercetin significantly reduced DNA damage in both B-13/H and B-13<sup>-TR/h1A2</sup>/H cells (figure 4.17). This result indicates that B-13/H cells express functional SULTs which are required for PhIP genotoxicity.

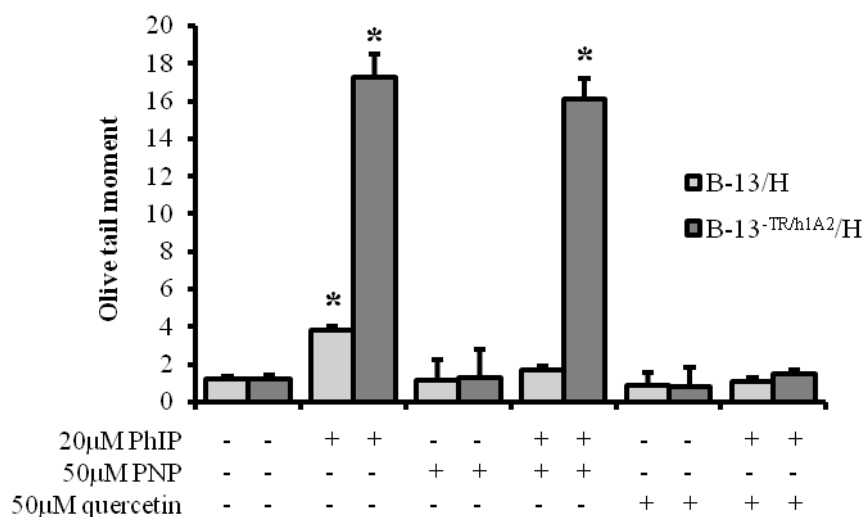


**Figure 4.17: PhIP genotoxicity is SULT dependent.** DNA damage in B-13/H and B-13<sup>-TR/h1A2</sup>/H cells treated with PhIP and SULT inhibitors measured by comet assay. B-13/H and B-13<sup>-TR/h1A2</sup>/H cells were treated with vehicle (0.1% (v/v) DMSO), PNP or quercetin for 6 hours then additionally with vehicle (1% (v/v) DMSO) or 20µM PhIP for 16 hours. Following treatment, cells were subject to the alkaline comet assay and DNA stained with SYBR gold. Slides were viewed using a fluorescence microscope and DNA damage calculated using cometscore software. Data are the mean and SE of 50 cells from a single experiment, typical of at least 3 separate experiments. \*significantly different to vehicle treated cells at  $p < 0.05$ .

#### 4.10 B-13/H cells express functional SULTs and are susceptible to 1-hydroxyestragole induced DNA damage

Based on the inhibition of PhIP induced DNA damage by SULT inhibitors, RT-PCR was carried out to determine which SULTs B-13 and B-13/H cells expressed. As shown

in figure 4.18A, RT-PCR showed that B-13 and B-13/H cells both expressed a number of SULT mRNA transcripts including SULT1A1 and SULT2B1. PAPS synthase 1 and 2 (PAPSS1 & 2) catalyse the production of the SULT cofactor PAPS from ATP and sulphate and are required for SULT function. Analysis of the sequenced B-13 genome suggested that the *Papss1* and *Papss2* genes contained exon deletions. To verify the presence or absence of the deletions, primers were designed around the predicted sites of deletion. RT-PCR showed (figure 4.18B) that neither *Papss1* nor *Papss2* contained deletions in B-13 cells as PAPSS1 mRNA could be detected in B-13 and B-13/H cells and PAPSS2 mRNA in B-13/H cells.

The dietary constituent estragole is an alkenylbenzene found in a range of herbs and spices, particularly in basil. As outlined in figure 4.19A, estragole can be bioactivated to a genotoxic metabolite. Specifically, it is primarily metabolised by CYP1A2 in humans to 1-hydroxyestragole which is then sulphated to the ultimate genotoxic metabolite, 1-sulfoxyestragole [235]. Due to the primary role of CYP1A2 in the bioactivation of estragole, B-13, B-13/H, B-13<sup>-TR/h1A2</sup> and B-13<sup>-TR/h1A2</sup>/H cells were treated with estragole, 1-hydroxyestragole (the hydroxylated form of estragole) or PhIP and DNA damage measured using the comet assay to determine if B-13<sup>-TR/h1A2</sup>/H cells were able to bioactivate estragole.

Figure 4.19B shows that no cells showed significant DNA damage in response to estragole whereas 1-hydroxyestragole caused significant DNA damage in B-13/H and B-13<sup>-TR/h1A2</sup>/H cells. This suggests that B-13<sup>-TR/h1A2</sup>/H cells were unable to significantly hydroxylate estragole but were, like B-13/H cells, able to sulphate 1-hydroxyestragole. Interestingly, B-13 cells, which expressed a similar range of SULT transcripts to B-13/H cells, were not sensitive to DNA damage resulting from 1-hydroxyestragole treatment. Treatment of B-13/H and B-13<sup>-TR/h1A2</sup>/H cells with a range of 1-hydroxyestragole concentrations showed that DNA damage was induced in both cell types in a dose dependent manner (figure 4.20A), but B-13<sup>-TR/h1A2</sup>/H cells were more sensitive. Importantly, DNA damage resulting from 1-hydroxyestragole treatment was not a consequence of cytotoxicity (figure 4.20B).

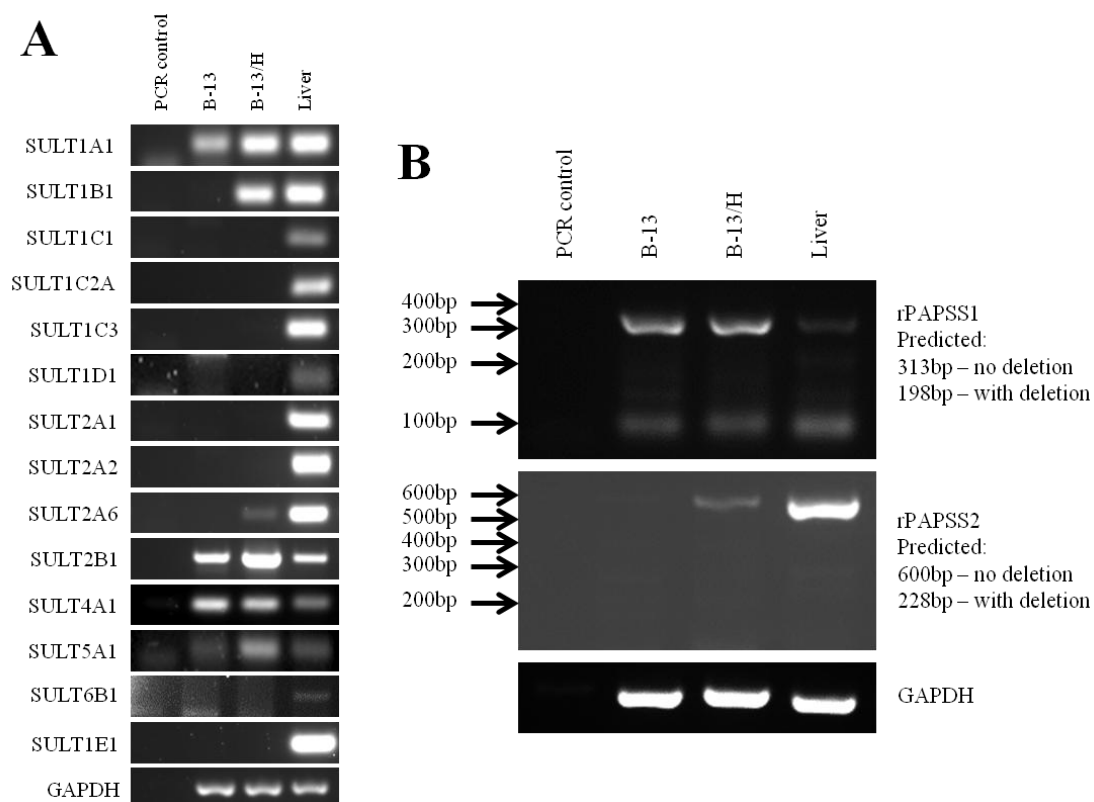


**Figure 4.18: B-13 and B-13/H cells express a number of SULTs and PAPS.** **A.** RT-PCR for the indicated transcripts. **B.** RT-PCR for PAPS1 and PAPS2 using primers designed around the potential deletion site. For **A** and **B**, total RNA was extracted using TRIzol from B-13 and B-13/H cells and cDNA produced which was used as the template for PCR alongside cDNA produced from untreated rat liver. Following PCR, samples were separated by agarose gel electrophoresis and visualised by UV transillumination. Results shown are representative of at least 3 separate experiments.

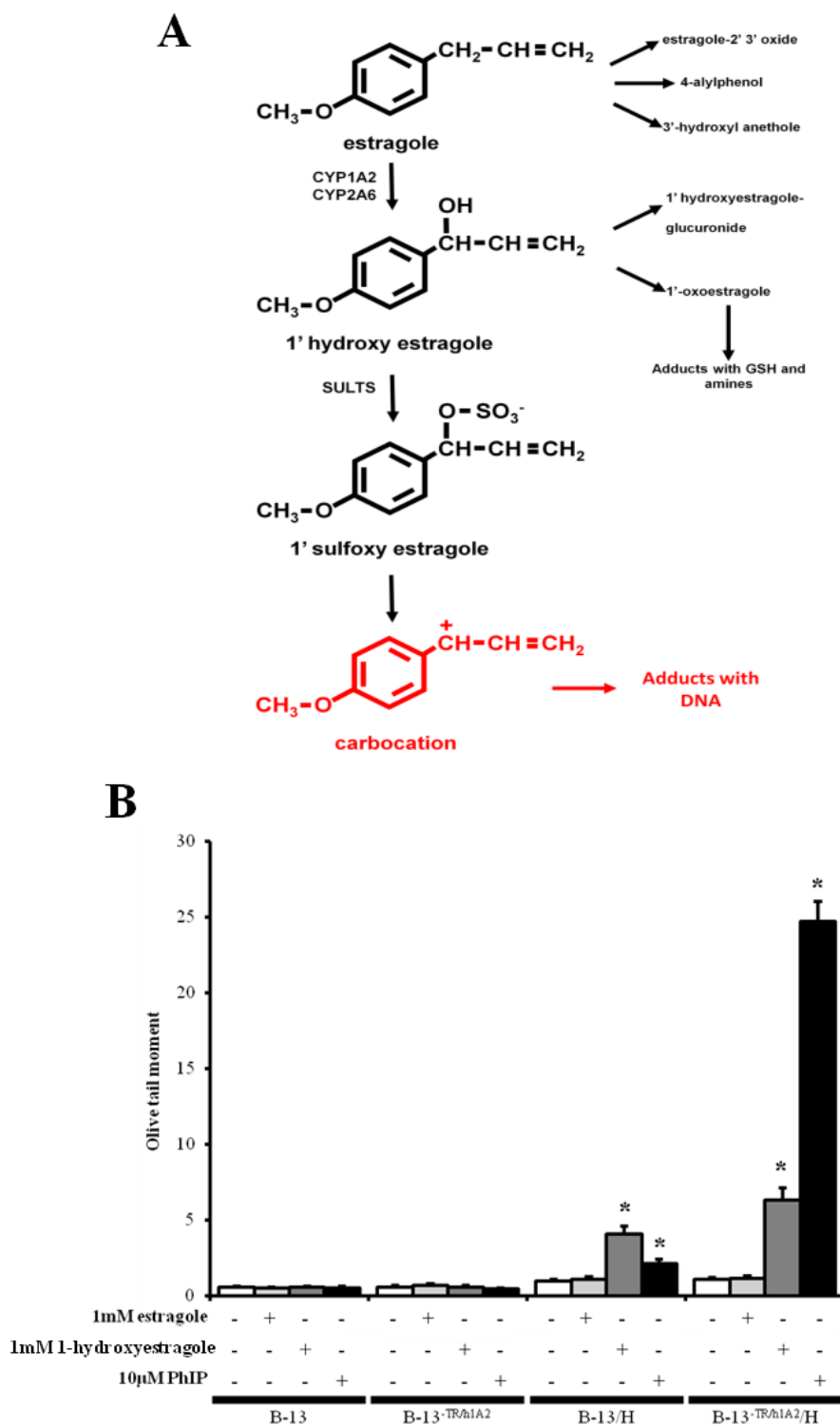


**Figure 4.19: B-13/H and B-13<sup>-TR/h1A2</sup>/H cells are sensitive to 1-hydroxyestragole. A. Metabolism of estragole to a genotoxic metabolite.** Adapted from Alhusainy *et al.*, (2012) [235]. **B. DNA damage in cells following estragole, 1-hydroxyestragole or PhIP treatment measured by comet assay.** B-13, B-13/H, B-13<sup>-TR/h1A2</sup> and B-13<sup>-TR/h1A2</sup>/H cells were treated with vehicle (1% (v/v) DMSO), 1mM estragole, 1mM 1-hydroxyestragole or 10µM PhIP for 16 hours. Following treatment, cells were subject to the alkaline comet assay and DNA stained with SYBR gold. Slides were viewed using a fluorescence microscope and DNA damage calculated using cometscore software. Data are the mean and SE of 50 cells from a single experiment, typical of at least 3 separate experiments. \*significant difference compared to respective vehicle control at  $p < 0.05$ .

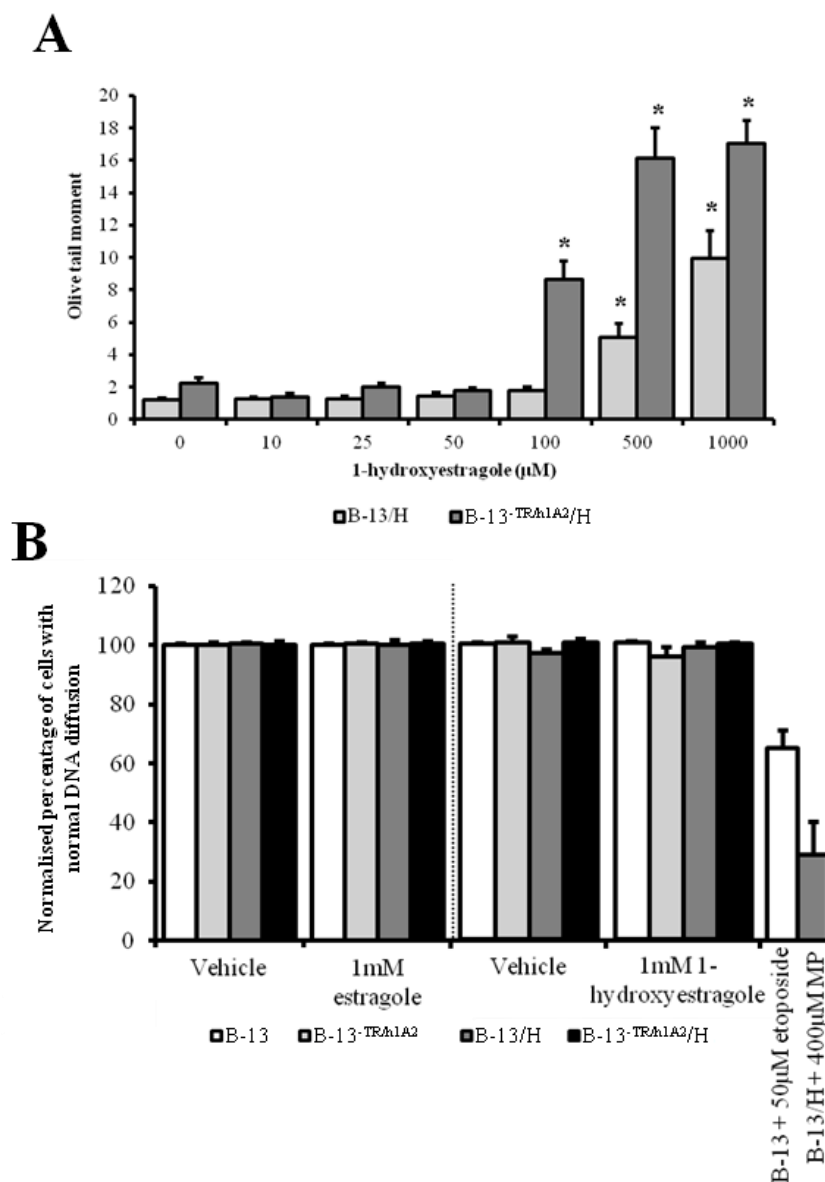


**Figure 4.20: B-13<sup>TRh1A2</sup>/H cells are more sensitive to 1-hydroxyestragole than B-13/H cells. A. Dose response of B-13/H and B-13<sup>TRh1A2</sup>/H cells treated with 1-hydroxyestragole measured by comet assay.** B-13/H and B-13<sup>TRh1A2</sup>/H cells were treated with vehicle (0.1% (v/v) DMSO) or different concentrations of 1-hydroxyestragole for 16 hours. Following treatment, cells were subject to the alkaline comet assay and DNA stained with SYBR gold. Data are the mean and SE of 50 cells from a single experiment, typical of at least 3 separate experiments. \*indicates significant difference compared to respective vehicle control at  $p < 0.05$  calculated by ANOVA followed by the Bonferroni-Holm post-hoc test. **B. DNA diffusion assay in cells following estragole or 1-hydroxyestragole treatment.** B-13, B-13/H, B-13<sup>TRh1A2</sup> and B-13<sup>TRh1A2</sup>/H cells were treated with vehicle (0.1% (v/v) DMSO), 1mM estragole, 1mM 1-hydroxyestragole or positive controls (50µM etoposide or 400µM methapyrilene (MP)) for 16 hours. Following treatment, cells were embedded in low melting point agarose, lysed and stained with SYBR gold. Slides were viewed using a fluorescence microscope and the percentage of cells with normal DNA diffusion (using the positive controls as a guide) calculated. Results are the mean and SD from 4 fields of view, with at least 100 individual cells counted in total, from a single experiment, typical of at least 3 separate experiments. No statistical analysis was performed.

#### 4.11 1-hydroxyestragole induced damage is sulphation dependent

To determine if DNA damage caused by 1-hydroxyestragole was dependent on SULT activity, B-13/H and B-13<sup>-TR/h1A2</sup>/H cells were pre-treated with a range of inhibitors prior to treatment with 1-hydroxyestragole. Figure 4.21 shows that treatment of cells with SULT inhibitors (quercetin, PNP and pentachlorophenol (PCP)) significantly inhibited 1-hydroxyestragole induced DNA damage. These results suggest that, as expected, 1-hydroxyestragole induced DNA damage is SULT dependent in B-13/H and B-13<sup>-TR/h1A2</sup>/H cells

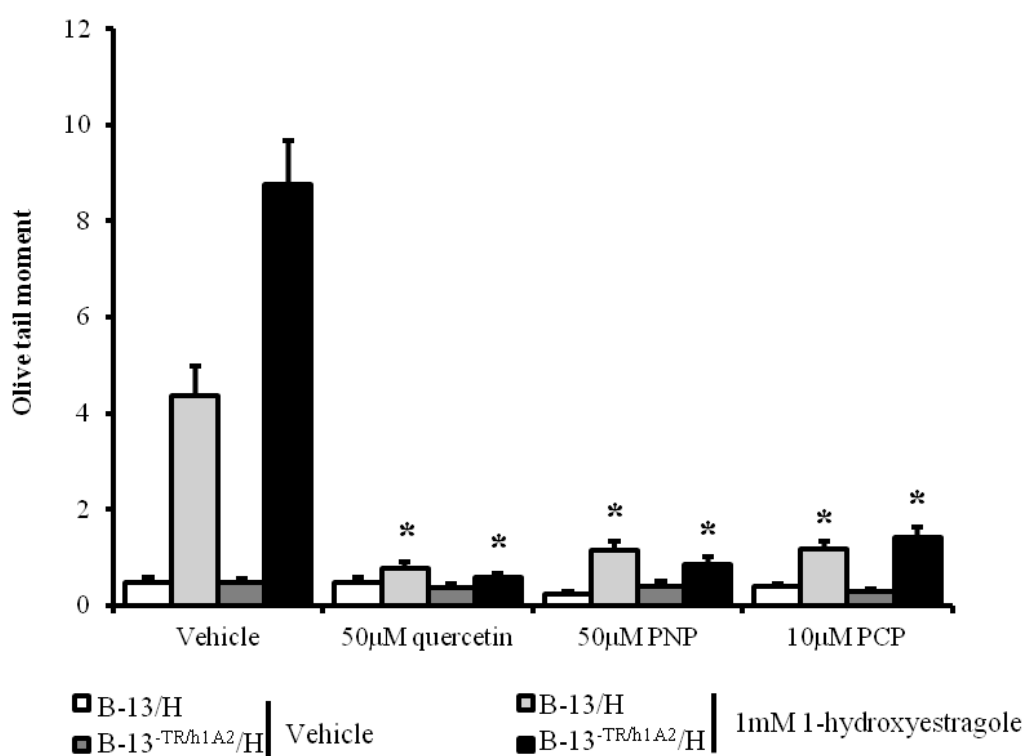


**Figure 4.21: 1-hydroxyestragole induced DNA damage is SULT dependent.** DNA damage in B-13/H and B-13<sup>-TR/h1A2</sup>/H cells treated with 1-hydroxyestragole and SULT inhibitors measured by comet assay. B-13/H and B-13<sup>-TR/h1A2</sup>/H cells were treated with vehicle (0.1% (v/v) DMSO), quercetin, PNP or PCP for 6 hours then additionally with vehicle (0.1% (v/v) DMSO) or 1mM 1-hydroxyestragole for 16 hours. Following treatment cells were subject to the alkaline comet assay and DNA stained with SYBR gold. Slides were viewed using a fluorescence microscope and DNA damage calculated using cometscore software. Data are the mean and SE of 50 cells from a single experiment, typical of at least 3 separate experiments. \*significant difference to cells treated with 1-hydroxyestragole alone at p<0.05.

## 4.12 Chapter discussion

Although most toxicity data obtained from non-human species is relevant to humans at least in some form, in the case of some specific compounds this is not the case. This is why human hepatocytes, but not those derived from other species, are the gold standard for toxicity screening. Variation exists in the specificity, affinity and regulation of homologous enzymes between species which account for the differences in metabolism that have been documented. In this chapter, it was shown that B-13 and B-13/H cells do not express functional CYP1A2. hCYP1A2, derived from a donor sample, was therefore cloned into the cells to create the B-13<sup>-TR/h1A2</sup> line. This line expressed hCYP1A2 and when transdifferentiated showed significantly increased and furafylline inhibitable MROD activity compared to wild type B-13/H cells. B-13<sup>-TR/h1A2</sup>/H cells were also shown to be significantly more sensitive to PhIP induced DNA damage. Undifferentiated B-13<sup>-TR/h1A2</sup> cells did not demonstrate any drug metabolising capacity and this is likely because undifferentiated B-13 cells do not express CYP reductase, which is required for CYP450 function [124].

hCYP1A2 was cloned into the B-13 line using a doxycycline inducible system, however the introduced hCYP1A2 was not doxycycline regulated as originally planned, even though TetR mRNA was expressed. The expression of hCYP1A2 in the absence of doxycycline was likely therefore a consequence of incomplete repression of expression by TetR. An additional factor is that the B-13<sup>-TR/h1A2</sup> line is a polyclonal population. Attempts were made to create a monoclonal line, selecting clones with low basal hCYP1A2 expression and high doxycycline inducible expression. However, when cells were sub-cultured as single cells/well they frequently died, likely due to lack of pro-survival paracrine signalling, which prevented the creation of a monoclonal line. If inducible expression was required, then hCYP1A2 could be fused to a fluorescent protein (eg. green fluorescent protein) and fluorescent activated cell sorting used to create a monoclonal population regulated by doxycycline in a more straightforward manner.

CYP450 hydroxylation of xenobiotics is often only the first step in the bioactivation process of a pro-drug. Conjugation reactions, particularly sulphation reactions, are frequently involved in the bioactivation of pro-carcinogenic xenobiotics following

CYP450 (often CYP1A) mediated hydroxylation [231]. If B-13/H cells (wild type or humanised versions) were to be used to screen genotoxins therefore, it was important that they expressed functional SULTs. A PCR array showed that B-13/H cells expressed 6/14 SULT transcripts and PAPSS1 and PAPSS2 mRNA. Undifferentiated B-13 cells expressed only 3/14 SULT transcripts and not PAPSS2, suggesting that transdifferentiation is associated with the up-regulation of phase II, as well as phase I, DMEs. SULTs were shown to be functional in B-13/H, but not B-13 cells, as their inhibition in B-13/H cells significantly reduced the DNA damage resulting from 2 SULT dependent pro-carcinogens, PhIP and 1-hydroxyestragole. Surprisingly, B-13<sup>TR/h1A2</sup>/H cells were more sensitive to 1-hydroxyestragole induced DNA damage than untransfected B-13/H cells. This may have been due to the presence of unhydroxylated estragole or other pro-carcinogenic impurities in the 1-hydroxyestragole we received which was metabolised by hCYP1A2 causing DNA damage.

The insensitivity of B-13<sup>TR/h1A2</sup>/H cells to estragole induced DNA damage was unexpected, as estragole is primarily bioactivated by CYP1A2 [235]. When B-13<sup>TR/h1A2</sup>/H cells were treated with 1-hydroxyestragole, DNA damage was only seen at doses greater than 100µM, a relatively high dose. Considering that estragole and 1-hydroxyestragole are substrates for numerous DMEs other than CYP1A2 and SULTs respectively, it is likely that a DNA damaging concentration of 1-sulfoxyestragole (the genotoxic metabolite) was unable to be produced, due to the rapid detoxification of estragole and 1-hydroxyestragole by competing DMEs.

The lack of DNA damage in B-13 cells treated with 1-hydroxyestragole suggests that the sulphation of 1-hydroxyestragole is catalysed by a SULT expressed by B-13/H, but not B-13 cells (SULT1B1, SULT2A6 and SULT5A1). Alternatively, it may be related to the lack of PAPSS2 expression in B-13 cells as, although PAPSS 1 and 2 both produce the universal SULT substrate PAPS, evidence to date suggests that they are differentially regulated and localised. PAPSS1 accumulates in the nucleus and in humans shows greater expression in the brain and skin compared to PAPSS2 which is more cytoplasmic based and shows greater expression in the liver and cartilage [236, 237]. Considering that SULTs are generally cytoplasmic and B-13 cells do not express PAPSS2, SULT mediated bioactivation of 1-hydroxyestragole could have been limited by a shortage of PAPS in B-13 cells.

The data presented in this chapter demonstrates that a human gene, stably introduced into the B-13 cell line, was expressed and functional following transdifferentiation, due to the expression of necessary coenzymes, thus proving the initial hypothesis. This work shows that, as a proof of concept, B-13 cells can be readily humanised with DMEs, which should be functional. It has also been shown that a humanised B-13 line could be used for genotoxicity screening, as B-13 cells, when transdifferentiated, express the enzymes required for complete bioactivation of pro-carcinogens. Commonly for genotoxicity screening, test compounds are bioactivated with exogenous metabolic activation systems (normally rat liver S9) before exposure to cells. However, these systems poorly recapitulate *in-vivo* metabolic activation where bioactivation is complex, requiring the activities of numerous enzymes, or where reactive intermediates are short lived and hence unable to reach target DNA. The use of B-13/H cells for genotoxicity screening could overcome these problems as they express a range of functional DMEs in proximity to the target DNA. The use of humanised B-13 cells (including B-13<sup>-TR/h1A2</sup> cells) would further improve their utility by enhancing the clinical relevance of any derived results.

**Chapter 5. Expression and function of transporters in B-13/H cells**

## 5.1 Introduction

The expression of transporters, and their polarisation, is required for efficient hepatocyte function *in-vivo*. They facilitate the removal of potentially toxic compounds from systemic circulation through active uptake and the partitioning of metabolites into the bile. As outlined in the introduction, hepatocytes express a range of transporters which can be broadly categorised by which membrane they localise to, whether they are involved in the influx or efflux of compounds and if they are ATP dependent for function. Similar to CYP450s, the expression of hepatic transporters is in part regulated by nuclear receptors, particularly the PXR, CAR, PPAR $\alpha$  and FXR [81]. Through these receptors, the rate and route of drug metabolism can be regulated from uptake through to modification/conjugation to efflux.

Certain drugs can inhibit specific transporters, resulting in alterations in metabolism of a second co-administered drug. An example of this is statins, which are primarily influxed by OATPs. Cyclosporin A and gemfibrozil both inhibit OATPs and significantly increase the bioavailability of statins when co-administered. In some patients administered cerivastatin with cyclosporin A, skeletal muscle toxicity was documented and it has been hypothesised that this may, at least in part, be due to increased bioavailability of cerivastatin resulting from inhibition of OATP-mediated uptake [238-240]. Due to the importance of BSEP in the export of bile acids, its inhibition can cause cholestasis and liver injury. Numerous drugs have been shown to inhibit BSEP function, including troglitazone and rifampicin, causing cholestatic liver injury [241, 242]. Inhibition of BSEP prevents sufficient bile acid export into the canaliculi, which leads to the intracellular accumulation of bile acids in hepatocytes. Through their detergent effect, this is thought to disrupt mitochondrial function, leading to necrosis and apoptosis [243, 244].

The assessment of the capacity of novel drugs and chemicals to inhibit transporter activity is therefore an important aspect of the characterisation of newly developed drugs and chemicals. Primary hepatocytes are the optimal model in which to evaluate drug-transporter interactions *in-vitro* as they, at least in the short term, express approximately physiological levels of transporters [245]. Additionally, metabolites of the parent compound, rather than the parent compound itself, may be inhibitors and

therefore testing in a metabolically competent cell is important to detect any effects. In hepatocytes *in-vitro*, apical transporter expression is generally relatively stable, however the expression of basal transporters including NTCP and OATP1 rapidly decreases over time [245-248]. Interestingly, the expression of transporters is more stable in human primary hepatocytes than rat primary hepatocytes in culture [245]. 3D culture of primary hepatocytes has been shown to help retain expression and polarisation of some hepatocyte transporters though it still only attenuates, rather than prevents, the loss of expression [245, 249].

As shown in chapter 3, B-13/H cells are metabolically competent in a manner quantitatively similar to primary hepatocytes. Based on this demonstrated similarity to primary hepatocytes, it was hypothesised that B-13/H cells express a physiologically relevant pattern of transporters, equivalent to that seen in the liver. Expression of hepatic transporters would improve the clinical relevance of B-13/H cells for the assessment of drug and chemical toxicity and allow them to be used in place of primary hepatocytes for the study of drug-transporter interactions.

## **5.2 Transdifferentiation of B-13 cells is associated with up-regulation of drug transporter mRNA expression**

To test the hypothesis, drug transporter mRNA expression was assessed in B-13 and B-13/H cells and rat liver using SABiosciences rat drug transporter qPCR arrays. Results for selected transporters (which were selected for all subsequent drug transporter arrays), chosen because of their known roles in xenobiotic and/or bile acid efflux/influx, are illustrated in figure 5.1. This shows that B-13 cells expressed detectable levels of drug transporter mRNA transcripts. Transdifferentiation of B-13 to B-13/H cells was associated with the up-regulation of almost all transcripts. Compared to intact rat liver, B-13 and B-13/H cells expressed approximately quantitatively equivalent mRNA levels of several important transporters including MDR1, MDR2, MRP1, MRP3-5, OCT2, OAT1 and OATP3 and 5. However, expression of the bile acid transporters BSEP and NTCP were low in comparison, as was expression of MRP2 amongst other important xenobiotic transporters. Comparing the average fold change in expression of all measured transcripts (table 5.1) showed that B-13/H cells expressed about 10 fold more transporter mRNA than B-13 cells, but around 100 fold less than rat liver.

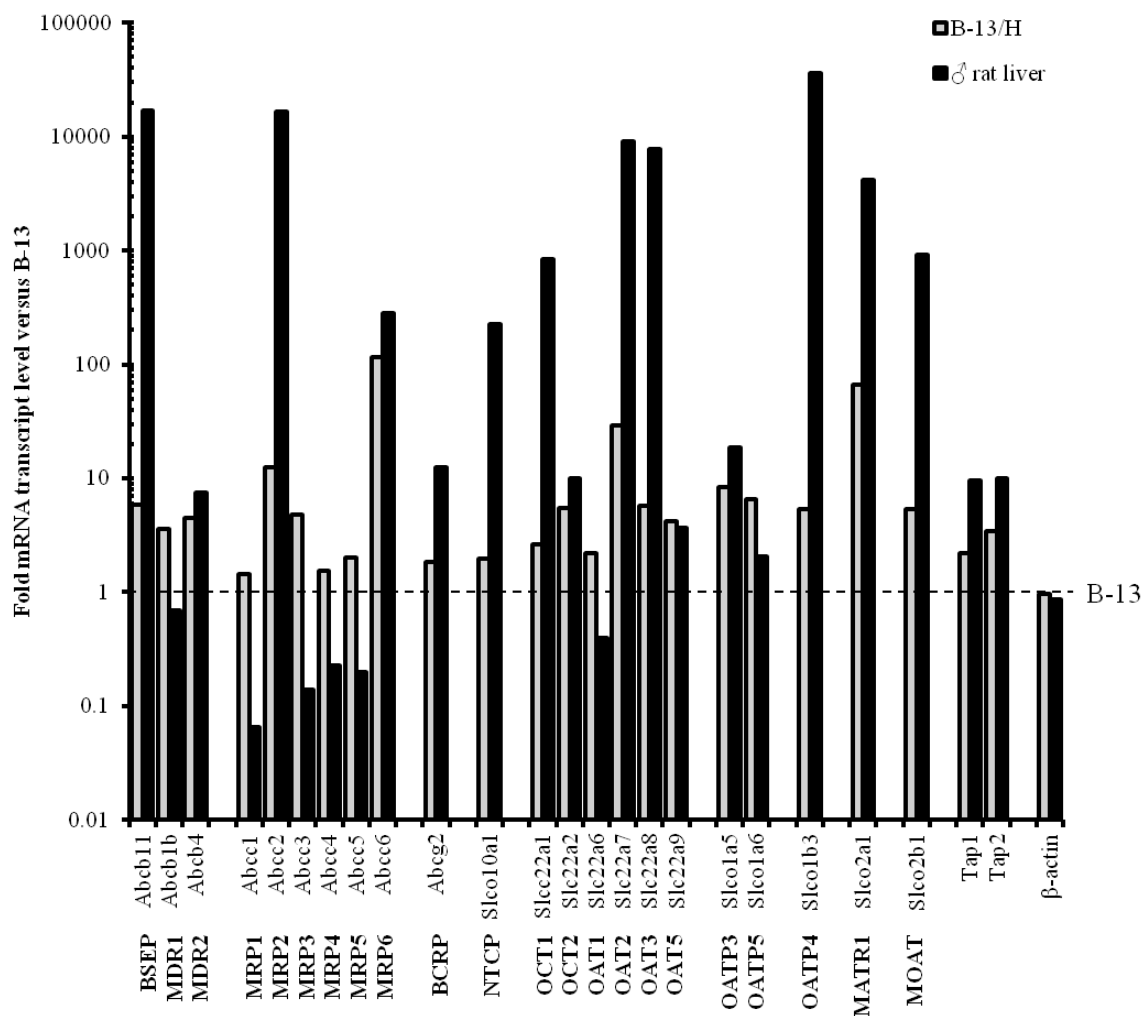


**Figure 5.1: B-13/H cells express several drug transporters at liver levels.** Fold mRNA expression of indicated transcripts in B-13/H cells and intact rat liver shown relative to B-13 cells, quantified using a rat drug transporter array. Total RNA was produced from samples using TRIzol, which was then cleaned up, reverse transcribed and the resulting cDNA used as a template for the rat drug transporter arrays. Results are the mean of 3 independent determinations from the same experiment. No statistical analysis was performed.

	B-13	B-13/H	♂ rat liver
Mean	1	11.12	1158.85
SD	0	43.28	4688.62

**Table 5.1: Average fold change in expression of all measured transcripts in B-13/H cells and rat liver relative to B-13 cells.**

### 5.3 3D culture does not markedly change B-13/H expression of drug transporters

Due to the low transcript expression of several key transporters in B-13/H cells, they may not be a good model in which to test for transporter interactions with novel drugs and chemicals. Culture of hepatocytes in 3D culture systems has been shown to help restore hepatocyte polarity and retain expression of various transporters including

BSEP, NTCP and MRP2 [245]. This normally involves the sandwich culture of hepatocytes between rat tail collagen I and matrigel. It was therefore hypothesised that modification of culture substratum would induce transporter expression in B-13/H cells. Alvetex is a porous polystyrene matrix which, unlike other commercially available matrices, is characterised by an open but interconnected pore structure. Published studies using alvetex have shown that it enhances the hepatic phenotype of HepG2 cells and reduces the rate of primary hepatocyte dedifferentiation [250-253]. In order to determine the effect of 3D culture on transporter expression in B-13/H cells, B-13 cells were seeded onto alvetex as outlined in the methods and transdifferentiated as normal over 14 days.

To assess if cells seeded onto the alvetex were viable, neutral red staining was carried out on cells. Figure 5.2A shows that cells seeded onto the alvetex accumulated neutral red, indicating that they were viable. To confirm the location of seeded cells on the scaffold, scaffolds containing B-13 and B-13/H cells were fixed, processed and embedded as outlined in the methods. They were then cut into 10 $\mu$ m sections and DAPI stained as shown in figure 5.2B. Both B-13 and B-13/H cells were localised to the top of the alvetex, the side they were originally seeded on, although B-13/H cells had invaded deeper into the scaffold. CYP2E1 immunostaining of B-13 and B-13/H cells on alvetex showed that B-13/H but not B-13 cells expressed CYP2E1, confirming that B-13 cells treated with DEX on alvetex were still able to transdifferentiate (figure 5.2C). RT-PCR confirmed that B-13 cells were able to transdifferentiate on the scaffold as B-13/H cells cultured on alvetex expressed the same markers as those grown as a monolayer (figure 5.3A).

The expression of drug transporter mRNA was measured in monolayer and alvetex cultured B-13/H cells as illustrated in figure 5.3B. Alvetex culture caused some changes in transporter mRNA expression compared to B-13/H cells cultured as a monolayer, however the differences were small and whilst alvetex culture induced the mRNA expression of several transporters, it also inhibited the expression of a similar number. Indeed, the average fold change in expression of all measured transcripts between alvetex cultured B-13/H cells and those cultured as a monolayer was  $1.18 \pm 2.30$ , demonstrating that alvetex had essentially no net effect on transporter expression.

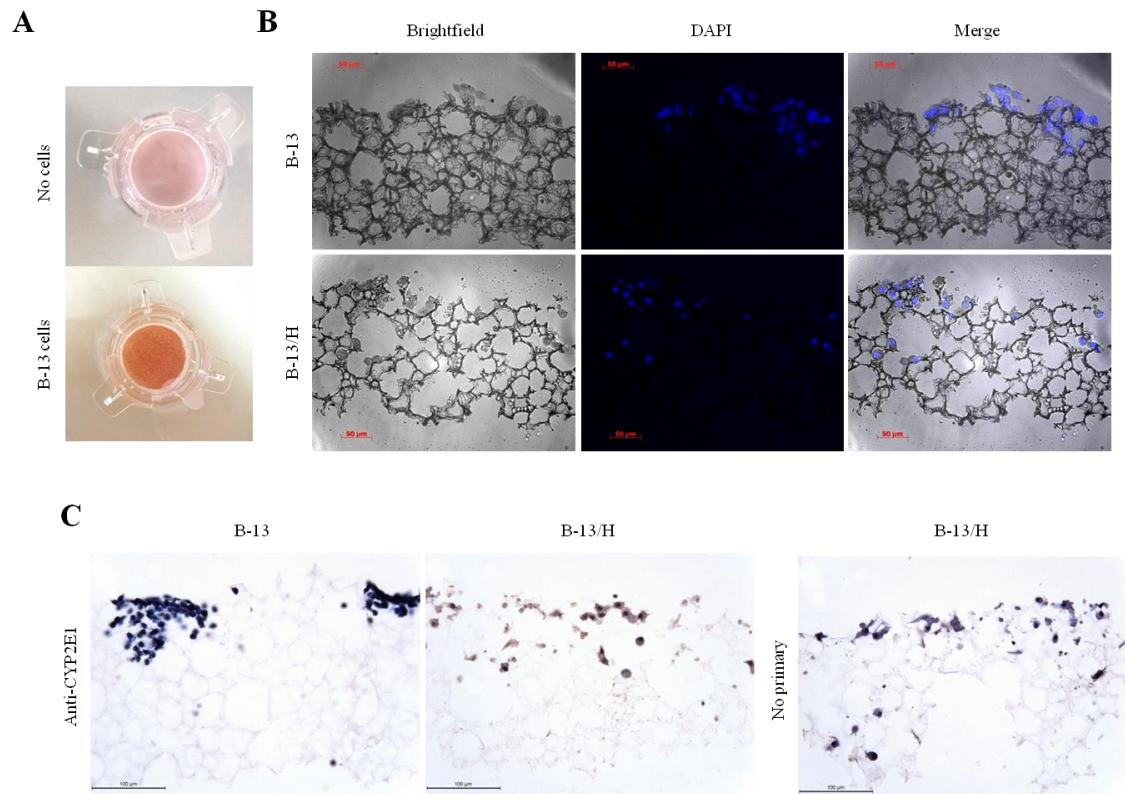


**Figure 5.2: B-13 cells adhere to and transdifferentiate on alvetex.** **A.** Neutral red stained alvetex seeded with or without B-13 cells. Scaffolds were incubated in 0.03% (w/v) neutral red in PBS for 1 hour before a PBS wash. Staining was carried out 2 days after B-13 seeding. **B.** DAPI staining of B-13 and B-13/H cells on alvetex. B-13 and B-13/H cells were cultured on alvetex for 3 and 14 days respectively before fixation. Scaffolds were fixed in 10% buffered formalin, embedded and cut into 10µm sections. Slides were dewaxed, rehydrated and stained with DAPI before imaging on a Zeiss fluorescence microscope. Scale bar indicates 50µm. **C.** CYP2E1 immunostaining of B-13 and B-13/H cells on alvetex. Scaffolds with cells cultured as in **B**, were fixed in 10% buffered formalin, embedded and cut into 10µm sections. Slides were then dewaxed, blocked and immunostained for CYP2E1 using DAB to detect bound antibody. Slides were then counterstained with haematoxylin. Slides were viewed using a Lecia upright microscope. Scale bar indicates 100µm. All images are representative of at least 3 separate experiments.

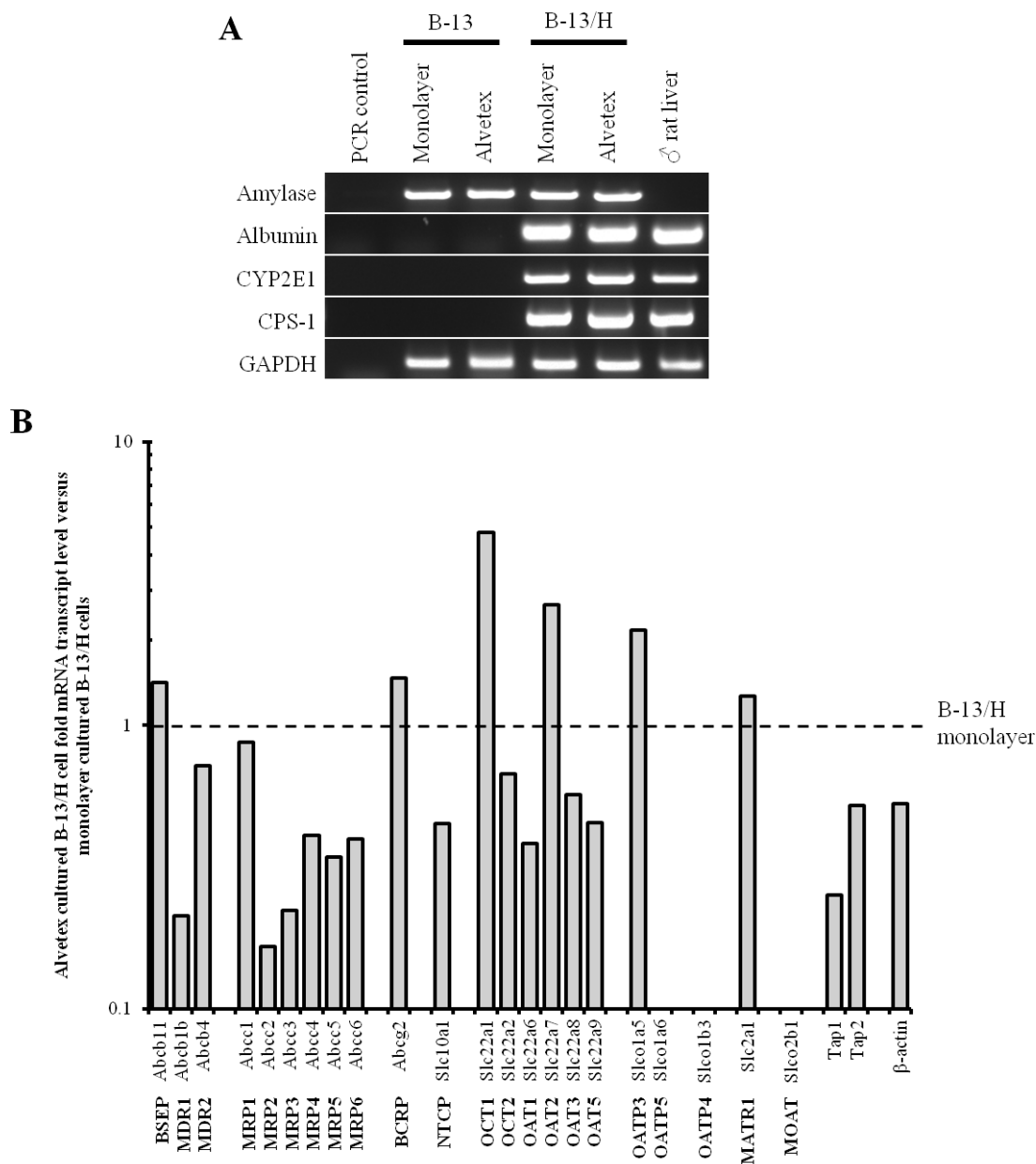


**Figure 5.3: Alvetex does not enhance B-13/H expression of drug transporters. A. RT-PCR for indicated transcripts in B-13 and B-13/H cells cultured as a monolayer or on alvetex.** B-13 cells and B-13/H cells were cultured for 3 and 14 days respectively as a monolayer or on alvetex. Total RNA was extracted from cells using TRIzol and cDNA produced which was used as the template for PCR. Following PCR, samples were separated by agarose gel electrophoresis and visualised by UV transillumination. **B. Fold mRNA expression of indicated transcripts in monolayer and alvetex cultured B-13/H cells.** Transporter mRNA expression in alvetex cultured B-13/H cells is shown relative to monolayer cultured B-13/H cells and was quantified using rat drug transporter array plates. Total RNA was produced from B-13/H cells cultured as a monolayer or on alvetex for 14 days using TRIzol, which was then cleaned up, reverse transcribed and the resulting cDNA used as a template for the rat drug transporter arrays. Results are the mean of 3 independent determinations from the same experiment. No statistical analysis was performed.

#### 5.4 Culture on PU134 does not up-regulate B-13/H expression of drug transporters

Recent interesting work has shown that hepatocyte-like cells derived from hESCs and cultured on PU134 show an improved hepatocyte phenotype compared to those cultured on plastic [254]. This use of PU134 was identified through a screen of 380 different polymers; hepatocyte-like cells were cultured on different polyurethane or polyacrylate polymers and then immunostained for albumin. The 6 polymers which induced the greatest increase in albumin expression were then tested for their ability to induce hepatocyte export proteins in the same cells. PU134 was identified as best at promoting a hepatocyte phenotype in these studies and was shown to improve CYP1A2 and CYP3A4 activity and CYP3A4 induction. It has been used in subsequent work to improve the predictive capacity of hESC and iPSC derived hepatocyte-like cells for toxicity screening [255]. Based on these findings, it was anticipated that culture of B-13/H cells on the polymer would improve their hepatic phenotype and up-regulate transporter expression. B-13 cells were therefore seeded onto PU134 coated slides in 24 well plates and either cultured as normal or transdifferentiated over 2 weeks. Figure 5.4 shows that B-13 and B-13/H cells cultured on PU134 had the same morphology as those cultured on plastic and transdifferentiated B-13 cells expressed CYP2E1 when transdifferentiated on plastic as normal, or on PU134.

RT-PCR and Western blotting confirmed that culture on PU134 did not have a marked effect on the expression of hepatic markers and did not lead to an up-regulation of MRP2, BSEP or NTCP mRNA expression (figure 5.5A & B). Drug transporter mRNA expression was analysed by qPCR as shown in figure 5.5C. B-13 and B-13/H cells on PU134 showed similar expression of transporters to those cultured on plastic as illustrated by the average fold change in expression of all measured transcripts (table 5.2). Several of the transcripts were poorly detected using the qPCR plates including BSEP and MRP2, presumably due to their low expression, which explains why the liver fold change in this experiment was relatively low in comparison to that seen previously.

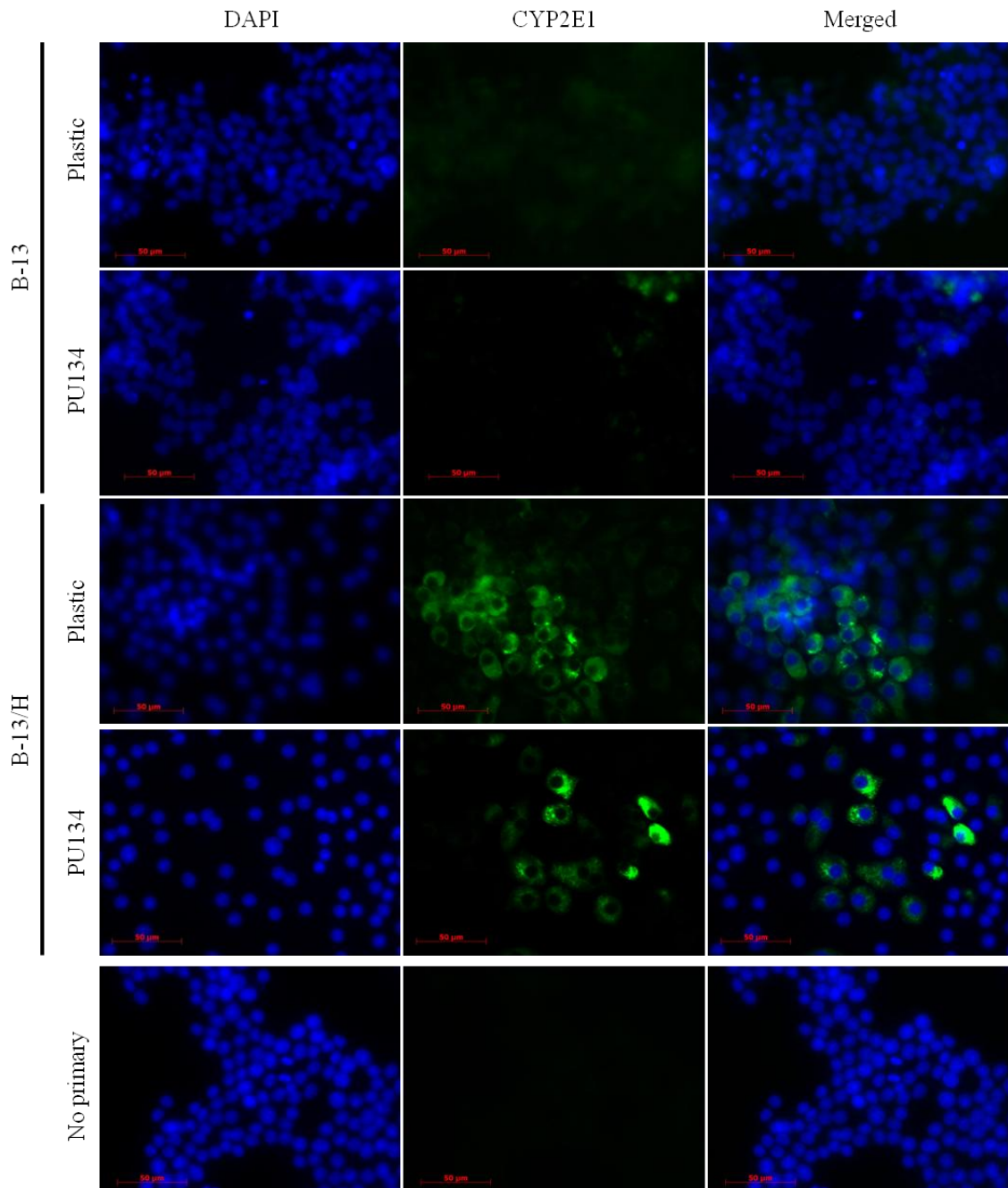


**Figure 5.4: Culture on PU134 does not affect B-13 transdifferentiation.** CYP2E1 fluorescence immunostaining of B-13 and B-13/H cells cultured on plastic as normal or on PU134 coated inserts for 14 days. Cells were fixed, blocked and immunostained for CYP2E1 and counterstained with DAPI. Cells were photographed using a Zeiss fluorescence microscope. Scale bar indicates 50 $\mu$ m. Results are typical of 2 separate experiments.

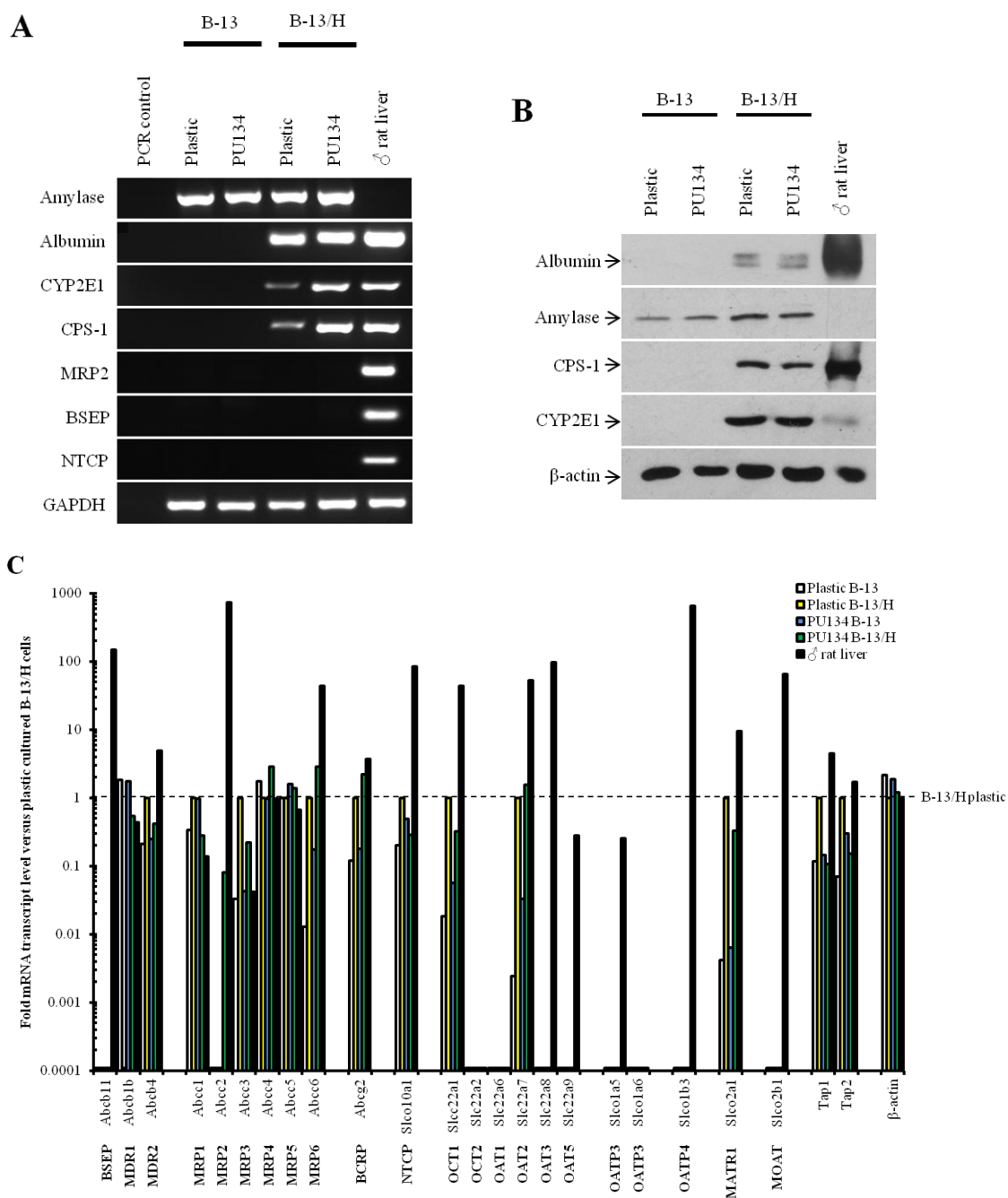


**Figure 5.5: Culture on PU134 does not cause up-regulation of transporter expression. A. RT-PCR for the indicated mRNA transcripts in B-13 and B-13/H cells cultured on plastic or PU134.** B-13 cells and B-13/H cells were cultured for 14 days on plastic or PU134. After culture, total RNA was extracted from samples using TRIzol and cDNA produced which was used as the template for PCR. Following PCR, samples were separated by agarose gel electrophoresis and visualised by UV transillumination. **B. Western blot for liver markers in samples cultured as in A.** Lysates were prepared from rat liver and samples treated as in A, and quantified by Lowry assay. 20 $\mu$ g of protein/well was separated by SDS-PAGE and transferred to a nitrocellulose membrane which was blocked and probed. Antibody binding was detected using ECL Western blot substrate. **C. Fold mRNA expression of indicated transcripts in plastic and PU134 cultured B-13 and B-13/H cells.** Expression is shown relative to plastic cultured B-13/H cells and was quantified using rat drug transporter array plates. From cells treated as in B, total RNA was produced using TRIzol which was cleaned up, reverse transcribed and the resulting cDNA used as a template for the rat drug transporter arrays. For A and B, results are typical of 2 separate experiments. For C, results are the fold change of single samples from the same experiment.

	B-13 plastic	B-13/H plastic	B-13 PU134	B-13/H PU134	♂ rat liver
Mean	0.58	1	0.67	1.03	39.32
SD	1	0	0.97	1.25	125.91

**Table 5.2: Average fold change in expression of all measured transcripts in rat liver and B-13 and B-13/H cells cultured on plastic or PU134 relative to B-13/H cells cultured on plastic.**

### 5.5 Introduction of liver enriched transcription factor HNF4 $\alpha$ increases expression of drug transporters

Liver transporter expression, and hepatocyte specification and phenotype more generally, is regulated by a complex network of liver enriched transcription factors (LETFs). The main LETFs are part of the HNF-1, -3, -4, -6 and C/EBP families [256]. To assess if overexpression of different LETFs could lead to up-regulation of hepatic transporters in B-13/H cells, B-13/H cells were infected with adenoviral constructs encoding C/EBP $\alpha$  (Ad-C/EBP $\alpha$ ), HNF1 $\alpha$  (Ad-HNF1 $\alpha$ ), HNF4 $\alpha$  (Ad-HNF4 $\alpha$ ), C/EBP $\beta$ -liver enriched activator protein (LAP, Ad-LAP) or C/EBP $\beta$ -liver enriched inhibitory protein (LIP, Ad-LIP). HNF1 $\alpha$  and 4 $\alpha$  are part of the HNF family of transcription factors. They regulate a broad range of hepatocyte-specific functions including energy and xenobiotic metabolism, but are also required for liver development and hepatocyte differentiation [256, 257]. C/EBP $\alpha$  and C/EBP $\beta$  are members of the C/EBP family of transcription factors, which, like HNF1 $\alpha$  and HNF4 $\alpha$ , regulate expression of liver specific genes including several CYP450s but also enzymes involved in gluconeogenesis [258]. C/EBP $\beta$  is also required for B-13 transdifferentiation, a physiologically conserved response *in-vivo*, which also shows that it has a role in specifying between pancreatic or hepatic differentiation [123, 126]. The C/EBP $\alpha$  and C/EBP $\beta$  genes are transcribed to full length mRNA which, due to the presence of downstream in-frame start sites, is translated to give several different N-truncated isoforms. C/EBP $\beta$ -LAP contains the activation domains and can therefore be activated and in turn promote gene transcription. Conversely, C/EBP $\beta$ -LIP lacks the activation domains and is therefore a dominant negative form of LAP and represses transcription [259, 260].

Prior to cell adenoviral infection, the MOI of B-13/H cells was established. This was determined as outlined in figure 5.6, as described in the methods. B-13/H cells were

infected with a serially diluted adenovirus encoding GFP and infection efficiency calculated (figure 5.6A & B). As the number of B-13/H cells that were infected was known, the MOI could be calculated, which for an infection efficiency of ~88%, was 2.37 pfu/cell (figure 5.6C).

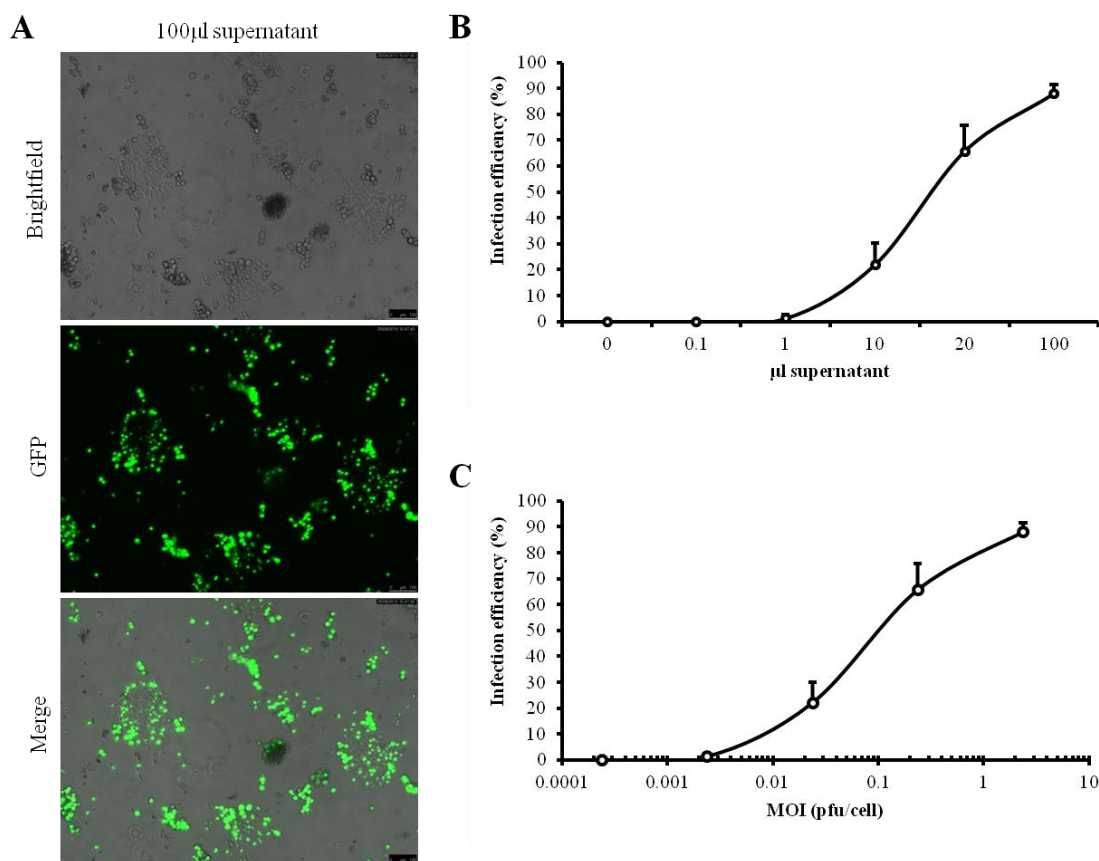


**Figure 5.6: Calculation of B-13/H MOI.** A. Brightfield and fluorescence photomicrographs of B-13/H cells infected with 100 µl of Ad-GFP crude supernatant. Images were taken at 100x magnification on a Leica fluorescence microscope 24 hours after infection. B. Plot of infection efficiency of B-13/H cells against volume of Ad-GFP crude supernatant used for infection. C. Plot of infection efficiency against MOI. For B and C, points are the mean and SD of 3 independent determinations from the same experiment.

B-13/H cells were subsequently infected with the different adenoviruses. Some B-13/H cells were infected with an adenovirus carrying an empty construct (Ad-null) as a control. Infection was carried out using an MOI of 2.37 pfu/cell. Following adenoviral infection, B-13/H cells were cultured, in DEX free medium, for 5 days then harvested. Ad-HNF4 $\alpha$  infected B-13/H cells showed a slight morphological change, flattening, forming more cell-cell contacts and appearing more hepatocyte-like (figure 5.7A). RT-PCR and Western blotting showed that adenoviral infection of B-13/H cells did not markedly affect expression of hepatocyte markers (figure 5.7B & C). RT-PCR for the transporters BSEP, MRP2 and NTCP demonstrated that Ad-HNF4 $\alpha$  infected B-13/H

cells showed detectable expression of BSEP and increased expression of MRP2 mRNA compared to the no virus and other adenoviral infected B-13/H cells. Adenoviral C/EBP $\alpha$ , HNF1 $\alpha$  and HNF4 $\alpha$  were detected by RT-PCR, indicating that B-13/H cells were expressing the relevant mRNA transcripts after adenoviral infection (figure 5.7B). C/EBP $\beta$  mRNA expression could not be detected by RT-PCR in either Ad-LAP or Ad-LIP infected B-13/H cells or human liver using species specific primers, preventing confirmation of adenoviral C/EBP $\beta$  expression in Ad-C/EBP $\beta$  infected B-13/H cells.

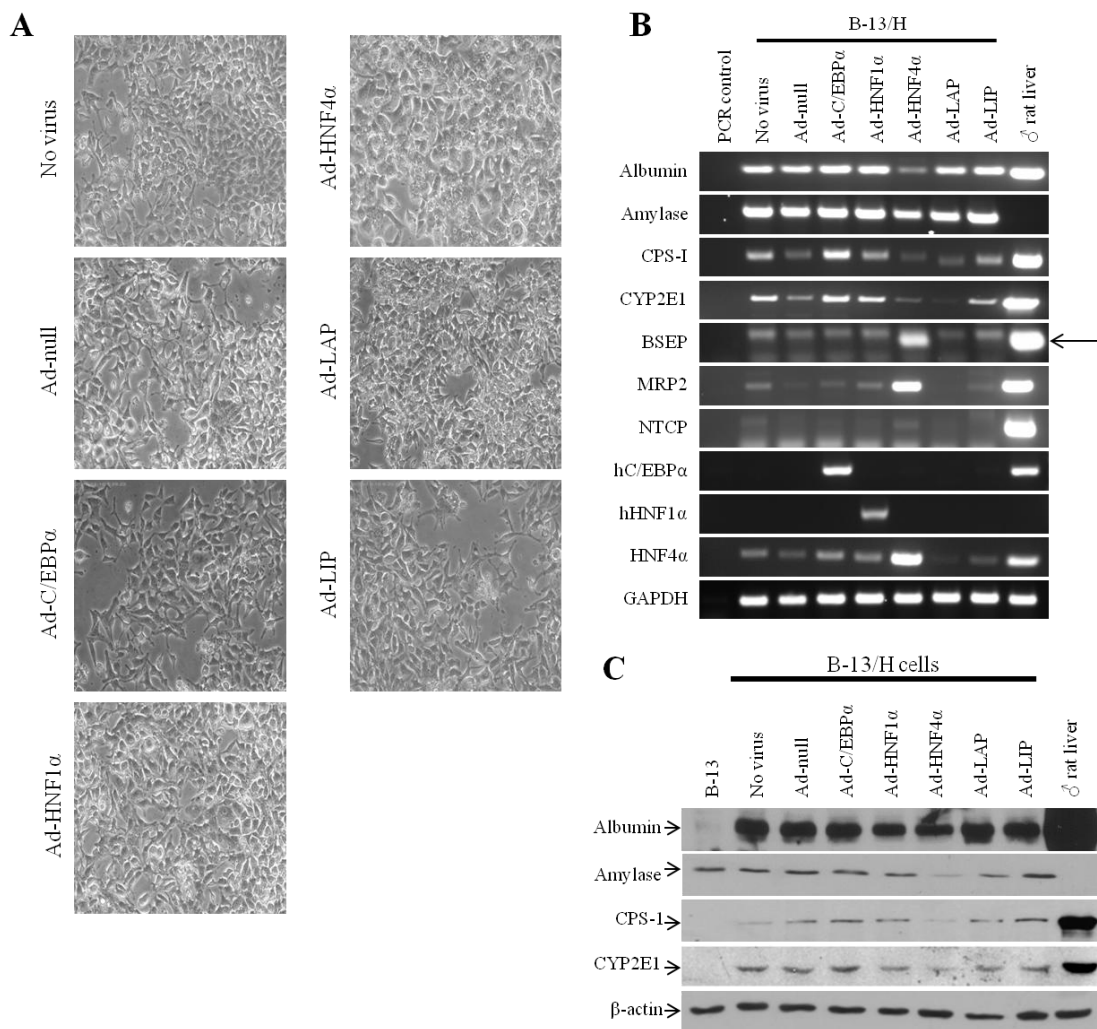


**Figure 5.7: Adenoviral infection with HNF4 $\alpha$  causes a phenotype change and induction of BSEP and MRP2 expression.** **A.** Photomicrograph of B-13/H cells 5 days after adenoviral infection. Images are at 100x magnification. **B.** RT-PCR for the indicated transcripts in adenoviral infected B-13/H cells. Total RNA was extracted from samples 5 days after infection using TRIzol and cDNA produced which was used as the template for PCR. Following PCR, samples were separated by agarose gel electrophoresis and visualised by UV transillumination. **C.** Western blotting for liver markers in B-13 cells, adenoviral infected B-13/H cells and rat liver. Lysates from rat liver, B-13 cells and B-13/H cells treated as in A and B, were prepared and quantified by Lowry assay. 20 $\mu$ g of protein/well was separated by SDS-PAGE and transferred to a nitrocellulose membrane which was blocked and probed. Antibody binding was detected using ECL Western blot substrate. All results are typical of at least 3 separate experiments.

Drug transporter mRNA expression was determined using drug transporter qPCR arrays as shown in figure 5.8. In agreement with the semi-quantitative RT-PCR data, it was confirmed that Ad-HNF4 $\alpha$  infection of B-13/H cells led to up-regulation of MRP2 and BSEP mRNA (by 96 and 73 fold respectively) compared to Ad-null infected cells. Several other transcripts, which could not be detected in Ad-null infected cells, were also measureable in Ad-HNF4 $\alpha$  infected cells such as OCT2 and OAT5. Although Ad-HNF4 $\alpha$  caused the up-regulation of several transporters, down-regulation was seen in other transcripts including all MRPs, excluding MRP2, and MDRs. Considering that these are expressed at greater levels in B-13/H cells in comparison to rat liver (excluding MRP6 and MDR2), the effect of their down-regulation brings their expression level more in line with that seen *in-vivo*. Compared to Ad-HNF4 $\alpha$  infected B-13/H cells, infection with other adenoviral constructs had little effect on the mRNA expression of transporters overall. The average fold change in expression of all measured transcripts is shown in table 5.3 and demonstrates that only HNF4 $\alpha$  overexpression markedly increased average drug transporter expression. This was in comparison to the other adenoviral constructs which had no net effect on expression.

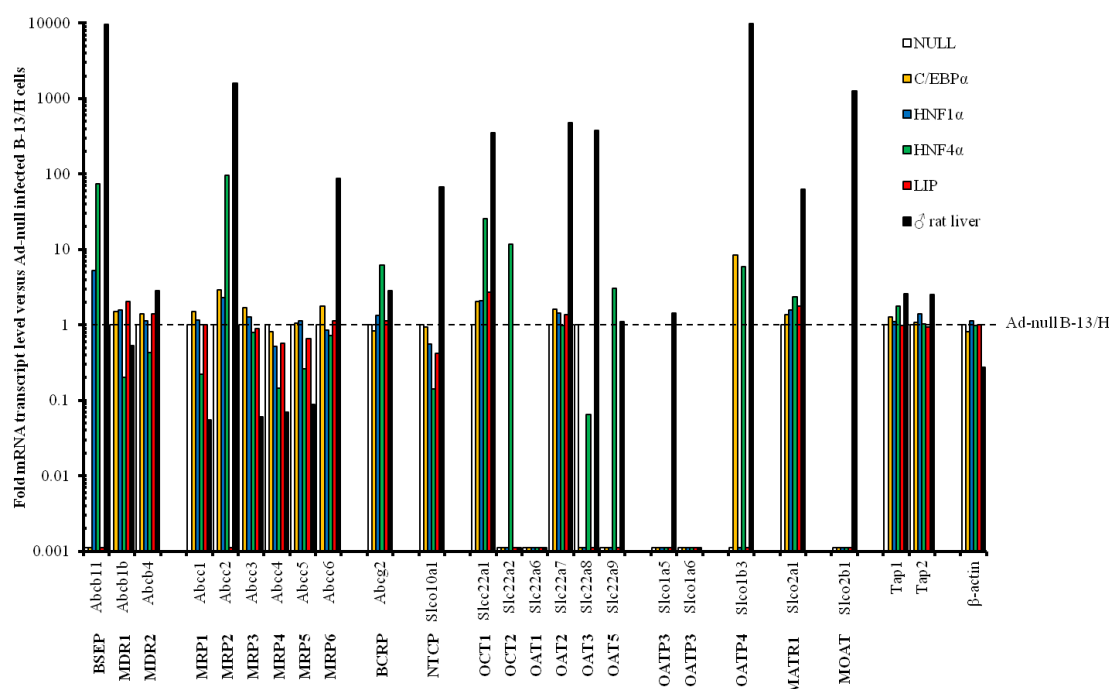


**Figure 5.8: Adenoviral overexpression of HNF4 $\alpha$  induces expression of transporters including MRP2 and BSEP.** Fold mRNA expression of indicated transcripts in adenoviral infected B-13/H cells quantified using rat drug transporter array plates. Expression is shown relative to Ad-null infected B-13/H cells. Total RNA was produced from B-13/H cells 5 days after infection using TRIzol, which was then cleaned up, reverse transcribed and the resulting cDNA used as a template for the rat drug transporter arrays. Legend corresponds to which adenovirus construct B-13/H cells were infected with. Results are the fold change of single samples from the same experiment.

	Ad-null	Ad-C/EBP $\alpha$	Ad-HNF1 $\alpha$	Ad-HNF4 $\alpha$	Ad-LIP	♂ rat liver
<b>Mean</b>	1.00	2.27	1.50	17.67	1.50	449.22
<b>SD</b>	0.00	5.55	0.95	108.24	1.37	1641.18

**Table 5.3: Average fold change in expression of all measured transcripts in rat liver or B-13/H cells following adenoviral infection relative to Ad-null infected B-13/H cells.**

## **5.6 Co-expression of HNF4 $\alpha$ with SGK1F or FOXA2 does not improve drug transporter expression**

Based on the net increase in drug transporter mRNA expression induced by HNF4 $\alpha$ , it was hypothesised that co-expression of HNF4 $\alpha$  with another transcription factor may have a cumulative effect on transporter expression. As C/EBP $\alpha$ , C/EBP $\beta$  and HNF1 $\alpha$  did not induce a net fold increase in the expression of transporter mRNA, the transcription factor FOXA2, and kinase SGK1F would be co-overexpressed with HNF4 $\alpha$ . Forkhead box A2 (FOXA2/ HNF3 $\beta$ ) is a transcription factor involved in liver specification during development [261]. It is considered a “pioneer” factor in that it facilitates access of LETFs to liver specific genes, which would otherwise be inaccessible due to significant DNA compaction and lack of co-activator binding [261, 262]. SGK1F is a human SGK1 isoform, similar to rat SGK1C, whose overexpression in B-13 cells is sufficient to initiate transdifferentiation [130].

B-13/H cells were therefore infected with either Ad-null, Ad-HNF4 $\alpha$ , Ad-SGK1F (encoding SGK1F) or Ad-FOXA2 (encoding FOXA2). Ad-SGK1F and Ad-FOXA2 were also separately infected in combination with Ad-HNF4 $\alpha$ . As previously, infection was at an MOI of 2.37 pfu/cell and over 5 days. B-13/H cells infected with Ad-SGK1F or Ad-FOXA2 in combination with Ad-HNF4 $\alpha$  appeared morphologically the same as those infected with Ad-HNF4 $\alpha$  alone, which appeared flatter with more cell-cell contacts (figure 5.9A). Infection with the adenoviral constructs did not affect hepatocyte phenotype as determined by mRNA and protein expression of hepatocyte markers (figure 5.9B & C). RT-PCR showed that, as expected, HNF4 $\alpha$  overexpression led to increased mRNA expression of BSEP and MRP2. Co-overexpression of HNF4 $\alpha$  with either FOXA2 or SGK1F did not appear to increase the expression of MRP2 or BSEP transcripts (figure 5.9B) in comparison with those infected with Ad-HNF4 $\alpha$  alone. Blotting for HNF4 $\alpha$  and SGK1 protein confirmed that adenoviral infection with Ad-

HNF4 $\alpha$  and Ad-SGK1F led to an up-regulation of the respective protein. No specific FOXA2 antibody could be identified and therefore expression of transduced hFOXA2 in Ad-FOXA2 infected B-13/H cells was confirmed by RT-PCR (figure 5.10).

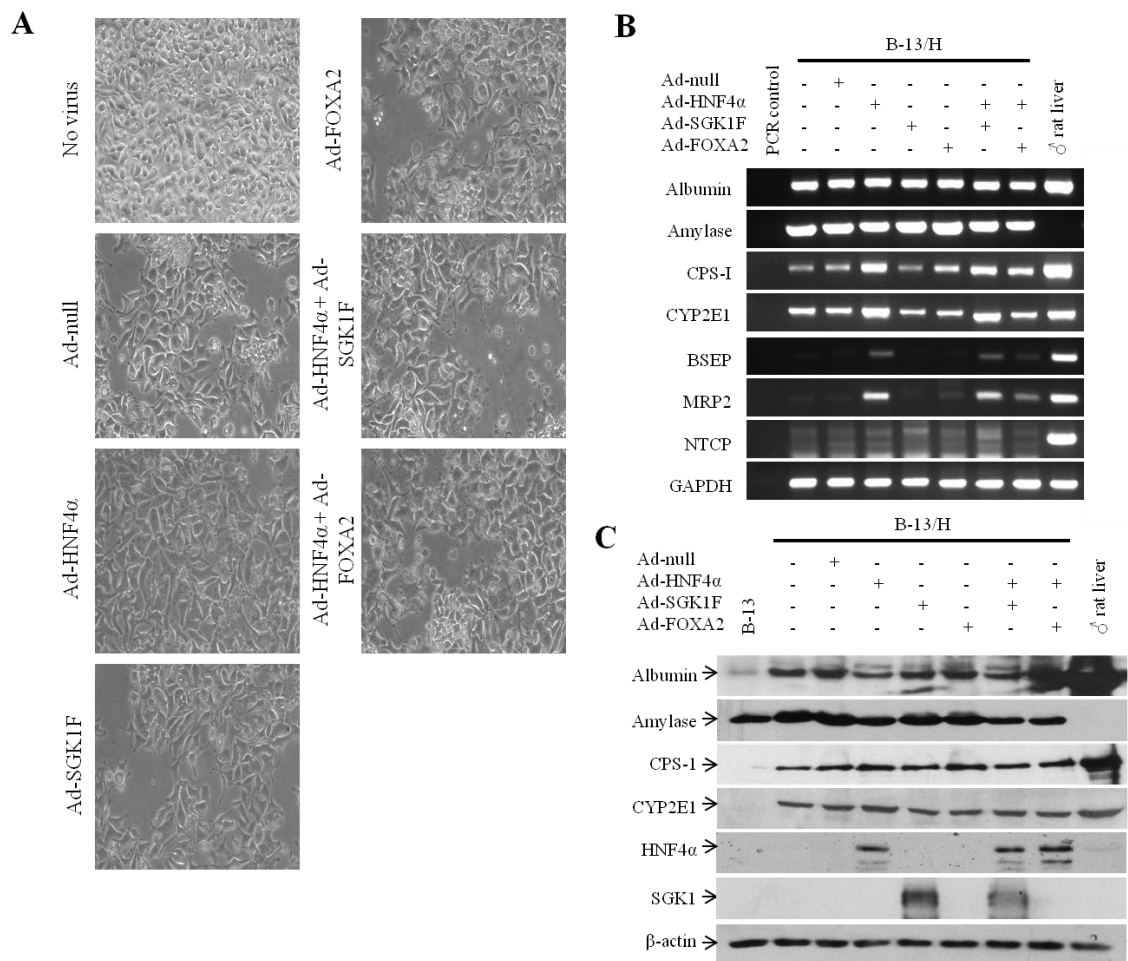


**Figure 5.9: Adenoviral overexpression of SGK1F or FOXA2 does not enhance transporter expression in B-13/H cells. A. Photomicrograph of B-13/H cells 5 days after adenoviral infection. Images are at 100x magnification. B. RT-PCR for the indicated transcripts in adenoviral infected B-13/H cells. Total RNA was extracted from samples 5 days after infection using TRIzol and cDNA produced which was used as the template for PCR. Following PCR, samples were separated by agarose gel electrophoresis and visualised by UV transillumination. C. Western blotting for liver markers in B-13 cells, adenoviral infected B-13/H cells and rat liver. Lysates from rat liver, B-13 cells and B-13/H cells treated as in A and B, were prepared and quantified by Lowry assay. 20 $\mu$ g of protein/well was separated by SDS-PAGE and transferred to a nitrocellulose membrane which was blocked and probed. Antibody binding was detected using ECL Western blot substrate. All results are typical of at least 3 separate experiments.**

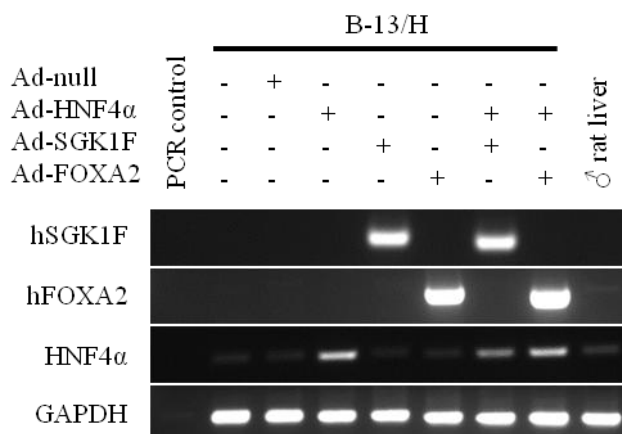


**Figure 5.10: RT-PCR for hSGK1F, hFOXA2 and HNF4 $\alpha$  in indicated cell samples.** Total RNA was extracted from samples 5 days after infection using TRIzol and cDNA produced which was used as the template for PCR. Following PCR, samples were separated by agarose gel electrophoresis and visualised by UV transillumination.

Quantitative measurement of transporter expression showed that, compared to Ad-null infected B-13/H cells, cells infected with Ad-HNF4 $\alpha$  expressed 691 and 385 fold more BSEP and MRP2 mRNA respectively. Cells infected with Ad-HNF4 $\alpha$  and Ad-SGK1F expressed 796 and 295 fold more BSEP and MRP2 mRNA respectively and those infected with Ad-HNF4 $\alpha$  and Ad-FOXA2 only 75 and 27 fold more BSEP and MRP2 mRNA respectively (figure 5.11). Indeed, B-13/H cells infected with Ad-HNF4 $\alpha$  and Ad-SGK1F had an essentially identical transporter expression profile compared to those infected with Ad-HNF4 $\alpha$  alone. In comparison, those infected with Ad-HNF4 $\alpha$  in combination with Ad-FOXA2 showed an intermediate up-regulation of transporters when compared with B-13/H cells infected with Ad-HNF4 $\alpha$  alone. The average fold change in expression of all measured transcripts supports this (table 5.4), as B-13/H cells infected with Ad-HNF4 $\alpha$  alone, or in combination with Ad-SGK1F, had essentially identical average fold changes. In contrast, B-13/H cells infected with Ad-HNF4 $\alpha$  in combination with Ad-FOXA2 had an average fold change of more than 3.5 fold less.

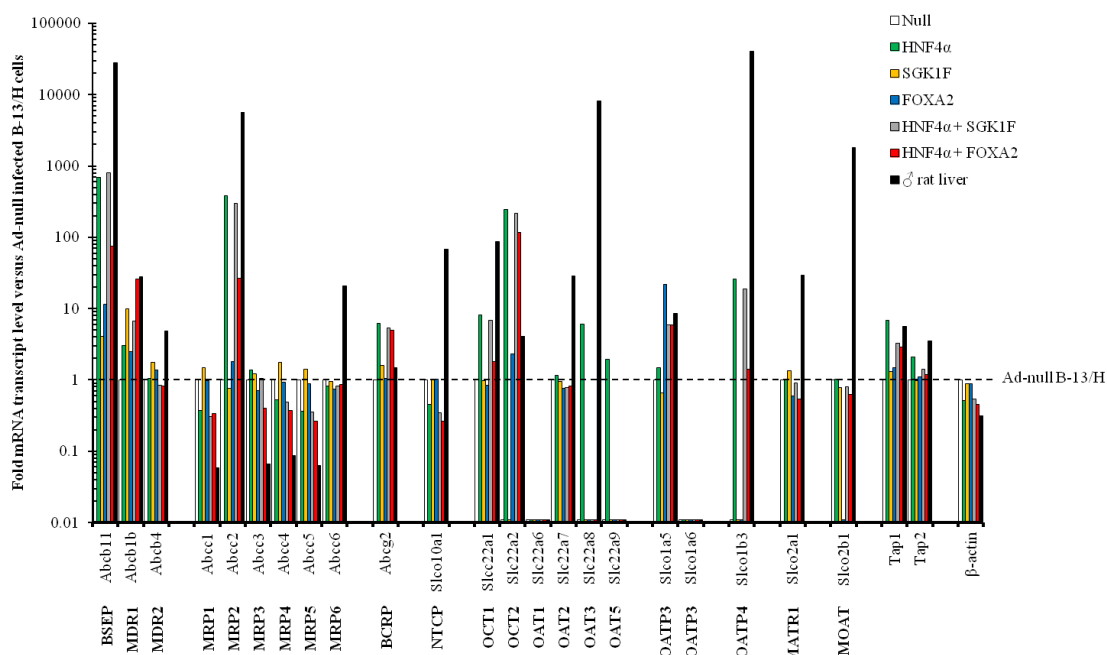


**Figure 5.11: Adenoviral overexpression of SGK1F or FOXA2 does not increase drug transporter expression.** Fold mRNA expression of indicated transcripts in adenoviral infected B-13/H cells quantified using rat drug transporter array plates. Expression is shown relative to Ad-null infected B-13/H cells. Total RNA was produced from B-13/H cells 5 days after infection using TRIzol, which was then cleaned up, reverse transcribed and the resulting cDNA used as a template for the rat drug transporter arrays. Legend corresponds to which adenovirus construct(s) B-13/H cells were infected with. Results are the fold change of single samples from the same experiment.

	Ad-null	Ad-HNF4 $\alpha$	Ad-SGK1F	Ad-FOXA2	Ad-HNF4 $\alpha$ + Ad-SGK1F	Ad-HNF4 $\alpha$ + Ad-FOXA2	♂ rat liver
<b>Mean</b>	1.00	25.42	1.58	1.65	25.33	6.79	1409.15
<b>SD</b>	0	105.19	1.37	2.98	105.85	22.39	5918.45

**Table 5.4: Average fold change in expression of all measured transcripts in B-13/H cells infected with different adenovirus constructs alone or in combination relative to Ad-null infected cells**

To determine if increased mRNA expression of transporters led to increased protein expression, Western blotting for MRP2 and NTCP was carried out (figure 5.12). MRP2 protein was detectable in Ad-HNF4 $\alpha$ , and Ad-HNF4 $\alpha$  and Ad-SGK1F infected B-13/H cells, but not in any other samples. This corresponded well to the matching increases in MRP2 mRNA expression seen in these 2 samples. As expected, no change in NTCP protein expression was seen following adenoviral infection of B-13/H cells as it was undetectable in all samples. Attempts were made to measure BSEP protein but the 2 different primary antibodies tried were found to be too non-specific for reliable measurement.

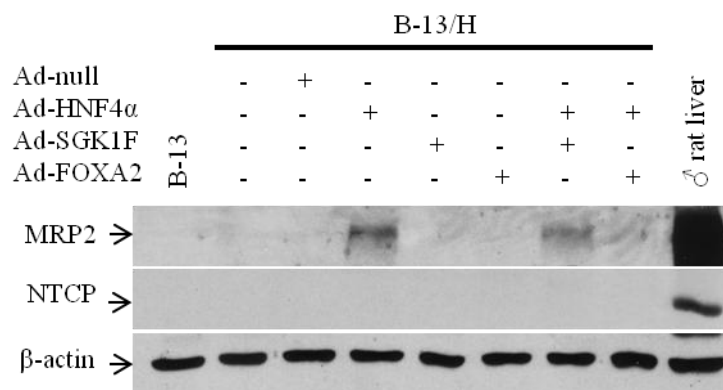


**Figure 5.12: Western blot for MRP2 and NTCP in B-13 cells, adenoviral infected B-13/H cells and rat liver.** Lysates from B-13/H cells infected for 5 days with the indicated adenovirus, B-13 cells and rat liver were prepared and quantified by Lowry assay. 20 $\mu$ g of protein/well was separated by SDS-PAGE and transferred to a nitrocellulose membrane which was blocked and probed. Antibody binding was detected using ECL Western blot substrate. MRP2 blot is typical of 4 separate experiments.

### 5.7 Ad-HNF4 $\alpha$ infected B-13/H cells show significantly increased MDR and BCRP activity.

To determine the effect of Ad-HNF4 $\alpha$  infection on B-13/H transporter activity, the activity of MDR, BCRP, MRP and BSEP was analysed using dye retention assays as outlined in the methods. The assays were carried out using the dyes H33342, CMFDA and H<sub>2</sub>FDA.

H33342 is a fluorescent dye which, like DAPI, fluoresces when bound to double stranded DNA and is effluxed from cells by MDR and BCRP. Cyclosporin A (CsA), at low concentrations (<10 $\mu$ M), inhibits MDR but not BCRP, allowing it to be used in combination with H33342 to determine MDR activity [263, 264]. Ko143 is a specific BCRP inhibitor meaning it can be used to determine the role of BCRP on H33342 efflux [265]. CMFDA is a non-fluorescent compound which, once it diffuses into cells, is conjugated to glutathione and cleaved by intracellular esterase to 5-chloromethylfluorescein, which is fluorescent and a substrate of MRP transporters [266]. The conjugation of CMFDA prevents its passive diffusion from the cell. Use of MK571, a specific MRP inhibitor [267], allows the relative activity of MRP transporters to be determined when used in conjugation with CMFDA. H<sub>2</sub>FDA is, like CMFDA, a non-fluorescent compound, which is cleaved by intracellular esterases to a fluorescent product. The fluorescent product is a substrate of BSEP [268]. No specific cell permeable BSEP inhibitors are commercially available. To measure BSEP activity

therefore, cells were treated with H<sub>2</sub>FDA in tandem with compounds which are known to inhibit BSEP, which were glibenclamide and troglitazone [269].

The results of the dye retention assays are shown in figure 5.13. Ad-null infected B-13/H cells showed significant retention of H33342 in response to CsA, indicative of MDR activity (figure 5.13A). This retention was significantly greater in Ad-HNF4 $\alpha$  infected cells. Similar findings were seen in terms of BCRP activity. Ad-null infected B-13/H cells showed significant retention of H33342 following treatment with the BCRP inhibitor Ko143 (figure 5.13B). B-13/H cells infected with Ad-HNF4 $\alpha$  however showed significantly greater retention when incubated with Ko143 compared to B-13/H cells infected with Ad-null. There was no difference in CMFDA retention in the presence or absence of the MRP inhibitor MK571, between B-13/H cells infected with Ad-null or those infected with Ad-HNF4 $\alpha$  (figure 5.13C), suggesting that there was no difference in MRP activity. However, both Ad-null and Ad-HNF4 $\alpha$  infected cells showed significantly increased fluorescence when treated with CMFDA and MK571 compared to those treated with CMFDA alone, indicating that B-13/H cells express functional MRP transporters.

Retention of H<sub>2</sub>FDA was significantly increased in B-13/H cells infected with Ad-null or Ad-HNF4 $\alpha$  in response to BSEP inhibitors glibenclamide or troglitazone (figure 5.13D). The degree of retention was equivalent between Ad-null and Ad-HNF4 $\alpha$  infected cells suggesting that HNF4 $\alpha$  overexpression had no effect on BSEP activity. Reaction of reactive oxygen species (ROS) with H<sub>2</sub>FDA causes fluorescence, meaning H<sub>2</sub>FDA is often used for measuring ROS production in cells [270]. To confirm that the increased fluorescence in troglitazone and glibenclamide treated B-13/H cells was from retention of H<sub>2</sub>FDA fluorescent metabolites and not from ROS production, B-13/H cells were treated with menadione, which causes ROS production through redox cycling [271], alongside the BSEP inhibitors. Treatment with 50 $\mu$ M menadione had no effect on fluorescence. This suggests that in these experiments, under the conditions used, that increased fluorescence following troglitazone and glibenclamide treatment was from inhibition of H<sub>2</sub>FDA metabolite efflux, not ROS production.

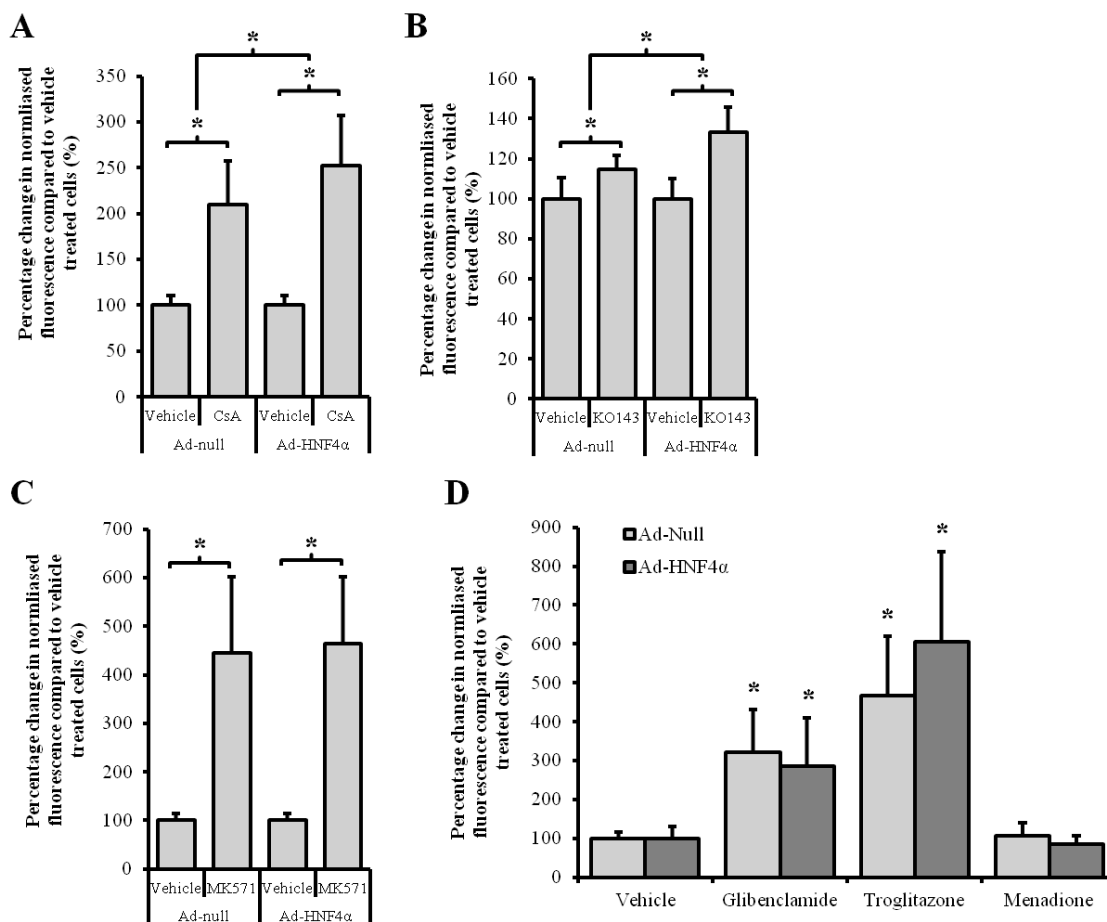


**Figure 5.13: HNF4α overexpression significantly increases MDR and BCRP, but not MRP or BSEP activity.** **A.** MDR activity in Ad-null and Ad-HNF4α infected B-13/H cells. Dye retention assay using H33342 as the dye and CsA as the inhibitor. **B.** BCRP activity in Ad-null and Ad-HNF4α infected B-13/H cells. Dye retention assay using H33342 as the dye and Ko143 as the inhibitor. **C.** MRP activity in Ad-null and Ad-HNF4α infected B-13/H cells. Dye retention assay using CMFDA as the dye and MK571 as the inhibitor. **D.** BSEP activity in Ad-null and Ad-HNF4α infected B-13/H cells. Dye retention assay using H<sub>2</sub>FDA as the dye and indicated compounds as the inhibitors. For A-D, values are expressed as the mean difference in fluorescence relative to vehicle controls (set at 100%) and SD. Retention assays were carried out on B-13/H cells infected for 5 days with either Ad-null or Ad-HNF4α. For A and C, results are the mean and SD of 15 independent determinations from 5 separate experiments. For B and D, results are the mean and SD of 9 independent determinations from 3 separate experiments. For A-C, \*significant difference between the indicated groups at p<0.05. In D, \*significant difference compared to respective vehicle control at p<0.05.

## 5.8 Chapter discussion

The interaction of drugs and their metabolites with hepatic transporters has historically been the cause of drug attrition during the late stages of clinical testing or after release, such as in the case of troglitazone [241], with significant financial consequences. These interactions are difficult to determine *in-vitro* due to the substrate promiscuity of transporters and the complex interactions between hepatic drug uptake/export and drug modifying enzymes [81]. Due to the difficulties of maintaining hepatocyte DME expression, including transporters, in culture, the potential of B-13/H cells as a model for assessment of hepatic transporter-drug interactions was investigated.

Measurement of drug transporter expression in B-13 and B-13/H cells showed that, although the expression of several transporters such as MDRs and some MRPs was similar or greater in B-13/H cells at the level of mRNA compared to rat liver, the mRNA expression of many others including BSEP and MRP2 was more than 10,000 fold lower. Consequently, it was hypothesised that modification of culture conditions would cause an up-regulation of transporter expression. However, culture of B-13/H cells on different substrata (alvetex or PU134) had no marked effect on transporter mRNA expression.

Hepatocyte transporter expression is regulated by a number of LETFs. Adenoviral based overexpression of B-13/H cells with selected LETFs showed that hepatocyte phenotype was broadly unchanged by LETF overexpression in terms of albumin, CPS-1 and CYP2E1 expression. However, B-13/H cells infected with Ad-HNF4 $\alpha$  showed an up-regulation in the mRNA expression of several transporters including BSEP and MRP2, not seen when any of the other LETFs were overexpressed. No evidence suggests that HNF4 $\alpha$  directly regulates the expression of BSEP and MRP2 and knockout of HNF4 $\alpha$  has no effect on BSEP or MRP2 expression [272]. However, the PXR and CAR do regulate transcription of a number of transporters including BSEP and MRP2, and HNF4 $\alpha$  has been documented to potentiate PXR and CAR mediated-transactivation [61, 273-275]. This may explain the documented up-regulation of PXR and CAR regulated transporters including BSEP and MRP2 in Ad-HNF4 $\alpha$  infected B-13/H cells. In terms of other up-regulated transporters, HNF4 $\alpha$  knockout represses expression of several transporters including BCRP and OCT1 [272], which were up-

regulated in Ad-HNF4 $\alpha$  infected B-13/H cells. This suggests that HNF4 $\alpha$  positively regulates the expression of a number of transporters including BCRP and OCT1 and explains the documented up-regulation in Ad-HNF4 $\alpha$  infected B-13/H cells.

Co-overexpression of HNF4 $\alpha$  with either SGK1F or FOXA2 did not enhance transporter mRNA expression. In fact, FOXA2 co-overexpression with HNF4 $\alpha$  attenuated the induction in transporter expression seen when HNF4 $\alpha$  was overexpressed alone. Although it has homeostatic regulatory roles in the adult liver, arguably the most important biological role of FOXA2 is in the hepatic specification of foregut endoderm during development, as targeted deletion of FOXA2 and FOXA1 in murine embryonic endoderm tissue is embryonic lethal due to the failure of liver development [261, 276]. This response is not seen in mice with deletion of FOXA1 or FOXA2 alone, presumably due to functional redundancy owing to the overlapping sequence affinity between FOXA family members. The overexpression of FOXA2, in Ad-FOXA2 infected B-13/H cells, may therefore promote a more plastic phenotype and an associated reduction in the expression of specific adult hepatocyte associated markers such as transporters. Alternatively, as the expression of adult hepatocyte markers albumin, CPS-1 and CYP2E1 were unaffected by FOXA2 overexpression in B-13/H cells, the antagonistic effect of FOXA2 on HNF4 $\alpha$  overexpression may be due to direct interaction inhibiting HNF4 $\alpha$  mediated transactivation. This is plausible considering that immunoprecipitation studies confirm that FOXA2 does interact with HNF4 $\alpha$  [277].

Dye retention assays to determine MDR, BCRP, MRP and BSEP activity in Ad-null and Ad-HNF4 $\alpha$  infected B-13/H cells showed that only MDR and BCRP activity were significantly increased by HNF4 $\alpha$  overexpression. The increase in BCRP activity was consistent with the BCRP qPCR results, which showed that Ad-HNF4 $\alpha$  infection was associated with an increase in BCRP mRNA expression. MDR mRNA expression was conversely not consistently increased so the difference documented may be due to inhibition of transporters, which also efflux H33342, other than MDR by CsA. The lack of difference in MRP activity between Ad-null and Ad-HNF4 $\alpha$  infected B-13/H cells may be because B-13/H cells overexpressing HNF4 $\alpha$  showed an up-regulation of MRP2 mRNA and protein, but reduced mRNA expression of MRP1 and MRP4-5. Considering that other MRP proteins may transport CMFDA, reduced transport by MRP1 and MRP4-5 may mask increased MRP2 activity. An MRP2 specific inhibitor would allow

for the activity of MRP2 alone to be determined, however no specific inhibitor is currently commercially available.

The H<sub>2</sub>FDA retention assays suggested that there was no difference in BSEP activity between Ad-null and Ad-HNF4 $\alpha$  infected B-13/H cells. The cause for the lack of effect may be that, although BSEP mRNA expression was strongly induced in Ad-HNF4 $\alpha$  infected B-13/H cells relative to Ad-null infected B-13/H cells, its relative expression was still more than 10-100 fold less than that expressed in the liver. The induction therefore may not have been sufficient to see a difference. Alternatively, no difference between Ad-null or Ad-HNF4 $\alpha$  infected cells may have been observed because HNF4 $\alpha$  induced BSEP mRNA was not translated and/or *de-novo* BSEP protein was not targeted to the plasma membrane. BSEP, like many other membrane localised proteins, cycles between the plasma membrane and endosomes in the cell [278]. Tauroursodeoxycholic has been shown to enhance targeting of BSEP to the plasma membrane and could, in combination with HNF4 $\alpha$  overexpression, improve BSEP activity and therefore H<sub>2</sub>FDA retention [279].

The data in this chapter demonstrates that B-13/H cells express a number of drug transporters but only a selection are expressed at mRNA levels equivalent to that seen in intact liver. Several physiologically important transporters were barely expressed, including bile acid transporters NTCP and BSEP. Of all approaches undertaken, only adenoviral mediated overexpression of HNF4 $\alpha$  resulted in a major change in transporter expression. However, although the activity of BCRP and MDR proteins was significantly increased following adenoviral infection, the activity of MRP proteins and BSEP under the conditions tested was not affected. The data overall suggests that, although B-13/H cells do not express a liver equivalent pattern of transporters as originally hypothesised, they could still be used as a model for particular transporters including BCRP, MDR, BSEP and MRP, with a phenotype improved by HNF4 $\alpha$  overexpression. Study of MRP2 specific function requires the identification of an MRP2 specific inhibitor and improved study of BSEP function may require further investigation to improve BSEP transcription and/or targeting to the plasma membrane.

**Chapter 6. Chronic administration of MP causes reversible and modulatable periportal fibrosis comparable to BDL**

## 6.1 Introduction

Chronic liver damage results in hepatic fibrosis that restricts liver regeneration and facilitates the development of cirrhosis, hepatocellular carcinoma and ultimately liver failure [16]. Hepatic fibrosis cannot be pharmacologically treated and it is largely responsible for the significant morbidity and mortality caused by liver disease worldwide [138]. There is therefore an ongoing utilisation of animal models of liver fibrosis to aid in the development of novel anti-fibrogenic drugs. Due to the differences in fibrogenesis in different regions of the liver lobule, as discussed in the introduction, prior to toxicity screening and initiation of clinical trials, the efficacy of novel anti-fibrogenic drugs should be determined in a periportal and centrilobular model of fibrosis [5, 16].

BDL is a surgical procedure involving the double ligation of the common bile duct as outlined in the introduction. It is the most frequently used model of periportal fibrosis and gives rise to cholestatic liver injury, causing robust activation of portal tract fibroblasts, hepatic stellate cells and a ductular reaction, all leading to development of portal-portal bridging fibrosis [161, 280, 281]. The procedure however has associated animal welfare issues. The ligation operation requires a degree of expertise and the surgery, together with the severity of the procedure, frequently results in a significant level of mortality [280, 282]. This restricts the long term use of BDL animals (generally no longer than 4 weeks [283]). The procedure can be reversed; however this requires further surgery and due to the associated risks and costs, including to animal welfare, is unlikely to occur. Under the Animals (Scientific Procedures) Act 1986 it is therefore classified as a “substantial” procedure due to its severity.

The H1 receptor antagonist methapyrilene (MP) [N,N-dimethyl-N'-Pyridyl-N'(2-thienylmethyl)-1,2-ethanediamine] was used clinically as a sedative and antihistamine in the late 1970s. It was withdrawn from use when rats chronically administered MP showed development of hepatocellular carcinomas [284]. Subsequent work has demonstrated that its carcinogenic effect appears not to be due to genotoxicity. Rather, studies have shown that MP is a periportal hepatotoxin in rats and its administration leads to hepatic damage [196, 285-292]. Specifically, MP is bioactivated in the liver by CYP450 activity leading to the production of a reactive intermediate (potentially a

thioether of MP S-oxide, figure 6.1) [196, 293]. The intermediate(s) are thought to disrupt mitochondria through opening of mitochondrial pores leading to mitochondrial depolarisation and  $\text{Ca}^{2+}$  loss. This causes hepatocyte apoptosis and necrosis and consequently hepatic inflammation [196, 291, 294].

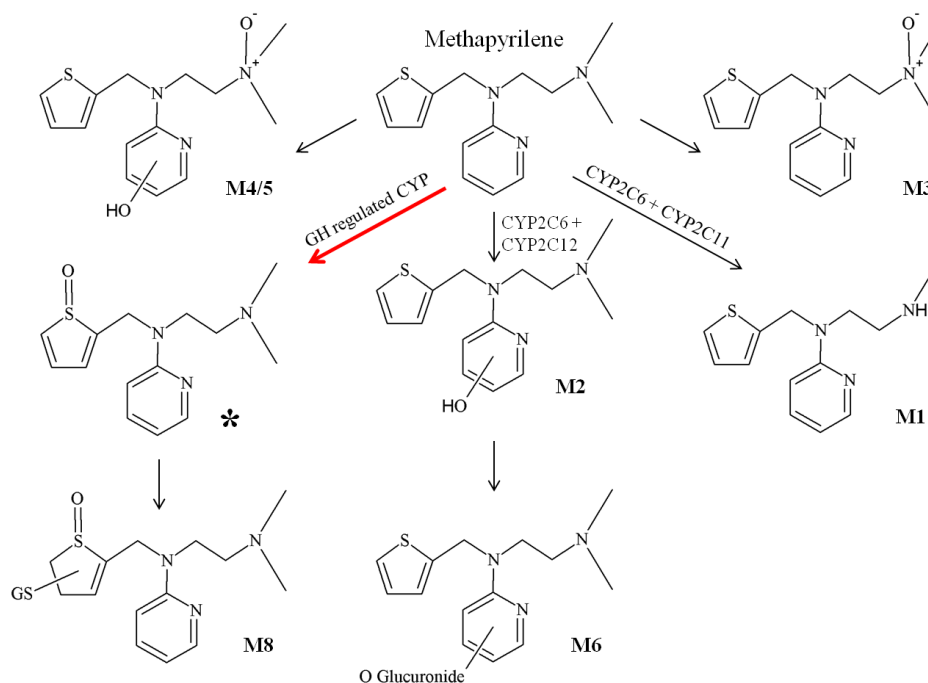


**Figure 6.1: Main MP metabolites produced *in-vitro* by male primary rat hepatocytes.** The indicated CYP450s have been shown to catalyse the designated reactions in enzymatic incubations *in-vitro*. Starred is the S-oxide thioether implicated in MP cytotoxicity. The glutathione adduct of MP is M8. Adapted from Graham *et al.*, (2008) [293]

Based on the observation that MP causes periportal hepatic damage, it was hypothesised that the chronic dosing of MP to rats would provide a more controllable reversible periportal fibrosis. The fibrosis generated in rats by MP treatment and BDL was therefore compared. Fibrosis in male Sprague-Dawley rats was generated by the chronic administration of MP, as outlined in table 6.1, at a dose of 150mg/kg 3 times per week for 3 or 6 weeks. In order to investigate the reversal of fibrosis, one group of rats was dosed with MP for 3 weeks followed by vehicle for 3 weeks. The dose of MP used was chosen based on pilot work [3].

<b>Group</b>	<b>Treatment</b>
<b>T0 (Control)</b>	Culled at initiation of study
<b>3 week MP (3wk MP)</b>	Dosed with 150mg/kg MP 3 times per week for 3 weeks
<b>6 week MP (6wk MP)</b>	Dosed with 150mg/kg MP 3 times per week for 6 weeks
<b>3 week MP/ 3 week vehicle (3wk MP/ 3wk veh.)</b>	Dosed with 150mg/kg MP 3 times per week for 3 weeks then with vehicle (PBS) 3 times per week for 3 weeks
MP was made up 1 x PBS (150mg MP/1ml) and dosed by oral gavage (1ml/kg)	

**Table 6.1: MP dosing regime**

## **6.2 Chronic administration of MP significantly inhibits weight gain**

All rats chronically dosed with MP gained weight over the course of the study. At 3 weeks, rats that began to receive vehicle began gaining weight at an accelerated rate compared to rats that continued to receive MP (figure 6.2). At termination (day 42), vehicle treated rats were significantly heavier than their MP treated counterparts indicating that MP inhibited weight gain. All MP treated rats also showed a significantly higher liver to body weight ratio than controls, indicating that MP significantly increased liver weight in treated animals. Importantly, the chronic dosing of MP caused no mortalities and treated rats did not appear to be in any distress.

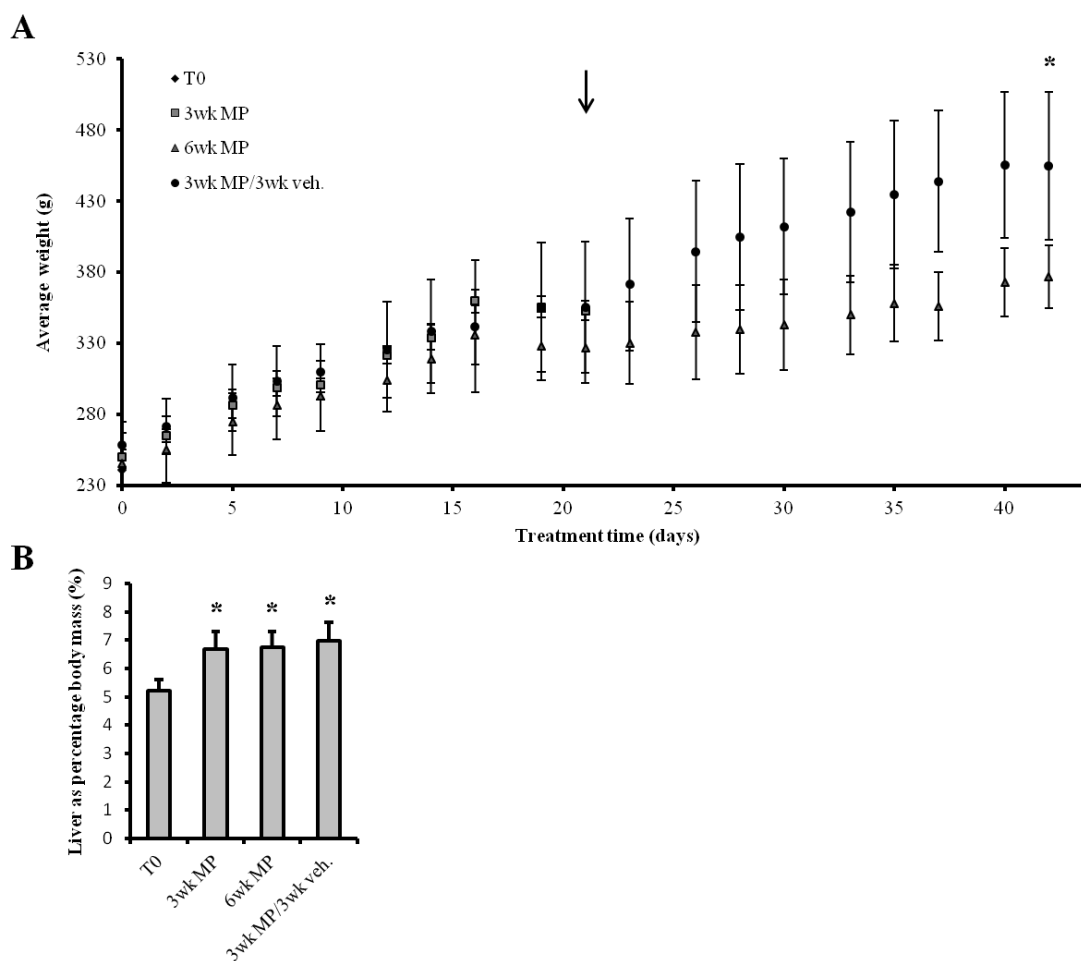


**Figure 6.2: MP treatment inhibits weight gain and increases relative liver size. A. Effect of MP treatment on body weight.** Arrow indicates half way point of study. **B. Liver weight as percentage body mass at harvest.** For A, \*indicates significant difference in weight between the indicated groups and for B, \*indicates significant difference compared to T0 control both at  $p < 0.05$ . For A and B, data are the mean and SD of the following animal numbers- for control,  $n=3$ ; for 3wk MP and 3wk MP/3 wk vehicle,  $n=5$  and for 6 wk MP,  $n=6$ .

### 6.3 Administration of MP causes significant and reversible portal tract inflammation

Liver sections from MP treated and control animals were stained with H&E and compared to liver sections from rats culled 14 days after BDL surgery (BDL liver tissue donated by Jelena Mann). Control animals showed occasional infiltrating leukocytes in the periportal region whereas both MP and BDL treated rats showed a marked significant increase in the number of periportal inflammatory cells (figure 6.3). The inflammation seen after 3 weeks of MP treatment was equivalent and not significantly different to that seen after 6 weeks of MP treatment or BDL. In the livers of animals that received MP for 3 weeks followed by vehicle for 3 weeks, portal tract inflammation

was no longer significant indicating that ceasing MP dosing led to a reversal of hepatic inflammation.

MP becomes toxic through its bioactivation by CYP450s [196]. Although the liver is the major organ of xenobiotic clearance, the kidney also has some xenobiotic metabolising activity, due to expression of some CYP450s [295]. Kidney sections were therefore also H&E stained to determine if MP induced toxicity was localised to the liver (figure 6.3). The staining and subsequent analysis of kidney sections showed that 6 weeks of MP treatment caused no discernible changes to kidney pathology, indicating that MP toxicity was likely restricted to the liver.

To further establish the specificity of MP to the liver, the lungs and spleen were also stained with H&E (figure 6.4) and this indicated that they too were unaffected, at least at the microscopic level, by chronic MP treatment.

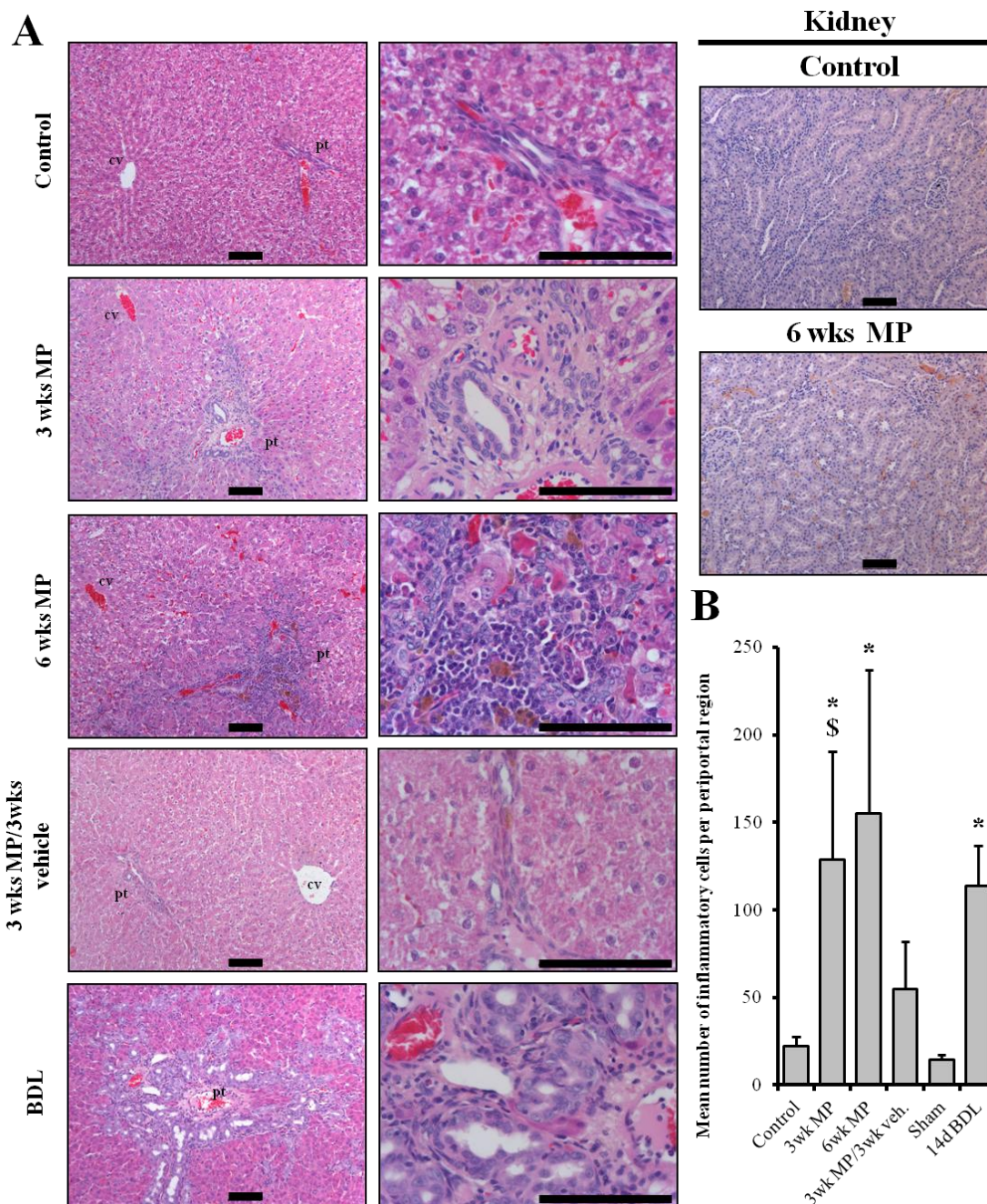


**Figure 6.3: MP treatment and 14 day BDL cause periportal inflammation. A. H&E stained sections of rat liver and kidney tissue after the indicated treatment.** Liver and kidney fixed in 10% formalin and paraffin embedded was cut into 5 $\mu$ m sections. Sections were dewaxed and rehydrated and stained with H&E prior to dehydration, mounting and analysis using a Leica upright microscope. Images are representative of groups and scale bar indicates 100 $\mu$ m. Note, control is from the T0 control group, which had an identical histopathological appearance to sections from sham BDL operated rats, hence only one view is shown and referred to as control. Abbreviations: pt, portal tract; cv, central vein. **B. Quantified mean number of periportal inflammatory cells.** The mean number of inflammatory cells in and around 5 random portal tracts was determined by an examiner blinded to the treatment groups, per section per animal. Data are the mean and SD of the following animal numbers - for control, n=3; for 3wk MP, 3wk MP/3 wk vehicle and sham, n=5; for 6wk MP, n=6; and for BDL, n=8. \*significant difference compared to the respective control group, \$ significant difference compared to the 3 week MP/3 week vehicle group both at p<0.05.

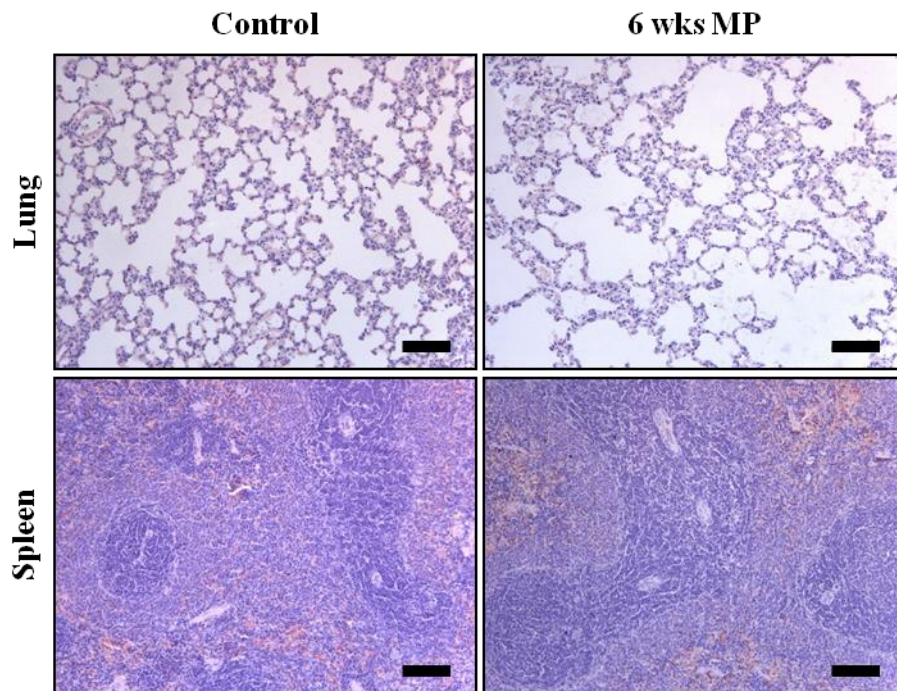


**Figure 6.4: MP causes liver specific injury.** H&E stained lung and spleen from control or 6 week MP treated rats. Lung and spleen fixed in 10% formalin and paraffin embedded were cut into 5 $\mu$ m sections. Sections were dewaxed and rehydrated and stained with H&E prior to dehydration, mounting and analysis using a Leica upright microscope. Scale bar indicates 100 $\mu$ m.

#### 6.4 MP treatment causes activation of hepatic regeneration pathways

The liver has significant regenerative capacity after injury and is able to fully regenerate mass and function when as much as 70% is irreversibly lost [16, 296]. The sources of parenchymal cells during regeneration are hepatic bipotent progenitor cells and undamaged hepatocytes that are induced to divide to replace damaged cells.

To determine the effect of the different MP dosing regimens on hepatic regeneration, proliferating cell nuclear antigen (PCNA) was immunostained in the liver sections. PCNA forms part of the DNA replication machinery required for DNA replication in S-phase. It can therefore be used as a marker of cellular proliferation [297]. The staining and subsequent quantification (figure 6.5) showed that the administration of MP for 3 weeks caused a significant increase in cholangiocyte PCNA expression. Conversely, rats that received MP for 6 weeks showed a significant increase in both periportal hepatocyte and cholangiocyte PCNA expression as seen in rats that had undergone BDL. The induction of cholangiocyte and hepatocyte division suggests that in MP treated and BDL rats, the liver was sufficiently damaged to induce cholangiocytes and

hepatocytes to divide to replace damaged cells. The animals that received MP for 3 weeks followed by vehicle for 3 weeks showed neither significant periportal hepatocyte nor cholangiocyte PCNA expression, suggesting that liver regeneration was complete.

### **6.5 MP administration causes expansion of hepatic pro-fibrogenic cell populations**

Hepatic fibrogenesis is dependent upon the deposition of ECM by (myo)fibroblasts, several different populations of which are involved in fibrogenesis with varying contributions [16]. Portal tract fibroblasts, although their contribution to fibrogenesis is currently controversial, proliferate and activate in response to periportal injury and are an identifying characteristic of periportal fibrosis [6, 161].

To determine the effect of MP on hepatic portal tract fibroblast populations, liver sections were examined for vimentin expression, which is expressed by portal tract fibroblasts [298]. The expression of vimentin, as illustrated in figure 6.6, appeared to be evenly spread throughout the lobule in control animals. In those animals treated with MP or subject to BDL however, vimentin staining of periportal regions was significantly increased. This implies that MP treatment, like BDL, caused an expansion of portal tract fibroblasts as has been documented during periportal fibrogenesis [161]. Rats that received MP for 6 weeks showed significantly more periportal vimentin staining than rats that received MP for only 3 weeks and rats that were treated with MP for 3 weeks followed by vehicle for 3 weeks did not show significant periportal vimentin staining.

Myofibroblasts express  $\alpha$ -SMA and are responsible for the majority of ECM deposition during fibrogenesis [5, 147].  $\alpha$ -SMA is therefore a commonly used biomarker of hepatic fibrosis. In control rat liver sections, only smooth muscle cells surrounding portal arterioles stained positive for  $\alpha$ -SMA (figure 6.7). In MP treated and BDL rat liver sections, a significant increase in periportal  $\alpha$ -SMA staining was observed. Liver sections of rats treated with MP for 6 weeks showed significantly more periportal  $\alpha$ -SMA staining than rats treated for only 3 weeks. Similar to periportal vimentin staining, the significant increase in periportal  $\alpha$ -SMA staining seen in rats after 3 weeks of MP treatment was reversible after 3 weeks of vehicle treatment.

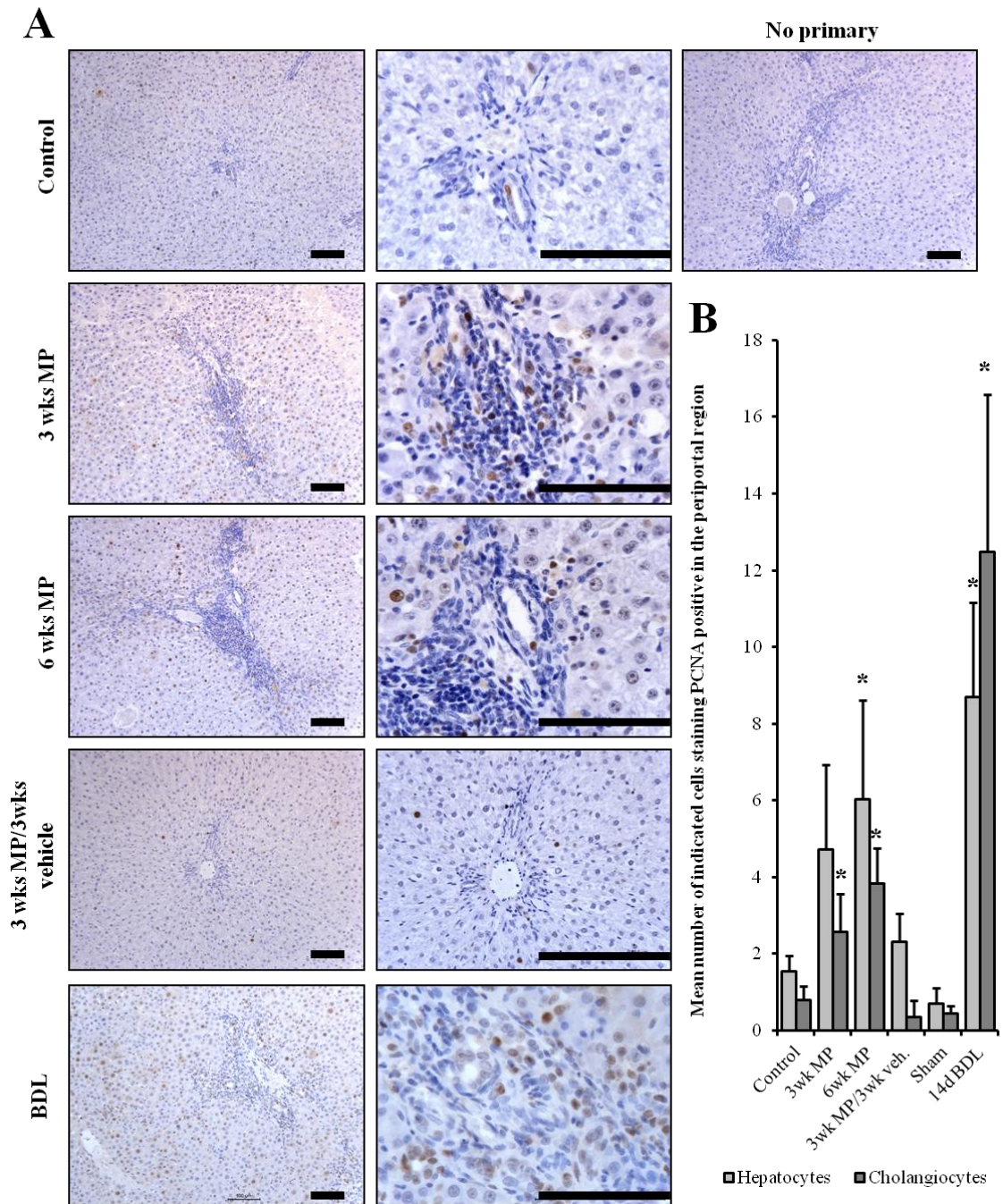


**Figure 6.5: 6 weeks chronic MP treatment and 14 day BDL cause hepatocyte and cholangiocyte proliferation. A. Rat liver sections immunostained for PCNA after the indicated treatment.** Liver fixed in 10% formalin and paraffin embedded was cut into 5 $\mu$ m sections. Sections were dewaxed, rehydrated and endogenous peroxidases blocked. Sections were then subject to trypsin-based antigen retrieval and serum blocking then immunostained for PCNA using DAB to detect bound antibody. Sections were then stained with haematoxylin prior to dehydration, mounting and analysis using a Leica upright microscope. Images are representative of groups and scale bar indicates 100 $\mu$ m. Note, control is from the T0 control group, which had an identical histopathological appearance to sections from sham BDL operated rats, hence only one view is shown and referred to as control. **B. Quantification of periportal PCNA positive hepatocytes and cholangiocytes.** The mean number of PCNA positive hepatocytes and cholangiocytes in and around 5 random portal tracts was determined by an examiner blinded to the treatment groups, per section per animal. Data are mean and SD of the following animal numbers - for control, n=3; for sham, n=4; for 3wk MP, 3wk MP/3 wk vehicle, n=5; for 6wk MP, n=6; and for BDL, n=8. \*significant difference compared to the respective control group at p<0.05.

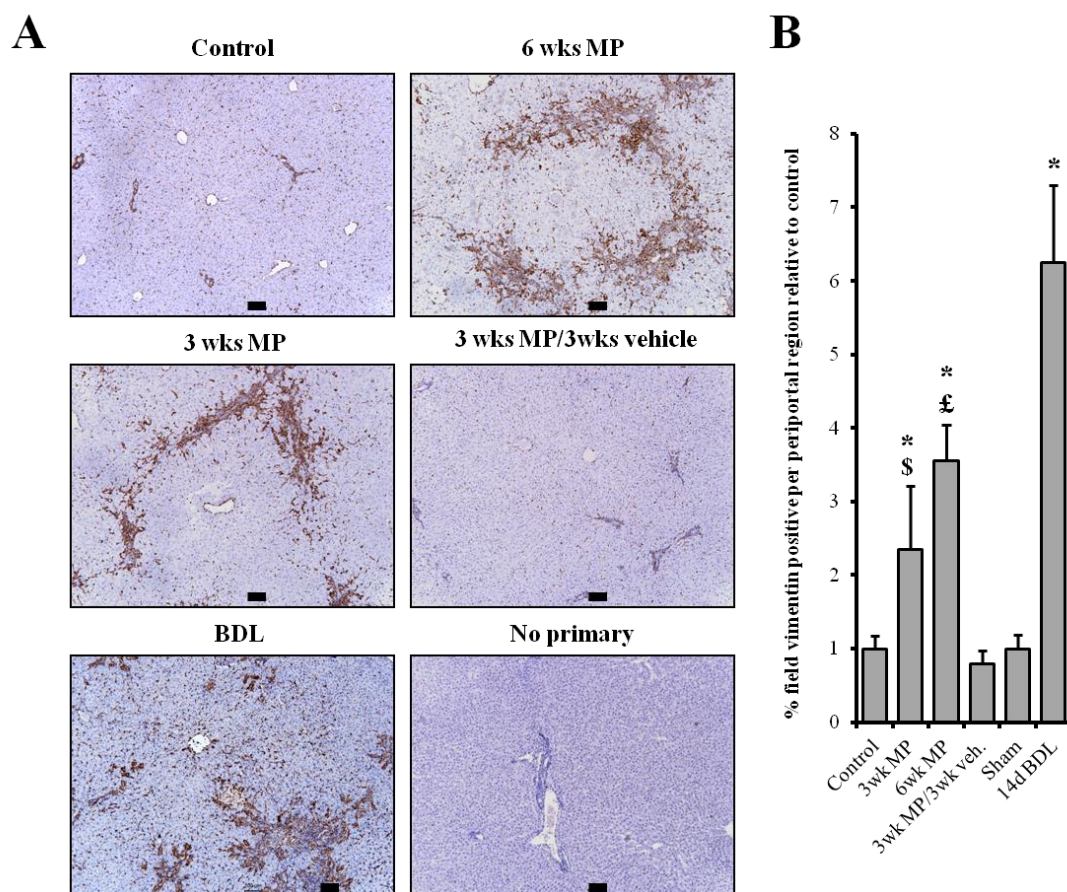


**Figure 6.6. Chronic MP treatment and 14 day BDL cause a significant increase in periportal vimentin staining. A. Rat liver sections immunostained for vimentin after the indicated treatment.** Liver fixed in 10% formalin and paraffin embedded was cut into 5µm sections. Sections were dewaxed, rehydrated and endogenous peroxidases blocked. Sections were then subject to sodium citrate antigen retrieval and serum blocking then immunostained for vimentin using DAB to detect bound antibody. Sections were then stained with haematoxylin prior to dehydration, mounting and analysis using a Leica upright microscope. Images are representative of groups and scale bar indicates 100µm. Note, control is from the T0 control group, which had an identical histopathological appearance to sections from sham BDL operated rats, hence only one view is shown and referred to as control. **B. Quantified vimentin labelling of periportal regions.** Vimentin staining was quantified using Qwin software: the percentage of periportal regions staining positive for vimentin was calculated around 10 random portal tracts per section per animal by an examiner blinded to the treatment groups. Values are expressed relative to respective controls. Data are the mean and SD of the following animal numbers - for control, n=3; for 3wk MP, 3wk MP/3 wk vehicle and sham, n=5; for 6wk MP, n=6; and for BDL n=8. \*significant difference compared to the respective control group, \$significant difference compared to the 3 week MP/3 week vehicle group and £significant difference compared to the 3 week MP group all at p<0.05.

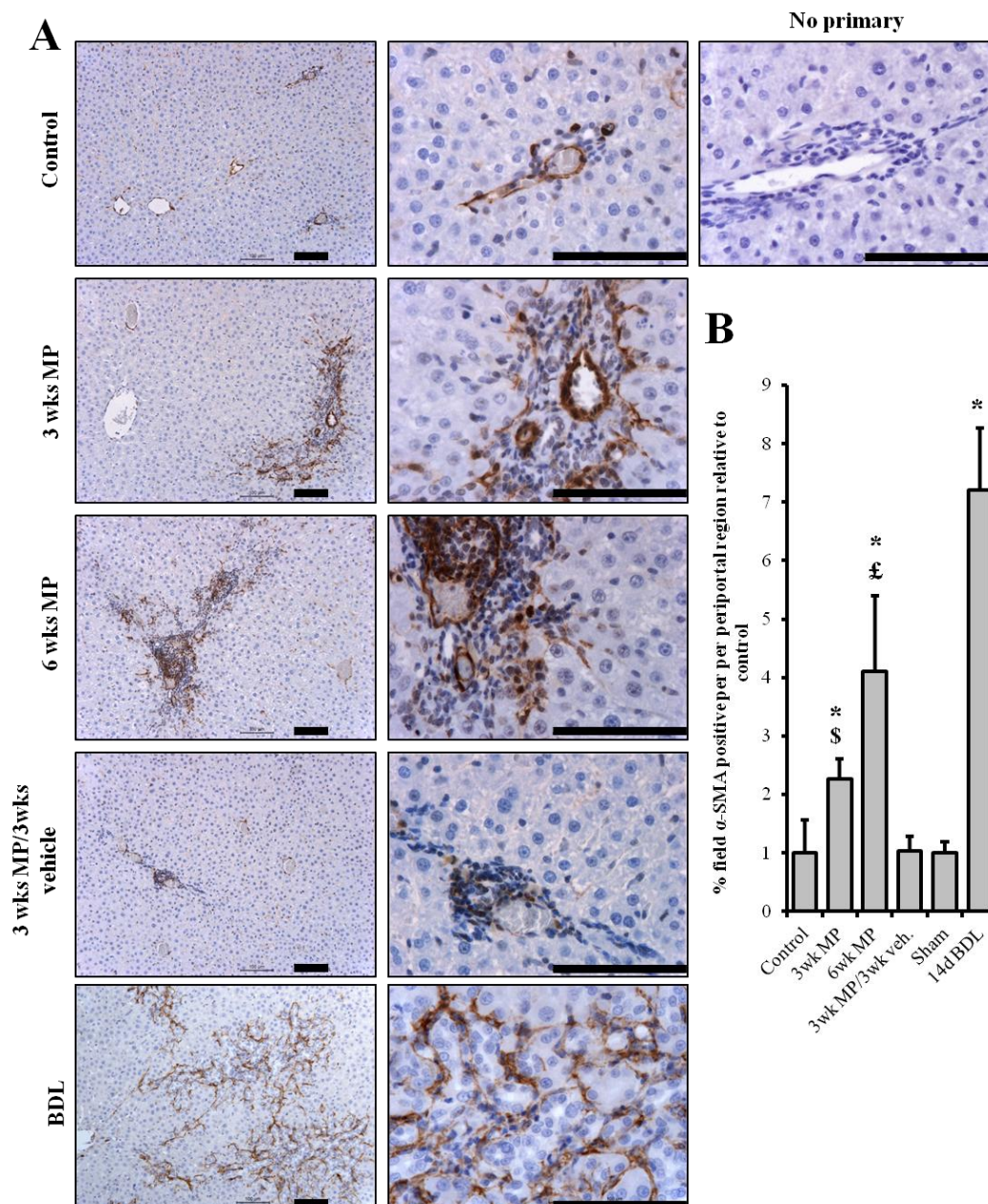


**Figure 6.7. Chronic MP treatment and 14 day BDL cause a significant increase in periportal  $\alpha$ -SMA staining.** **A.** Rat liver sections immunostained for  $\alpha$ -SMA after the indicated treatment. Liver fixed in 10% formalin and paraffin embedded was cut into 5 $\mu$ m sections. Sections were dewaxed, rehydrated and endogenous peroxidases blocked. Sections were then subject to sodium citrate antigen retrieval and serum blocking then immunostained for  $\alpha$ -SMA using DAB to used to detect bound antibody. Sections were then stained with haematoxylin prior to dehydration, mounting and analysis using a Leica upright microscope. Images are representative of groups and scale bar indicates 100 $\mu$ m. Note, control is from the T0 control group, which had an identical histopathological appearance to sections from sham BDL operated rats, hence only one view is shown and referred to as control. **B.** **Quantified  $\alpha$ -SMA labelling of periportal regions.**  $\alpha$ -SMA staining was quantified using Qwin software: the percentage of periportal regions staining positive for  $\alpha$ -SMA was calculated around 10 random portal tracts per section per animal by an examiner blinded to the treatment groups. Values are expressed relative to respective controls. Data are the mean and SD of the following animal numbers - for control, n=3; for 3wk MP, 3wk MP/3 wk vehicle and sham, n=5; for 6wk MP, n=6; and for BDL, n=8. \*significant difference compared to the respective control group, §significant difference compared to the 3 week MP/3 week vehicle group and £significant difference compared to the 3 week MP group all at p<0.05.

### **6.6 MP administration causes significant and reversible periportal fibrosis**

To determine the severity of fibrosis in rats chronically dosed with MP, sirius red staining (which stains for collagen) was carried out on liver sections. This showed that both MP treatment and BDL induced significant periportal fibrosis compared to controls (figure 6.8). Prolonged treatment with MP (6 weeks) led to a significant increase in periportal fibrosis compared to that seen after 3 weeks of MP treatment or 14 day BDL. The increase in periportal fibrosis after 3 weeks of MP treatment was reversible because the rats treated with MP for 3 weeks followed by vehicle for 3 weeks no longer showed significant periportal collagen deposition. Central veins appeared similar in MP treated and control animals indicating that MP primarily caused periportal damage and fibrosis.

Assessment of whole liver fibrosis showed that administration of MP, like BDL, caused a significant increase in whole lobule collagen deposition (figure 6.9A). Administration of MP for 6 weeks did increase collagen deposition compared to only 3 weeks but the difference was not significant. Similar to when collagen deposition was measured around periportal regions, 3 weeks of MP treatment followed by 3 weeks of vehicle treatment did not lead to a significant increase in whole liver collagen deposition. As shown in figure 6.9B, assessment of hepatic hydroxyproline content, which is a quantitative measure of fibrosis severity [183], gave similar results to the whole liver sirius red measurement. Specifically, 3 and 6 weeks of MP administration caused a significant increase in liver hydroxyproline content whereas the group that received MP for 3 weeks followed by vehicle for 3 weeks did not show a significant difference in hepatic hydroxyproline content. Unfortunately the effect of 14 day BDL on liver hydroxyproline content could not be measured for comparison due to a shortage of liver tissue.

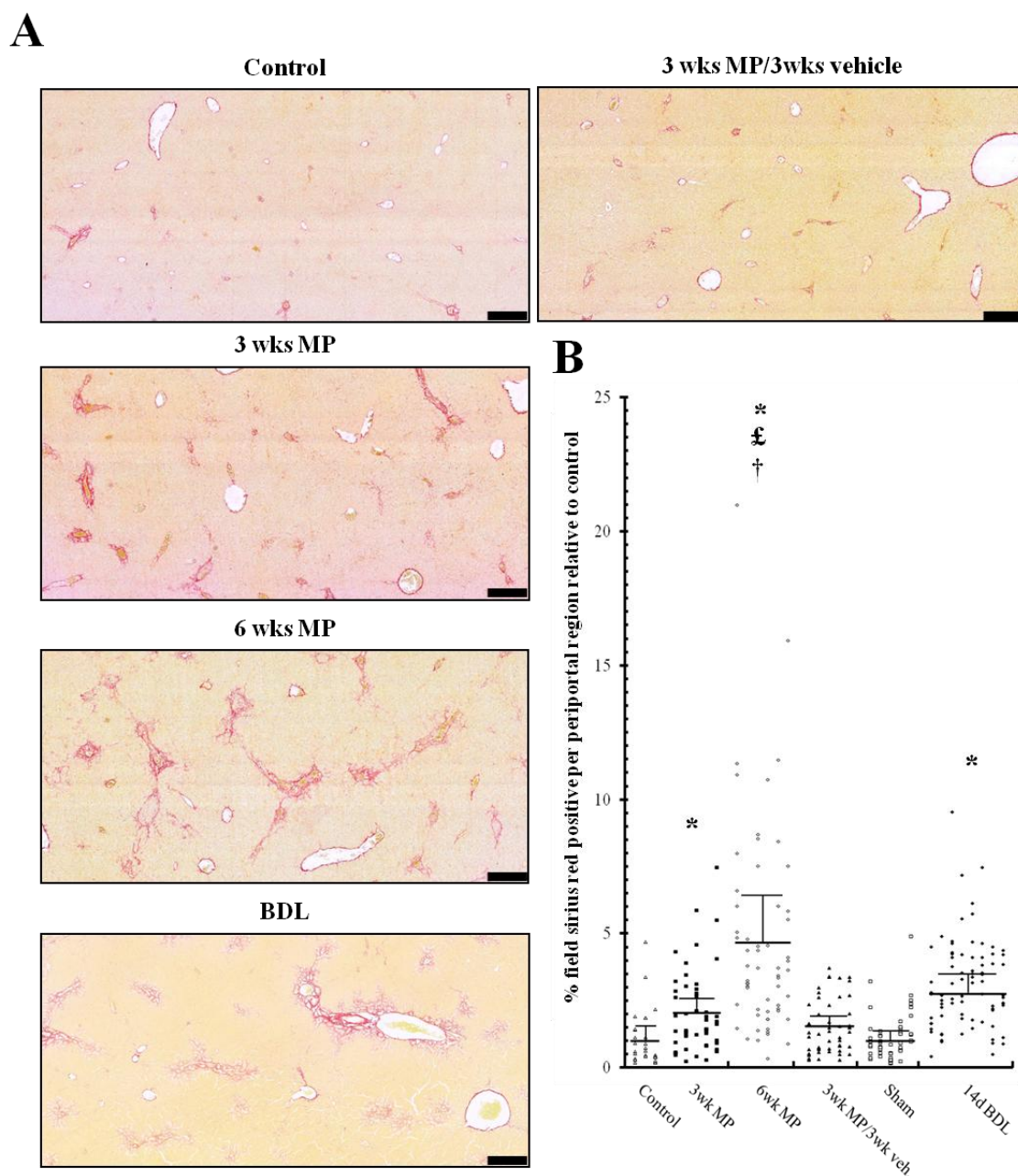


**Figure 6.8. Chronic MP treatment and 14 day BDL cause significant periportal fibrosis. A. Rat liver sections stained with sirius red after the indicated treatment.** Liver fixed in 10% formalin and paraffin embedded was cut into 5 $\mu$ m sections. Sections were dewaxed and rehydrated and stained with picosirius red prior to dehydration, mounting and analysis using a Leica upright microscope. Images are representative of groups and scale bar indicates 400 $\mu$ m. Note, control is from the T0 control group, which had an identical histopathological appearance to sections from sham BDL operated rats, hence only one view is shown and referred to as control. **B. Quantified sirius red staining of periportal fibrosis.** Sirius red staining was quantified using Qwin software: the percentage of periportal regions staining positive for sirius red was calculated around 10 random portal tracts per section per animal by an examiner blinded to the treatment groups. All individual readings are shown, lower lines are the means and the upper lines are the SD. Values are expressed relative to respective controls. \*significant difference compared to the respective control group, †significant difference compared to the 3 week MP group (all  $p < 0.05$ ) and ‡significant difference compared to the 14d BDL group. Animal numbers - for control,  $n=3$ ; for 3wk MP, 3wk MP/3 wk vehicle and sham,  $n=5$ ; for 6wk MP,  $n=6$ ; and for BDL,  $n=8$ .

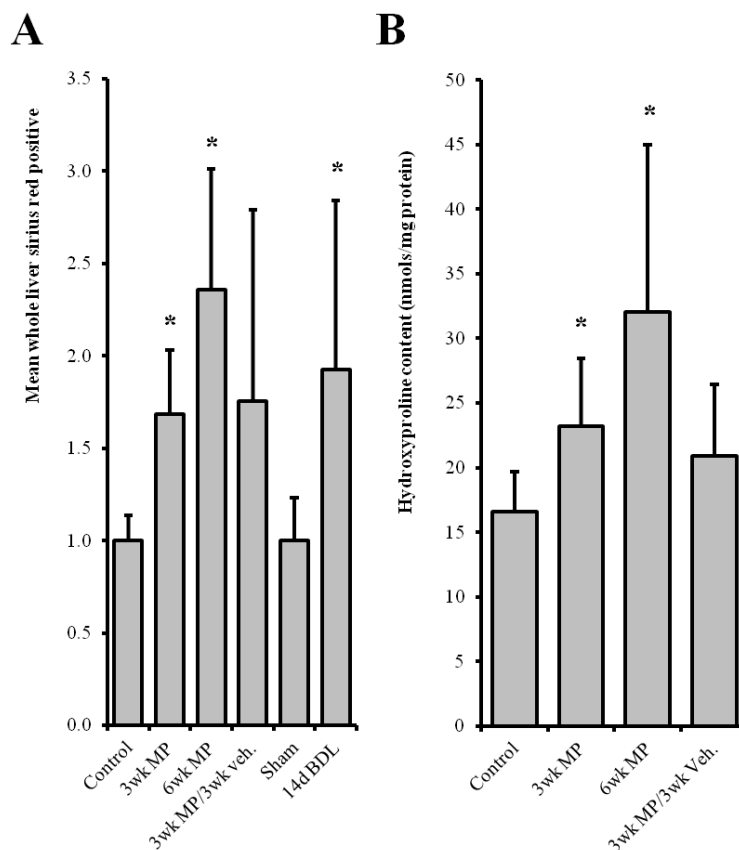


**Figure 6.9: Chronic MP treatment and BDL cause significant hepatic fibrosis. A. Quantification of sirius red staining.** Sirius red stained liver sections were scanned using a Leica SCN400 slide scanner and once scanned the liver masked to exclude large vessels. Analysis of whole liver staining was then carried out using optimised settings. **B. Liver hydroxyproline content following the indicated treatments.** Frozen liver tissue was weighed and acid hydrolysed before calculation of hydroxyproline content. Results were normalised to protein concentration calculated by Lowry assay. For **A**, data are expressed relative to respective controls and for **A** and **B**, data are the mean and SD of the following animal numbers - for control, n=3; for 3wk MP, 3wk MP/3 wk vehicle and sham (A only), n=5; for 6wk MP, n=6; and for BDL (A only), n=8. \*significant difference compared to respective control group at  $p < 0.05$ .

### 6.7 MP treatment causes a ductular reaction

Ductular reaction is a regenerative response involving the proliferation of a hepatic bipotent progenitor population (“oval cells” in rats) which can differentiate into cholangiocytes or hepatocytes. It is also thought to play an important role in fibrogenesis [4]. Oval cells have a cholangiocyte phenotype and express CK-19. MP treatment and BDL significantly increased periportal CK-19 staining (figure 6.10) indicating that they both caused a ductular reaction. The reaction was significantly more severe after 6 weeks than 3 weeks of MP treatment and the significant increase seen after 3 weeks of MP treatment was reversible after 3 weeks of vehicle treatment.

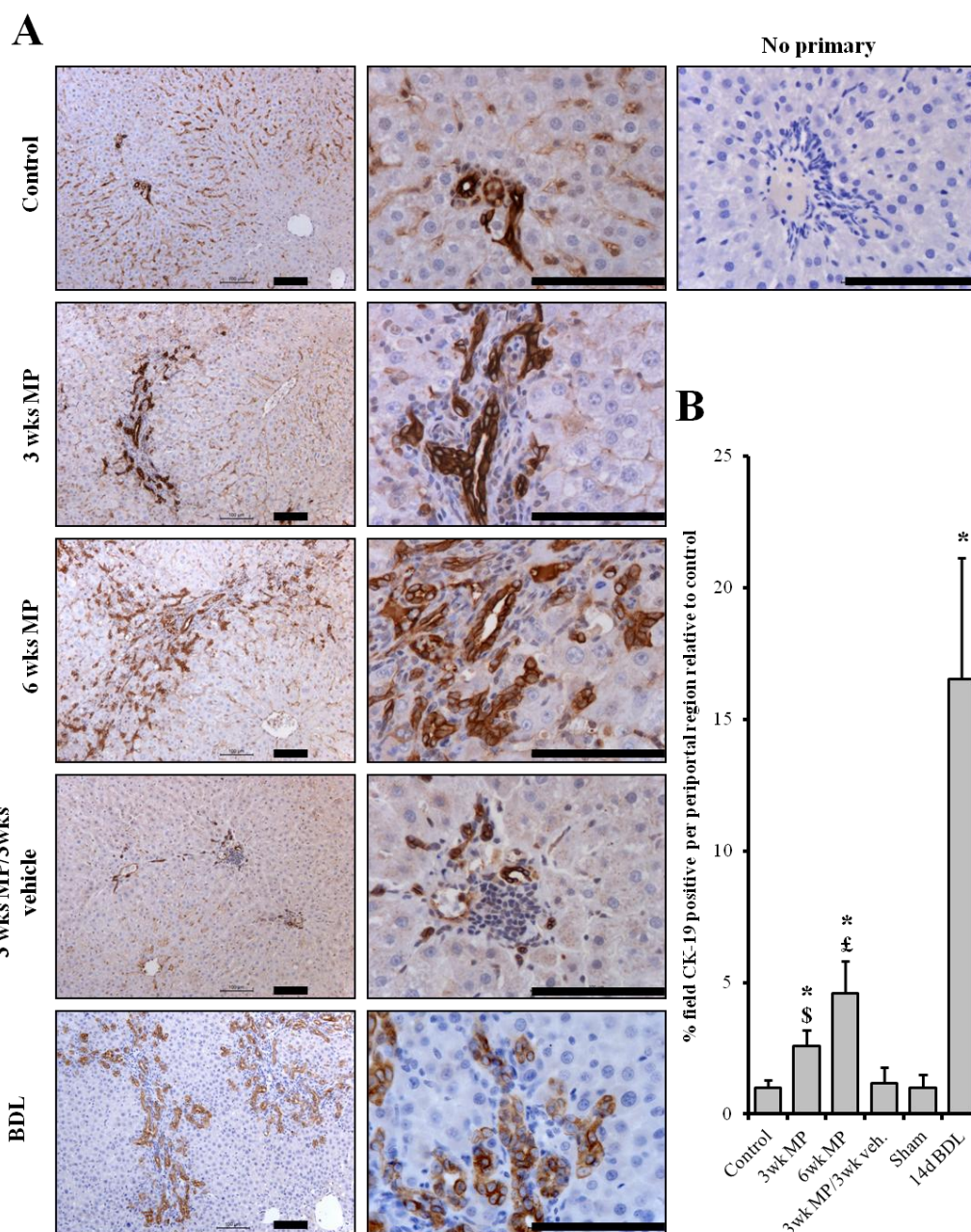


**Figure 6.10: Chronic MP treatment and 14 day BDL cause activation of a ductular reaction. A. Rat liver sections stained with CK-19 after the indicated treatment.** Liver fixed in 10% formalin and paraffin embedded was cut into 5 $\mu$ m sections. Sections were dewaxed, rehydrated and endogenous peroxidases blocked. Sections were then subject to sodium citrate antigen retrieval and serum blocking then immunostained for CK-19 using DAB to detect bound antibody. Sections were then stained with haematoxylin prior to dehydration, mounting and analysis using a Leica upright microscope. Images are representative of groups and scale bar indicates 100 $\mu$ m. Note, control is from the T0 control group, which had an identical histopathological appearance to sections from sham BDL operated rats, hence only one view is shown and referred to as control. **B. Quantified CK-19 labelling of liver sections.** CK-19 staining was quantified using Qwin software: the percentage of periportal regions staining positive for CK-19 was calculated around 10 random portal tracts per section per animal by an examiner blinded to the treatment groups. Values are expressed relative to respective controls. Data are the mean and SD of the following animal numbers - for control, n=3; for 3wk MP, 3wk MP/3 wk vehicle and sham, n=5; for 6wk MP, n=6; and for BDL, n=8. \*significant difference compared to the respective control group, §significant difference compared to the 3 week MP/3 week vehicle group and †significant difference compared to the 3 week MP group all at p<0.05.

### **6.8 MP treatment significantly up-regulates expression of fibrosis-associated markers**

To further characterise how chronic MP treatment and its withdrawal affects the liver, the expression of fibrogenesis associated genes was measured using qPCR (table 6.2). In support of the histology, administration of MP for 3 and 6 weeks was associated with the significant up-regulation of  $\alpha$ -SMA, COL1A1 and vimentin mRNA expression similar to that seen after BDL. TGF- $\beta$ 1 is a key pro-fibrogenic growth factor produced by inflammatory leukocytes during fibrogenesis that promotes ECM deposition by myofibroblasts [5]. Chronic dosing of MP led to the significant up-regulation of TGF- $\beta$ 1 mRNA expression to similar levels to that seen after BDL. Similarly, the hepatic mRNA expression of TGF- $\beta$ 2, another TGF isoform also implicated in promotion of fibrosis, was significantly increased after 6 weeks of chronic MP treatment.

Fibrosis occurs due to an imbalance in deposition of ECM versus its degradation. However, enhanced breakdown of ECM can be pro-fibrogenic by releasing pro-fibrogenic ECM bound growth factors and by enhancing motility of pro-fibrogenic cell types (eg. myofibroblasts and leukocytes). Matrix metalloproteinase-2 (MMP-2) is a myofibroblast derived matrix metalloproteinase that is generally considered pro-fibrogenic [5, 299] and its mRNA expression was significantly up-regulated following 6 weeks of MP treatment, but not 3 weeks of MP treatment or BDL. Tissue inhibitor of metalloproteinase-1 (TIMP-1) is part of the tissue inhibitor of metalloproteinase family which competitively inhibit the matrix metalloproteinases; they promote fibrogenesis through inhibition of ECM remodelling and inhibition of apoptosis of activated hepatic stellate cells [5]. The expression of TIMP-1 mRNA was significantly increased following MP treatment and BDL. Importantly, in terms of reversal of MP induced hepatic fibrosis, for all the markers of fibrogenesis measured, the rats treated with MP for 3 weeks followed by vehicle for 3 weeks showed reversion of mRNA expression to control levels. This is in agreement with the histology and suggests that after 3 weeks of vehicle treatment the hepatic injury caused by 3 weeks of MP treatment was essentially repaired.

Group	mRNA transcript (fold control levels)						
	$\alpha$ -SMA	COL1A1	MMP-2	TGF- $\beta$ 1	TGF- $\beta$ 2	TIMP-1	Vimentin
Control	1 $\pm$ 0.24	1 $\pm$ 0.24	1 $\pm$ 0.89	1 $\pm$ 0.23	1 $\pm$ 0.47	1 $\pm$ 0.85	1 $\pm$ 0.33
3wk MP	2.19 $\pm$ 0.47*	3.26 $\pm$ 2.1*	1.87 $\pm$ 1.22	2.82 $\pm$ 0.56*	2.05 $\pm$ 1.79	3.46 $\pm$ 2.34*	2.18 $\pm$ 1.21*
6wk MP	4.84 $\pm$ 6.63*	4.03 $\pm$ 6.43*	4.62 $\pm$ 6.41*	3.97 $\pm$ 3.7*	3.82 $\pm$ 3.89*	7.8 $\pm$ 15.56*	3.42 $\pm$ 2.62*
3wk MP/3 wk veh.	1.01 $\pm$ 0.26	1.39 $\pm$ 0.78	2.12 $\pm$ 1.05	1.28 $\pm$ 0.38	0.88 $\pm$ 0.3	1.14 $\pm$ 0.33	0.68 $\pm$ 0.27
14d BDL	3.88 $\pm$ 1.83*	25.06 $\pm$ 13.74*	1.43 $\pm$ 5.09	2.71 $\pm$ 0.44*	5.78 $\pm$ 8.31*	2.83 $\pm$ 9.77	8.83 $\pm$ 2.95*

**Table 6.2: Whole liver changes in gene expression after MP treatment or 14 day BDL as measured by qPCR.** Total RNA was extracted from liver samples using TRIzol and then subject to reverse transcription to produce cDNA. The cDNA was used as template for real-time PCR and relative expression calculated using 18S rRNA as the endogenous control and fold change expressed relative to control liver. Values are the mean and SD of the following animal numbers - for control liver, 3wk MP and 3wk MP/3wk vehicle, n=5; for 6wk MP, n=6 and for 14d BDL, n=8. \*Significant difference compared to control, all at p<0.05.

## 6.9 Chapter discussion

Models of periportal fibrosis are important for research into anti-fibrogenics; prior to clinical testing, it is recommended that anti-fibrogenic drugs are tested in both a centrilobular model as well as a periportal model of fibrosis due to their different pathologies [5, 6, 16]. Due to the limitations associated with the BDL model of periportal fibrosis, chronic MP dosing was investigated as an alternative.

Assessment of pathology following BDL and MP treatment showed that the 2 models induced a similar pattern of liver injury. Chronic inflammation is a key driver of fibrogenesis in chronically injured liver [16]. H&E staining of liver from MP treated and BDL rats showed that both treatments caused significant periportal inflammation. MP induced inflammation was also shown to be reversible. PCNA immunostaining showed that 6 weeks of MP treatment and BDL both significantly increased hepatocyte and cholangiocyte proliferation, demonstrating that both treatments lead to hepatic damage and activation of hepatic regenerative pathways.

In terms of fibrogenic cells, the numbers of myofibroblasts and portal tract fibroblasts in the periportal region positively correlated with the length of MP administration and numbers significantly decreased following the cessation of MP treatment. Sirius red staining showed that MP treatment and BDL were both associated with significant

periportal collagen deposition, in a manner that mirrored the changes in fibrogenic cell populations. Specifically, MP induced periportal fibrosis that significantly increased in severity with treatment time and reversed when treatment was ceased.

Spontaneous reversal of fibrosis is recognised to occur in some patients where the underlying cause of hepatic insult is successfully treated, however the processes that underlie this reversal are poorly understood [16]. The severity of periportal fibrosis in MP treated rats correlated with the number of pro-fibrogenic cells. The resolution of fibrosis seen in rats treated with MP for 3 weeks followed by vehicle for 3 weeks is therefore likely to be the result of apoptosis or reversal of the pro-fibrogenic phenotype of these populations. This may result from a decline in inflammation and associated pro-fibrogenic growth factors released from inflammatory cells. That the mRNA expression of hepatic TGF- $\beta$ 1 and TGF- $\beta$ 2 returned to control levels in rats treated with MP for 3 weeks followed by vehicle for 3 weeks (table 6.2) supports this hypothesis. The ease of reversal in this model facilitates its use as a method to study the reversal of periportal fibrosis.

Increasing evidence suggests that reactive ductules, arising from ductular reaction activation, are important mediators of fibrogenesis through secretion of pro-fibrogenic and inflammatory factors [4]. CK-19 staining demonstrated that both MP treatment and BDL were associated with the activation of a ductular reaction. The reaction induced by MP treatment was also shown to be reversible.

Similar to periportal fibrosis, ductular reaction is commonly studied in BDL rats. However the severity of hepatic damage caused by BDL means that it is currently difficult to model the initiation and progression of ductular reactions in this model. This is because within a very short period of time after ligation surgery, a significant ductular reaction develops [300]. Chronic MP treatment causes liver damage and activation of a ductular reaction less rapidly than BDL. The use of a MP model for the study of this phenomenon would give a longer time frame for the investigation into the early stages of a ductular reaction. Additionally, the examination of ductular reaction reversal would also be simplified compared to the use of BDL for the reasons previously mentioned.

In terms of potential drug interactions, MP administration has been shown to reduce CYP2C11 and CYP3A activity in rats *in-vivo* whilst CYP1A and CYP2B activity were unaffected [196]. Although MP is a H1 receptor antagonist, knockout of the H1 receptor has been demonstrated to have no effect on hepatic injury in a murine model of liver damage [301]. The antagonistic action of MP on the H1 receptor is therefore not predicted to have a significant effect on MP induced hepatic injury. Although MP drug interactions may need to be taken into account when analysing results, MP is not unique in having “off-target” effects. Most compounds used to generate liver fibrosis have similar “off-target” activity. For example, CCl<sub>4</sub>, the commonly used centrilobular hepatotoxin, is also a relatively potent inhibitor of protein kinase C activity [302].

The data presented in this chapter demonstrates that, in agreement with the initial hypothesis, chronic MP treatment of male rats causes periportal fibrosis with characteristics qualitatively equivalent to that seen following BDL, but without the requirement for surgery, distress and high mortality rates. The severity of fibrosis could be easily modulated and generated fibrosis was reversible on cessation of treatment. Chronic MP treatment is therefore, compared to BDL, a refined and alternative model for the generation of reversible periportal fibrosis in the rat.

**Chapter 7. The PXR is anti-fibrogenic in an  $\alpha$ -  
naphthylisothiocyanate-induced model of periportal fibrosis in  
the mouse**

## 7.1 Introduction

Mice are the most commonly used mammalian species in biomedical research due to their ease of care and the huge range of genetically engineered mouse strains that have been created. Mice subject to BDL are a frequently used model of periportal fibrosis [16, 163, 283]. However, similar to its use in rats, the use of BDL in mice is associated with animal welfare and methodology problems. These include, but are not limited to, high rates of mortality, practical irreversibility of the procedure and inability to modulate the intensity of the hepatic injury.

Non-surgical models of periportal and biliary fibrosis in mice are limited. Previous work in this lab has shown that MP, although hepatotoxic in rats, does not cause significant liver injury in mice [3]. This appears to be because its metabolism differs between the two species. Evidence to date shows that mouse hepatocytes do not produce the S-oxide thioether of MP that is postulated to be the cause of MP toxicity in rat hepatocytes [293].

$\alpha$ -naphthylisothiocyanate (ANIT) is a hepatotoxic compound which is known to cause portal and periportal liver injury in rats and mice [303, 304]. Rather than causing liver injury through hepatocyte toxicity directly, ANIT is thought to accumulate in bile where it causes necrosis in surrounding biliary epithelia through modification of cellular proteins [305, 306]. Hepatocyte damage may come secondarily to cholangiocyte death, recruitment of neutrophils and initiation of inflammation.

Several studies have demonstrated that the chronic administration of ANIT also causes ductular reaction as well as portal fibrosis leading to cirrhosis when given chronically [307-310]. The pattern of fibrosis seen however has not been thoroughly explored, particularly in respect to its potential as an alternative to BDL in mice. It was therefore hypothesised that the chronic administration of mice with ANIT would cause periportal fibrosis qualitatively similar to that seen after BDL.

## 7.2 ANIT treatment causes hepatic injury

Before the hypothesis was tested, pilot work was carried out to confirm and examine the distribution and dynamics of ANIT induced liver injury. To confirm the distribution of injury and identify an appropriate dose for treatment, a small pilot study was carried out as outlined in table 7.1.

Number of animals	Treatment	Notes
2 male C57BL/6	Vehicle (olive oil)	Animals were dosed twice per week for 4 weeks. Dosing was by oral gavage.
1 male C57BL/6	10mg/kg ANIT	
1 male C57BL/6	25mg/kg ANIT	
1 male C57BL/6	50mg/kg ANIT	

**Table 7.1: Pilot animal dosing groups**

Figure 7.1A shows that the administration of ANIT at the doses tested had no effect on weight gain in the treated mice over the course of the study. At harvest, measurement of liver weight to body mass ratios showed that ANIT treatment increased this ratio in a dose dependent manner (figure 7.1B). In terms of serum markers of liver injury, ALT activity was not increased by ANIT treatment and appeared to decrease in mice treated with 10 or 25mg/kg ANIT. ALP activity was almost twice as high in the mouse treated with 50mg/kg ANIT compared to all other treatment groups (figure 7.1C).

Assessment of liver pathology and fibrosis showed that 50mg/kg ANIT treatment caused marked portal tract inflammation and collagen deposition around portal tracts which was not apparent in other treatment groups (figure 7.2A). The severity of periportal fibrosis increased in a dose responsive manner (figure 7.2B).

Following this pilot study, it was realised that ANIT was incompletely dissolved in the olive oil vehicle during preparation. A consequence of this is that mice in the pilot study may have received less than the dose planned. Constant agitation was found to be required for more complete dissolution of ANIT into the vehicle. This method was used for all subsequent ANIT work.

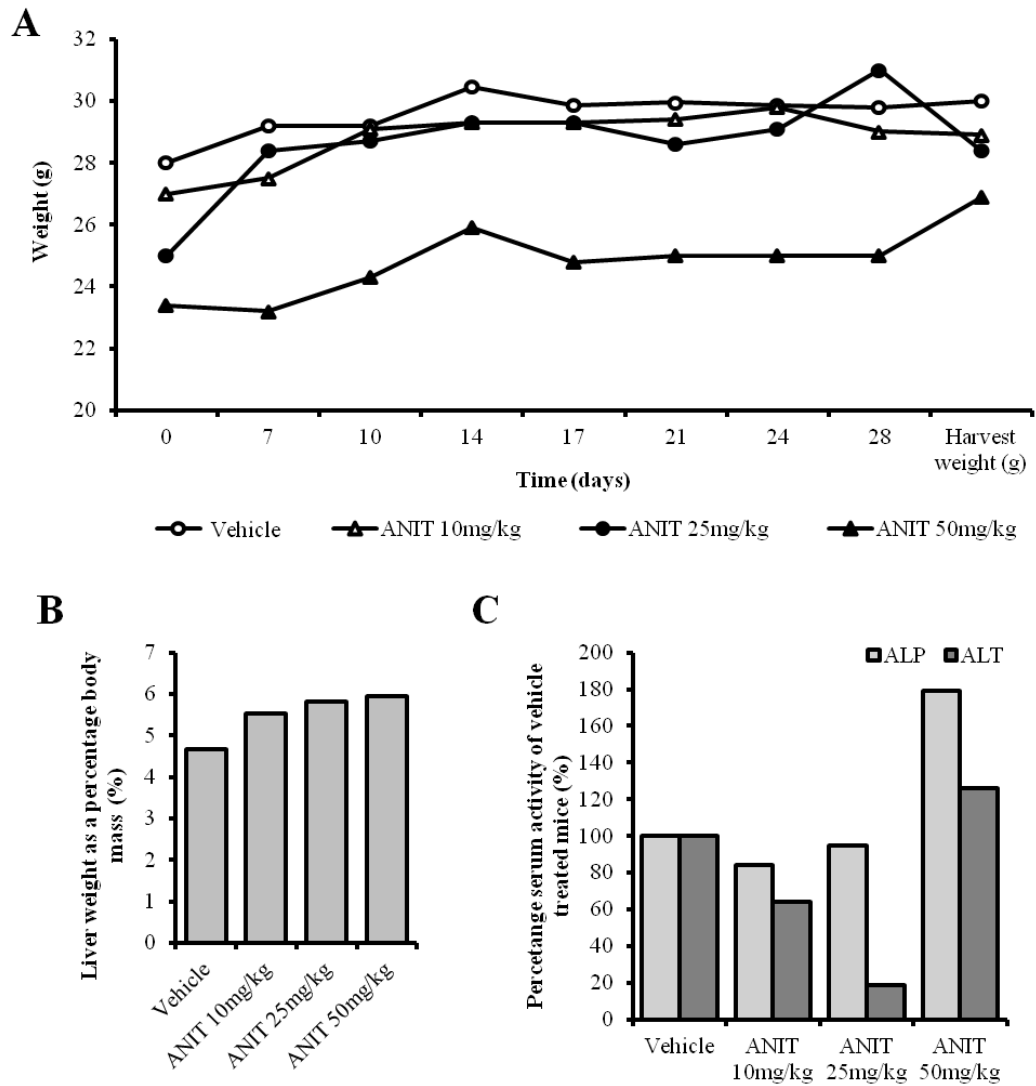


**Figure 7.1: ANIT treatment does not give rise to weight loss but does increase serum ALP activity. A. Weights of treated mice over the study. B. Liver weight as percentage body mass at harvest. C. Serum ALT and ALP values of treated mice. Values are expressed relative to the vehicle treated mice. Results are the mean of the following animal numbers - for vehicle, n=2; for ANIT treated animals, n=1.**

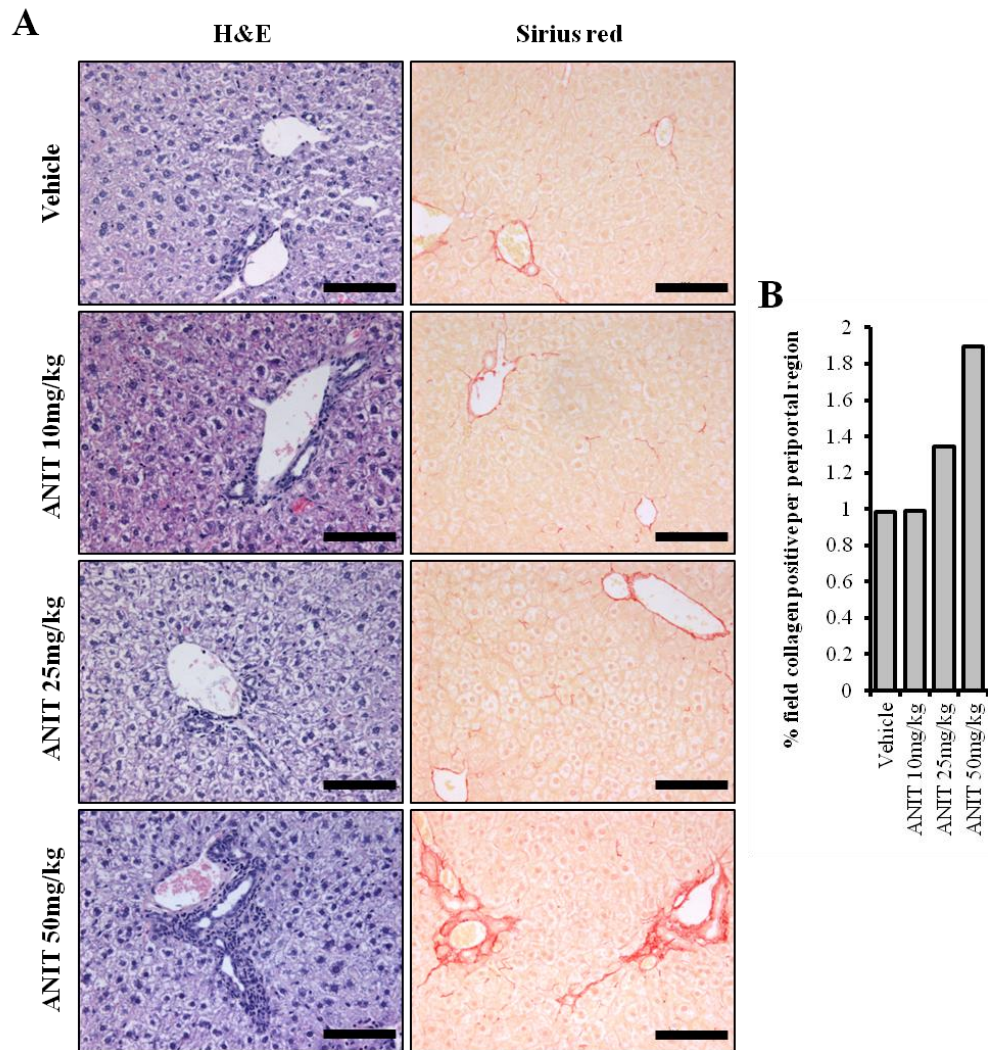


**Figure 7.2: ANIT treatment causes portal tract inflammation and fibrosis. A. H&E and sirius red stained livers of vehicle and ANIT treated mice.** Liver fixed in 10% formalin and paraffin embedded was cut into 5 $\mu$ m sections. Sections were dewaxed, rehydrated and stained with H&E or sirius red prior to dehydration and mounting and analysis using a Leica upright microscope. Scale bar indicates 100 $\mu$ m. **B. Quantified sirius red staining of periportal fibrosis.** Sirius red staining was quantified using Qwin software: the percentage of periportal regions staining positive for collagen was determined by an examiner blinded to the treatment groups, from 10 random portal tracts per section per animal. Results are the mean of the following animal numbers - for vehicle, n=2; for ANIT treated animals, n=1.

### 7.3 Acute ANIT administration induces hepatic NF- $\kappa$ B signalling *in-vivo*

The development of *in-vivo* imaging systems, in combination with fluorescent or luminescent reporters, allows for live imaging of animals. 3x- $\kappa$ B-luc C57BL/6 mice (NF- $\kappa$ B -luc mice) express luciferase under control of a NF- $\kappa$ B response element [164, 311]. In cells with active NF- $\kappa$ B signalling, luciferase is therefore expressed. Through administration of luciferin, which is metabolised by luciferase to produce light, the localisation of NF- $\kappa$ B transcriptional activity can be determined. NF- $\kappa$ B signalling is

activated by a range of stimuli, including tissue damage, and initiates and regulates inflammation, tissue regeneration and immune responses [312, 313]. It is consequently active in all chronic liver diseases and is generally considered pro-fibrogenic. Amongst other effects, NF- $\kappa$ B inhibits apoptosis of myofibroblasts and drives inflammation through promotion of the release of pro-fibrogenic/inflammatory cytokines from various cell types, particularly TGF $\beta$ 1 release from Kupffer cells/macrophages [314-317]. Monitoring its expression in NF- $\kappa$ B-luc mice therefore permits the extent of hepatic injury and inflammation caused by a given treatment to be determined.

To assess if ANIT treatment would cause hepatic NF- $\kappa$ B activation and inflammation measurable *in-vivo*, and to determine the dynamics of ANIT induced liver injury more generally, NF- $\kappa$ B-luc mice were treated with a single dose of vehicle, or a low (30mg/kg) or high dose (50mg/kg) of ANIT (outlined in table 7.2). CCl<sub>4</sub> was used as a positive control as it is known to cause hepatic damage and activation of NF- $\kappa$ B signalling [318]. Luminescence was measured over 7 days.

Number of animals	Treatment	Notes
2 female NF- $\kappa$ B -luc	Vehicle (olive oil)	Animals were given a single dose of vehicle, ANIT or CCl <sub>4</sub> at T0 and luminescence measured periodically over 7 days
1 female NF- $\kappa$ B -luc	50mg/kg ANIT	
1 female NF- $\kappa$ B -luc	30mg/kg ANIT	
1 female NF- $\kappa$ B -luc	0.6g/kg CCl <sub>4</sub>	

**Table 7.2: Pilot NF- $\kappa$ B-luc mouse study groups**

Results showed that CCl<sub>4</sub> treatment led to peak signal in the upper abdominal region of the mouse (location of the liver) at 24 hours (figure 7.3). The 50mg/kg ANIT treated mouse showed peak signal at 48 hours. 30mg/kg ANIT treatment conversely had little effect on luminescence. The increase in luminescence induced by CCl<sub>4</sub> treatment rapidly dropped back to control levels by day 7 whereas luminescence induced by 50mg/kg ANIT remained elevated at the end of the study.

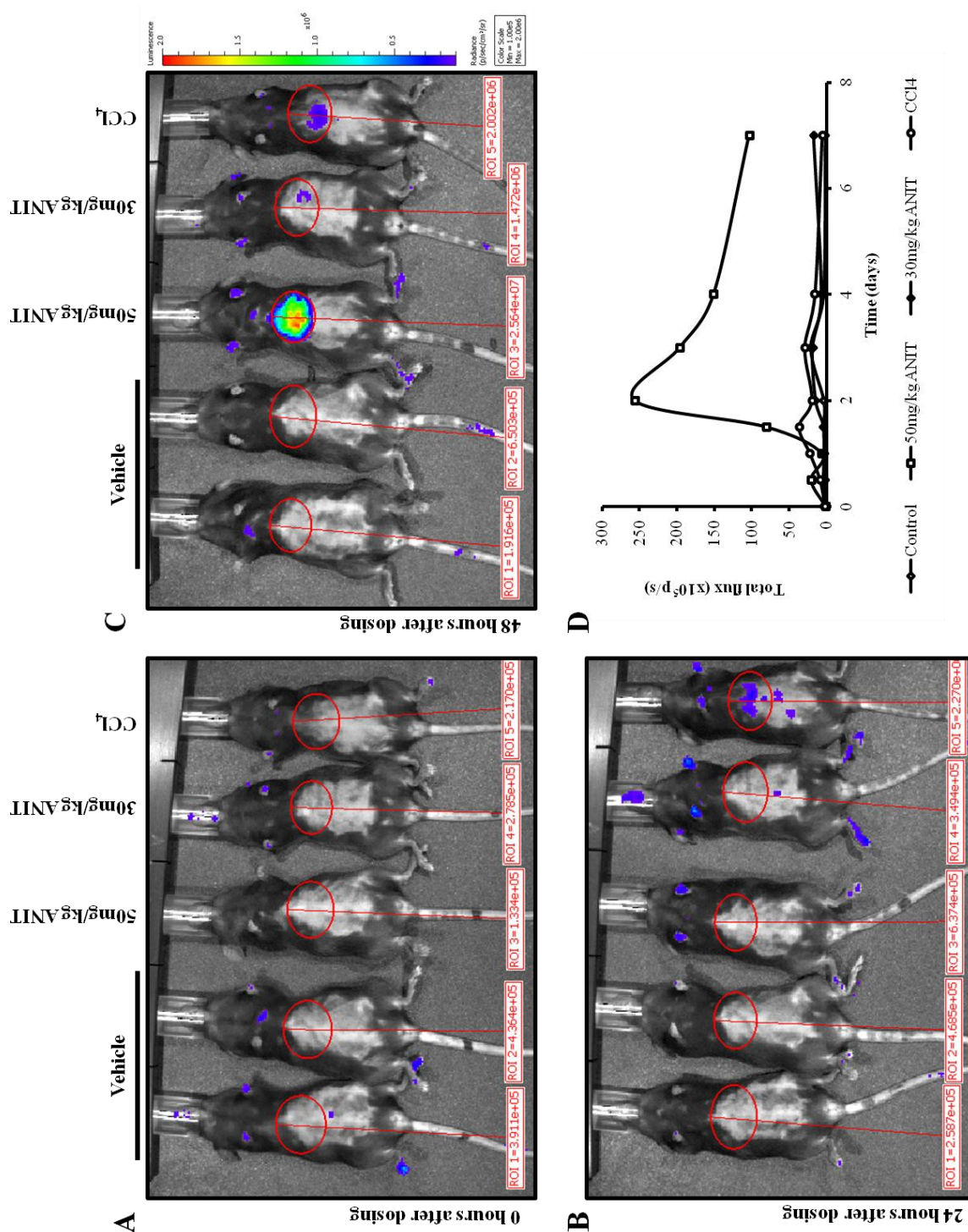


**Figure 7.3: Acute dosing of 50mg/kg but not 30mg/kg ANIT causes long term hepatic inflammation.** A-C: IVIS images of treated mice at 0, 24 and 48 hours respectively. Mice were treated with the indicated compounds and imaged at different time points. For imaging, mice were anesthetised with isoflurane and injected i.p. with 200 $\mu$ l of D-luciferin at 15mg/ml. Images are from scans 10 minutes after injection. D. Quantified abdominal luminescence of treated mice.

In order to be able to carry out statistical tests, the study was repeated using more mice treated, as previously, with a single dose of either vehicle, ANIT (50mg/kg) or CCl<sub>4</sub>.

Luminescence was measured over 39 days and following the end of the study organs were excised, *ex-vivo* scans performed and tissue histology assessed.

As shown in figure 7.4 and figure 7.5A, luminescent signal was again apparent in the upper abdominal region of ANIT treated mice by 36 hours and which peaked at 60 hours ( $2.33 \times 10^7 \pm 7.49 \times 10^6$  p/s (photons/second)). CCl<sub>4</sub> treatment caused upper abdominal luminescence which peaked at 24 hours with a total flux of  $3.23 \times 10^6 \pm 9.58 \times 10^5$  p/s and the difference was not significantly different to mice at time point zero. Measurement of luminescence over time indicated that the increase in upper abdominal luminescence caused by ANIT remained elevated and was significantly different compared to time point zero till day 10 following treatment. At the end of the study, total flux was still  $1.57 \times 10^6 \pm 3.87 \times 10^5$  p/s (3 fold higher than control mouse values), compared to CCl<sub>4</sub> treated mice in which luminescence had dropped to control levels by day 6. To confirm the source of luminescence in the treated mice, organs were excised following the termination of the study and immediately imaged (figure 7.5B). This showed that significantly more luminescence could be detected in the livers of ANIT treated mice compared to those of control animals. This suggests that the upper abdominal signal detected during the *in-vivo* imaging was from liver luminescence. Livers from CCl<sub>4</sub> treated mice showed no difference in luminescence. ALP serum activity of treated mice showed no difference regardless of treatment (figure 7.5C).

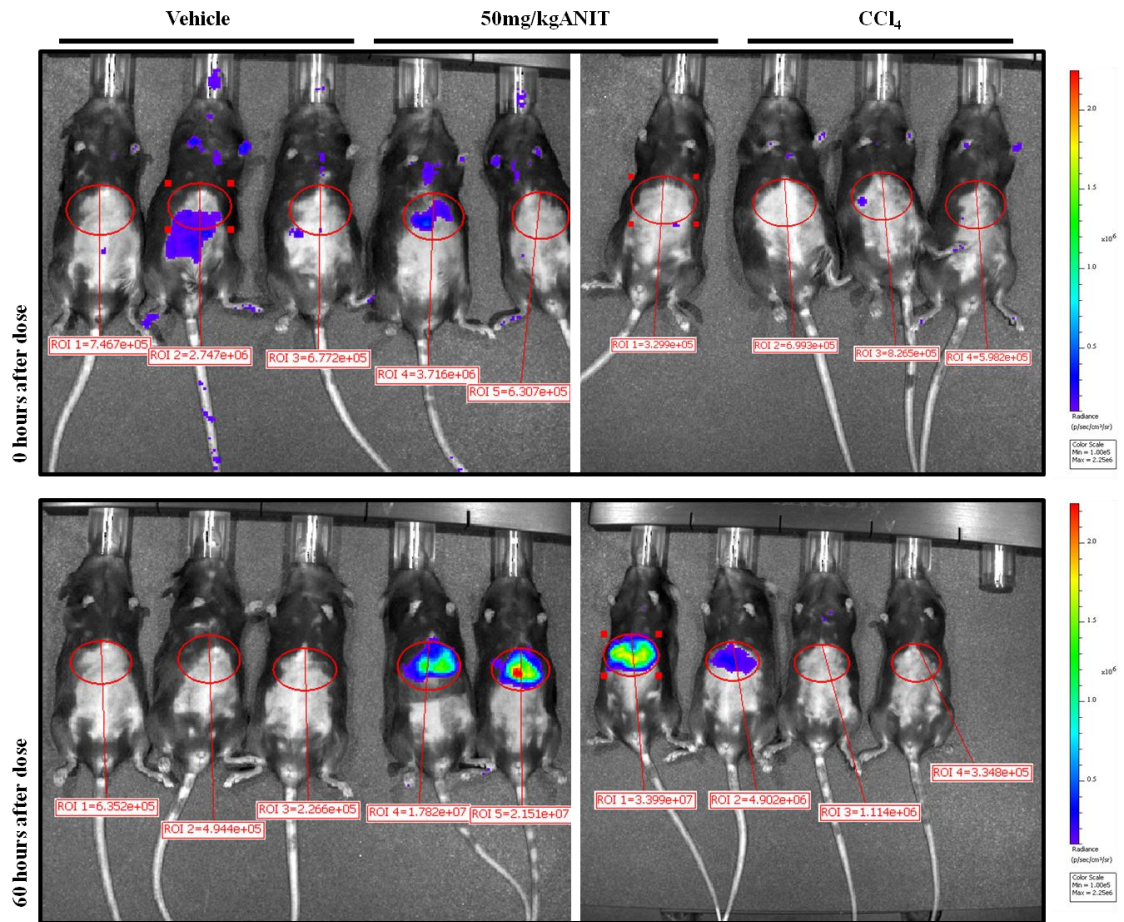


**Figure 7.4: Acute dosing of 50mg/kg ANIT causes long term hepatic inflammation. IVIS images of treated mice at 0 and 60 hours after dosing.** Mice were treated with the indicated compounds and imaged at different timepoints. For imaging, mice were anesthetised with isoflurane and injected i.p. with 200 $\mu$ l of D-luciferin at 15mg/ml. Images are from scans 10 minutes after injection.

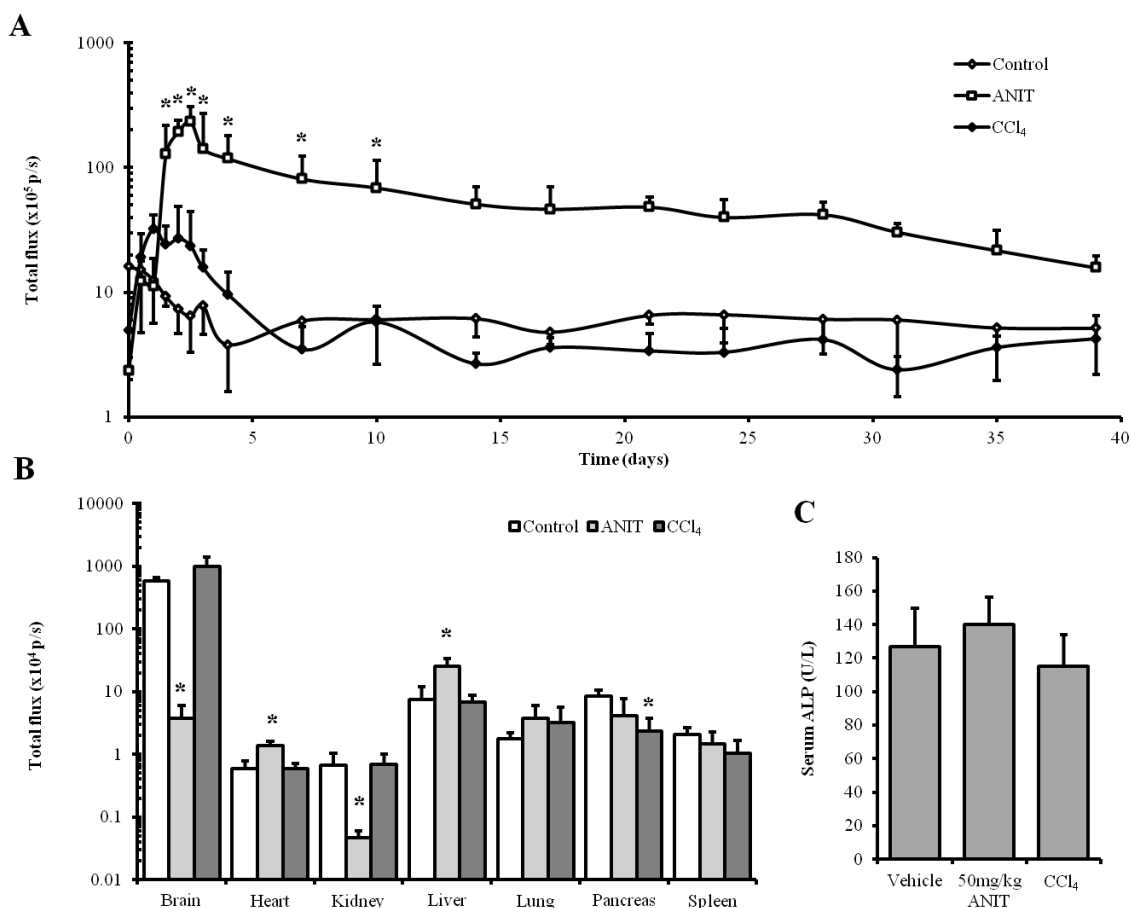


**Figure 7.5: Acute treatment of 50mg/kg ANIT causes long term significant hepatic inflammation. A. Quantified abdominal luminescence of treated mice. B. Quantified *ex-vivo* luminescence of harvested organs. C. Serum ALP measurements of treated mice.** Serum was taken at harvest. For **A** and **B**, points and bars respectively are the mean and SD of the following animal numbers - vehicle, n=3; CCL<sub>4</sub> and ANIT, n=4. For **C**, bars are the mean and SD of the following animal numbers - vehicle, n=3; CCL<sub>4</sub> and ANIT, n=4. In **A**, \*indicates significant difference compared to respective time point zeros at p<0.05; statistical significance was determined by a repeated measures ANOVA followed by a Dunnett's multiple comparisons test using Graphpad prism 6. For **B**, \*indicates significantly different total organ flux compared to those from control mice determined by 2-tailed Student's t-test at p<0.05. Pilot animal readings, culled on day 46 following treatment, were included in mean and SD values.

To assess for an inflammatory response in the livers of the treated mice, the livers were fixed, embedded and stained with H&E. Histologically, portal tract inflammation and bile duct hyperplasia were only apparent in the livers of ANIT treated mice (figure 7.6A). Quantification of portal tract inflammation confirmed that ANIT caused significant periportal inflammation (figure 7.6B). These data suggest that the NF- $\kappa$ B activity measured in this study is a measure of hepatic inflammation. In support of this, figure 7.6C depicts the result of plotting the mean number of periportal inflammatory cells against total liver flux, indicating a correlation between the two parameters.

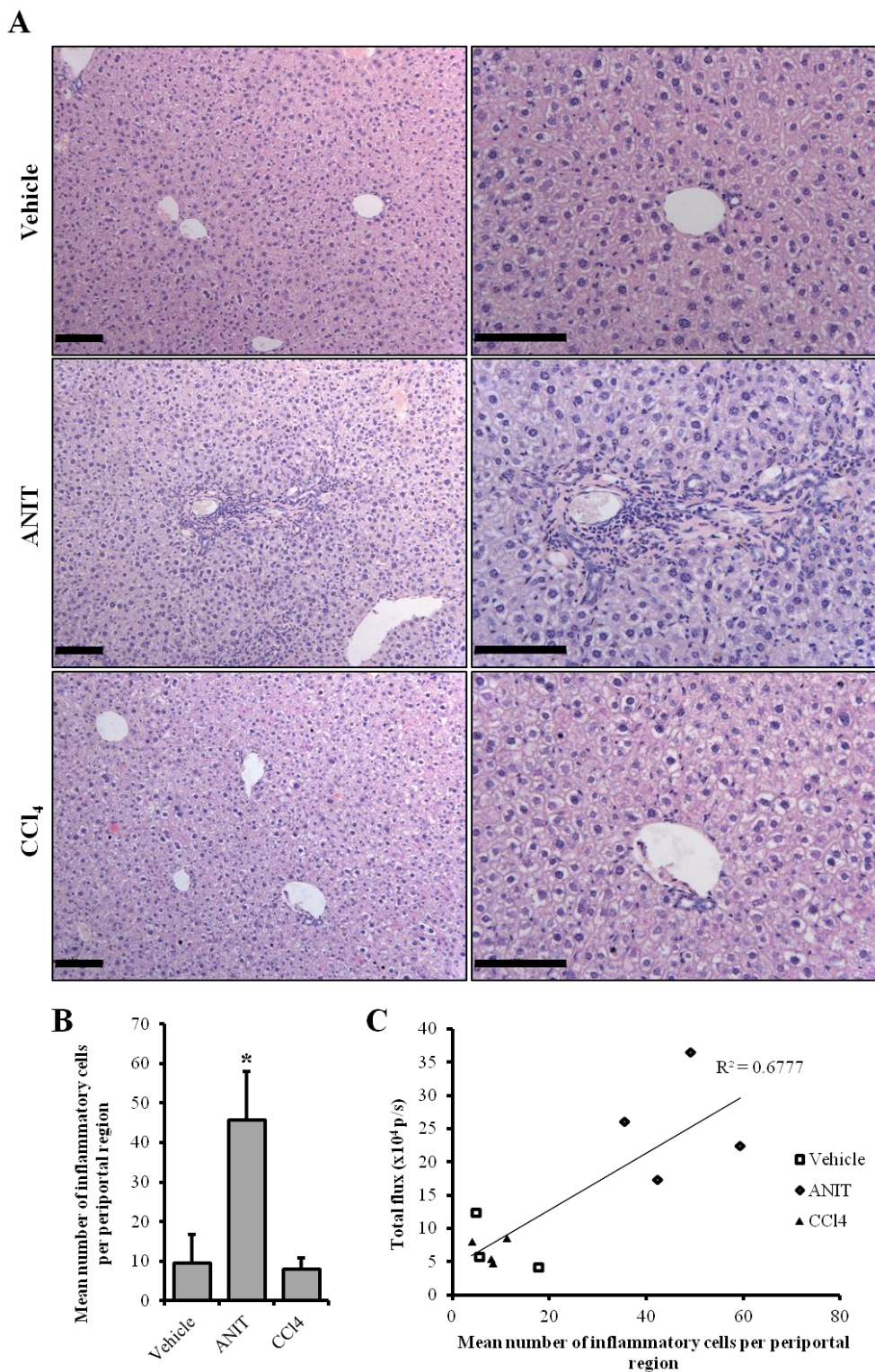


**Figure 7.6: Abdominal luminescence was proportional to hepatic inflammation following acute 50mg/kg ANIT treatment.** Liver fixed in 10% formalin and paraffin embedded was cut into 5 $\mu$ m sections. Sections were dewaxed, rehydrated and stained with H&E prior to dehydration, mounting and analysis using a Leica upright microscope. Images are representative of groups and scale bar indicates 100 $\mu$ m. **B. Quantified periportal inflammation.** The mean number of inflammatory cells around 6 random portal tracts, per section per animal, was determined by an examiner blinded to the treatment groups. Data are the mean and SD of the following animal numbers - for vehicle, n=3; CCl<sub>4</sub> and ANIT, n=4 \*significant difference compared to vehicle treated mice at p<0.05. **C. Correlation between total flux and periportal inflammation.** Flux values are from the *ex-vivo* liver scan.

#### 7.4 ANIT treatment causes portal tract inflammation in WT and PXR KO mice

Based on the pilot work, which suggested that ANIT caused liver injury localised to and around portal tracts in agreement with the literature, the initial hypothesis (that chronic administration of mice with ANIT would cause periportal fibrosis qualitatively similar to that seen after BDL) was still appropriate and would therefore be tested.

ANIT treatment causes intrahepatic cholestasis through biliary epithelial cell damage [319]. Human cholestatic liver disease may result from a wide range of diseases with a number of different aetiologies. These disorders cause a reduction of bile flow and an associated retention of substances that are secreted into the bile leading to biliary tree obstruction and intrahepatic accumulation of bile acids and hepatotoxicity. Chronic hepatic cholestasis is generally associated with the development of biliary and periportal fibrosis within the liver [58, 320]. Evidence to date indicates that activation of the PXR, the nuclear receptor xenosensor, is hepatoprotective in experimental animal models of liver injury [56, 60, 61, 311]. It has also been shown to be anti-fibrogenic in a CCl<sub>4</sub> model of fibrosis [321]. To date, however, a role for the PXR in modulating the severity of fibrosis in a periportal model has not been established. Therefore, to further test the hypothesised ANIT model of periportal fibrosis, ANIT was dosed in wild type (WT) mice and mice lacking expression of a functional PXR (PXR KO). The hypothesis was that the expression of a functional PXR protects against liver fibrosis.

ANIT was dosed as outlined in table 7.3, 3 times per week for 8 weeks. ANIT was dosed at 30mg/kg as administration of 50mg/kg led to weight loss in treated mice following a single dose. The mice were culled the day following the final treatment.

Group	Treatment	Number of mice	Notes
Vehicle	3ml/kg olive oil by oral gavage	4 WT & 3 PXR KO	Mice used were all male
ANIT	30mg/kg ANIT (by oral gavage)	5 WT & 4 PXR KO	

**Table 7.3: Animal dosing groups for ANIT and PCN study**

In terms of serum markers of liver injury, treatment of mice with ANIT led to a significant increase in serum ALP activity in both WT and PXR KO animals compared to vehicle controls (figure 7.7A). Figure 7.7B shows that WT mice, but not PXR KO

mice, also had significantly increased ALT serum activity in response to ANIT treatment. The liver to body mass ratio however was unaffected by treatment (figure 7.7C). Importantly, the chronic dosing of ANIT caused no mortalities and treated mice did not appear to be in any distress.

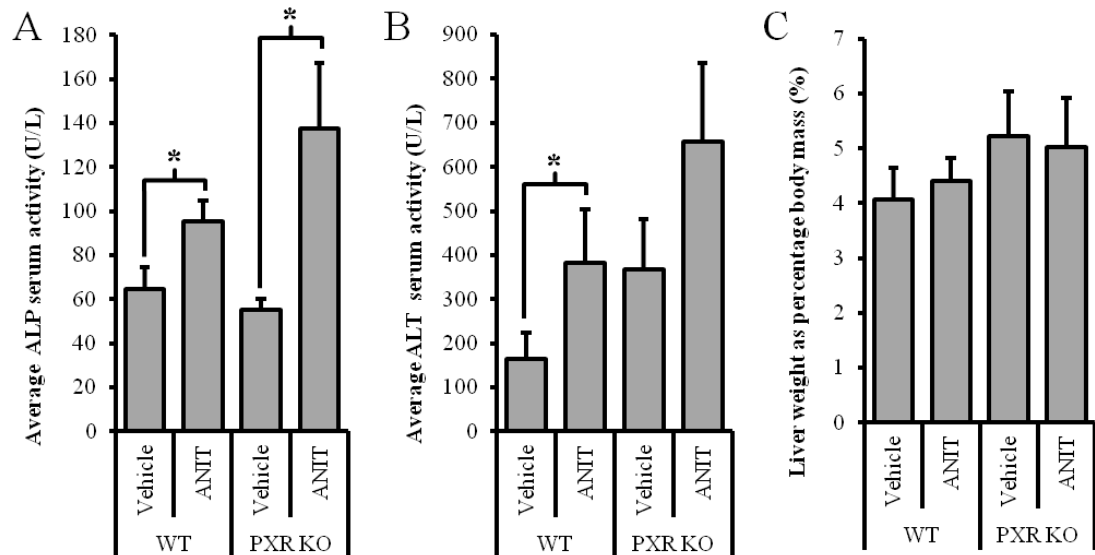


**Figure 7.7: Chronic ANIT treatment significantly increases serum ALP and ALT activity. A. ALP serum values of treated mice. B. ALT serum values of treated mice. C. Liver weight as percentage body mass at harvest.** Data are the mean and SD of the following animal numbers – for PXR KO vehicle, n=3; for WT vehicle, and PXR KO ANIT, n=4; for WT ANIT, n=5. \*significantly different to respective control at  $p < 0.05$ .

At harvest, livers were dissected from treated mice, fixed and processed. Sections were then stained with H&E in order to assess changes in liver histology following treatment. Archived tissue from a 21 day BDL study was similarly stained (donated by Fiona Oakley). Figure 7.8A shows that ANIT administration was associated with increased numbers of infiltrating leukocytes in and around the portal tracts in both WT and PXR KO mice similar to that seen after BDL. Aside from inflammation, no major histological abnormalities were seen and central veins appeared unaffected by ANIT treatment. Figure 7.8B shows that periportal inflammation was significantly increased by treatment with ANIT, the severity of which was unaffected by the lack of a functional PXR.

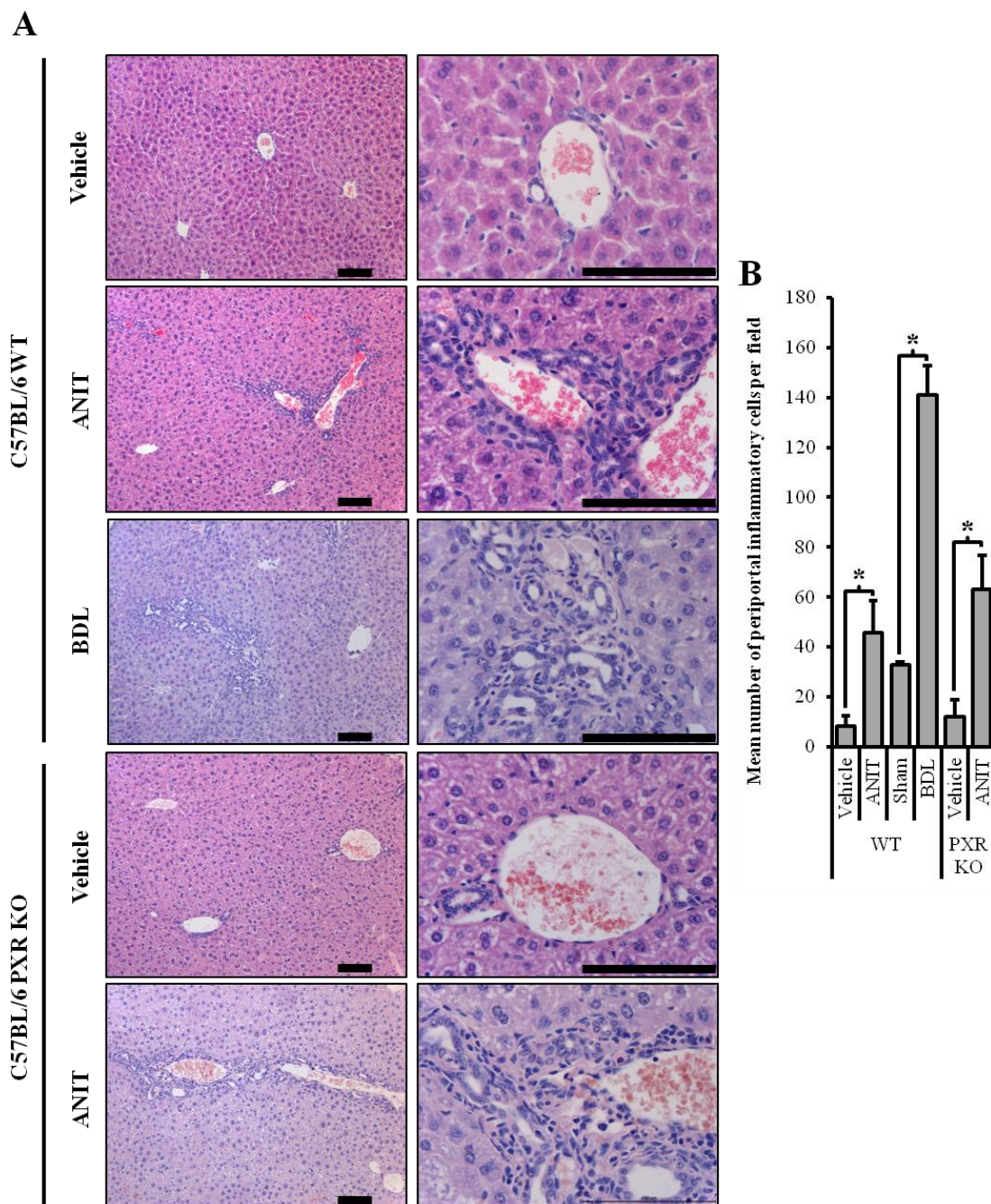


**Figure 7.8: Chronic ANIT treatment causes significant portal tract inflammation. A. H&E stained liver tissue.** Liver fixed in 10% formalin and paraffin embedded was cut into 5 $\mu$ m sections. Sections were dewaxed and rehydrated and stained with H&E prior to dehydration, mounting and analysis using a Leica upright microscope. Images are representative of groups and scale bar indicates 100 $\mu$ m. Note, control is from the vehicle control group, which had an identical histopathological appearance to sections from sham BDL operated mice, hence only one view is shown. **B. Quantified mean number of periportal inflammatory cells per portal tract.** The mean number of inflammatory cells around 5 random periportal regions, per section per animal, was determined by an examiner blinded to the treatment groups. Data are the mean and SD of the following animal numbers – for PXR KO vehicle, n=3; for WT vehicle, sham and BDL, and PXR KO ANIT, n=4; for WT ANIT, n=5. \*significant difference compared to the respective control group at p<0.05.

### **7.5 Hepatic pro-fibrogenic cell populations expand in response to ANIT treatment**

As in rats, hepatic fibrogenesis is a consequence of ECM deposition by different populations of fibroblasts and portal tract fibroblasts are an identifying characteristic of periportal fibrogenesis [6, 161]. To assess the effect of ANIT treatment upon portal tract fibroblasts, the expression of vimentin, which is expressed by portal tract fibroblasts [298], was examined by immunostaining. Figure 7.9A shows that ANIT treatment, similar to BDL, caused an increase in periportal vimentin staining compared to controls. Quantification of the staining (figure 7.9B) showed that ANIT treatment significantly increased periportal vimentin staining in both WT and PXR KO animals by around 2 fold. BDL significantly increased periportal vimentin staining by approximately 3 fold compared to sham operated animals.

To determine if ANIT caused activation of fibroblasts to myofibroblasts,  $\alpha$ -SMA was immunolabelled. Figure 7.10A shows that following ANIT treatment in WT and PXR KO animals, there was an apparent increase in the number of  $\alpha$ -SMA positive cells around portal tracts, particularly surrounding bile ducts. The increase however was less pronounced than that seen after BDL in which more  $\alpha$ -SMA staining was evident both in and around the portal tracts. The results of quantification of the staining is shown in figure 7.10B. Treatment with ANIT in both WT and PXR KO mice caused a small but significant increase in the number of periportal  $\alpha$ -SMA positive cells, qualitatively similar to that seen after BDL.

### **7.6 The PXR protects against ANIT-induced periportal fibrosis**

Fibrosis severity following treatment was assessed by sirius red staining (figure 7.11A). Treatment of mice with ANIT caused increased periportal collagen deposition in both WT and PXR KO mice, with central veins appearing unaffected by treatment. However, the degree of deposition appeared more severe in the PXR KO animals. Quantification of staining (figure 7.11B) indicated that ANIT treatment significantly increased periportal fibrosis in both WT and PXR KO mice similar to that seen after BDL. In the PXR KO mice, periportal fibrosis was significantly more severe than that seen in ANIT treated WT mice. This suggests that the PXR inhibits ANIT induced periportal fibrogenesis.

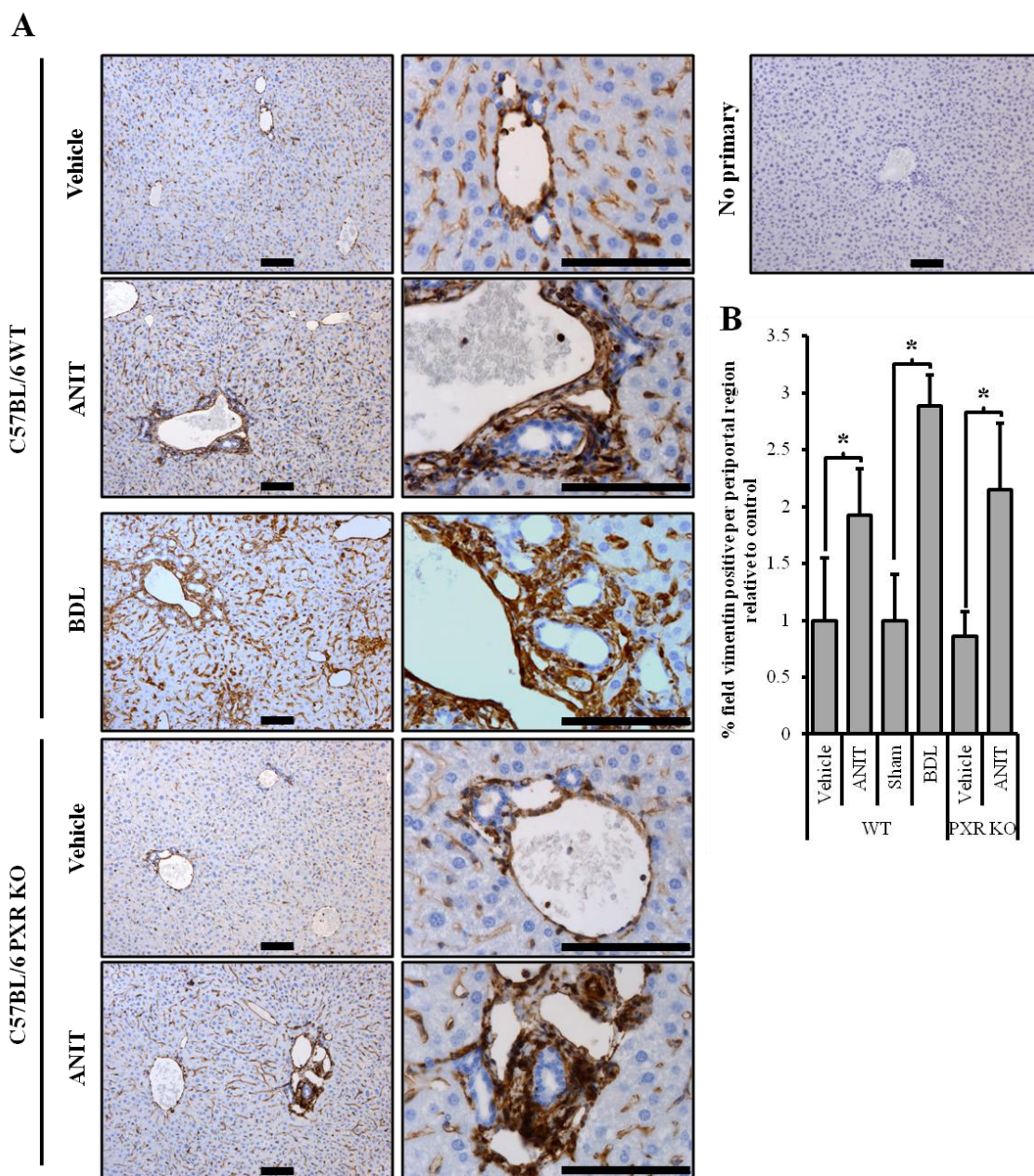


**Figure 7.9: Chronic ANIT treatment causes a significant increase in periportal vimentin staining.**  
**A. Vimentin immunostained liver sections.** Liver fixed in 10% formalin and paraffin embedded was cut into 5 $\mu$ m sections. Sections were dewaxed, rehydrated and endogenous peroxidases blocked. Sections were then subject to sodium citrate antigen retrieval and serum blocking then immunostained for vimentin using DAB to detect bound antibody. Sections were then stained with haematoxylin prior to dehydration, mounting and analysis using a Leica upright microscope. Images are representative of groups and scale bar indicates 100 $\mu$ m. Note, control is from the vehicle control group, which had an identical histopathological appearance to sections from sham BDL operated mice, hence only one view is shown.  
**B. Quantified periportal vimentin staining.** Vimentin staining was quantified using Qwin software: the percentage of periportal regions staining positive for vimentin was calculated around 10 random portal tracts per section per animal by an examiner blinded to the treatment groups. Values are expressed relative to WT vehicle treated mice (or sham for sham and BDL measurements). Data are the mean and SD of the following. Animal numbers – for PXR KO vehicle, n=3; for WT vehicle and BDL, and PXR KO ANIT, n=4; for WT ANIT and sham, n=5. \*significant difference compared to the respective control group at p<0.05.

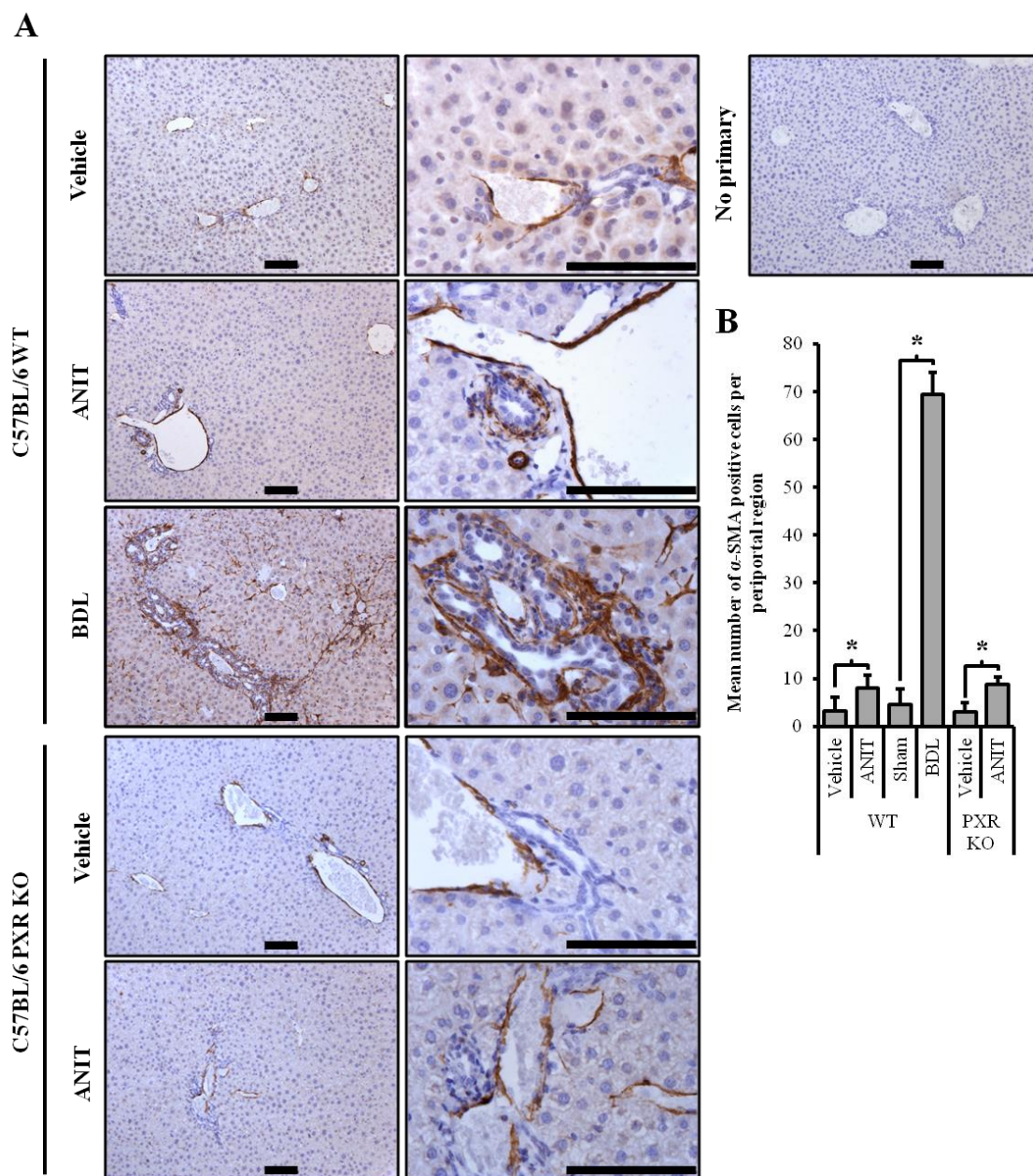


**Figure 7.10: Chronic ANIT treatment causes a significant increase in periportal myfibroblast recruitment/activation. A.  $\alpha$ -SMA immunostained liver sections.** Liver fixed in 10% formalin and paraffin embedded was cut into 5 $\mu$ m sections. Sections were dewaxed, rehydrated and endogenous peroxidases blocked. Sections were then subject to sodium citrate antigen retrieval and serum blocking then immunostained for  $\alpha$ -SMA using DAB to detect bound antibody. Sections were then stained with haematoxylin prior to dehydration, mounting and analysis using a Leica upright microscope. Images are representative of groups and scale bar indicates 100 $\mu$ m. Note, control is from the vehicle control group, which had an identical histopathological appearance to sections from sham BDL operated mice, hence only one view is shown. **B. Quantified number of  $\alpha$ -SMA positive cells per periportal region.** The mean number of  $\alpha$ -SMA positive cells around 6 random portal tracts was calculated per section per animal by an examiner blinded to the treatment groups. Data are the mean and SD of the following animal numbers – for PXR KO vehicle, n=3; for WT vehicle, sham and BDL, and PXR KO ANIT, n=4; for WT ANIT, n=5. \*significant difference compared to the respective control group at  $p < 0.05$ .

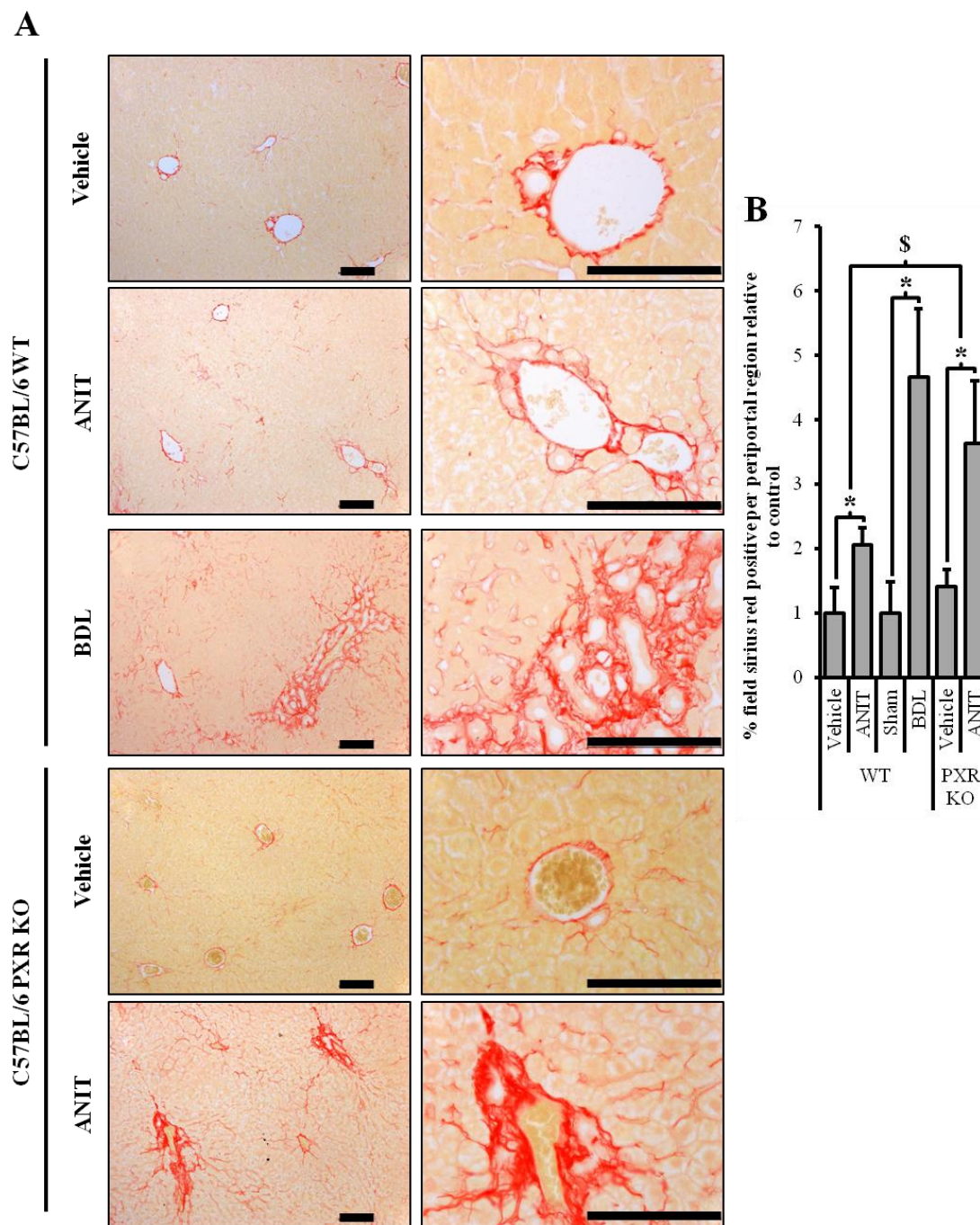


**Figure 7.11: Chronic ANIT treatment causes periportal fibrosis significantly more severe in PXR KO mice. A. Sirius red stained liver sections.** Liver fixed in 10% formalin and paraffin embedded was cut into 5 $\mu$ m sections. Sections were dewaxed and rehydrated and stained with sirius red prior to dehydration, mounting and analysis using a Leica upright microscope. Images are representative of groups and scale bar indicates 100 $\mu$ m. Note, control is from the vehicle control group, which had an identical histopathological appearance to sections from sham BDL operated mice, hence only one view is shown. **B. Quantification of sirius red staining.** Sirius red staining was quantified using Qwin software: the percentage of periportal regions staining positive for collagen was calculated around 10 random portal tracts per section per animal by an examiner blinded to the treatment groups. Values are expressed relative to WT vehicle treated mice (or sham for sham and BDL measurements). Data are the mean and SD of the following animal numbers – for PXR KO vehicle, n=3; for WT vehicle, and PXR KO ANIT, n=4; for WT ANIT, sham and BDL, n=5. \*significant difference compared to the respective control group and § significantly more severe fibrosis compared to WT ANIT treated mice at  $p < 0.05$ .

### **7.7 ANIT administration causes a ductular reaction and induces NTCP expression**

To determine if a ductular reaction was initiated by chronic ANIT treatment, liver sections were stained for CK-19. Figure 7.12A shows that in response to ANIT administration, there was an increase in CK-19 staining around portal tracts in WT and PXR KO mice as seen after BDL. Quantification of the staining (figure 7.12B) confirmed this as ANIT treatment significantly increased periportal CK-19 staining in both WT and PXR KO mice. This confirms that chronic ANIT administration, like BDL, causes initiation of a ductular reaction.

In response to cholestatic disease, the expression of proteins involved in bile acid metabolism are modulated to minimise hepatic damage caused by bile acid accumulation and reduce the synthesis of bile acids from cholesterol [84]. The PXR has been shown to play a role in this homeostatic response and is thought to function to protect against cholestatic injury through regulation of bile acid metabolism [56-59]. It was hypothesised that ANIT treatment would lead to a similar pattern of CYP450 and transporter expression to that seen after BDL.

To test the hypothesis, the expression of the hepatic CYP450s that regulate bile acid synthesis was analysed by qPCR (figure 7.13A). In mice lacking expression of a functional PXR, greater basal levels of CYP7A1 and CYP8B1 mRNA expression were seen compared to WT mice, although the increase was not significant. The chronic administration of ANIT, to WT or PXR KO mice, was not associated with a significant change in the expression of any of the CYP450 mRNAs tested. BDL conversely led to a significant increase in the expression of CYP7A1 mRNA and decreased expression of CYP8B1 mRNA as has been reported previously [61].

The expression of transporters has been shown to change in response to cholestatic disease in the liver in order to ameliorate cellular injury resulting from the intracellular accumulation of bile acids [61, 273]. Analysis of the expression of sinusoidal transporters involved in hepatocyte bile acid influx in this study (figure 7.13B), showed that the mRNA expression of NTCP was significantly higher in ANIT treated WT but not PXR KO mice compared to vehicle treated controls.

In terms of canalicular transporters (figure 7.13C), in BDL mice, the expression of MRP2, MDR1A and MDR2 mRNA, but not BSEP, was significantly increased. No significant changes were seen in WT or PXR KO mice treated with ANIT.

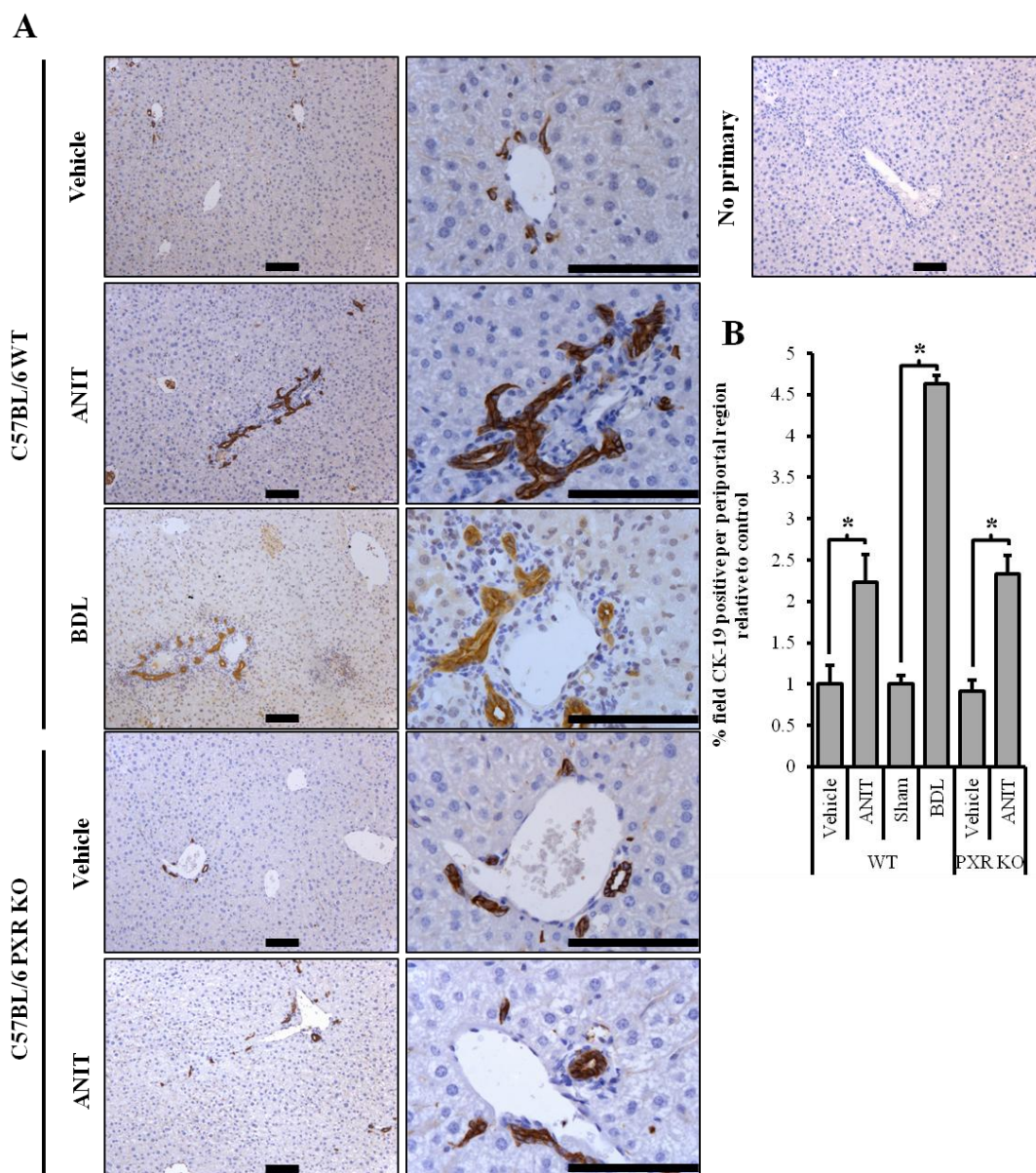


**Figure 7.12: Chronic ANIT treatment causes activation of a ductular reaction. A. CK-19 immunostained liver sections.** Sections were dewaxed, rehydrated and endogenous peroxidases blocked. Sections were then subject to sodium citrate antigen retrieval and serum blocking then immunostained for CK-19 using DAB to detect bound antibody. Sections were then stained with haematoxylin prior to dehydration, mounting and analysis using a Leica upright microscope. Images are representative of groups and scale bar indicates 100 $\mu$ m. Note, control is from the vehicle control group, which had an identical histopathological appearance to sections from sham BDL operated mice, hence only one view is shown. **B. Quantified liver periportal CK-19 staining.** CK-19 staining was quantified using Qwin software: the percentage of periportal regions staining positive for CK-19 was calculated around 10 portal tracts per section per animal by an examiner blinded to the treatment groups. Values are expressed relative to WT vehicle treated mice (or sham for sham and BDL measurements). Data are the mean and SD of the following animal numbers – for WT sham and BDL, and PXR KO vehicle, n=3; for WT vehicle, and PXR KO ANIT, n=4; for WT ANIT, n=5. \*significant difference compared to the respective control group at p<0.05.

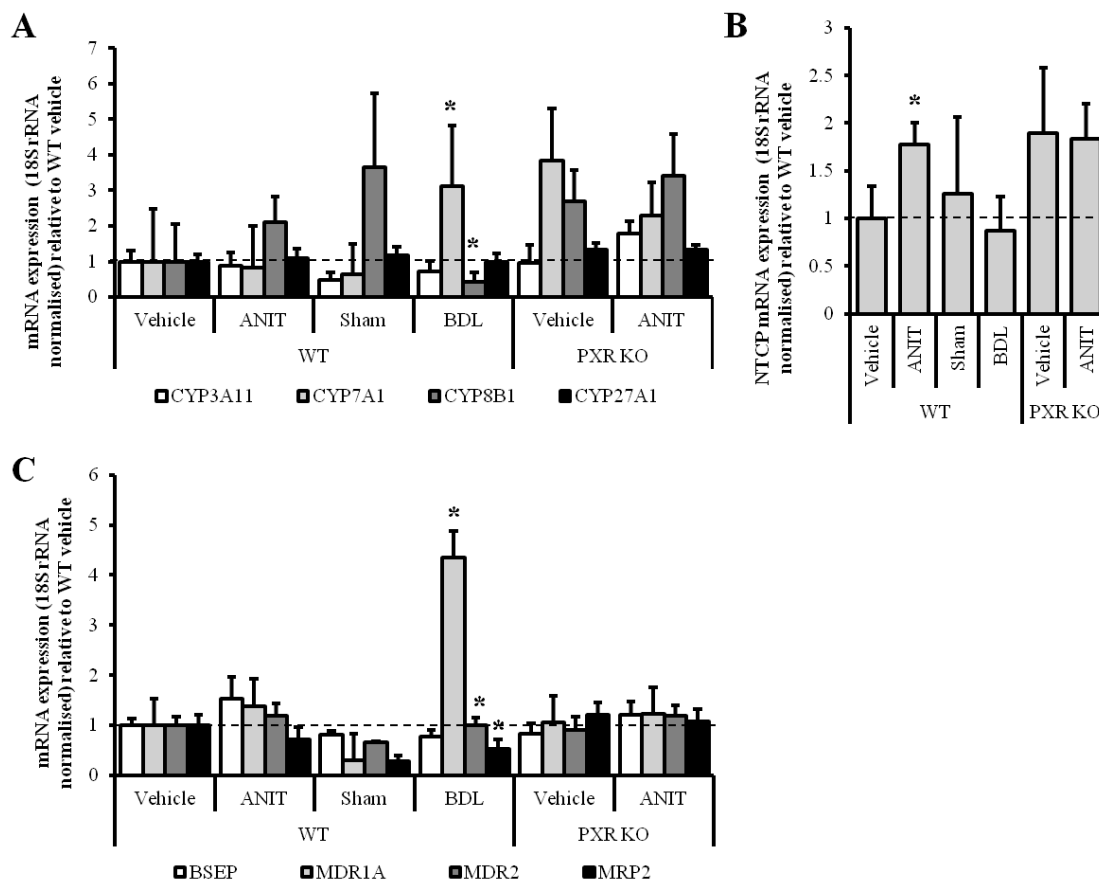


**Figure 7.13: Chronic ANIT treatment significantly increases NTCP expression.** A. Relative mRNA expression of CYP450s involved in bile metabolism. B. Relative mRNA expression of the sinusoidal transporter NTCP. C. Relative mRNA expression of the canalicular transporters BSEP, MDR1A, MDR2 and MRP2. RNA was isolated from liver samples using TRIzol, reverse transcribed and the cDNA used as template for qPCR. Results were normalised to 18S rRNA expression. Data are expressed relative to vehicle treated WT mice and are the mean and SD of the following animal numbers – for PXR KO vehicle, n=3; for WT vehicle and sham, and PXR KO ANIT, n=4; for WT ANIT, n=5; for BDL, n=10. \*indicates significant difference compared to respective control at  $p < 0.05$ .

## 7.8 Chapter discussion

Mice subjected to BDL are a frequently used model for the study of liver disease and periportal fibrosis. Due to severity and practical issues associated with the use of BDL, liver injury resulting from ANIT treatment was investigated and compared to that seen after BDL. The data in this chapter shows that ANIT treatment gives rise to periportal fibrosis qualitatively similar to that seen following BDL. Furthermore, through administration of ANIT in mice lacking expression of a functional PXR, it was seen that the PXR plays an anti-fibrogenic role in this model.

As part of the pilot work, the effect of ANIT on hepatic inflammation was investigated. This showed that a single dose of 50mg/kg ANIT gave rise to long term hepatic inflammation still detectable 39 days after dosing. This was in contrast to CCl<sub>4</sub>, which caused inflammation that peaked around 24 hours before dropping to control levels by day 6. ANIT is detoxified by glutathione conjugation in hepatocytes and effluxed into the bile by MRP2 [306, 322, 323]. Cannulation of the bile duct to prevent enterohepatic recirculation is known to prevent ANIT induced cholestasis and therefore it is expected that a significant proportion of metabolised ANIT is re-absorbed in the gut [324]. In the bile, glutathione conjugated ANIT is documented to be unstable, potentially limiting the efficient clearance of ANIT [322]. The enterohepatic cycling of ANIT would prolong its associated toxicity which could explain the long term inflammation observed. However, the systemic half-life of orally administered ANIT in rats has been shown to be 6 hours and it is likely that the majority of dosed ANIT would be cleared by 48 hours, including from the bile [325, 326]. The long term inflammation observed after a single dose of ANIT could alternatively be due to initiation of a self-sustaining leukocyte-mediated inflammatory response, similar to that seen in human autoimmune liver disorders such as primary biliary cirrhosis. This response may be targeted to/maintained by cholangiocytes, as it is in primary biliary cirrhosis [327], which is plausible considering that they are the primary target of ANIT-mediated toxicity in the liver and ANIT induces cholangiocytes to release leukocyte chemo-attractants [328]. It is clear however that further study is required to ascertain the cause of the prolonged inflammatory response induced by ANIT.

The ability of an acute dose of ANIT to cause significant hepatic inflammation, which can be detected in real time, means that this could be a valuable model in which to test anti-inflammatory compounds. Compared to other *in-vivo* models, this model would allow relatively rapid screening of compounds and reduced group sizes, due to the ability to repeatedly measure an inflammation endpoint in the same animals.

The pattern of hepatic injury seen following chronic ANIT administration was qualitatively similar to that seen after BDL in terms of all measured markers of liver injury. However, for all tested markers, the magnitude of injury was greater in BDL mice compared to ANIT treated mice. This likely reflects that BDL causes constant and

uncontrollable hepatic injury in contrast to the periodic dosing regimen of ANIT. The severity of liver injury resulting from ANIT treatment could possibly be increased by dosing ANIT more regularly or at a higher dose.

Administration of ANIT in both WT mice and mice lacking a functional PXR allowed the role of the PXR in ANIT-induced periportal fibrogenesis to be examined. At the level of inflammation, equivalent severity of portal tract inflammation was observed between WT and PXR KO mice treated with ANIT. Previously published work suggests that activation of the PXR suppresses portal tract inflammation in SJL/J mice, which show chronic hepatic portal tract inflammation [311]. No difference was seen in the severity of portal tract inflammation between SJL/J mice expressing functional PXR and those that did not express functional PXR (SJL-PXR<sup>-/-</sup> mice). This indicates that activation of the PXR is required for its anti-inflammatory role which, considering that the PXR was not activated in this work, is consistent with the similar severity of portal tract inflammation seen in ANIT treated WT and PXR KO mice in this study.

In terms of fibrogenic cell populations, vimentin immunostaining, corresponding to portal tract fibroblasts, was significantly increased by ANIT treatment but unaffected by genotype (no difference between WT or PXR KO mice). The number of  $\alpha$ -SMA positive cells was similarly significantly increased by ANIT treatment although not to a marked extent in comparison with BDL. Using a CCl<sub>4</sub> model of hepatic fibrosis, Marek *et al.*, (2005) showed that, unlike WT mice in which CCl<sub>4</sub> treatment significantly increased both the numbers of  $\alpha$ -SMA positive and negative (myo)fibroblasts, in mice lacking a functional PXR, only the number of  $\alpha$ -SMA negative cells was increased by CCl<sub>4</sub> treatment [321]. These results are in contrast to this study in which ANIT treated WT and PXR KO mice both showed equivalent increases in the numbers of periportal vimentin and  $\alpha$ -SMA positive cells. These differences may be due to the different pattern and localisation of hepatic injury induced by ANIT and CCl<sub>4</sub> treatment.

Interestingly, although the relative increase in the number of (myo)fibroblasts was equivalent between WT and PXR KO mice following ANIT treatment, the severity of periportal fibrosis was significantly greater in the PXR KO mice compared to the mice expressing intact PXR. This finding suggests that the PXR, in WT mice, attenuates fibrogenesis resulting from chronic ANIT treatment. In a CCl<sub>4</sub> induced model of hepatic

fibrosis in contrast, the severity of fibrosis caused by chronic CCl<sub>4</sub> treatment was not markedly changed between WT mice and those lacking expression of a functional PXR [321]. An anti-fibrogenic PXR-dependent effect was only seen, in WT mice, when the PXR was activated by PCN treatment and this effect was lost in mice with a PXR knockout. The role of the PXR, in respect to modulation of fibrogenesis, therefore appears to vary depending on the location of fibrosis development.

Activation of a ductular reaction following ANIT treatment was determined by CK-19 staining. This showed that chronic ANIT administration, similar to BDL, causes activation of a ductular reaction the severity of which was not affected by the absence of a functional PXR.

Evidence suggests that the PXR regulates bile acid synthesis through repression of CYP7A1, which catalyses the rate limiting step in the synthesis of bile acids from cholesterol, but also of CYP8B1, which is required for cholic acid synthesis [60, 329]. The increased basal, though not significant, expression of CYP7A1 and CYP8B1 mRNA in PXR KO mice compared to WT mice is therefore likely due to a loss of transcriptional repression by the PXR.

NTCP is the main hepatocyte transporter involved in influx of bile acids [72]. During cholestasis, the expression of NTCP is repressed by the FXR, as a hepatoprotective mechanism to prevent the intracellular accumulation of bile acids to cytotoxic concentrations [83, 330]. ANIT treatment was shown in this study to significantly increase the expression of NTCP mRNA in WT mice compared to those treated with vehicle alone [321]. The reason and mechanism for the observed induction of NTCP mRNA expression is unclear. Potentially, it may be due to ANIT, or a metabolite, binding and activating the glucocorticoid receptor leading to up-regulation of NTCP expression. DEX treatment has been shown to induce NTCP expression *in-vivo*, acting through the glucocorticoid receptor. The effect was not seen with specific PXR or CAR activators (PCN and TCPOBOP respectively) and was lost in DEX treated mice lacking a functional PXR [331]. However, although functional PXR expression appears to be required for the response, the NTCP promoter lacks a PXR consensus sequence, suggesting that PXR dependency is likely a consequence of cross-talk between the glucocorticoid receptor and PXR signalling pathways such as occurs during CAR and

PXR-mediated DME induction [332]. That the induction of NTCP mRNA was seen in WT mice alone, not in those lacking functional PXR expression, indicates that ANIT or its metabolites may induce NTCP in an equivalent manner to DEX, through the glucocorticoid receptor or downstream.

Up-regulation of canalicular transporter expression is hepatoprotective in order to reduce intracellular accumulation of bile acids and bilirubin. Several canalicular transporters have been shown to be regulated by the PXR including MDR1 and MRP2, but not MDR2 [61, 273, 274]. In this study, BDL, but not ANIT, caused a significant up-regulation of MDR1A, MDR2 and MRP2 mRNA expression, as has been previously shown [61, 273]. Analysis of mRNA expression of enzymes and hepatic transporters involved in bile acid and xenobiotic metabolism indicated that the chronic administration of ANIT was not associated with changes to bile acid synthesis. The expression analysis of CYP450s and transporters involved in hepatobiliary homeostasis are in contrast to previously published studies demonstrating that a single high dose of ANIT (75mg/kg) caused a significant reduction in the mRNA expression of CYP450s CYP7A1, CYP27A1 and CYP8B1 when measured 48 hours after dosing [326, 330]. The mRNA expression of apical transporters MRP2, BSEP and MDR2 were also shown to significantly increase and NTCP expression to decrease in the same study. The markedly different patterns of ANIT administration (75mg/kg ANIT over 48 hours compared to 30mg/kg ANIT dosed over 8 weeks) between this study and those aforementioned are likely the reason for the contrasting results seen.

The data presented in this chapter has shown that chronic administration of ANIT gives rise to significant periportal fibrosis which is qualitatively equivalent to that induced by BDL in mice, thus successfully proving the initial hypothesis. Furthermore, in this model the PXR was shown to play an anti-fibrogenic role in periportal fibrogenesis although the mechanism by which it exerts this effect requires further elucidation. The uncovering of the mechanism is likely complicated by the functional redundancy between nuclear receptors, such as between the PXR and CAR, acting to mask the effect of the PXR knockout [203].

The use of the ANIT model of periportal fibrosis as an alternative to BDL would improve animal welfare and reduce mortality rates whilst likely allowing the severity of

fibrosis generated to be modulated similar to the MP model of periportal fibrosis in the rat. Mice lacking the expression of a functional PXR showed significantly more severe periportal fibrosis in response to chronic ANIT treatment. This result, together with findings from this lab demonstrating reduced severity of CCl<sub>4</sub> induced fibrosis in rodents when treated with the PXR activator PCN [321], suggests that PXR activators could be used for treatment of hepatic fibrosis. The PXR agonists ursodeoxycholic acid and rifampicin are currently used for the treatment of chronic cholestasis and its complications. Unfortunately, rifampicin is associated with hepatotoxicity if administered chronically and the efficacy of ursodeoxycholic acid for the treatment of cholestatic liver disease remains controversial [333-335]. However these compounds are also agonists for targets other than the PXR [335, 336] and there is no evidence that PXR activation alone is toxic [337]. Non-hepatotoxic but potent PXR activators could therefore be a superior approach to treat hepatic fibrosis in a wide range of chronic liver diseases.

## **Chapter 8. General discussion**

Liver disease and the associated fibrosis is prevalent worldwide, the 14<sup>th</sup> leading cause of mortality [138]. Due to the unique architecture and resident cell populations of the liver, liver disease is complex, involving the contributions of, and interactions between, numerous different cell types. Furthermore, the defining cell of the liver, the hepatocyte, is not amenable to tissue culture, rapidly dedifferentiating within a few days to lose all liver specific functions. The complexity of liver disease pathogenesis limits the use of *in-vitro* models in this field of research and necessitates the use of animal models. However many of these models are in need of refinement, including the BDL model of periportal fibrosis. Hepatocytes are responsible for the drug metabolising activity of the liver and human hepatocytes are the gold standard for drug and chemical toxicity screening. However, the limited availability of quality human hepatocytes means that animals are culled to derive hepatocytes and the number of animals required to source hepatocytes is exacerbated by the rapid dedifferentiation and lack of proliferation of hepatocytes in culture. The primary aims of this thesis were to address these issues through the refinement of the BDL model of rodent periportal fibrosis and characterisation of the B-13/H cell as an alternative to primary hepatocytes for drug and chemical toxicity screening.

Investigation of the drug metabolising properties of B-13/H cells demonstrated that they are metabolically competent as the 3 main families of rat CYP450s could be induced (at the mRNA level) and in the case of CYP1A1 and CYP3A1, induced mRNA was translated into functional protein. Furthermore, although CYP4A could not be reliably induced to any marked extent, peroxisome proliferation could be. As B-13 cells are derived from rats, potentially species differences could limit extrapolation of derived results to humans. The stable B-13<sup>TR/h1A2</sup> line was therefore created which stably expressed human CYP1A2. The expressed hCYP1A2 was shown to be functional, as were SULT enzymes required for the bioactivation of the pro-genotoxins PhIP and 1-hydroxyestragole. This work showed the potential in humanising the B-13 line with human genes in order to improve the clinical relevance of the line. Assessment of the drug transporter expression profile of B-13/H cells indicated that they expressed a range of transporters, at least at the level of mRNA, at levels similar to that seen in liver. However, several important hepatic transporters were poorly expressed including MRP2 and BSEP and therefore different strategies were investigated to enhance transporter

expression. HNF4 $\alpha$  overexpression was uniquely shown to induce transporter expression, although no change in MRP or BSEP activity was seen, even with the strong induction of MRP2 protein and BSEP mRNA.

The data presented in this thesis in regard to B-13/H cells suggests that they could be used as an alternative to primary hepatocytes for the study of drug metabolism and drug and chemical toxicity screening. In respect to screening, the suitability for genotoxicity screening in the form of comet assays using B-13/H cells has been validated, however sensitivity to other hepatotoxins such as paracetamol, flutamide and troglitazone has also been recorded although it is not presented in this thesis. In comparison to the most commonly used model of hepatocytes, HepG2 cells, B-13/H cells are a superior model; HepG2 cells show only limited CYP450 activity when compared to primary hepatocytes whereas B-13/H cells show a quantitatively similar pattern of expression, including inducibility in response to prototypical inducers of the primary CYP450 isoforms. Consequently, HepG2 cells are relatively insensitive to hepatotoxins requiring bioactivation by CYP450s other than CYP1A1, which they express [89]. The expression of phase II and III enzymes in HepG2 cells is similar to that of B-13/H cells, with many genes expressed at liver equivalent levels. Although, similar to B-13/H cells, HepG2 cells show low expression of several important transporters including BSEP and NTCP [338].

The use of B-13/H cells as an alternative to primary hepatocytes could solve the issues associated with primary hepatocyte sourcing and culture. An unlimited number of B-13/H cells can be quickly and cheaply generated from B-13 cells, which don't require culling of rats to generate, therefore significantly reducing the number of animals culled to derive hepatocytes. In culture, B-13/H cells have a stable phenotype and unlike primary hepatocytes, B-13 cells can be stably transfected. This allows human genes to be introduced into B-13 cells to increase the clinical predictivity of B-13/H cells. Based on their drug metabolising capacity, further elucidation of the mechanism of B-13 transdifferentiation could allow for the isolation of a human equivalent, which would express human DMEs. This human equivalent would have significant utility for drug and chemical toxicity screening and also for use in bioartificial liver devices.

Investigation of alternatives to BDL in rodents demonstrated that the chronic administration of MP in rats and ANIT in mice gave rise to periportal fibrosis qualitatively equivalent to that seen following BDL. The similarity was seen in terms of significant portal tract inflammation, proliferation of pro-fibrogenic cell populations and development of periportal fibrosis. The MP model of periportal fibrosis in the rat was also reversible when dosing was ceased. This work shows the potential in the chronic administration of MP and ANIT, as alternatives to BDL, for the generation of periportal fibrosis in rats and mice respectively. Compared to BDL, they are not associated with significant mortality or surgical associated complications. In the case of MP, it was also shown that unlike BDL, which causes uncontrollable hepatic injury, MP caused periportal fibrosis of which the severity could be modulated by increasing the dose. Although not tested, this is also likely the case for ANIT induced periportal fibrosis.

Pilot work with ANIT showed that a single dose could cause long term liver portal tract inflammation. Although the mechanism responsible for the long term effect documented was not clear, this model may provide a useful system with which to study hepatic inflammation and therapeutics. Chronic administration of ANIT to PXR KO mice caused significantly more severe periportal fibrosis than that seen in WT mice. This, together with the previously published work showing the hepatoprotective action of the PXR [56, 60, 61, 311], suggests that PXR specific activators could be used as a therapy for patients with liver damage and fibrosis.

The use of chronic administration of hepatotoxins to generate fibrosis is a common method in the study of liver fibrosis, for example the commonly used model of centrilobular fibrosis in rodents involves the chronic administration of CCl<sub>4</sub> over 4-8 weeks [153]. The use of ANIT or MP to generate periportal fibrosis may also therefore help standardise models of liver fibrosis, due to the similar method of fibrosis generation to the CCl<sub>4</sub> model. CCl<sub>4</sub> induced fibrosis for example, will spontaneously reverse when dosing is ceased [163], similar to MP induced fibrosis. Considering the recommendation that novel anti-fibrogenic drugs are tested in a centrilobular and periportal model of fibrosis [16], the similar method of generation of fibrosis between the CCl<sub>4</sub>, MP and ANIT models may help with the comparison of results.

The data presented in this thesis demonstrates the application of the “3Rs” (replacement, refinement and reduction) to liver research. Through the use of B-13/H cells and chronic hepatotoxin administration models of periportal fibrosis, fewer animals would be required for less severe procedures. Further validation of the described models and consideration of the “3Rs” in existing animal based models would ultimately improve research outcomes whilst reducing the number of animals used in scientific procedures.

## References

1. Malarkey, D.E., et al., *New insights into functional aspects of liver morphology*. Toxicologic pathology, 2005. **33**(1): p. 27-34.
2. Schiff, E.R., M.F. Sorrell, and W.C. Maddrey, *Schiff's diseases of the liver*. 10th ed. / [edited by] Eugene R. Schiff, Michael F. Sorrell, Willis C. Maddrey. ed. 2007, Philadelphia ; London: Lippincott Williams & Wilkins. 2 v. (xxxiv, 1576, I-48 p.).
3. Probert, P., *Methapyrilene as an alternative to bile duct ligation for the generation of reproducible hepatic periportal fibrosis*, in *Institute of Cellular Medicine*. MRes Thesis 2011, Newcastle University.
4. Glaser, S.S., et al., *Cholangiocyte proliferation and liver fibrosis*. Expert Rev Mol Med, 2009. **11**: p. e7.
5. Hernandez-Gea, V. and S.L. Friedman, *Pathogenesis of liver fibrosis*. Annual review of pathology, 2011. **6**: p. 425-56.
6. Dranoff, J.A. and R.G. Wells, *Portal fibroblasts: Underappreciated mediators of biliary fibrosis*. Hepatology, 2010. **51**(4): p. 1438-44.
7. Kruglov, E.A., D. Jain, and J.A. Dranoff, *Isolation of primary rat liver fibroblasts*. J Investig Med, 2002. **50**(3): p. 179-84.
8. Li, Z., et al., *Transforming growth factor-beta and substrate stiffness regulate portal fibroblast activation in culture*. Hepatology, 2007. **46**(4): p. 1246-56.
9. Magness, S.T., et al., *A dual reporter gene transgenic mouse demonstrates heterogeneity in hepatic fibrogenic cell populations*. Hepatology, 2004. **40**(5): p. 1151-9.
10. Desmouliere, A., et al., *Extracellular matrix deposition, lysyl oxidase expression, and myofibroblastic differentiation during the initial stages of cholestatic fibrosis in the rat*. Lab Invest, 1997. **76**(6): p. 765-78.
11. Sleyster, E.C. and D.L. Knook, *Relation between localization and function of rat liver Kupffer cells*. Lab Invest, 1982. **47**(5): p. 484-90.
12. Roberts, R.A., et al., *Role of the Kupffer cell in mediating hepatic toxicity and carcinogenesis*. Toxicol Sci, 2007. **96**(1): p. 2-15.
13. Benhamouche, S., et al., *Apc tumor suppressor gene is the "zonation-keeper" of mouse liver*. Dev Cell, 2006. **10**(6): p. 759-70.

14. Sekine, S., et al., *Liver-specific loss of beta-catenin blocks glutamine synthesis pathway activity and cytochrome p450 expression in mice*. *Hepatology*, 2006. **43**(4): p. 817-25.
15. Colnot, S. and C. Perret, *Liver Zonation*, in *Molecular Pathology of Liver Diseases*, S.P.S. Monga, Editor. 2011, Springer. p. 7-16.
16. Wallace, K., A.D. Burt, and M.C. Wright, *Liver fibrosis*. *Biochem J*, 2008. **411**(1): p. 1-18.
17. Apte, U. and P. Krishnamurthy, *Detoxification Functions of the Liver*, in *Molecular Pathology of Liver Diseases*, S.P.S. Monga, Editor. 2011, Springer. p. 147-163.
18. Ogilvie, B.W., et al., *Glucuronidation converts gemfibrozil to a potent, metabolism-dependent inhibitor of CYP2C8: implications for drug-drug interactions*. *Drug Metab Dispos*, 2006. **34**(1): p. 191-7.
19. James, L.P., P.R. Mayeux, and J.A. Hinson, *Acetaminophen-induced hepatotoxicity*. *Drug Metab Dispos*, 2003. **31**(12): p. 1499-506.
20. Guengerich, F.P., *Cytochrome p450 and chemical toxicology*. *Chem Res Toxicol*, 2008. **21**(1): p. 70-83.
21. Lehmann, J.M., et al., *The human orphan nuclear receptor PXR is activated by compounds that regulate CYP3A4 gene expression and cause drug interactions*. *J Clin Invest*, 1998. **102**(5): p. 1016-23.
22. Zanger, U.M., S. Raimundo, and M. Eichelbaum, *Cytochrome P450 2D6: overview and update on pharmacology, genetics, biochemistry*. *Naunyn Schmiedebergs Arch Pharmacol*, 2004. **369**(1): p. 23-37.
23. Oostenbrink, C., et al., *Malleability and versatility of cytochrome P450 active sites studied by molecular simulations*. *Curr Drug Metab*, 2012. **13**(2): p. 190-6.
24. Park, H., S. Lee, and J. Suh, *Structural and dynamical basis of broad substrate specificity, catalytic mechanism, and inhibition of cytochrome P450 3A4*. *J Am Chem Soc*, 2005. **127**(39): p. 13634-42.
25. Walsh, J.S. and G.T. Miwa, *Bioactivation of drugs: risk and drug design*. *Annu Rev Pharmacol Toxicol*, 2011. **51**: p. 145-67.
26. Lee, W.M., *Drug-induced hepatotoxicity*. *N Engl J Med*, 2003. **349**(5): p. 474-85.
27. Holt, M.P. and C. Ju, *Mechanisms of drug-induced liver injury*. *AAPS J*, 2006. **8**(1): p. E48-54.

28. Schuster, D., C. Laggner, and T. Langer, *Why drugs fail--a study on side effects in new chemical entities*. *Curr Pharm Des*, 2005. **11**(27): p. 3545-59.
29. Senior, J.R., *Drug hepatotoxicity from a regulatory perspective*. *Clin Liver Dis*, 2007. **11**(3): p. 507-24, vi.
30. Park, B.K., et al., *Managing the challenge of chemically reactive metabolites in drug development*. *Nat Rev Drug Discov*, 2011. **10**(4): p. 292-306.
31. Tompkins, L.M., T.L. Sit, and A.D. Wallace, *Unique transcription start sites and distinct promoter regions differentiate the pregnane X receptor (PXR) isoforms PXR 1 and PXR 2*. *Drug Metab Dispos*, 2008. **36**(5): p. 923-9.
32. Beischlag, T.V., et al., *The aryl hydrocarbon receptor complex and the control of gene expression*. *Crit Rev Eukaryot Gene Expr*, 2008. **18**(3): p. 207-50.
33. Ma, Q. and A.Y. Lu, *CYP1A induction and human risk assessment: an evolving tale of in vitro and in vivo studies*. *Drug Metab Dispos*, 2007. **35**(7): p. 1009-16.
34. Hankinson, O., *The aryl hydrocarbon receptor complex*. *Annu Rev Pharmacol Toxicol*, 1995. **35**: p. 307-40.
35. Ciolino, H.P., P.J. Daschner, and G.C. Yeh, *Dietary flavonols quercetin and kaempferol are ligands of the aryl hydrocarbon receptor that affect CYP1A1 transcription differentially*. *Biochem J*, 1999. **340** ( Pt 3): p. 715-22.
36. Ciolino, H.P., et al., *Effect of curcumin on the aryl hydrocarbon receptor and cytochrome P450 1A1 in MCF-7 human breast carcinoma cells*. *Biochem Pharmacol*, 1998. **56**(2): p. 197-206.
37. Whitelaw, M.L., et al., *Heat shock protein hsp90 regulates dioxin receptor function in vivo*. *Proc Natl Acad Sci U S A*, 1995. **92**(10): p. 4437-41.
38. Fernandez-Salguero, P., et al., *Immune system impairment and hepatic fibrosis in mice lacking the dioxin-binding Ah receptor*. *Science*, 1995. **268**(5211): p. 722-6.
39. Walisser, J.A., et al., *Gestational exposure of Ahr and Arnt hypomorphs to dioxin rescues vascular development*. *Proc Natl Acad Sci U S A*, 2004. **101**(47): p. 16677-82.
40. Baba, T., et al., *Intrinsic function of the aryl hydrocarbon (dioxin) receptor as a key factor in female reproduction*. *Mol Cell Biol*, 2005. **25**(22): p. 10040-51.
41. Opitz, C.A., et al., *An endogenous tumour-promoting ligand of the human aryl hydrocarbon receptor*. *Nature*, 2011. **478**(7368): p. 197-203.

42. Wang, Y.M., et al., *Role of CAR and PXR in xenobiotic sensing and metabolism*. *Expert Opin Drug Metab Toxicol*, 2012. **8**(7): p. 803-17.
43. Kobayashi, K., et al., *Cytoplasmic accumulation of the nuclear receptor CAR by a tetratricopeptide repeat protein in HepG2 cells*. *Mol Pharmacol*, 2003. **64**(5): p. 1069-75.
44. Yoshinari, K., et al., *Identification of the nuclear receptor CAR:HSP90 complex in mouse liver and recruitment of protein phosphatase 2A in response to phenobarbital*. *FEBS Lett*, 2003. **548**(1-3): p. 17-20.
45. Forman, B.M., et al., *Androstane metabolites bind to and deactivate the nuclear receptor CAR-beta*. *Nature*, 1998. **395**(6702): p. 612-5.
46. Moore, L.B., et al., *Orphan nuclear receptors constitutive androstane receptor and pregnane X receptor share xenobiotic and steroid ligands*. *J Biol Chem*, 2000. **275**(20): p. 15122-7.
47. Mutoh, S., et al., *Dephosphorylation of threonine 38 is required for nuclear translocation and activation of human xenobiotic receptor CAR (NR1I3)*. *J Biol Chem*, 2009. **284**(50): p. 34785-92.
48. Hosseinpour, F., et al., *Serine 202 regulates the nuclear translocation of constitutive active/androstane receptor*. *Mol Pharmacol*, 2006. **69**(4): p. 1095-102.
49. Swales, K. and M. Negishi, *CAR, driving into the future*. *Mol Endocrinol*, 2004. **18**(7): p. 1589-98.
50. Mutoh, S., et al., *Phenobarbital indirectly activates the constitutive active androstane receptor (CAR) by inhibition of epidermal growth factor receptor signaling*. *Sci Signal*, 2013. **6**(274): p. ra31.
51. Saradhi, M., et al., *Pregnane and Xenobiotic Receptor (PXR/SXR) resides predominantly in the nuclear compartment of the interphase cell and associates with the condensed chromosomes during mitosis*. *Biochim Biophys Acta*, 2005. **1746**(2): p. 85-94.
52. Squires, E.J., T. Sueyoshi, and M. Negishi, *Cytoplasmic localization of pregnane X receptor and ligand-dependent nuclear translocation in mouse liver*. *J Biol Chem*, 2004. **279**(47): p. 49307-14.
53. Xie, W., et al., *Reciprocal activation of xenobiotic response genes by nuclear receptors SXR/PXR and CAR*. *Genes Dev*, 2000. **14**(23): p. 3014-23.

54. Sueyoshi, T., et al., *The repressed nuclear receptor CAR responds to phenobarbital in activating the human CYP2B6 gene*. J Biol Chem, 1999. **274**(10): p. 6043-6.
55. di Masi, A., et al., *Nuclear receptors CAR and PXR: Molecular, functional, and biomedical aspects*. Mol Aspects Med, 2009. **30**(5): p. 297-343.
56. Xie, W., et al., *An essential role for nuclear receptors SXR/PXR in detoxification of cholestatic bile acids*. Proceedings of the National Academy of Sciences of the United States of America, 2001. **98**(6): p. 3375-80.
57. Teng, S. and M. Piquette-Miller, *Hepatoprotective role of PXR activation and MRP3 in cholic acid-induced cholestasis*. British journal of pharmacology, 2007. **151**(3): p. 367-76.
58. Jonker, J.W., C. Liddle, and M. Downes, *FXR and PXR: potential therapeutic targets in cholestasis*. The Journal of steroid biochemistry and molecular biology, 2012. **130**(3-5): p. 147-58.
59. Goodwin, B., et al., *Identification of bile acid precursors as endogenous ligands for the nuclear xenobiotic pregnane X receptor*. Proceedings of the National Academy of Sciences of the United States of America, 2003. **100**(1): p. 223-8.
60. Staudinger, J.L., et al., *The nuclear receptor PXR is a lithocholic acid sensor that protects against liver toxicity*. Proceedings of the National Academy of Sciences of the United States of America, 2001. **98**(6): p. 3369-74.
61. Stedman, C.A., et al., *Nuclear receptors constitutive androstane receptor and pregnane X receptor ameliorate cholestatic liver injury*. Proceedings of the National Academy of Sciences of the United States of America, 2005. **102**(6): p. 2063-8.
62. Zhang, J., et al., *The constitutive androstane receptor and pregnane X receptor function coordinately to prevent bile acid-induced hepatotoxicity*. J Biol Chem, 2004. **279**(47): p. 49517-22.
63. Pyper, S.R., et al., *PPARalpha: energy combustion, hypolipidemia, inflammation and cancer*. Nucl Recept Signal, 2010. **8**: p. e002.
64. Chakravarthy, M.V., et al., *Identification of a physiologically relevant endogenous ligand for PPARalpha in liver*. Cell, 2009. **138**(3): p. 476-88.
65. Lee, S.S., et al., *Targeted disruption of the alpha isoform of the peroxisome proliferator-activated receptor gene in mice results in abolishment of the*

- pleiotropic effects of peroxisome proliferators*. Mol Cell Biol, 1995. **15**(6): p. 3012-22.
66. Kersten, S., et al., *Peroxisome proliferator-activated receptor alpha mediates the adaptive response to fasting*. J Clin Invest, 1999. **103**(11): p. 1489-98.
67. Bays, H. and E.A. Stein, *Pharmacotherapy for dyslipidaemia--current therapies and future agents*. Expert Opin Pharmacother, 2003. **4**(11): p. 1901-38.
68. Gonzalez, F.J. and Y.M. Shah, *PPARalpha: mechanism of species differences and hepatocarcinogenesis of peroxisome proliferators*. Toxicology, 2008. **246**(1): p. 2-8.
69. Peters, J.M., C. Cheung, and F.J. Gonzalez, *Peroxisome proliferator-activated receptor-alpha and liver cancer: where do we stand?* J Mol Med (Berl), 2005. **83**(10): p. 774-85.
70. Huber, W.W., B. Grasl-Kraupp, and R. Schulte-Hermann, *Hepatocarcinogenic potential of di(2-ethylhexyl)phthalate in rodents and its implications on human risk*. Crit Rev Toxicol, 1996. **26**(4): p. 365-481.
71. Hurst, C.H. and D.J. Waxman, *Activation of PPARalpha and PPARgamma by environmental phthalate monoesters*. Toxicol Sci, 2003. **74**(2): p. 297-308.
72. Dawson, P.A., T. Lan, and A. Rao, *Bile acid transporters*. Journal of lipid research, 2009. **50**(12): p. 2340-57.
73. Sekine, T., H. Miyazaki, and H. Endou, *Molecular physiology of renal organic anion transporters*. American journal of physiology. Renal physiology, 2006. **290**(2): p. F251-61.
74. Eckhardt, U., et al., *Polyspecific substrate uptake by the hepatic organic anion transporter Oatp1 in stably transfected CHO cells*. The American journal of physiology, 1999. **276**(4 Pt 1): p. G1037-42.
75. Hagenbuch, B. and C. Gui, *Xenobiotic transporters of the human organic anion transporting polypeptides (OATP) family*. Xenobiotica; the fate of foreign compounds in biological systems, 2008. **38**(7-8): p. 778-801.
76. Cusatis, G., et al., *Pharmacogenetics of ABCG2 and adverse reactions to gefitinib*. Journal of the National Cancer Institute, 2006. **98**(23): p. 1739-42.
77. Muller, M. and P.L. Jansen, *Molecular aspects of hepatobiliary transport*. The American journal of physiology, 1997. **272**(6 Pt 1): p. G1285-303.
78. Kruh, G.D. and M.G. Belinsky, *The MRP family of drug efflux pumps*. Oncogene, 2003. **22**(47): p. 7537-52.

79. Rius, M., et al., *Substrate specificity of human ABCC4 (MRP4)-mediated cotransport of bile acids and reduced glutathione*. American journal of physiology. Gastrointestinal and liver physiology, 2006. **290**(4): p. G640-9.
80. Arias, I.M., *The liver : biology and pathobiology*. 5th ed. ed. 2009, Oxford: Wiley-Blackwell. xxii, 1191 p. [24] p. of plates.
81. Funk, C., *The role of hepatic transporters in drug elimination*. Expert Opin Drug Metab Toxicol, 2008. **4**(4): p. 363-79.
82. Pauli-Magnus, C. and P.J. Meier, *Hepatobiliary transporters and drug-induced cholestasis*. Hepatology, 2006. **44**(4): p. 778-87.
83. Eloranta, J.J. and G.A. Kullak-Ublick, *Coordinate transcriptional regulation of bile acid homeostasis and drug metabolism*. Arch Biochem Biophys, 2005. **433**(2): p. 397-412.
84. Handschin, C. and U.A. Meyer, *Regulatory network of lipid-sensing nuclear receptors: roles for CAR, PXR, LXR, and FXR*. Arch Biochem Biophys, 2005. **433**(2): p. 387-96.
85. Bass, A.S., et al., *Exploratory drug safety: a discovery strategy to reduce attrition in development*. J Pharmacol Toxicol Methods, 2009. **60**(1): p. 69-78.
86. Fraczek, J., et al., *Primary hepatocyte cultures for pharmaco-toxicological studies: at the busy crossroad of various anti-dedifferentiation strategies*. Arch Toxicol, 2013. **87**(4): p. 577-610.
87. Russell, W.M.S. and R.L. Burch, *The principles of humane experimental technique*. 1959, London: Methuen & Co. 252p.
88. Madan, A., et al., *Effects of prototypical microsomal enzyme inducers on cytochrome P450 expression in cultured human hepatocytes*. Drug Metab Dispos, 2003. **31**(4): p. 421-31.
89. Hewitt, N.J., et al., *Primary hepatocytes: current understanding of the regulation of metabolic enzymes and transporter proteins, and pharmaceutical practice for the use of hepatocytes in metabolism, enzyme induction, transporter, clearance, and hepatotoxicity studies*. Drug Metab Rev, 2007. **39**(1): p. 159-234.
90. Guguen-Guillouzo, C. and A. Guillouzo, *General review on in vitro hepatocyte models and their applications*. Methods Mol Biol, 2010. **640**: p. 1-40.
91. Paine, A.J. and E. Andreakos, *Activation of signalling pathways during hepatocyte isolation: relevance to toxicology in vitro*. Toxicol In Vitro, 2004. **18**(2): p. 187-93.

92. Hodgkinson, C.P., M.C. Wright, and A.J. Paine, *Fibronectin-mediated hepatocyte shape change reprograms cytochrome P450 2C11 gene expression via an integrin-signaled induction of ribonuclease activity*. *Mol Pharmacol*, 2000. **58**(5): p. 976-81.
93. Rodriguez-Antona, C., et al., *Cytochrome P450 expression in human hepatocytes and hepatoma cell lines: molecular mechanisms that determine lower expression in cultured cells*. *Xenobiotica*, 2002. **32**(6): p. 505-20.
94. Mizuguchi, T., et al., *Alteration of expression of liver-enriched transcription factors in the transition between growth and differentiation of primary cultured rat hepatocytes*. *J Cell Physiol*, 1998. **174**(3): p. 273-84.
95. Baker, T.K., et al., *Temporal gene expression analysis of monolayer cultured rat hepatocytes*. *Chem Res Toxicol*, 2001. **14**(9): p. 1218-31.
96. Beigel, J., et al., *Genomics and proteomics analysis of cultured primary rat hepatocytes*. *Toxicol In Vitro*, 2008. **22**(1): p. 171-81.
97. Richert, L., et al., *Evaluation of the effect of culture configuration on morphology, survival time, antioxidant status and metabolic capacities of cultured rat hepatocytes*. *Toxicol In Vitro*, 2002. **16**(1): p. 89-99.
98. Sidhu, J.S., F. Liu, and C.J. Omiecinski, *Phenobarbital responsiveness as a uniquely sensitive indicator of hepatocyte differentiation status: requirement of dexamethasone and extracellular matrix in establishing the functional integrity of cultured primary rat hepatocytes*. *Exp Cell Res*, 2004. **292**(2): p. 252-64.
99. Isom, H.C., et al., *Maintenance of differentiated rat hepatocytes in primary culture*. *Proc Natl Acad Sci U S A*, 1985. **82**(10): p. 3252-6.
100. Henkens, T., et al., *Trichostatin A, a critical factor in maintaining the functional differentiation of primary cultured rat hepatocytes*. *Toxicol Appl Pharmacol*, 2007. **218**(1): p. 64-71.
101. Kia, R., et al., *Stem cell-derived hepatocytes as a predictive model for drug-induced liver injury: are we there yet?* *Br J Clin Pharmacol*, 2013. **75**(4): p. 885-96.
102. Baxter, M.A., et al., *Generating hepatic cell lineages from pluripotent stem cells for drug toxicity screening*. *Stem Cell Res*, 2010. **5**(1): p. 4-22.
103. Chen, Y.F., et al., *Rapid generation of mature hepatocyte-like cells from human induced pluripotent stem cells by an efficient three-step protocol*. *Hepatology*, 2012. **55**(4): p. 1193-203.

104. Duan, Y., et al., *Differentiation and characterization of metabolically functioning hepatocytes from human embryonic stem cells*. *Stem Cells*, 2010. **28**(4): p. 674-86.
105. Rowe, C., et al., *Proteome-wide analyses of human hepatocytes during differentiation and dedifferentiation*. *Hepatology*, 2013. **58**(2): p. 799-809.
106. Aden, D.P., et al., *Controlled synthesis of HBsAg in a differentiated human liver carcinoma-derived cell line*. *Nature*, 1979. **282**(5739): p. 615-6.
107. Knowles, B.B., C.C. Howe, and D.P. Aden, *Human hepatocellular carcinoma cell lines secrete the major plasma proteins and hepatitis B surface antigen*. *Science*, 1980. **209**(4455): p. 497-9.
108. Aninat, C., et al., *Expression of cytochromes P450, conjugating enzymes and nuclear receptors in human hepatoma HepaRG cells*. *Drug Metab Dispos*, 2006. **34**(1): p. 75-83.
109. Gerets, H.H., et al., *Characterization of primary human hepatocytes, HepG2 cells, and HepaRG cells at the mRNA level and CYP activity in response to inducers and their predictivity for the detection of human hepatotoxins*. *Cell Biol Toxicol*, 2012. **28**(2): p. 69-87.
110. Westerink, W.M. and W.G. Schoonen, *Cytochrome P450 enzyme levels in HepG2 cells and cryopreserved primary human hepatocytes and their induction in HepG2 cells*. *Toxicol In Vitro*, 2007. **21**(8): p. 1581-91.
111. Wilkening, S., F. Stahl, and A. Bader, *Comparison of primary human hepatocytes and hepatoma cell line Hepg2 with regard to their biotransformation properties*. *Drug Metab Dispos*, 2003. **31**(8): p. 1035-42.
112. Hart, S.N., et al., *A comparison of whole genome gene expression profiles of HepaRG cells and HepG2 cells to primary human hepatocytes and human liver tissues*. *Drug Metab Dispos*, 2010. **38**(6): p. 988-94.
113. Castell, J.V., et al., *Hepatocyte cell lines: their use, scope and limitations in drug metabolism studies*. *Expert Opin Drug Metab Toxicol*, 2006. **2**(2): p. 183-212.
114. Yoshitomi, S., et al., *Establishment of the transformants expressing human cytochrome P450 subtypes in HepG2, and their applications on drug metabolism and toxicology*. *Toxicol In Vitro*, 2001. **15**(3): p. 245-56.

115. Tolosa, L., et al., *HepG2 cells simultaneously expressing five P450 enzymes for the screening of hepatotoxicity: identification of bioactivable drugs and the potential mechanism of toxicity involved*. Arch Toxicol, 2013. **87**(6): p. 1115-27.
116. Gripon, P., et al., *Infection of a human hepatoma cell line by hepatitis B virus*. Proc Natl Acad Sci U S A, 2002. **99**(24): p. 15655-60.
117. Parent, R., et al., *Origin and characterization of a human bipotent liver progenitor cell line*. Gastroenterology, 2004. **126**(4): p. 1147-56.
118. Antherieu, S., et al., *Stable expression, activity, and inducibility of cytochromes P450 in differentiated HepaRG cells*. Drug Metab Dispos, 2010. **38**(3): p. 516-25.
119. Longnecker, D.S., et al., *Transplantation of azaserine-induced carcinomas of pancreas in rats*. Cancer letters, 1979. **7**(4): p. 197-202.
120. Christophe, J., *Pancreatic tumoral cell line AR42J: an amphicrine model*. Am J Physiol, 1994. **266**(6 Pt 1): p. G963-71.
121. Mashima, H., et al., *Formation of insulin-producing cells from pancreatic acinar AR42J cells by hepatocyte growth factor*. Endocrinology, 1996. **137**(9): p. 3969-76.
122. Mashima, H., et al., *Betacellulin and activin A coordinately convert amylase-secreting pancreatic AR42J cells into insulin-secreting cells*. The Journal of clinical investigation, 1996. **97**(7): p. 1647-54.
123. Shen, C.N., J.M. Slack, and D. Tosh, *Molecular basis of transdifferentiation of pancreas to liver*. Nat Cell Biol, 2000. **2**(12): p. 879-87.
124. Marek, C.J., et al., *Generation of hepatocytes expressing functional cytochromes P450 from a pancreatic progenitor cell line in vitro*. Biochem J, 2003. **370**(Pt 3): p. 763-9.
125. Tosh, D., C.N. Shen, and J.M. Slack, *Differentiated properties of hepatocytes induced from pancreatic cells*. Hepatology, 2002. **36**(3): p. 534-43.
126. Wallace, K., et al., *Exocrine pancreas trans-differentiation to hepatocytes--a physiological response to elevated glucocorticoid in vivo*. J Steroid Biochem Mol Biol, 2009. **116**(1-2): p. 76-85.
127. Wallace, K., et al., *Disrupted pancreatic exocrine differentiation and malabsorption in response to chronic elevated systemic glucocorticoid*. Am J Pathol, 2010. **177**(3): p. 1225-32.

128. Fairhall, E.A., et al., *Adult human exocrine pancreas differentiation to hepatocytes – potential source of a human hepatocyte progenitor for use in toxicology research*. Toxicology Research, 2013(2): p. 80-87.
129. Wallace, K., et al., *Glucocorticoid-dependent transdifferentiation of pancreatic progenitor cells into hepatocytes is dependent on transient suppression of WNT signalling*. J Cell Sci, 2010. **123**(Pt 12): p. 2103-10.
130. Wallace, K., et al., *Serine/threonine protein kinase SGK1 in glucocorticoid-dependent transdifferentiation of pancreatic acinar cells to hepatocytes*. J Cell Sci, 2011. **124**(Pt 3): p. 405-13.
131. Maiyar, A.C., et al., *Repression of glucocorticoid receptor transactivation and DNA binding of a glucocorticoid response element within the serum/glucocorticoid-inducible protein kinase (sgk) gene promoter by the p53 tumor suppressor protein*. Mol Endocrinol, 1997. **11**(3): p. 312-29.
132. Webster, M.K., et al., *Characterization of sgk, a novel member of the serine/threonine protein kinase gene family which is transcriptionally induced by glucocorticoids and serum*. Mol Cell Biol, 1993. **13**(4): p. 2031-40.
133. Wu, S.Y., et al., *Differentiation of pancreatic acinar cells to hepatocytes requires an intermediate cell type*. Gastroenterology, 2010. **138**(7): p. 2519-30.
134. Hafezi-Moghadam, A., et al., *Acute cardiovascular protective effects of corticosteroids are mediated by non-transcriptional activation of endothelial nitric oxide synthase*. Nat Med, 2002. **8**(5): p. 473-9.
135. Cross, D.A., et al., *Inhibition of glycogen synthase kinase-3 by insulin mediated by protein kinase B*. Nature, 1995. **378**(6559): p. 785-9.
136. Pearce, L.R., D. Komander, and D.R. Alessi, *The nuts and bolts of AGC protein kinases*. Nat Rev Mol Cell Biol, 2010. **11**(1): p. 9-22.
137. Burke, Z.D., et al., *Characterization of liver function in transdifferentiated hepatocytes*. J Cell Physiol, 2006. **206**(1): p. 147-59.
138. Lim, Y.S. and W.R. Kim, *The global impact of hepatic fibrosis and end-stage liver disease*. Clinics in liver disease, 2008. **12**(4): p. 733-46, vii.
139. Alter, M.J., *Epidemiology of viral hepatitis and HIV co-infection*. J Hepatol, 2006. **44**(1 Suppl): p. S6-9.
140. NHS. *Alcoholic liver disease*. [NHS. (2009). Alcoholic liver disease, [online] Available at

- [http://www.nhs.uk/Conditions/Liver\\_disease\\_\(alcoholic\)/Pages/Introduction.aspx](http://www.nhs.uk/Conditions/Liver_disease_(alcoholic)/Pages/Introduction.aspx). [accessed 4 July 2011].] 2009 [cited 2011 4 July].
141. Williams, R., *Global challenges in liver disease*. Hepatology, 2006. **44**(3): p. 521-6.
  142. NHS. *Primary biliary cirrhosis*. [NHS. (2011). Primary biliary cirrhosis, [online] Available at <http://www.nhs.uk/conditions/Primary-biliary-cirrhosis/Pages/Introduction.aspx>. [accessed 25 April 2011].] 2011 [cited 2011 25 April].
  143. Wynn, T.A. and T.R. Ramalingam, *Mechanisms of fibrosis: therapeutic translation for fibrotic disease*. Nat Med, 2012. **18**(7): p. 1028-40.
  144. Anthony, P.P., et al., *The morphology of cirrhosis: definition, nomenclature, and classification*. Bulletin of the World Health Organization, 1977. **55**(4): p. 521-40.
  145. Wells, R.G., *The Portal Fibroblast: Not Just a Poor Man's Stellate Cell*. Gastroenterology.
  146. Beaussier, M., et al., *Prominent contribution of portal mesenchymal cells to liver fibrosis in ischemic and obstructive cholestatic injuries*. Lab Invest, 2007. **87**(3): p. 292-303.
  147. Mederacke, I., et al., *Fate tracing reveals hepatic stellate cells as dominant contributors to liver fibrosis independent of its aetiology*. Nat Commun. **4**: p. 2823.
  148. Sedlacek, N., et al., *Proliferating bile duct epithelial cells are a major source of connective tissue growth factor in rat biliary fibrosis*. Am J Pathol, 2001. **158**(4): p. 1239-44.
  149. Milani, S., et al., *Transforming growth factors beta 1 and beta 2 are differentially expressed in fibrotic liver disease*. Am J Pathol, 1991. **139**(6): p. 1221-9.
  150. Grappone, C., et al., *Expression of platelet-derived growth factor in newly formed cholangiocytes during experimental biliary fibrosis in rats*. J Hepatol, 1999. **31**(1): p. 100-9.
  151. Omenetti, A., et al., *Hedgehog-mediated mesenchymal-epithelial interactions modulate hepatic response to bile duct ligation*. Lab Invest, 2007. **87**(5): p. 499-514.

152. Friedman, S.L., et al., *Isolated hepatic lipocytes and Kupffer cells from normal human liver: morphological and functional characteristics in primary culture*. *Hepatology*, 1992. **15**(2): p. 234-43.
153. Starkel, P. and I.A. Leclercq, *Animal models for the study of hepatic fibrosis*. *Best Pract Res Clin Gastroenterol*, 2011. **25**(2): p. 319-33.
154. Wong, F.W., W.Y. Chan, and S.S. Lee, *Resistance to carbon tetrachloride-induced hepatotoxicity in mice which lack CYP2E1 expression*. *Toxicol Appl Pharmacol*, 1998. **153**(1): p. 109-18.
155. Yoo, J.S., H. Ishizaki, and C.S. Yang, *Roles of cytochrome P450IIE1 in the dealkylation and denitrosation of N-nitrosodimethylamine and N-nitrosodiethylamine in rat liver microsomes*. *Carcinogenesis*, 1990. **11**(12): p. 2239-43.
156. Pegg, A.E., W. Perry, and R.A. Bennett, *Effect of partial hepatectomy on removal of O6-methylguanine from alkylated DNA by rat liver extracts*. *Biochem J*, 1981. **197**(1): p. 195-201.
157. Hirata, K., et al., *Hepatic sinusoidal cell destruction in the development of intravascular coagulation in acute liver failure of rats*. *J Pathol*, 1989. **158**(2): p. 157-65.
158. Chilakapati, J., et al., *Toxicokinetics and toxicity of thioacetamide sulfoxide: a metabolite of thioacetamide*. *Toxicology*, 2007. **230**(2-3): p. 105-16.
159. Kang, J.S., et al., *Role of CYP2E1 in thioacetamide-induced mouse hepatotoxicity*. *Toxicol Appl Pharmacol*, 2008. **228**(3): p. 295-300.
160. Palmeira, C.M. and A.P. Rolo, *Mitochondrially-mediated toxicity of bile acids*. *Toxicology*, 2004. **203**(1-3): p. 1-15.
161. Tuchweber, B., et al., *Proliferation and phenotypic modulation of portal fibroblasts in the early stages of cholestatic fibrosis in the rat*. *Lab Invest*, 1996. **74**(1): p. 265-78.
162. Cassiman, D., et al., *Hepatic stellate cell/myofibroblast subpopulations in fibrotic human and rat livers*. *Journal of hepatology*, 2002. **36**(2): p. 200-9.
163. Iredale, J.P., *Models of liver fibrosis: exploring the dynamic nature of inflammation and repair in a solid organ*. *J Clin Invest*, 2007. **117**(3): p. 539-48.
164. Carlsen, H., et al., *In vivo imaging of NF-kappa B activity*. *J Immunol*, 2002. **168**(3): p. 1441-6.

165. de la Iglesia, N., et al., *The role of the regulatory protein of glucokinase in the glucose sensory mechanism of the hepatocyte*. J Biol Chem, 2000. **275**(14): p. 10597-603.
166. Vogelstein, B. and D. Gillespie, *Preparative and analytical purification of DNA from agarose*. Proc Natl Acad Sci U S A, 1979. **76**(2): p. 615-9.
167. Shuman, S., *Novel approach to molecular cloning and polynucleotide synthesis using vaccinia DNA topoisomerase*. J Biol Chem, 1994. **269**(51): p. 32678-84.
168. Thorvaldsdottir, H., J.T. Robinson, and J.P. Mesirov, *Integrative Genomics Viewer (IGV): high-performance genomics data visualization and exploration*. Brief Bioinform, 2013. **14**(2): p. 178-92.
169. Chomczynski, P. and N. Sacchi, *Single-step method of RNA isolation by acid guanidinium thiocyanate-phenol-chloroform extraction*. Anal Biochem, 1987. **162**(1): p. 156-9.
170. Barbas, C.F., 3rd, et al., *Quantitation of DNA and RNA*. CSH Protoc, 2007. **2007**: p. pdb ip47.
171. Lundberg, K.S., et al., *High-fidelity amplification using a thermostable DNA polymerase isolated from Pyrococcus furiosus*. Gene, 1991. **108**(1): p. 1-6.
172. Yuan, J.S., et al., *Statistical analysis of real-time PCR data*. BMC Bioinformatics, 2006. **7**: p. 85.
173. Lowry, O.H., et al., *Protein measurement with the Folin phenol reagent*. J Biol Chem, 1951. **193**(1): p. 265-75.
174. Laemmli, U.K., *Cleavage of structural proteins during the assembly of the head of bacteriophage T4*. Nature, 1970. **227**(5259): p. 680-5.
175. Junqueira, L.C., G. Bignolas, and R.R. Brentani, *Picosirius staining plus polarization microscopy, a specific method for collagen detection in tissue sections*. Histochem J, 1979. **11**(4): p. 447-55.
176. Kubista, M., B. Akerman, and B. Norden, *Characterization of interaction between DNA and 4',6-diamidino-2-phenylindole by optical spectroscopy*. Biochemistry, 1987. **26**(14): p. 4545-53.
177. Schneider, C.A., W.S. Rasband, and K.W. Eliceiri, *NIH Image to ImageJ: 25 years of image analysis*. Nature Methods, 2012. **9**: p. 671-675.
178. Burke, M.D. and R.T. Mayer, *Ethoxyresorufin: direct fluorimetric assay of a microsomal O-dealkylation which is preferentially inducible by 3-methylcholanthrene*. Drug Metab Dispos, 1974. **2**(6): p. 583-8.

179. Lubet, R.A., et al., *Dealkylation of pentoxyresorufin: a rapid and sensitive assay for measuring induction of cytochrome(s) P-450 by phenobarbital and other xenobiotics in the rat*. Arch Biochem Biophys, 1985. **238**(1): p. 43-8.
180. Nerurkar, P.V., et al., *Methoxyresorufin and benzyloxyresorufin: substrates preferentially metabolized by cytochromes P4501A2 and 2B, respectively, in the rat and mouse*. Biochem Pharmacol, 1993. **46**(5): p. 933-43.
181. Singh, N.P., et al., *A simple technique for quantitation of low levels of DNA damage in individual cells*. Exp Cell Res, 1988. **175**(1): p. 184-91.
182. Omura, T. and R. Sato, *The Carbon Monoxide-Binding Pigment of Liver Microsomes. I. Evidence for Its Hemoprotein Nature*. J Biol Chem, 1964. **239**: p. 2370-8.
183. Toyoki, Y., et al., *Semiquantitative evaluation of hepatic fibrosis by measuring tissue hydroxyproline*. Hepatogastroenterology, 1998. **45**(24): p. 2261-4.
184. Fairhall, E.A., et al., *The "3Rs" hepatocyte progenitor B-13 cell resists pluripotency induction and differentiation to non-hepatocyte cells*. Toxicology Research, 2013(2): p. 308-320.
185. Yamazaki, H., et al., *Roles of NADPH-P450 reductase and apo- and holo-cytochrome b5 on xenobiotic oxidations catalyzed by 12 recombinant human cytochrome P450s expressed in membranes of Escherichia coli*. Protein Expr Purif, 2002. **24**(3): p. 329-37.
186. Waxman, D.J. and M.G. Holloway, *Sex differences in the expression of hepatic drug metabolizing enzymes*. Mol Pharmacol, 2009. **76**(2): p. 215-28.
187. Tannenbaum, G.S. and J.B. Martin, *Evidence for an endogenous ultradian rhythm governing growth hormone secretion in the rat*. Endocrinology, 1976. **98**(3): p. 562-70.
188. Eden, S., *Age- and sex-related differences in episodic growth hormone secretion in the rat*. Endocrinology, 1979. **105**(2): p. 555-60.
189. Morgan, E.T., C. MacGeoch, and J.A. Gustafsson, *Hormonal and developmental regulation of expression of the hepatic microsomal steroid 16 alpha-hydroxylase cytochrome P-450 apoprotein in the rat*. J Biol Chem, 1985. **260**(22): p. 11895-8.
190. MacGeoch, C., et al., *Purification, characterization, and pituitary regulation of the sex-specific cytochrome P-450 15 beta-hydroxylase from liver microsomes of untreated female rats*. J Biol Chem, 1984. **259**(24): p. 15433-9.

191. Pampori, N.A. and B.H. Shapiro, *Feminization of hepatic cytochrome P450s by nominal levels of growth hormone in the feminine plasma profile*. Mol Pharmacol, 1996. **50**(5): p. 1148-56.
192. Thangavel, C., M.C. Garcia, and B.H. Shapiro, *Intrinsic sex differences determine expression of growth hormone-regulated female cytochrome P450s*. Mol Cell Endocrinol, 2004. **220**(1-2): p. 31-9.
193. Henderson, C.J., et al., *Sexual differentiation and regulation of cytochrome P-450 CYP2C7*. Biochim Biophys Acta, 1992. **1118**(2): p. 99-106.
194. Yano, M., E. Falvey, and F.J. Gonzalez, *Role of the liver-enriched transcription factor DBP in expression of the cytochrome P450 CYP2C6 gene*. Mol Cell Biol, 1992. **12**(6): p. 2847-54.
195. Thangavel, C., W. Dworakowski, and B.H. Shapiro, *Inducibility of male-specific isoforms of cytochrome p450 by sex-dependent growth hormone profiles in hepatocyte cultures from male but not female rats*. Drug Metab Dispos, 2006. **34**(3): p. 410-9.
196. Ratra, G.S., S. Cottrell, and C.J. Powell, *Effects of induction and inhibition of cytochromes P450 on the hepatotoxicity of methapyrilene*. Toxicol Sci, 1998. **46**(1): p. 185-96.
197. McFadyen, M.C. and G.I. Murray, *Cytochrome P450 1B1: a novel anticancer therapeutic target*. Future Oncol, 2005. **1**(2): p. 259-63.
198. Tompkins, L.M. and A.D. Wallace, *Mechanisms of cytochrome P450 induction*. J Biochem Mol Toxicol, 2007. **21**(4): p. 176-81.
199. Tassaneeyakul, W., et al., *Specificity of substrate and inhibitor probes for human cytochromes P450 1A1 and 1A2*. J Pharmacol Exp Ther, 1993. **265**(1): p. 401-7.
200. Shimada, T., et al., *Metabolic activation of polycyclic aromatic hydrocarbons and other procarcinogens by cytochromes P450 1A1 and P450 1B1 allelic variants and other human cytochromes P450 in Salmonella typhimurium NM2009*. Drug Metab Dispos, 2001. **29**(9): p. 1176-82.
201. Choucroun, P., et al., *Comet assay and early apoptosis*. Mutat Res, 2001. **478**(1-2): p. 89-96.
202. Mosesso, P., et al., *The use of cyprinodont fish, *Aphanius fasciatus*, as a sentinel organism to detect complex genotoxic mixtures in the coastal lagoon ecosystem*. Mutat Res, 2012. **742**(1-2): p. 31-6.

203. Kliewer, S.A., B. Goodwin, and T.M. Willson, *The nuclear pregnane X receptor: a key regulator of xenobiotic metabolism*. *Endocr Rev*, 2002. **23**(5): p. 687-702.
204. Greenblatt, D.J., et al., *Mechanism of cytochrome P450-3A inhibition by ketoconazole*. *J Pharm Pharmacol*, 2011. **63**(2): p. 214-21.
205. Watkins, P.B., et al., *Erythromycin breath test as an assay of glucocorticoid-inducible liver cytochromes P-450. Studies in rats and patients*. *J Clin Invest*, 1989. **83**(2): p. 688-97.
206. Hildebrandt, A.G., *The binding of metyrapone to cytochrome P-450 and its inhibitory action on liver microsomal mixed-function oxidase reactions*. *Biochem J*, 1971. **125**(2): p. 6P-8P.
207. Marshall, F.N. and H.E. Williamson, *Natruetic Response during Infusion of Beta-Diethylaminoethyl-Diphenylpropyl Acetate Hydrochloride (Skf 525-a)*. *J Pharmacol Exp Ther*, 1964. **143**: p. 395-400.
208. Frederick, C.B., et al., *Cytochrome P-450- and flavin-containing monooxygenase-catalyzed formation of the carcinogen N-hydroxy-2-aminofluorene and its covalent binding to nuclear DNA*. *Cancer Res*, 1982. **42**(7): p. 2671-7.
209. Kelly, J.D., et al., *Aflatoxin B1 activation in human lung*. *Toxicol Appl Pharmacol*, 1997. **144**(1): p. 88-95.
210. Yamazaki, H., et al., *Procarcinogen activation by cytochrome P450 3A4 and 3A5 expressed in Escherichia coli and by human liver microsomes*. *Carcinogenesis*, 1995. **16**(9): p. 2167-70.
211. Rogakou, E.P., et al., *DNA double-stranded breaks induce histone H2AX phosphorylation on serine 139*. *J Biol Chem*, 1998. **273**(10): p. 5858-68.
212. Kuo, L.J. and L.X. Yang, *Gamma-H2AX - a novel biomarker for DNA double-strand breaks*. *In Vivo*, 2008. **22**(3): p. 305-9.
213. Nakamura, Y., et al., *Silencing HSF1 by short hairpin RNA decreases cell proliferation and enhances sensitivity to hyperthermia in human melanoma cell lines*. *J Dermatol Sci*, 2010. **60**(3): p. 187-92.
214. Imanaka, T., et al., *The 70-kDa peroxisomal membrane protein (PMP70), an ATP-binding cassette transporter*. *Cell Biochem Biophys*, 2000. **32 Spring**: p. 131-8.

215. Austin, K.L., et al., *Intersubject and dose-related variability after intravenous administration of erythromycin*. Br J Clin Pharmacol, 1980. **10**(3): p. 273-9.
216. Wolbold, R., et al., *Sex is a major determinant of CYP3A4 expression in human liver*. Hepatology, 2003. **38**(4): p. 978-88.
217. Jansson, J.O., S. Eden, and O. Isaksson, *Sexual dimorphism in the control of growth hormone secretion*. Endocr Rev, 1985. **6**(2): p. 128-50.
218. Holloway, M.G., E.V. Laz, and D.J. Waxman, *Codependence of growth hormone-responsive, sexually dimorphic hepatic gene expression on signal transducer and activator of transcription 5b and hepatic nuclear factor 4alpha*. Mol Endocrinol, 2006. **20**(3): p. 647-60.
219. Acharya, P., J.J. Chen, and M.A. Correia, *Hepatic heme-regulated inhibitor (HRI) eukaryotic initiation factor 2alpha kinase: a protagonist of heme-mediated translational control of CYP2B enzymes and a modulator of basal endoplasmic reticulum stress tone*. Mol Pharmacol, 2010. **77**(4): p. 575-92.
220. Toyooka, T. and Y. Ibuki, *Co-exposure to benzo[a]pyrene and UVA induces phosphorylation of histone H2AX*. FEBS Lett, 2005. **579**(28): p. 6338-42.
221. Yan, C., et al., *Benzo[a]pyrene induces complex H2AX phosphorylation patterns by multiple kinases including ATM, ATR, and DNA-PK*. Toxicol In Vitro, 2011. **25**(1): p. 91-9.
222. Bogaards, J.J., et al., *Determining the best animal model for human cytochrome P450 activities: a comparison of mouse, rat, rabbit, dog, micropig, monkey and man*. Xenobiotica, 2000. **30**(12): p. 1131-52.
223. Kuribayashi, S., et al., *Human cytochrome P450 1A2 involvement in the formation of reactive metabolites from a species-specific hepatotoxic pyrazolopyrimidine derivative, 5-n-butyl-7-(3,4,5-trimethoxybenzoylamino)pyrazolo[1,5-a]pyrimidine*. Chem Res Toxicol, 2009. **22**(2): p. 323-31.
224. Soltanpour, Y., et al., *Characterization of THLE-cytochrome P450 (P450) cell lines: gene expression background and relationship to P450-enzyme activity*. Drug Metab Dispos, 2012. **40**(11): p. 2054-8.
225. Venkatakrisnan, K., et al., *Five distinct human cytochromes mediate amitriptyline N-demethylation in vitro: dominance of CYP 2C19 and 3A4*. J Clin Pharmacol, 1998. **38**(2): p. 112-21.

226. Metry, K.J., et al., *2-amino-1-methyl-6-phenylimidazo [4,5-b] pyridine-induced DNA adducts and genotoxicity in chinese hamster ovary (CHO) cells expressing human CYP1A2 and rapid or slow acetylator N-acetyltransferase 2*. Mol Carcinog, 2007. **46**(7): p. 553-63.
227. Sesardic, D., et al., *Furafylline is a potent and selective inhibitor of cytochrome P450IA2 in man*. Br J Clin Pharmacol, 1990. **29**(6): p. 651-63.
228. Zhao, K., et al., *Metabolism of the food derived mutagen and carcinogen 2-amino-1-methyl-6-phenylimidazo(4,5-b)pyridine (PhIP) by human liver microsomes*. Carcinogenesis, 1994. **15**(6): p. 1285-8.
229. Gooderham, N.J., et al., *Molecular and genetic toxicology of 2-amino-1-methyl-6-phenylimidazo[4,5-b]pyridine (PhIP)*. Mutat Res, 2002. **506-507**: p. 91-9.
230. Gu, D., et al., *A comprehensive approach to the profiling of the cooked meat carcinogens 2-amino-3,8-dimethylimidazo[4,5-f]quinoxaline, 2-amino-1-methyl-6-phenylimidazo[4,5-b]pyridine, and their metabolites in human urine*. Chem Res Toxicol, 2010. **23**(4): p. 788-801.
231. Glatt, H., *Sulfation and sulfotransferases 4: bioactivation of mutagens via sulfation*. FASEB J, 1997. **11**(5): p. 314-21.
232. Ozawa, S., et al., *Activation of 2-hydroxyamino-1-methyl-6-phenylimidazo[4,5-b] pyridine by cDNA-expressed human and rat arylsulfotransferases*. Jpn J Cancer Res, 1994. **85**(12): p. 1220-8.
233. Glatt, H., et al., *Human cytosolic sulphotransferases: genetics, characteristics, toxicological aspects*. Mutat Res, 2001. **482**(1-2): p. 27-40.
234. Allali-Hassani, A., et al., *Structural and chemical profiling of the human cytosolic sulfotransferases*. PLoS Biol, 2007. **5**(5): p. e97.
235. Alhusainy, W., et al., *Matrix modulation of the bioactivation of estragole by constituents of different alkenylbenzene-containing herbs and spices and physiologically based biokinetic modeling of possible in vivo effects*. Toxicol Sci, 2012. **129**(1): p. 174-87.
236. Besset, S., et al., *Nuclear localization of PAPS synthetase 1: a sulfate activation pathway in the nucleus of eukaryotic cells*. FASEB J, 2000. **14**(2): p. 345-54.
237. Venkatachalam, K.V., *Human 3'-phosphoadenosine 5'-phosphosulfate (PAPS) synthase: biochemistry, molecular biology and genetic deficiency*. IUBMB Life, 2003. **55**(1): p. 1-11.

238. Shitara, Y., et al., *In vitro and in vivo correlation of the inhibitory effect of cyclosporin A on the transporter-mediated hepatic uptake of cerivastatin in rats*. Drug Metab Dispos, 2004. **32**(12): p. 1468-75.
239. Shitara, Y., et al., *Inhibition of transporter-mediated hepatic uptake as a mechanism for drug-drug interaction between cerivastatin and cyclosporin A*. J Pharmacol Exp Ther, 2003. **304**(2): p. 610-6.
240. Tamraz, B., et al., *OATP1B1-related drug-drug and drug-gene interactions as potential risk factors for cerivastatin-induced rhabdomyolysis*. Pharmacogenet Genomics, 2013. **23**(7): p. 355-64.
241. Funk, C., et al., *Troglitazone-induced intrahepatic cholestasis by an interference with the hepatobiliary export of bile acids in male and female rats. Correlation with the gender difference in troglitazone sulfate formation and the inhibition of the canalicular bile salt export pump (Bsep) by troglitazone and troglitazone sulfate*. Toxicology, 2001. **167**(1): p. 83-98.
242. Stieger, B., et al., *Drug- and estrogen-induced cholestasis through inhibition of the hepatocellular bile salt export pump (Bsep) of rat liver*. Gastroenterology, 2000. **118**(2): p. 422-30.
243. Kass, G.E. and S.C. Price, *Role of mitochondria in drug-induced cholestatic injury*. Clin Liver Dis, 2008. **12**(1): p. 27-51, vii.
244. Gores, G.J., et al., *Induction of the mitochondrial permeability transition as a mechanism of liver injury during cholestasis: a potential role for mitochondrial proteases*. Biochim Biophys Acta, 1998. **1366**(1-2): p. 167-75.
245. Ramboer, E., et al., *Primary hepatocyte cultures as prominent in vitro tools to study hepatic drug transporters*. Drug Metab Rev, 2013. **45**(2): p. 196-217.
246. Ripplin, S.J., et al., *Cholestatic expression pattern of sinusoidal and canalicular organic anion transport systems in primary cultured rat hepatocytes*. Hepatology, 2001. **33**(4): p. 776-82.
247. Borlak, J. and T. Klutcka, *Expression of basolateral and canalicular transporters in rat liver and cultures of primary hepatocytes*. Xenobiotica, 2004. **34**(11-12): p. 935-47.
248. Jigorel, E., et al., *Functional expression of sinusoidal drug transporters in primary human and rat hepatocytes*. Drug Metab Dispos, 2005. **33**(10): p. 1418-22.

249. Turncliff, R.Z., X. Tian, and K.L. Brouwer, *Effect of culture conditions on the expression and function of Bsep, Mrp2, and Mdr1a/b in sandwich-cultured rat hepatocytes*. *Biochem Pharmacol*, 2006. **71**(10): p. 1520-9.
250. Bokhari, M., et al., *Culture of HepG2 liver cells on three dimensional polystyrene scaffolds enhances cell structure and function during toxicological challenge*. *J Anat*, 2007. **211**(4): p. 567-76.
251. Bokhari, M., et al., *Novel cell culture device enabling three-dimensional cell growth and improved cell function*. *Biochem Biophys Res Commun*, 2007. **354**(4): p. 1095-100.
252. Schutte, M., et al., *Rat primary hepatocytes show enhanced performance and sensitivity to acetaminophen during three-dimensional culture on a polystyrene scaffold designed for routine use*. *Assay Drug Dev Technol*, 2011. **9**(5): p. 475-86.
253. Burkard, A., et al., *Generation of proliferating human hepatocytes using Upcyte(R) technology: characterisation and applications in induction and cytotoxicity assays*. *Xenobiotica*, 2012. **42**(10): p. 939-56.
254. Hay, D.C., et al., *Unbiased screening of polymer libraries to define novel substrates for functional hepatocytes with inducible drug metabolism*. *Stem Cell Res*, 2011. **6**(2): p. 92-102.
255. Medine, C.N., et al., *Developing high-fidelity hepatotoxicity models from pluripotent stem cells*. *Stem Cells Transl Med*, 2013. **2**(7): p. 505-9.
256. Schrem, H., J. Klempnauer, and J. Borlak, *Liver-enriched transcription factors in liver function and development. Part I: the hepatocyte nuclear factor network and liver-specific gene expression*. *Pharmacol Rev*, 2002. **54**(1): p. 129-58.
257. Gonzalez, F.J., *Regulation of hepatocyte nuclear factor 4 alpha-mediated transcription*. *Drug Metab Pharmacokinet*, 2008. **23**(1): p. 2-7.
258. Schrem, H., J. Klempnauer, and J. Borlak, *Liver-enriched transcription factors in liver function and development. Part II: the C/EBPs and D site-binding protein in cell cycle control, carcinogenesis, circadian gene regulation, liver regeneration, apoptosis, and liver-specific gene regulation*. *Pharmacol Rev*, 2004. **56**(2): p. 291-330.
259. Descombes, P., et al., *LAP, a novel member of the C/EBP gene family, encodes a liver-enriched transcriptional activator protein*. *Genes Dev*, 1990. **4**(9): p. 1541-51.

260. Descombes, P. and U. Schibler, *A liver-enriched transcriptional activator protein, LAP, and a transcriptional inhibitory protein, LIP, are translated from the same mRNA*. Cell, 1991. **67**(3): p. 569-79.
261. Lee, C.S., et al., *The initiation of liver development is dependent on Foxa transcription factors*. Nature, 2005. **435**(7044): p. 944-7.
262. Zaret, K.S. and J.S. Carroll, *Pioneer transcription factors: establishing competence for gene expression*. Genes Dev, 2011. **25**(21): p. 2227-41.
263. Ejendal, K.F. and C.A. Hrycyna, *Differential sensitivities of the human ATP-binding cassette transporters ABCG2 and P-glycoprotein to cyclosporin A*. Mol Pharmacol, 2005. **67**(3): p. 902-11.
264. Xia, C.Q., et al., *Interactions of cyclosporin a with breast cancer resistance protein*. Drug Metab Dispos, 2007. **35**(4): p. 576-82.
265. Allen, J.D., et al., *Potent and specific inhibition of the breast cancer resistance protein multidrug transporter in vitro and in mouse intestine by a novel analogue of fumitremorgin C*. Mol Cancer Ther, 2002. **1**(6): p. 417-25.
266. Roelofsen, H., et al., *Increased levels of the multidrug resistance protein in lateral membranes of proliferating hepatocyte-derived cells*. Gastroenterology, 1997. **112**(2): p. 511-21.
267. Gekeler, V., et al., *The leukotriene LTD4 receptor antagonist MK571 specifically modulates MRP associated multidrug resistance*. Biochem Biophys Res Commun, 1995. **208**(1): p. 345-52.
268. Wang, E.J., et al., *Fluorescent substrates of sister-P-glycoprotein (BSEP) evaluated as markers of active transport and inhibition: evidence for contingent unequal binding sites*. Pharm Res, 2003. **20**(4): p. 537-44.
269. Kis, E., et al., *Effect of membrane cholesterol on BSEP/Bsep activity: species specificity studies for substrates and inhibitors*. Drug Metab Dispos, 2009. **37**(9): p. 1878-86.
270. Hempel, S.L., et al., *Dihydrofluorescein diacetate is superior for detecting intracellular oxidants: comparison with 2',7'-dichlorodihydrofluorescein diacetate, 5(and 6)-carboxy-2',7'-dichlorodihydrofluorescein diacetate, and dihydrorhodamine 123*. Free Radic Biol Med, 1999. **27**(1-2): p. 146-59.
271. Loor, G., et al., *Menadione triggers cell death through ROS-dependent mechanisms involving PARP activation without requiring apoptosis*. Free Radic Biol Med, 2010. **49**(12): p. 1925-36.

272. Lu, H., F.J. Gonzalez, and C. Klaassen, *Alterations in hepatic mRNA expression of phase II enzymes and xenobiotic transporters after targeted disruption of hepatocyte nuclear factor 4 alpha*. *Toxicol Sci*, 2010. **118**(2): p. 380-90.
273. Wagner, M., et al., *CAR and PXR agonists stimulate hepatic bile acid and bilirubin detoxification and elimination pathways in mice*. *Hepatology*, 2005. **42**(2): p. 420-30.
274. Teng, S. and M. Piquette-Miller, *The involvement of the pregnane X receptor in hepatic gene regulation during inflammation in mice*. *J Pharmacol Exp Ther*, 2005. **312**(2): p. 841-8.
275. Tirona, R.G., et al., *The orphan nuclear receptor HNF4alpha determines PXR- and CAR-mediated xenobiotic induction of CYP3A4*. *Nat Med*, 2003. **9**(2): p. 220-4.
276. Le Lay, J. and K.H. Kaestner, *The Fox genes in the liver: from organogenesis to functional integration*. *Physiol Rev*, 2010. **90**(1): p. 1-22.
277. Wallerman, O., et al., *Molecular interactions between HNF4a, FOXA2 and GABP identified at regulatory DNA elements through ChIP-sequencing*. *Nucleic Acids Res*, 2009. **37**(22): p. 7498-508.
278. Wakabayashi, Y., J. Lippincott-Schwartz, and I.M. Arias, *Intracellular trafficking of bile salt export pump (ABCB11) in polarized hepatic cells: constitutive cycling between the canalicular membrane and rab11-positive endosomes*. *Mol Biol Cell*, 2004. **15**(7): p. 3485-96.
279. Dombrowski, F., B. Stieger, and U. Beuers, *Tauroursodeoxycholic acid inserts the bile salt export pump into canalicular membranes of cholestatic rat liver*. *Lab Invest*, 2006. **86**(2): p. 166-74.
280. Symeonidis, A. and E.G. Trams, *Morphologic and functional changes in the livers of rats after ligation or excision of the common bile duct*. *The American journal of pathology*, 1957. **33**(1): p. 13-27.
281. Tarcin, O., et al., *Time course of collagen peak in bile duct-ligated rats*. *BMC gastroenterology*, 2011. **11**: p. 45.
282. Deems, R.O. and M.I. Friedman, *Macronutrient selection in an animal model of cholestatic liver disease*. *Appetite*, 1988. **11**(2): p. 73-80.
283. Georgiev, P., et al., *Characterization of time-related changes after experimental bile duct ligation*. *Br J Surg*, 2008. **95**(5): p. 646-56.

284. Lijinsky, W., M.D. Reuber, and B.N. Blackwell, *Liver tumors induced in rats by oral administration of the antihistaminic methapyrilene hydrochloride*. Science, 1980. **209**(4458): p. 817-9.
285. Brennan, L.M. and D.A. Creasia, *The effects of methapyrilene hydrochloride on hepatocarcinogenicity and pentobarbital-induced sleeping time in rats and mice*. Toxicol Appl Pharmacol, 1982. **66**(2): p. 252-8.
286. Graichen, M.E., et al., *Effects of methapyrilene on rat hepatic xenobiotic metabolizing enzymes and liver morphology*. Fundam Appl Toxicol, 1985. **5**(1): p. 165-74.
287. Steinmetz, K.L., et al., *Examination of genotoxicity, toxicity and morphologic alterations in hepatocytes following in vivo or in vitro exposure to methapyrilene*. Carcinogenesis, 1988. **9**(6): p. 959-63.
288. Richardson, F.C., D.M. Copple, and P.I. Eacho, *Effects of methapyrilene on DNA synthesis in mice and rats following continuous dietary exposure*. Carcinogenesis, 1992. **13**(12): p. 2453-7.
289. Cunningham, M.L., et al., *The hepatocarcinogen methapyrilene but not the analog pyrilamine induces sustained hepatocellular replication and protein alterations in F344 rats in a 13-week feed study*. Toxicology and applied pharmacology, 1995. **131**(2): p. 216-23.
290. Hamadeh, H.K., et al., *Methapyrilene toxicity: anchorage of pathologic observations to gene expression alterations*. Toxicol Pathol, 2002. **30**(4): p. 470-82.
291. Mercer, A.E., et al., *Functional and toxicological consequences of metabolic bioactivation of methapyrilene via thiophene S-oxidation: Induction of cell defence, apoptosis and hepatic necrosis*. Toxicol Appl Pharmacol, 2009. **239**(3): p. 297-305.
292. Priestley, C.C., et al., *The genotoxic potential of methapyrilene using the alkaline Comet assay in vitro and in vivo*. Toxicology, 2011. **290**(2-3): p. 249-57.
293. Graham, E.E., et al., *Identification of the thiophene ring of methapyrilene as a novel bioactivation-dependent hepatic toxicophore*. J Pharmacol Exp Ther, 2008. **326**(2): p. 657-71.

294. Ratra, G.S., et al., *Methapyrilene hepatotoxicity is associated with oxidative stress, mitochondrial dysfunction and is prevented by the Ca<sup>2+</sup> channel blocker verapamil*. Toxicology, 1998. **130**(2-3): p. 79-93.
295. Lock, E.A. and C.J. Reed, *Xenobiotic metabolizing enzymes of the kidney*. Toxicologic pathology, 1998. **26**(1): p. 18-25.
296. Michalopoulos, G.K., *Liver regeneration*. J Cell Physiol, 2007. **213**(2): p. 286-300.
297. Galand, P. and C. Degraef, *Cyclin/PCNA immunostaining as an alternative to tritiated thymidine pulse labelling for marking S phase cells in paraffin sections from animal and human tissues*. Cell Tissue Kinet, 1989. **22**(5): p. 383-92.
298. Libbrecht, L., et al., *The correlation between portal myofibroblasts and development of intrahepatic bile ducts and arterial branches in human liver*. Liver, 2002. **22**(3): p. 252-8.
299. Du, X., et al., *Involvement of matrix metalloproteinase-2 in the development of renal interstitial fibrosis in mouse obstructive nephropathy*. Lab Invest, 2012. **92**(8): p. 1149-60.
300. Azmaiparashvili, E., et al., *Ductular reaction at the early terms of common bile duct ligation in the rats*. Acta Biol Hung, 2012. **63**(3): p. 321-32.
301. Masaki, T., et al., *The role of histamine H1 receptor and H2 receptor in LPS-induced liver injury*. FASEB J, 2005. **19**(10): p. 1245-52.
302. Pentyala, S.N., et al., *Effect of carbon tetrachloride on inositol 1,4,5-trisphosphate dependent and independent regulation of rat brain microsomal Ca<sup>2+</sup> flux*. Cell Signal, 1994. **6**(5): p. 561-7.
303. Desmet, V.J., B. Krstulovic, and B. Van Damme, *Histochemical study of rat liver in alpha-naphthyl isothiocyanate (ANIT) induced cholestasis*. The American journal of pathology, 1968. **52**(2): p. 401-21.
304. Kossor, D.C., et al., *Temporal relationship of changes in hepatobiliary function and morphology in rats following alpha-naphthylisothiocyanate (ANIT) administration*. Toxicology and applied pharmacology, 1993. **119**(1): p. 108-14.
305. Tang, W., *Drug metabolite profiling and elucidation of drug-induced hepatotoxicity*. Expert Opin Drug Metab Toxicol, 2007. **3**(3): p. 407-20.
306. Jean, P.A. and R.A. Roth, *Naphthylisothiocyanate disposition in bile and its relationship to liver glutathione and toxicity*. Biochemical pharmacology, 1995. **50**(9): p. 1469-74.

307. Moran, E. and H. Ungar, *The Effect of Intermittent Administration of Alpha-Naphthyl Isothiocyanate to Rats*. The American journal of pathology, 1964. **44**: p. 947-60.
308. Lesage, G., et al., *Regression of cholangiocyte proliferation after cessation of ANIT feeding is coupled with increased apoptosis*. American journal of physiology. Gastrointestinal and liver physiology, 2001. **281**(1): p. G182-90.
309. Xu, J., et al., *Limited role for CXC chemokines in the pathogenesis of alpha-naphthylisothiocyanate-induced liver injury*. American journal of physiology. Gastrointestinal and liver physiology, 2004. **287**(3): p. G734-41.
310. Chang, M.L., et al., *Comparison of murine cirrhosis models induced by hepatotoxin administration and common bile duct ligation*. World J Gastroenterol, 2005. **11**(27): p. 4167-72.
311. Wallace, K., et al., *The PXR is a drug target for chronic inflammatory liver disease*. J Steroid Biochem Mol Biol, 2010. **120**(2-3): p. 137-48.
312. Li, Q. and I.M. Verma, *NF-kappaB regulation in the immune system*. Nat Rev Immunol, 2002. **2**(10): p. 725-34.
313. Luedde, T. and R.F. Schwabe, *NF-kappaB in the liver--linking injury, fibrosis and hepatocellular carcinoma*. Nat Rev Gastroenterol Hepatol, 2011. **8**(2): p. 108-18.
314. Wright, M.C., et al., *Gliotoxin stimulates the apoptosis of human and rat hepatic stellate cells and enhances the resolution of liver fibrosis in rats*. Gastroenterology, 2001. **121**(3): p. 685-98.
315. Oakley, F., et al., *Inhibition of inhibitor of kappaB kinases stimulates hepatic stellate cell apoptosis and accelerated recovery from rat liver fibrosis*. Gastroenterology, 2005. **128**(1): p. 108-20.
316. Anan, A., et al., *Proteasome inhibition induces hepatic stellate cell apoptosis*. Hepatology, 2006. **43**(2): p. 335-44.
317. Sunami, Y., et al., *Hepatic activation of IKK/NFkappaB signaling induces liver fibrosis via macrophage-mediated chronic inflammation*. Hepatology, 2012. **56**(3): p. 1117-28.
318. Gieling, R.G., et al., *The c-Rel subunit of nuclear factor-kappaB regulates murine liver inflammation, wound-healing, and hepatocyte proliferation*. Hepatology, 2010. **51**(3): p. 922-31.

319. Ogawa, K., et al., *Characterization of inducible nature of MRP3 in rat liver*. Am J Physiol Gastrointest Liver Physiol, 2000. **278**(3): p. G438-46.
320. Osterreicher, C.H. and M. Trauner, *Xenobiotic-induced liver injury and fibrosis*. Expert opinion on drug metabolism & toxicology, 2012. **8**(5): p. 571-80.
321. Marek, C.J., et al., *Pregnenolone-16alpha-carbonitrile inhibits rodent liver fibrogenesis via PXR (pregnane X receptor)-dependent and PXR-independent mechanisms*. The Biochemical journal, 2005. **387**(Pt 3): p. 601-8.
322. Carpenter-Deyo, L., et al., *Involvement of glutathione in 1-naphthylisothiocyanate (ANIT) metabolism and toxicity to isolated hepatocytes*. Biochemical pharmacology, 1991. **42**(11): p. 2171-80.
323. Dietrich, C.G., et al., *Role of MRP2 and GSH in intrahepatic cycling of toxins*. Toxicology, 2001. **167**(1): p. 73-81.
324. Roberts, R.J. and G.L. Plaa, *The effect of bile duct ligation, bile duct cannulation, and hypothermia on alpha-naphthylisothiocyanate-induced hyperbilirubinemia and cholestasis in rats*. Gastroenterology, 1966. **50**(6): p. 768-74.
325. Hu, K. and M.E. Morris, *Pharmacokinetics of alpha-naphthyl isothiocyanate in rats*. J Pharm Sci, 2005. **94**(11): p. 2441-51.
326. Tanaka, Y., et al., *ANIT-induced intrahepatic cholestasis alters hepatobiliary transporter expression via Nrf2-dependent and independent signaling*. Toxicol Sci, 2009. **108**(2): p. 247-57.
327. Jones, D.E., *Pathogenesis of primary biliary cirrhosis*. Gut, 2007. **56**(11): p. 1615-24.
328. Hill, D.A., P.A. Jean, and R.A. Roth, *Bile duct epithelial cells exposed to alpha-naphthylisothiocyanate produce a factor that causes neutrophil-dependent hepatocellular injury in vitro*. Toxicol Sci, 1999. **47**(1): p. 118-25.
329. Chiang, J.Y., *Bile acids: regulation of synthesis*. J Lipid Res, 2009. **50**(10): p. 1955-66.
330. Cui, Y.J., et al., *Compensatory induction of liver efflux transporters in response to ANIT-induced liver injury is impaired in FXR-null mice*. Toxicol Sci, 2009. **110**(1): p. 47-60.
331. Cheng, X., D. Buckley, and C.D. Klaassen, *Regulation of hepatic bile acid transporters Ntcp and Bsep expression*. Biochem Pharmacol, 2007. **74**(11): p. 1665-76.

332. Wang, H., et al., *Glucocorticoid receptor enhancement of pregnane X receptor-mediated CYP2B6 regulation in primary human hepatocytes*. *Drug Metab Dispos*, 2003. **31**(5): p. 620-30.
333. Chan, C.W., et al., *Long-term ursodeoxycholic acid therapy for primary biliary cirrhosis: a follow-up to 12 years*. *Aliment Pharmacol Ther*, 2005. **21**(3): p. 217-26.
334. Festi, D., et al., *Clinical efficacy and effectiveness of ursodeoxycholic acid in cholestatic liver diseases*. *Curr Clin Pharmacol*, 2007. **2**(2): p. 155-77.
335. Prince, M.I., A.D. Burt, and D.E. Jones, *Hepatitis and liver dysfunction with rifampicin therapy for pruritus in primary biliary cirrhosis*. *Gut*, 2002. **50**(3): p. 436-9.
336. Amaral, J.D., et al., *p53 is a key molecular target of ursodeoxycholic acid in regulating apoptosis*. *J Biol Chem*, 2007. **282**(47): p. 34250-9.
337. Szabo, S., S. Komblos, and Z. Ignjatovic, *Effect of pregnenolone-16alpha-carbonitrile (PCN) on drug response in man*. *J Pharm Pharmacol*, 1975. **27**(2): p. 113-8.
338. Guo, L., et al., *Similarities and differences in the expression of drug-metabolizing enzymes between human hepatic cell lines and primary human hepatocytes*. *Drug Metab Dispos*, 2011. **39**(3): p. 528-38.

## Appendix A. List of primers used for PCR

Oligo ID	Primer sequence (5'-3')		Comments
<b>18S rRNA</b>	<b>US</b>	CCCGAAGCGTTTACTTTGAA	Will amplify 136bp fragment of rat, mouse and human 18S rRNA
	<b>DS</b>	CCCTCTTAATCATGGCCTCA	
<b>r<math>\alpha</math>-collagen</b>	<b>US</b>	TGTGTTGCTGAAAGACTACCTCGT	Will amplify 53bp fragment of rat collagen 1A1 (NM_053304)
	<b>DS</b>	AGTTGCCCCGGTGACACACAA	
<b>r<math>\alpha</math>-SMA</b>	<b>US</b>	TGCCATGTATGTGGCTATTCA	Will amplify 55bp fragment of rat $\alpha$ -SMA (NM_031004)
	<b>DS</b>	ACCAGTTGTACGTCCAGAAGC	
<b>rAhR</b>	<b>US</b>	TGGCTGTGATGCCAAAGGGCAG	Will amplify 100bp fragment of rat AhR (NM_013149.2)
	<b>DS</b>	AAGCATGTCAGCGGCGTGGA	
<b>rAlbumin</b>	<b>US</b>	TGGTCGCAGCTGTCCGTCAGA	Will amplify 182bp fragment of rat albumin (NM_134326.2)
	<b>DS</b>	CAGGTCGCCGTGACAGCACTC	
<b>rAmylase</b>	<b>US</b>	CAAAATGGTTCTCCCAAGGA	Will amplify 224bp fragment of rat pancreatic amylase 2 (NM_031502.1 )
	<b>DS</b>	AAGGGCTCTGTCAGTAGGCA	
<b>rARNT</b>	<b>US</b>	GGTTTGCCAGGTCGGATGAT	Will amplify 219bp fragment of rat ARNT (NM_012780.1 )
	<b>DS</b>	CCGTTCCCCTCAAGGACTTC	
<b>mBSEP</b>	<b>US</b>	TGGCCGTGCTCATCGCCTTC	Will amplify 200bp fragment of mouse BSEP (NM_021022.3)
	<b>DS</b>	TCCAATTCCAGCCACGGTGCG	
<b>rBSEP</b>	<b>US</b>	GCCAGGGGAAACGACGGCTC	Will amplify 113bp fragment of rat BSEP (NM_031760.1)
	<b>DS</b>	GGCCGTCCAGAGTCACCATGC	
<b>rCAR</b>	<b>US</b>	CTCTCCTGACAGGCCTGGGGT	Will amplify 156bp fragment of rat CAR (NM_022941.3)
	<b>DS</b>	CGAAGCTCAGCTAGCAGGCC	
<b>hC/EBP<math>\alpha</math></b>	<b>US</b>	CCATGCCGGGAGAACTCTAA	Will amplify 218bp fragment of human C/EBP $\alpha$ (NM_004364.4)
	<b>DS</b>	ATGTCGATGGACGTCTCGTG	
<b>rCPS-1</b>	<b>US</b>	ATACAACGGCACGTGATGAA	Will amplify 390bp fragment of rat CPS-1 (NM_017072.1)
	<b>DS</b>	GCTTAACTAGCAGGCGGATG	
<b>rCYP1A1</b>	<b>US</b>	TCCCTGGGGTCTAGAGAACTCT	Will amplify 109bp fragment of rat CYP1A1 (NM_012540.2)
	<b>DS</b>	TGTGGCTGATGTGAAGGCTGGG	
<b>hCYP1A2</b>	<b>US</b>	CACACCAGCCATTACAACCCTGCC	Will amplify 1608bp coding sequence of human CYP1A2 (NM_000761.3)
	<b>DS</b>	TCAGTTGATGGAGAAGCGCAGCC	

<b>gCYP1A2</b>	<b>US</b>	GTGGTCACTGGCATCCACACCA	Will amplify 460bp fragment of genomic rat CYP1A2 (NC_005107.3)
	<b>DS</b>	AAGGGCAAGCCCCAGGGTCC	
<b>rCYP1A2</b>	<b>US</b>	CGCATTGGCTCCACACCCGT	Will amplify 412bp fragment of rat CYP1A2 (NM_012541.3)
	<b>DS</b>	TCTCCTCGCTCTTCTGGGGA	
<b>rCYP1A2</b>	<b>US</b>	CTACAACCTGCGCAGTCTCCAG	Will amplify 130bp fragment of rat CYP1A2 (NM_012541.3) - used for qPCR
	<b>DS</b>	CCTCTCAACACCCAGAACACT	
<b>rCYP1B1</b>	<b>US</b>	CAGCTTTTTGCCTGTCACCC	Will amplify 180bp fragment of rat CYP1B1 (NM_012940.2)
	<b>DS</b>	ATGAAGCCGTCCTTGTCCAG	
<b>rCYP2A1</b>	<b>US</b>	ATGCTGCTTTCTCCCTTTC	Will amplify 64bp fragment of rat CYP2A1 (NM_012692.1)
	<b>DS</b>	ATCTTAGCCAGGCCATCTCC	
<b>rCYP2B1</b>	<b>US</b>	CGCATGGAGAAGGAGAAGTCGAACC	Will amplify 151bp fragment of rat CYP2B1 (NM_001134844.1 )
	<b>DS</b>	CGACATGGGGTACTTGAGCATCAG	
<b>rCYP2B2</b>	<b>US</b>	CGCCTGTTGGAGCTGTTCTA	Will amplify 151bp fragment of rat CYP2B2 (NM_001198676.1)
	<b>DS</b>	ACTTCTCCTCTCTCATCCATGC	
<b>rCYP2B3</b>	<b>US</b>	CCCTTCTCCATAGGAAAGCGTA	Will amplify 269bp fragment of rat CYP2B3 (NM_173294.1)
	<b>DS</b>	CCAGCAGGTCTCCAGAATC	
<b>rCYP2C6</b>	<b>US</b>	CTGTGACCAACCAGCTAAAGTCCAG	Will amplify 82bp fragment of rat CYP2C6 (XM_003748910.1)
	<b>DS</b>	CTCCATGCGGGCTAGGCCCT	
<b>rCYP2C7</b>	<b>US</b>	AGATGTGAAGAACATCAGCCA	Will amplify 84bp fragment of CYP2C7 (NM_017158.2)
	<b>DS</b>	GGCTGTGAGCCCAAATACAG	
<b>rCYP2C11</b>	<b>US</b>	CTGCCATGGATCCAGTCTTAGTCC	Will amplify 88bp fragment of rat CYP2C11 (NM_019184.2 )
	<b>DS</b>	TTCCCTCTCCAAAGCTCTGTCTCC	
<b>rCYP2C12</b>	<b>US</b>	TGTGAGCACTCCTGCATTTTCAGG	Will amplify 317bp fragment of rat CYP2C12 (NM_031572.1)
	<b>DS</b>	AGAGCAAAAGTGCAAATCTCAGCGT	
<b>rCYP2C13</b>	<b>US</b>	CCCACCTTCCAGATGCGCTTCA	Will amplify 165bp fragment of rat CYP2C13 (NM_138514.1)
	<b>DS</b>	CCGAAGCTGTGAGAAGAAGGAAGG	
<b>rCYP2E1</b>	<b>US</b>	TCGACTACAATGACAAGAAGTGT	Will amplify 525bp fragment of rat CYP2E1 (NM_031543)
	<b>DS</b>	CAAGATTGATGAATCTCTGGATCTC	
<b>rCYP3A1/23</b>	<b>US</b>	TGGCCCAGTGGGGATTATGGGG	Will amplify 183bp fragment of rat CYP3A1/23 (NM_013105.2)
	<b>DS</b>	GGGACAGGTTTGCCTTTCTCTTGCC	
<b>rCYP3A2</b>	<b>US</b>	TGGCAAGGTCTGTGATGGAAC	Will amplify 72bp fragment of rat CYP3A2 (NM_153312.2)
	<b>DS</b>	ACCAGATGTGGATGGAGATGG	
<b>rCYP3A2</b>	<b>US</b>	ACCCGTCTGGATTCTAAGCA	Will amplify 73bp fragment of rat CYP3A2 (NM_153312.2) - used for qPCR

	<b>DS</b>	TGGAATTATTATGAGCGTTCAGC	
<b>mCYP3A11</b>	<b>US</b>	GGATCACACACACAGTTGTAGGGAG	Will amplify 194bp fragment of mouse CYP3A11 (NM_007818.3)
	<b>DS</b>	GCAGAGGTTTGGGCCCAGGAA	
<b>rCYP3A18</b>	<b>US</b>	GGAGGCCTGAACTGCTGAAGGAG	Will amplify 166bp fragment of rat CYP3A18 (NM_145782.1)
	<b>DS</b>	AAGGCACAGTTTGGGTCCAGGA	
<b>rCYP3A19</b>	<b>US</b>	GCCCTGAAAGGTTCAAGCAAG	Will amplify 282bp fragment of rat CYP3A19 (NM_147206.2)
	<b>DS</b>	AGGCCATTCTACATCAAGCTCC	
<b>rCYP4A1</b>	<b>US</b>	TGCACCATGAGCGTCTCTGCACT	Will amplify 85bp fragment of rat CYP4A1 (NM_175837.1)
	<b>DS</b>	GACCAAGCACGGAGGCCACTT	
<b>rCYP4A2</b>	<b>US</b>	AGTCCAAAGCTTTTACTCCAGA	Will amplify 219bp fragment of rat CYP4A2 ( NM_001044770.2)
	<b>DS</b>	TGCCGATTGTCCCAAGACTC	
<b>rCYP4A3</b>	<b>US</b>	GGAGGAGCAAGGAACTGCAT	Will amplify 225bp fragment of rat CYP4A3 (NM_175760.2)
	<b>DS</b>	TATTGCAGGCAGCAGACCTC	
<b>mCYP7A1</b>	<b>US</b>	TGCGAAGGCATTTGGACACAGA	Will amplify 163bp fragment of mouse CYP7A1 (NM_007824.2)
	<b>DS</b>	AGGAAGGCCCGGAGGTCTCA	
<b>mCYP8B1</b>	<b>US</b>	CCCCGGCAGTTCTTTGCC	Will amplify 119bp fragment of mouse CYP8B1 (NM_007742.3)
	<b>DS</b>	AGCGCCTTGGGTCAATGGGG	
<b>mCYP27A1</b>	<b>US</b>	GGCTGGGGTGGACACGACAT	Will amplify 116bp fragment of mouse CYP27A1 (NM_024264.4)
	<b>DS</b>	TCCCGAAGGGCACACACCA	
<b>hFOXA2</b>	<b>US</b>	CACTTGAGTCCCAGCCTGA	Will amplify 333bp fragment of human FOXA2 (BC011780.2)
	<b>DS</b>	GTCGTTGAAGGAGAGCGAGT	
<b>rmhGAPDH</b>	<b>US</b>	TGACATCAAGAAGGTGGTGAAG	Will amplify 243bp of rat GAPDH (NM_017008.3)(also human and mouse)
	<b>DS</b>	TTGTCATACCAGGAAATGAGCT	
<b>hHNF1<math>\alpha</math></b>	<b>US</b>	ACAGCTTGGAGCAGACATCC	Will amplify 55bp fragment of human HNF1 $\alpha$ (BC104910.1)
	<b>DS</b>	ATGAGCATAGTCTGCGGGAG	
<b>rhHNF4<math>\alpha</math></b>	<b>US</b>	ACATGGACATGGCCGACTAC	Will amplify 202bp fragment of human HNF4 $\alpha$ (NM_178849.2)(also rat)
	<b>DS</b>	CTCGAGGCACCGTAGTGTTT	
<b>mMDR1a</b>	<b>US</b>	GGAACAGCGTTTCCAGGAGCTG	Will amplify 136bp fragment of mouse MDR1a (NM_011076.2)
	<b>DS</b>	CCATCACGACCTCACGTGTCTCT	
<b>mMDR2</b>	<b>US</b>	AGCGAGAAACGGAACAGCACGG	Will amplify 175bp fragment of mouse MDR2 (NM_008830.2)
	<b>DS</b>	AGCTATGGCCATGAGGGTGCC	
<b>rMMP-2</b>	<b>US</b>	GCACCGTCGCCATCATCAAGT	Will amplify 55bp fragment of rat MMP2 (NM_031054.2)
	<b>DS</b>	TTGCGGGGAAAGAAGTTGTAGT	

<b>mMRP2</b>	<b>US</b>	CGTGCGCTCTCCTCCCAGACT	Will amplify 167bp fragment of mouse MRP2 (NM_013806.2 )
	<b>DS</b>	CACAGCCGACAGGGGGTTCGT	
<b>rMRP2</b>	<b>US</b>	GCGCCCTGGGTGACTGACAA	Will amplify 164bp fragment of rat MRP2 (NM_012833.1)
	<b>DS</b>	GTCCTGCCCACTACGCCGAC	
<b>mNTCP</b>	<b>US</b>	ATCCAAGCTGCAGACGCACCA	Will amplify 248bp fragment of mouse NTCP (NM_001177561.1)
	<b>DS</b>	AGCATCTTCTGTTGCAGCAGCCT	
<b>rNTCP</b>	<b>US</b>	GCATCATGCCCTCGCTGCT	Will amplify 164bp fragment of rat NTCP (NM_017047.1)
	<b>DS</b>	GGTGGTCATCACGATGCTGAGGT	
<b>rPAPSS1</b>	<b>US</b>	CTCTCTTACCACTCGGCCTC	Will amplify 313bp fragment of rat PAPSS1 (NM_001106471.1)
	<b>DS</b>	AAGTGTAGCACGGAATGCCA	
<b>rPAPSS2</b>	<b>US</b>	CCGTGTTACTCCCTGGATGG	Will amplify 600bp fragment of rat PAPSS2 (NM_001106375.2 )
	<b>DS</b>	AAAGCCTTTGAGCGGAGTGG	
<b>rPPAR<math>\alpha</math></b>	<b>US</b>	CGGGGATCTTAGAGGCGAGCCAA	Will amplify 126bp fragment of rat PPAR $\alpha$ (NM_013196.1)
	<b>DS</b>	GCGGGCCACAGAGACCAAT	
<b>rPXR</b>	<b>US</b>	GCTCCTGCTGGACCCGTTGA	Will amplify 115bp fragment of rat PXR (NM_052980.2)
	<b>DS</b>	GCCAGGGCGATCTGGGGAGAA	
<b>rRXR<math>\alpha</math></b>	<b>US</b>	TCTTCATCCCTGAGCTCTCCA	Will amplify 263bp fragment of rat RXR $\alpha$ (NM_012805.2)
	<b>DS</b>	TTCATGGGTGAGTTGAGCTGG	
<b>rRXR<math>\beta</math></b>	<b>US</b>	GACAGCTCCTCCCCAAATCC	Will amplify 213bp fragment of rat RXR $\beta$ (NM_206849.3)
	<b>DS</b>	GGAGTTAATCTGAGGGCTGC	
<b>hSGK1F</b>	<b>US</b>	TCTCCTCCTTCATCCACAGCTTTCA	Will amplify 211bp fragment of human SGK1F (CAI19718)
	<b>DS</b>	TGGACGACGGGCCAAGGTTG	
<b>rSULT1A1</b>	<b>US</b>	ACACATCTGCCCTGTCTT	Will amplify 77bp fragment of rat SULT1A1 (NM_031834.1)
	<b>DS</b>	GCATTTGCGGGCAATGTAGA	
<b>rSULT1B1</b>	<b>US</b>	CGAGATGTTATTACCTCTAAAGTTCCA	Will amplify 88bp fragment of rat SULT1B1 (NM_025513.1)
	<b>DS</b>	GAGTTTTCTTCAAGAGTTCAACACC	
<b>rSULT1C2</b>	<b>US</b>	TCTGCCCTTGAGGTATCCAG	Will amplify 90bp fragment of rat SULT1C2 (NM_133547.4)
	<b>DS</b>	GCGGCTGTAATCTGCTCAA	
<b>rSULT1C2A</b>	<b>US</b>	TCTGCCCTTGAGGTATCCAG	Will amplify 87bp fragment of rat SULT1C2A (NM_001013177.2)
	<b>DS</b>	CAGGAAGAAGGTTTAGTTCCA	
<b>rSULT1C3</b>	<b>US</b>	GGTACCCTGGGAGAATACATTG	Will amplify 84bp fragment of rat SULT1C3 (NM_031732.2)
	<b>DS</b>	CCACCATCCCTTTACATGGT	
<b>rSULT1D1</b>	<b>US</b>	CCTCGACTGGTGAAGACACA	Will amplify 87bp fragment of rat SULT1D1 (NM_021769.1)

	<b>DS</b>	CCGTGCCACATAAATCATCTT	
<b>rSULT1E1</b>	<b>US</b>	GAGAAATTTATGGAAGGGCAAG	Will amplify 103bp fragment of rat SULT1E1 (NM_012883.1)
	<b>DS</b>	CATAGAACATAAAACAAAACACGTGAA	
<b>rSULT2A1</b>	<b>US</b>	TGGGGTAATTCAACTCTTGTGA	Will amplify 102bp fragment of at rat SULT2A1 (NM_131903.1 )
	<b>DS</b>	GATGTGCTCAAACCATGATCC	
<b>rSULT2A2</b>	<b>US</b>	TCTTCAGTTCCAAGGCCAAG	Will amplify 118bp fragment of rat SULT2A2 (NM_001025131.1)
	<b>DS</b>	GTTCCCAGCGAGTCTGGTT	
<b>rSULT2A6</b>	<b>US</b>	AAGACAACCTCTTGCGAAGAAGC	Will amplify 96bp fragment of rat SULT2A6 (NM_012695.3)
	<b>DS</b>	GATGTGCTCAAACCATGATCC	
<b>rSULT2B1</b>	<b>US</b>	GGTGATTTACTTGGGCCGGA	Will amplify 420bp fragment of rat SULT2B1 (NM_001039665.1)
	<b>DS</b>	CAGTCGCCACTGATCCCTTT	
<b>rSULT2B12</b>	<b>US</b>	GGTGATTTACTTGGGCCGGA	Will amplify 420bp fragment of rat SULT2B12 (NM_001039665.1)
	<b>DS</b>	CAGTCGCCACTGATCCCTTT	
<b>rSULT4A1</b>	<b>US</b>	CGGAAGTTGCTTGAAACAG	Will amplify 60bp fragment of rat SULT4A1 (NM_031641.1)
	<b>DS</b>	CATCTCACTCCTCGGCTCTC	
<b>rSULT5A1</b>	<b>US</b>	CTCCAGAAGGACCTAACTTTGC	Will amplify 69bp fragment of rat SULT5A1 (NM_001106194.1)
	<b>DS</b>	AATGGTTGAGCGAGGTTC	
<b>rSULT6B1</b>	<b>US</b>	TCCGAGCTTTGGATGCCTTT	Will amplify 608bp fragment of rat SULT6B1 (NM_001192017.1)
	<b>DS</b>	CTGGGATTTTGCTCGCATCG	
<b>rTGFβ1</b>	<b>US</b>	CGAGCCCGAGGCGGACTACT	Will amplify 73bp fragment of rat TGFβ1 (NM_021578.2)
	<b>DS</b>	ATAGATTGCGTTGTTGCGGTCCACC	
<b>rTGFβ2</b>	<b>US</b>	TTCAGAATCGTCCGCTTCGAT	Will amplify 114bp fragment of rat TGFβ2 (NM_031131.1)
	<b>DS</b>	TTGTTCAGCCACTCTGGCCTT	
<b>rTIMP1</b>	<b>US</b>	GACCACCTTATACCAGCGTT	Will amplify 60bp fragment of rat TIMP1 (NM_053819.1)
	<b>DS</b>	GTCACTCTCCAGTTTGCAAG	
<b>rVimentin</b>	<b>US</b>	CAGGCCACCTCGTCTTCGAAG	Will amplify 84bp fragment of rat vimentin (NM_031140.1 )
	<b>DS</b>	TGTGCCGGAGCCACCGAACAT	

## **Appendix B. Published papers**